Universidad Pública de Navarra

Electric and Electronic Departament

CONTRIBUTION TO THE DEVELOPMENT OF FUNCTIONAL NANOSTRUCTURED COATINGS BASED ON SILVER NANOPARTICLES

PhD dissertation by

Pedro José Rivero Fuente

Advisors:

Dr. Javier Goicoechea Fernández

Prof. Francisco J. Arregui San Martín

Pamplona, July 2014

Universidad Pública de Navarra

Departamento de Ingeniería Eléctrica y Electrónica

CONTRIBUCIÓN AL DESARROLLO DE RECUBRIMIENTOS NANOESTRUCTURADOS FUNCIONALES BASADOS EN NANOPARTÍCULAS DE PLATA

Memoria de la tesis doctoral realizada por

Pedro José Rivero Fuente

Directores:

Dr. Javier Goicoechea Fernández

Prof. Francisco J. Arregui San Martín

Pamplona, Julio 2014

TESIS DOCTORAL: **"CONTRIBUTION TO THE DEVELOPMENT OF FUNCTIONAL NANOSTRUCTURED COATINGS BASED ON SILVER NANOPARTICLES"**

Autor: Pedro José Rivero Fuente

Directores: Dr. Javier Goicoechea Fernández

Prof. Francisco J. Arregui San Martín

Tribunal nombrado para evaluar la citada Tesis Doctoral:

Presidente: _____

Secretario: _____

Vocal: _____

Revisores externos:

_____

_____

Acuerda otorgar la calificación de:

_____

En Pamplona, a _____ de _____ de 20___

"Ten cuidado con tu forma de interpretar el mundo,
porque el mundo es tal como tú lo interpretes"
Erich Heller

RECONOCIMIENTOS

La realización de este tesis ha sido posible gracias a la obtención de una beca predoctoral de la Universidad Pública de Navarra (UPNA) y a las aportaciones económicas recibidas por parte del Gobierno de Navarra mediante sus programas de apoyo a la investigación, además de la colaboración de la Comisión Interministerial de Ciencia y Tecnología a través de la financiación de los proyectos CICYT fondos FEDER TEC2010-17805.

AGRADECIMIENTOS

Por fin ha llegado el momento después de muchos días de trabajo, esfuerzo y dedicación. Son muchos los experimentos realizados, las horas sin dormir, el buscar explicaciones a los resultados obtenidos. Ahora comienza una nueva etapa de mi vida que afronto con muchas ganas e ilusión.

Esta tesis está dedicada a muchas personas que me conocen, me quieren, me valoran y me aprecian. En primer lugar, quiero recordar a dos personas que ya no están entre nosotros y que son muy especiales para mí. A mi madre Teresa, gracias por todo el cariño que me has dado mamá, por enseñarme a convivir con una enfermedad, por hacerme ver que no hay retos imposibles y por estar siempre presente aunque ausente en todos los momentos de mi vida en los que he tomado decisiones importantes. También quiero recordar a la abuelita Mercedes, una segunda madre para mí. Gracias abuelita por todas las muestras de cariño que siempre me dabas y que para mí eran un estímulo para seguir trabajando. Gracias por contarme tus historias de vida, con las que tanto aprendía y disfrutaba, que me servían para desconectar del laboratorio.

A mi padre Manuel, un luchador nato de los pies a la cabeza. Gracias papá por enseñarme a ser un trapero del tiempo, por creer en mí, por apoyarme en los momento más difíciles de mi vida en los que no veía el final del túnel y por hacerme ver que los sueños siempre se pueden cumplir. Y ahora quiero recordar a mi mujer, María, por estar siempre conmigo, por todos sus consejos, por escucharme cuando tenía que desahogarme, por decirme alegra esa cara cuando las cosas no salían como se esperaban o por decirme que soy un químico fantástico. Ya sabes que a esto llegamos los dos juntos, siempre juntos, como diría la abuelita.

Ahora me gustaría mencionar a mis directores de tesis. De manera especial, quiero hablar en un primer momento de Javier Goicoechea, una gran persona en todos los sentidos, tanto humanamente como científicamente. Gracias Javi por introducirme en la Universidad Pública de Navarra, por darme la oportunidad de trabajar en el laboratorio de sensores, por animarme a hacer la tesis y por haberme enseñado a pensar desde un punto de vista ingenieril, buscando la aplicación de los resultados. Gracias por saber aconsejarme en todo momento, por darme ideas cuando las cosas no salían bien. Pero no sólo por esto, gracias por ser un gran amigo. Siempre tendrás todo mi aprecio.

Asimismo, también quiero agradecer a Nacho Matías y Patxi Arregui todo el apoyo que me han brindado durante estos años. Gracias Nacho por poner todos los medios para que esta aventura llegase a su fin. Y a ti, Patxi, por todos

los consejos y sugerencias a lo largo de estos años en los que tanto he aprendido y que me han hecho madurar como persona e investigador.

Ahora quiero recordar a mis compañeros de fatigas, mis amigos del laboratorio UPNA SENSORS. A los que ya son doctores, Carlos, César y Miguel, quienes son un ejemplo a seguir. A los que están haciendo el doctorado, Aitor, Abián y Pedro S., a los cuales les llegará este momento, así que mucho ánimo y para adelante. A todos los proyectandos y a Paula, por su gran ayuda. A mis buenos amigos de Nadetech Innovations SL., Edu, Edorta y Juanmari, que siempre me han escuchado.

También me gustaría agradecer a los miembros del Departamento de Ingeniería de Materiales, en especial a los doctores Javier, Carlos e Iñaki, por confiar en mí y darme la oportunidad de hacer horas de docencia. Ya sabéis que ha sido una experiencia única e inolvidable.

A los miembros de la Dublin City University (DCU), por acogerme con tanto cariño durante mi estancia en Irlanda. Gracias a la catedrática Colette McDonagh y a los doctores, Paul, Gemma, Barbara y Dorota Wencel, por ayudarme en todo momento. Gracias Dorota por hacerme pensar de una manera más crítica y selectiva.

Son muchas las personas de las que uno se acuerda cuando se escriben estas líneas. Pero no me quiero olvidar de dos grandes amigos que me han ayudado mucho cuando estaba haciendo la carrera de Química. La primera de ellas, eres tú, Chema. Muchas gracias por el apoyo que me diste, por preocuparte de mí y animarme en todo momento. También aprovecho para agradecer el cariño que recibí de tu familia. Y en segundo lugar, me quiero acordar de mi gran amigo Felipe, un hermano para mí, al que siempre estaré agradecido. De sus padres y hermanos, por acogerme con tanto cariño en su casa de Peralta. Gracias por todos los momentos que compartí con vosotros y por hacerme sentir importante cuando más lo necesitaba.

Como buen gallego no me puedo olvidar de mi tierra gallega, de mi Ferrol querido, de mis amigos de siempre. Gracias por esos momentos de diversión y por esos veranos inolvidables. Tampoco me quiero olvidar de mi cuadrilla de Pamplona y, como no, de mis compañeros de piso. Muchas gracias Nacho por ser como eres, el mejor compañero que uno puede tener. De mis compañeros de carrera, por recordar todos esos momentos que aún parecen recientes.

Y para concluir, me quiero acordar de mi tía Julia, mi abuela Gabriela, mi abuelo Pedro (un gran hombre), mi tía Carmiña y demás familiares. Asimismo, no me quiero olvidar de mi nueva familia, Mercedes, una santa, y Alejandro. Muchas gracias por cuidarme y quererme.

RESUMEN

Esta tesis se centra en la síntesis de nanopartículas de plata (AgNPs) y su posterior incorporación en recubrimientos delgados usando dos métodos alternativos: el proceso de síntesis *in situ* (ISS) de AgNPs y la técnica de embebido capa a capa (LbL-E) de AgNPs. Un preciso control de varios parámetros tales como la forma, tamaño, estado de agregación o la distribución de las nanopartículas de plata en los recubrimientos tiene una gran influencia en la posición final de la longitud de onda de la resonancia localizada de plasmones superficiales (LSPR). Además, estas películas que incorporan nanopartículas de plata han sido estudiadas para dos aplicaciones diferentes. La primera aplicación es la fabricación de recubrimientos antibacterianos eficientes. La segunda aplicación es la fabricación de un nuevo tipo de sensores de fibra óptica basados en la incorporación de nanopartículas de plata en películas nanoestructuradas, que hace posible obtener y observar dos resonancias ópticas diferentes, (LSPR) y resonancias de modos con pérdidas (LMR), en un mismo dispositivo.

ABSTRACT

This thesis is focused on the synthesis of silver nanoparticles (AgNPs) and their further incorporation into thin films using two alternative methods, the *In Situ* Synthesis (ISS) process and the Layer-by-Layer Embedding (LbL-E) deposition technique. A precise control of several parameters such as the shape, size, aggregation state or distribution of the AgNPs into the films has a great influence in the wavelength position of the Localized Surface Plasmon Resonance (LSPR) of the AgNPs. With this aim, two deposition methods such as sol-gel process and Layer-by-Layer (LbL) assembly have been studied and applied in order to deposit different nanocoatings based on AgNPs onto glass slides and optical fibers. In addition, these thin films that incorporate AgNPs have been studied for two different applications. The first application is the fabrication of efficient antibacterial surfaces. The second application is the implementation of new optical fiber sensors based on the incorporation of these AgNPs in nanostructured films, making possible to obtain and display two optical resonances, (LSPR) and Lossy Mode Resonances (LMR), in the same device.

CONTENTS

CHAPTER 1. Introduction

1.1. Motivation and objectives

Nanotechnology is an area of the science devoted to the manipulation of atoms and molecules. This discipline leads to the fabrication of structures in the nanometric scale [1, 2]. The ability of controlling the structure of matter at this atomic or molecular level makes possible the fabrication of devices or systems with new and unique properties as a result of their small size. Within the field of nanotechnology, noble metal nanoparticles (silver, gold, palladium, platinum) [3-5] are one of the most promising candidates for technological applications in fields as diverse as biology [6], catalysis [7], electronics [8], medicine [9] or optics [10]. These nanoparticles exhibit remarkable features such as their highly tunable optical properties and their high surface to volume ratios [11, 12]. For example, palladium or platinum nanoparticles are used as catalysts in a wide number of chemical reactions and, in these cases, the shape of the nanoparticles has a great influence in the catalytic activity [13, 14]. Gold and silver nanoparticles are very widely used in biomedical applications such as biomolecular detection or medical diagnostics [15], creating biosensing platforms with a high sensitivity for molecular recognition in the early-stage of the disease. Concretely, gold-nanoprobes are based on the functionalization of gold nanoparticles (AuNPs) with oligonucleotides or antibodies for recognition of specific DNA sequences [16-18] or for the detection of protein cancer markers [19-21].

In addition, it has been demonstrated that noble metal nanoparticles have been used for signal enhancement in fluorescence assays when the fluorophores molecules are in the vicinity of noble metal nanostructures [22-24]. This enhancement is a result of the dramatic electric improvement in the dielectric surrounding medium at the noble metal surface when light excites the nanoparticle under certain conditions. This rise in the intensity of the electromagnetic field around the fluorophore leads to an increase in the emitted fluorescence. Potential applications include the improvement of the signal obtained from optical biochips which results in better limits of detection [25]. The shape of the noble metal nanoparticles has an important influence in the emitted fluorescence. For example, enhanced fluorescence emission by noble metal nanoparticles with a rod shape is more than 1 order of magnitude larger in comparison with the enhancement achieved by nanoparticles with spherical shape [26]. Noble metal nanoparticles are also used for Surface-Enhancement Raman Scattering (SERS) for the identification of analyte

molecules [27-29] and this enhancement is obtained through the excitation of electronic transitions in the analyte by using a laser source with an appropriate frequency. It has been also demonstrated that noble metal nanoparticles with unusual shapes (star), non-spherical (rod, prism, cube) or anisotropic shape show higher enhancement surface factors than spherical nanoparticles [3, 4, 30, 31]. According to these results, the control of the metal nanoparticles morphology is of vital importance for biosensing and plasmonic applications [32-34]. In addition, metal nanoparticles show a strong absorption band in the visible, known as Localized Surface Plasmon Resonance (LSPR), which occurs when conduction electrons in metal nanostructures oscillate, as a result of their interaction with the incident electromagnetic radiation. The wavelength position of the LSPR absorption band displays a high dependence on the shape and size of the nanoparticles, and also with the refractive index of their surrounding medium [35]. This makes metallic nanoparticles good candidates for optical sensing applications.

Furthermore, among all metallic materials, silver is of particular interest because it is a powerful antibacterial agent, showing antimicrobial efficacy against bacteria, viruses and microorganisms [36-39]. This excellent antibacterial activity makes possible the use of silver nanoparticles in food preservation [40], safe cosmetics [41], medical devices [42, 43], textile fabrics [44] or water treatment [45]. In addition, silver shows a low toxicity to human cells, broad spectrum biocide effect, biocompatibility, high thermal stability and low volatility [46]. These antibacterial properties related to the AgNPs are of great interest in optical fiber sensors [47-49]. The presence of AgNPs in the sensitive coatings of optical fiber sensors contributes to enhance the lifetime of the devices submitted to high Relative Humidity (RH) environments. In such RH conditions, the biocide behavior of AgNPs prevents the adverse bacteria growth which could damage the sensitive coating [50-52].

Regarding to synthetic methods, metal nanoparticles can be synthesized from solid, liquid or gaseous state, using two approaches known as “top-down” and “bottom-up” [53]. The top-down approach uses physical (evaporation, laser ablation, arc discharge) and lithographic methods to pattern nanoscale structures, starting from a bulk material. The bottom-up approach uses interactions between molecules or colloidal particles to assemble nanoscale structures. Most of these deposition methods related to both approaches require specific experimental conditions (plasma, gas-phase, elevated temperature) to obtain thin films onto a substrate [54, 55]. However, solution-phase bottom-up synthetic methods are inexpensive, versatile and simple to implement, making possible the fabrication of nanoparticles as well as nanostructures of a wide range of materials [3, 4].

Although different chemical approaches to synthesize AgNPs have been reported [56-61], this thesis will focus on water-based wet synthesis routes of

stable and well-controlled morphology (shape and size) AgNPs [62], and their incorporation into thin films [63]. More specifically, two different processes as *In Situ* Synthesis (ISS) process and Layer-by-Layer Embedding (LbL-E) deposition technique are studied. Remarkable differences between both processes are observed in terms of the location of the LSPR absorption bands as well as the shape and size of the synthesized AgNPs. In addition, this work will also analyze in detail the incorporation of the AgNPs into the coatings, preserving their aggregation as well as maintaining the initial shape and size [63]. The use of adequate encapsulating and reducing agents will be one of the keys for the synthesis and a further incorporation into the films. This work will use two deposition techniques, sol-gel method and Layer-by-Layer (LbL) assembly, for the fabrication of thin films because of their simplicity, flexibility, versatility and the possibility of assembling inorganic nanoparticles and organic materials for the synthesis of hybrid nanostructures [64-67].

Finally, once AgNPs have been successfully synthesized and incorporated into thin films, the features of such AgNPs loaded coatings will be analyzed in two different applications. Firstly, the implementation of highly efficient and low-cost antibacterial surfaces against bacteria growth is shown due to the biocide effect of the AgNPs. And secondly, in the field of optical fiber sensors [68] for measuring relative humidity changes, the use of nanostructured thin films makes possible the generation of optical effects which cannot be appreciable with the utilization of thicker coatings. One of these optical effects is known as Lossy Mode Resonance (LMR) [69], enabling the fabrication of optical fiber sensors with tunable spectral response. Furthermore, the presence of the AgNPs in the nanostructured sensitive coating makes possible the generation of two optical resonances (LSPR and LMR) in a same spectral range [47]. This dual reference makes possible to obtain more accurate measurements because it is possible to monitor both LSPR and LMR as a function of Relative Humidity changes (RH), observing notable differences in their sensitivity.

1.2. Organization

First of all, a method for the in situ synthesis (ISS) process of metallic silver nanoparticles (AgNPs) into thin films is presented in Chapter 2, using two different deposition techniques, the sol-gel process and the Layer-by-Layer (LbL) assembly, techniques which have been specifically explained in Appendixes 1 and 2. In this ISS method, firstly, a thin film is obtained using sol-gel process or LbL assembly, and secondly, the in situ synthesis of the silver nanoparticles is performed into these thin films. The ISS of AgNPs is based on chemical reactions in solution (often termed wet chemistry) that yields loading metal ions (Ag^{+}) and a further reduction from metal ions to silver nanoparticles (Ag^{0}) [50, 51]. Several parameters have been evaluated, such as the use of an adequate weak polyelectrolyte poly(acrylic acid, sodium salt) (PAA), a specific pH value, thickness or effect of the temperature.

The first part of Chapter 3 is devoted to the synthesis of multicolored silver nanoparticles, as a function of the fine control of two parameters: the protective and reducing agents concentration, making possible the synthesis of AgNPs with different shapes [62]. The second part of this chapter is focused on the incorporation of these colored AgNPs into thin films using the LbL assembly [63]. The successive incorporation of AgNPs using the LbL assembly will be named Layer-by-Layer Embedding (LbL-E) deposition technique. A study of the color formation in the resultant LbL-E films will be investigated as a function of the thickness and the pH of the dipping polyelectrolyte solutions.

In chapter 4, the possibility of combining organic polymeric chains with inorganic materials (AgNPs) opens the door to the design of hybrid materials with a high functionality. These thin films based on the incorporation of AgNPs have been studied as antibacterial surfaces. It is well known that silver is considered a very good antibacterial agent, showing a broad spectrum biocide effect. Consequently, this chapter deals with the development of efficient antibacterial surfaces [51].

Finally, the fabrication of optical fiber humidity sensors based on Localized Surface Plasmon Resonance (LSPR) [47], Lossy mode resonance (LMR) [48] and both optical phenomena (LSPR and LMR) [49] will be presented in Chapter 5. The apparition of the optical resonances will be evaluated as a function of the resultant thickness, when a waveguide is coated with a sensitive coating using the ISS process or the LbL-E deposition technique. The differences in their sensitivities to Relative Humidity (RH) changes will be also analyzed.

A graphical summary about the organization of this thesis is plotted in Figure 1.1.

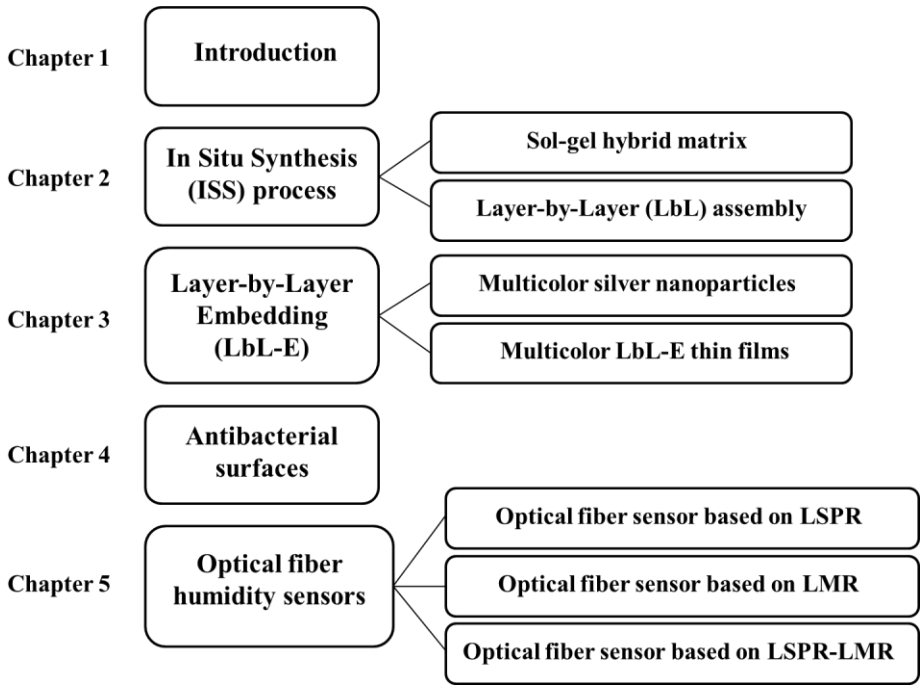

Figure 1.1. A schematic representation of the chapters of this work.

Bibliography

[1] Moghimi, S. M.; Hunter, A. C.; Murray, J. C. Nanomedicine: Current Status and Future Prospects. FASEB Journal 2005, 19, 311-330.
[2] Roco, M. C. Nanotechnology: Convergence with Modern Biology and Medicine. Curr. Opin. Biotechnol. 2003, 14, 337-346.
[3] Sau, T. K.; Rogach, A. L. Nonspherical Noble Metal Nanoparticles: Colloid-Chemical Synthesis and Morphology Control. Adv Mater 2010, 22, 1781-1804.
[4] Sau, T. K.; Rogach, A. L.; Jäckel, F.; Klar, T. A.; Feldmann, J. Properties and Applications of Colloidal Nonspherical Noble Metal Nanoparticles. Adv Mater 2010, 22, 1805-1825.
[5] Grzelczak, M.; Vermant, J.; Furst, E. M.; Liz-Marzán, L. M. Directed Self-Assembly of Nanoparticles. ACS Nano 2010, 4, 3591-3605.
[6] Daniel, M. -.; Astruc, D. Gold Nanoparticles: Assembly, Supramolecular Chemistry, Quantum-Size-Related Properties, and Applications Toward Biology, Catalysis, and Nanotechnology. Chem. Rev. 2004, 104, 293-346.
[7] Kidambi, S.; Dai, J.; Li, J.; Bruening, M. L. Selective Hydrogenation by Pd Nanoparticles Embedded in Polyelectrolyte Multilayers. J. Am. Chem. Soc. 2004, 126, 2658-2659.
[8] Xi, Q.; Chen, X.; Evans, D. G.; Yang, W. Gold Nanoparticle-Embedded Porous Graphene Thin Films Fabricated Via Layer-by-Layer Self-Assembly and Subsequent Thermal Annealing for Electrochemical Sensing. Langmuir 2012, 28, 9885-9892.
[9] Dreaden, E. C.; Alkilany, A. M.; Huang, X.; Murphy, C. J.; El-Sayed, M. A. The Golden Age: Gold Nanoparticles for Biomedicine. Chem. Soc. Rev. 2012, 41, 2740-2779.
[10] Anker, J. N.; Hall, W. P.; Lyandres, O.; Shah, N. C.; Zhao, J.; Van Duyne, R. P. Biosensing with Plasmonic Nanosensors. Nature Materials 2008, 7, 442-453.
[11] Doria, G.; Conde, J.; Veigas, B.; Giestas, L.; Almeida, C.; Assunção, M.; Rosa, J.; Baptista, P. V. Noble Metal Nanoparticles for Biosensing Applications. Sensors 2012, 12, 1657-1687.
[12] Larguinho, M.; Baptista, P. V. Gold and Silver Nanoparticles for Clinical Diagnostics - from Genomics to Proteomics. Journal of Proteomics 2012, 75, 2811-2823.
[13] Haruta, M. Size- and Support-Dependency in the Catalysis of Gold. Catalysis Today 1997, 36, 153-166.
[14] Haruta, M.; Daté, M. Advances in the Catalysis of Au Nanoparticles. Applied Catalysis A: General 2001, 222, 427-437.
[15] Cheng, M. M. -.; Cuda, G.; Bunimovich, Y. L.; Gaspari, M.; Heath, J. R.; Hill, H. D.; Mirkin, C. A.; Nijdam, A. J.; Terracciano, R.; Thundat, T.; Ferrari, M. Nanotechnologies for Biomolecular Detection and Medical Diagnostics. Curr. Opin. Chem. Biol. 2006, 10, 11-19.
[16] Elghanian, R.; Storhoff, J. J.; Mucic, R. C.; Letsinger, R. L.; Mirkin, C. A. Selective Colorimetric Detection of Polynucleotides Based on the Distance-Dependent Optical Properties of Gold Nanoparticles. Science 1997, 277, 1078-1081.
[17] Storhoff, J. J.; Elghanian, R.; Mucic, R. C.; Mirkin, C. A.; Letsinger, R. L. One-Pot Colorimetric Differentiation of Polynucleotides with Single Base Imperfections using Gold Nanoparticle Probes. J. Am. Chem. Soc. 1998, 120, 1959-1964.
[18] Thaxton, C. S.; Georganopoulou, D. G.; Mirkin, C. A. Gold Nanoparticle Probes for the Detection of Nucleic Acid Targets. Clinica Chimica Acta 2006, 363, 120-126.
[19] Byrne, J. D.; Betancourt, T.; Brannon-Peppas, L. Active Targeting Schemes for Nanoparticle Systems in Cancer Therapeutics. Adv. Drug Deliv. Rev. 2008, 60, 1615-1626.
[20] Kim, D.; Daniel, W. L.; Mirkin, C. A. Microarray-Based Multiplexed Scanometric Immunoassay for Protein Cancer Markers using Gold Nanoparticle Probes. Anal. Chem. 2009, 81, 9183-9187.
[21] Liu, X.; Dai, Q.; Austin, L.; Coutts, J.; Knowles, G.; Zou, J.; Chen, H.; Huo, Q. A One-Step Homogeneous Immunoassay for Cancer Biomarker Detection using Gold Nanoparticle Probes Coupled with Dynamic Light Scattering. J. Am. Chem. Soc. 2008, 130, 2780-2782.
[22] Lee, K. -.; El-Sayed, M. A. Gold and Silver Nanoparticles in Sensing and Imaging: Sensitivity of Plasmon Response to Size, Shape, and Metal Composition. J Phys Chem B 2006, 110, 19220-19225.

[23] Cheng, Y.; Stakenborg, T.; Van Dorpe, P.; Lagae, L.; Wang, M.; Chen, H.; Borghs, G. Fluorescence Near Gold Nanoparticles for DNA Sensing. Anal. Chem. 2011, 83, 1307-1314.
[24] Matveeva, E. G.; Gryczynski, I.; Barnett, A.; Leonenko, Z.; Lakowicz, J. R.; Gryczynski, Z. Metal Particle-Enhanced Fluorescent Immunoassays on Metal Mirrors. Anal. Biochem. 2007, 363, 239-245.
[25] Stranik, O.; Nooney, R.; McDonagh, C.; MacCraith, B. D. Optimization of Nanoparticle Size for Plasmonic Enhancement of Fluorescence. Plasmonics 2007, 2, 15-22.
[26] Varnavski, O. P.; Mohamed, M. B.; El-Sayed, M. A.; Goodson III, T. Relative Enhancement of Ultrafast Emission in Gold Nanorods. J Phys Chem B 2003, 107, 3101-3104.
[27] Keating, C. D.; Kovaleski, K. M.; Natan, M. J. Protein: Colloid Conjugates for Surface Enhanced Raman Scattering: Stability and Control of Protein Orientation. J Phys Chem B 1998, 102, 9404-9413.
[28] Smith, W. E. Practical Understanding and use of Surface Enhanced Raman scattering/surface Enhanced Resonance Raman Scattering in Chemical and Biological Analysis. Chem. Soc. Rev. 2008, 37, 955-964.
[29] Yang, M.; Chen, T.; Lau, W. S.; Wang, Y.; Tang, Q.; Yang, Y.; Chen, H. Development of Polymer-Encapsulated Metal Nanoparticles as Surface-Enhanced Raman Scattering Probes. Small 2009, 5, 198-202.
[30] Jana, N. R.; Pal, T. Anisotropic Metal Nanoparticles for use as Surface-Enhanced Raman Substrates. Adv Mater 2007, 19, 1761-1765.
[31] Rodríguez-Lorenzo, L.; Álvarez-Puebla, R. A.; De Abajo, F. J. G.; Liz-Marzán, L. M. Surface Enhanced Raman Scattering using Star-Shaped Gold Colloidal Nanoparticles. Journal of Physical Chemistry C 2010, 114, 7336-7340.
[32] Rycenga, M.; Cobley, C. M.; Zeng, J.; Li, W.; Moran, C. H.; Zhang, Q.; Qin, D.; Xia, Y. Controlling the Synthesis and Assembly of Silver Nanostructures for Plasmonic Applications. Chem. Rev. 2011, 111, 3669-3712.
[33] Angelomé, P. C.; Mezerji, H. H.; Goris, B.; Pastoriza-Santos, I.; Pérez-Juste, J.; Bals, S.; Liz-Marzán, L. M. Seedless Synthesis of Single Crystalline Au Nanoparticles with Unusual Shapes and Tunable LSPR in the Near-IR. Chemistry of Materials 2012, 24, 1393-1399.
[34] Anker, J. N.; Hall, W. P.; Lyandres, O.; Shah, N. C.; Zhao, J.; Van Duyne, R. P. Biosensing with Plasmonic Nanosensors. Nature Materials 2008, 7, 442-453.
[35] Liz-Marzán, L. M. Nanometals: Formation and Color. Materials Today 2004, 7, 26-31.
[36] Morones, J. R.; Elechiguerra, J. L.; Camacho, A.; Holt, K.; Kouri, J. B.; Ramírez, J. T.; Yacaman, M. J. The Bactericidal Effect of Silver Nanoparticles. Nanotechnology 2005, 16, 2346-2353.
[37] Panácek, A.; Kvítek, L.; Prucek, R.; Kolár, M.; Vecerová, R.; Pizúrová, N.; Sharma, V. K.; Nevecná, T.; Zboril, R. Silver Colloid Nanoparticles: Synthesis, Characterization, and their Antibacterial Activity. J Phys Chem B 2006, 110, 16248-16253.
[38] Moritz, M.; Geszke-Moritz, M. The Newest Achievements in Synthesis, Immobilization and Practical Applications of Antibacterial Nanoparticles. Chem. Eng. J. 2013, 228, 596-613.
[39] Sondi, I.; Salopek-Sondi, B. Silver Nanoparticles as Antimicrobial Agent: A Case Study on E. Coli as a Model for Gram-Negative Bacteria. J. Colloid Interface Sci. 2004, 275, 177-182.
[40] Mohammed Fayaz, A.; Balaji, K.; Girilal, M.; Kalaichelvan, P. T.; Venkatesan, R. Mycobased Synthesis of Silver Nanoparticles and their Incorporation into Sodium Alginate Films for Vegetable and Fruit Preservation. J. Agric. Food Chem. 2009, 57, 6246-6252.
[41] Jain, J.; Arora, S.; Rajwade, J. M.; Omray, P.; Khandelwal, S.; Paknikar, K. M. Silver Nanoparticles in Therapeutics: Development of an Antimicrobial Gel Formulation for Topical use. Molecular Pharmaceutics 2009, 6, 1388-1401.
[42] Chaloupka, K.; Malam, Y.; Seifalian, A. M. Nanosilver as a New Generation of Nanoproduct in Biomedical Applications. Trends Biotechnol. 2010, 28, 580-588.
[43] Furno, F.; Morley, K. S.; Wong, B.; Sharp, B. L.; Arnold, P. L.; Howdle, S. M.; Bayston, R.; Brown, P. D.; Winship, P. D.; Reid, H. J. Silver Nanoparticles and Polymeric Medical Devices: A New Approach to Prevention of Infection? J. Antimicrob. Chemother. 2004, 54, 1019-1024.
[44] Lee, H. J.; Yeo, S. Y.; Jeong, S. H. Antibacterial Effect of Nanosized Silver Colloidal Solution on Textile Fabrics. J. Mater. Sci. 2003, 38, 2199-2204.

[45] Li, Q.; Mahendra, S.; Lyon, D. Y.; Brunet, L.; Liga, M. V.; Li, D.; Alvarez, P. J. J. Antimicrobial Nanomaterials for Water Disinfection and Microbial Control: Potential Applications and Implications. Water Res. 2008, 42, 4591-4602.
[46] Sharma, V. K.; Yngard, R. A.; Lin, Y. Silver Nanoparticles: Green Synthesis and their Antimicrobial Activities. Adv. Colloid Interface Sci. 2009, 145, 83-96.
[47] Rivero, P. J.; Urrutia, A.; Goicoechea, J.; Arregui, F. J.; Matías, I. R. Humidity Sensor Based on Silver Nanoparticles Embedded in a Polymeric Coating. International Journal on Smart Sensing and Intelligent Systems 2012, 5, 71-83.
[48] Rivero, P. J.; Urrutia, A.; Goicoechea, J.; Matias, I. R.; Arregui, F. J. A Lossy Mode Resonance Optical Sensor using Silver Nanoparticles-Loaded Films for Monitoring Human Breathing. Sensors and Actuators, B: Chemical 2013, 187, 40-44.
[49] Rivero, P. J.; Urrutia, A.; Goicoechea, J.; Arregui, F. J. Optical Fiber Humidity Sensors Based on Localized Surface Plasmon Resonance (LSPR) and Lossy-Mode Resonance (LMR) in Overlays Loaded with Silver Nanoparticles. Sensors and Actuators, B: Chemical 2012, 173, 244-249.
[50] Rivero, P. J.; Urrutia, A.; Goicoechea, J.; Rodríguez, Y.; Corres, J. M.; Arregui, F. J.; Matías, I. R. An Antibacterial Submicron Fiber Mat with in Situ Synthesized Silver Nanoparticles. J Appl Polym Sci 2012, 126, 1228-1235.
[51] Rivero, P. J.; Urrutia, A.; Goicoechea, J.; Zamarreño, C. R.; Arregui, F. J.; Matías, I. R. An Antibacterial Coating Based on a polymer/sol- Gel Hybrid Matrix Loaded with Silver Nanoparticles. Nanoscale Research Letters 2011, 6, X1-7.
[52] Urrutia, A.; Rivero, P. J.; Ruete, L.; Goicoechea, J.; Matías, I. R.; Arregui, F. J. Single-Stage in Situ Synthesis of Silver Nanoparticles in Antibacterial Self-Assembled Overlays. Colloid Polym. Sci. 2012, 290, 785-792.
[53] Gates, B. D.; Xu, Q.; Stewart, M.; Ryan, D.; Willson, C. G.; Whitesides, G. M. New Approaches to Nanofabrication: Molding, Printing, and Other Techniques. Chem. Rev. 2005, 105, 1171-1196.
[54] Kamiya, S.; Takahashi, H.; Saka, M.; Abé, H. Evaluation and Improvement of the Adhesive Fracture Toughness of CVD Diamond on Silicon Substrate. J Electron Packag, Trans ASME 2002, 124, 271-276.
[55] Shin, D. O.; Lee, D. H.; Moon, H. -.; Jeong, S. -.; Kim, J. Y.; Mun, J. H.; Cho, H.; Park, S.; Kim, S. O. Sub-Nanometer Level Size Tuning of a Monodisperse Nanoparticle Array Via Block Copolymer Lithography. Advanced Functional Materials 2011, 21, 250-254.
[56] Pastorizo-Santos, I.; Liz-Marzán, L. M. N,N-Dimethylformamide as a Reaction Medium for Metal Nanoparticle Synthesis. Advanced Functional Materials 2009, 19, 679-688.
[57] Evanoff Jr., D. D.; Chumanov, G. Size-Controlled Synthesis of Nanoparticles. 1. "Silver-Only" Aqueous Suspensions Via Hydrogen Reduction. J Phys Chem B 2004, 108, 13948-13956.
[58] Wang, H.; Qiao, X.; Chen, J.; Wang, X.; Ding, S. Mechanisms of PVP in the Preparation of Silver Nanoparticles. Mater. Chem. Phys. 2005, 94, 449-453.
[59] Martinez-Castanon, G. A.; Niño-Martínez, N.; Martínez-Gutierrez, F.; Martínez-Mendoza, J. R.; Ruiz, F. Synthesis and Antibacterial Activity of Silver Nanoparticles with Different Sizes. Journal of Nanoparticle Research 2008, 10, 1343-1348.
[60] Pillai, Z. S.; Kamat, P. V. What Factors Control the Size and Shape of Silver Nanoparticles in the Citrate Ion Reduction Method? J Phys Chem B 2004, 108, 945-951.
[61] Kan, C. -.; Zhu, J. -.; Zhu, X. -. Silver Nanostructures with Well-Controlled Shapes: Synthesis, Characterization and Growth Mechanisms. J. Phys. D 2008, 41.
[62] Rivero, P. J.; Goicoechea, J.; Urrutia, A.; Arregui, F. J. Effect of both Protective and Reducing Agents in the Synthesis of Multicolor Silver Nanoparticles. Nanoscale Research Letters 2013, 8, 1-9.
[63] Rivero, P. J.; Goicoechea, J.; Urrutia, A.; Matias, I. R.; Arregui, F. J. Multicolor Layer-by-Layer Films using Weak Polyelectrolyte Assisted Synthesis of Silver Nanoparticles. Nanoscale Research Letters 2013, 8, 1-10.
[64] Wencel, D.; Barczak, M.; Borowski, P.; McDonagh, C. The Development and Characterisation of Novel Hybrid Sol-Gel-Derived Films for Optical pH Sensing. Journal of Materials Chemistry 2012, 22, 11720-11729.
[65] Estella, J.; Wencel, D.; Moore, J. P.; Sourdaine, M.; McDonagh, C. Fabrication and Performance Evaluation of Highly Sensitive Hybrid Sol-Gel-Derived Oxygen Sensor Films Based on a Fluorinated Precursor. Anal.Chim.Acta 2010, 666, 83-90.

[66] Berg, M. C.; Choi, J.; Hammond, P. T.; Rubner, M. F. Tailored Micropatterns through Weak Polyelectrolyte Stamping. Langmuir 2003, 19, 2231-2237.
[67] Yoo, D.; Shiratori, S. S.; Rubner, M. F. Controlling Bilayer Composition and Surface Wettability of Sequentially Adsorbed Multilayers of Weak Polyelectrolytes. Macromolecules 1998, 31, 4309-4318.
[68] Matias I. R.; Arregui F. J.; Claus R. O. Optical Fiber Sensors. New York (USA): American Scientific Publishers 2006.
[69] Del Villar, I.; Hernaez, M.; Zamarreno, C. R.; Sánchez, P.; Fernández-Valdivielso, C.; Arregui, F. J.; Matias, I. R. Design Rules for Lossy Mode Resonance Based Sensors. Appl. Opt. 2012, 51, 4298-4307.

CHAPTER 2. *In situ* synthesis of silver nanoparticles into thin films

In this chapter, a method for the in situ synthesis (ISS) of silver nanoparticles (AgNPs) into thin films is presented, using two different host matrices fabricated by the sol-gel process and the Layer-by-Layer (LbL) assembly. Several parameters such as thickness evolution, pH value, thermal treatment or morphology of the coatings have been evaluated. The great simplicity, repeatability and versatility of this method based on a metal-ion exchange and a further in situ chemical reduction of silver cations to obtain the silver nanoparticles makes possible the fabrication of organic-inorganic hybrid coatings, opening up new opportunities to obtain thin films with a high functionality.

2.1. Introduction

One of the main factors that have helped to the explosion of the nanotechnology in the last years is the existence of several deposition methods on the nanometric scale. There are two approaches, known as top-down and bottom-up, which are used to fabricate nanotechnology products. The first one consists of starting with a bulk material and then breaks it into smaller pieces using mechanical, chemical or other form of energy (top-down). The second one is based on the synthesis of the material from atomic or molecular species via chemical reactions and makes possible to grow in size (bottom-up). Both approaches are of great interest to obtain thin films with special properties [1-12]. Due to this, the development of nanoscale materials and their corresponding fabrication processes are so attractive in the scientific community because of their potential applications in many areas such as biology, biochemistry, medicine, chemistry, physics, electronics, photonics, sensing, among others [13-22].

It is important to remark that a higher number of deposition methods related to both approaches have been developed in the last decades. Most of these deposition techniques such as lithography, chemical vapor deposition (CVD), laser ablation, atomic layer deposition or molecular beam epitaxy require expensive equipment and specific experimental conditions (plasma, gas-phase, elevated temperature or high energy) in order to deposit the thin films on a desired substrate [23-26]. However, liquid phase methods are a good alternative to make nanomaterials because of their low cost and the possibility

of being upscalable. The focus of this chapter is the use of bottom-up fabrication processes based on liquid phase methods for the production of advanced nanomaterials. Of all them, sol-gel process and the Layer-by-Layer assembly are investigated for the fabrication of thin films [27-37]. The main advantages of both methods are their flexibility, simplicity and versatility.

In addition, the synthesis of metal nanoparticles [38, 39] to be incorporated into thin films has attracted the attention of the researches due to their unique properties and potential applications, range from antibacterial to optical applications. A precise control of the shape, size, agglomeration degree, composition and distribution of the nanoparticles are key parameters during the synthesis process. Generally, this control can be achieved by varying the synthesis method, reducing agent, protective agent or the pH of the reaction system. According to this, the sol-gel method and the Layer-by-Layer (LbL) assembly are some of the most suitable methods of synthesis that can be used to prepare metal nanoparticles (gold, silver, copper) with a great control of the nanoparticle size, size distribution, composition and cristallinity.

The optical properties of the metal nanostructures are very attractive because of the existence of a plasmon resonance band, known as Localized Surface Plasmon Resonance (LSPR), which occurs when conduction electrons in metal nanostructures collectively oscillate, as a result of their interaction with an incident electromagnetic radiation [40-43]. A specific wavelength position of the LSPR displays a high dependence on the resultant shape and size of the nanoparticles. Such nanoplasmonic properties of the metal nanostructures with a well-controlled shape and size of the nanoparticles by adjusting the synthesizing parameters are being investigated because of their unique or improved electronic, catalytic or optical properties [44-48].

In this chapter, a novel method is presented for the *in situ* synthesis (ISS) of silver nanoparticles (AgNPs) into thin films (host matrixes) which are previously obtained by the sol-gel process and the Layer-by-Layer (LbL) assembly. The *in situ* synthesis (ISS) of silver nanoparticles is based on chemical reactions in solution (often termed wet chemistry) that yields loading metal ions and a further synthesis of the metal nanoparticles. In the next section, a host matrix obtained by sol-gel process for the *in situ* synthesis of silver nanoparticles is presented. This sol-gel deposition technique has been selected by its simplicitiy, quite inexpensive approach and the possibility of obtaining organic-inorganic hybrid materials with a high functionality.

2.2. In situ synthesis (ISS) of the silver nanoparticles into a hybrid sol-gel matrix

In this Section, an organic/inorganic hybrid matrix has been developed by sol-gel process using the dip-coating technique. More details about sol-gel deposition technique, chemical reactions and experimental conditions can be found in Appendix 1.

An organic/inorganic hybrid matrix was prepared by mixing an aqueous polymeric solution of poly(acrylic acid, sodium salt) (PAA), tetraethyl ortosilicate (TEOS) and absolute ethanol (EtOH) under vigorous stirring at pH 8.0 [49]. The use of PAA in the sol-gel hybrid matrix is of great interest due to the presence of free carboxylic acid groups, known as nanoreactor host sites, which are available for a subsequent metal ion exchange for the introduction of inorganic ions such as silver. More specifically, the free acid groups are responsible for binding Ag-ions by metal-ion exchange with the proton [50].

The PAA polymeric solution was prepared using ultrapure water and its concentration was varied from 1 mM to 20 mM respect to the repetitive unit. The molar ratio in the initial precursor solution of TEOS:EtOH:PAA was 0.11:0.77:0.12 and was aged for one day at room temperature. Then, the substrates (glass slides) were immersed into the precursor solution for 15 seconds and lifted from the solution at a speed of 0.4 cm/s using a ND-DC dip-coater from Nadetech Innovations. In order to evaporate very gently the remaining solvents and to allow the consolidation of the films, the samples were stored at room temperature for 3 hours. As a result, high quality transparent films were obtained in this fabrication step. The next step is based on the *in situ* synthesis (ISS) of the silver nanoparticles (AgNPs) into the previous hybrid matrix obtained by sol-gel process.

The experimental process consists of the use of the hybrid matrix as a host for the *in situ* synthesis of the AgNPs. Firstly, silver ions were immobilized into the hybrid matrix by via ion exchange by simply immersing the coated samples into the silver nitrate ($AgNO_3$) solution (0.01 N). During this loading step, silver cations (Ag^+) formed electrostatic pairs with some of the carboxylate groups (COO^-) from PAA. This loading step was carried out for 5 minutes. Secondly, the silver ions loaded into the coatings were reduced by immersing the samples into dimethylamine borane complex (DMAB) solution (0.01 N) which acted as a reducing agent [49, 51-55]. In this step, the carboxylate-bonded Ag^+ ions were reduced to produce zero valent silver nanoparticles (Ag^0). This reducing step was carried out for 5 minutes. Between each loading and reduction step, samples were thoroughly rinsed in ultrapure water for 30 seconds. This Loading/Reduction (L/R) cycle can be repeated as

many times as desired to induce a growth of the silver nanoparticles into the films.

A schematic representation of this experimental process can be observed in Figure 2.1.

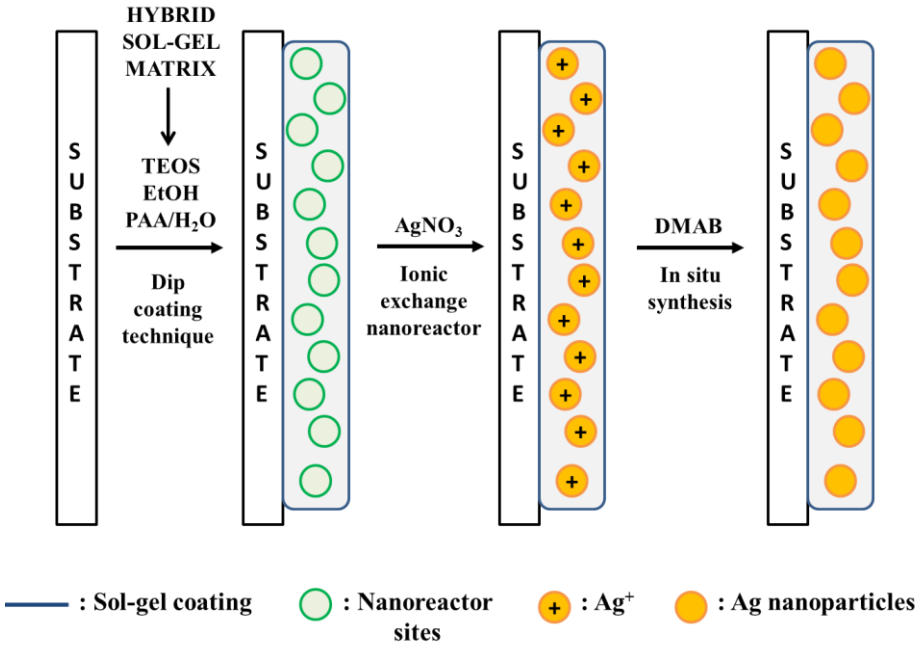

Figure 2.1. Schematic illustration of the metal ion exchange in the hybrid matrix obtained by sol-gel deposition technique and a further *in situ* synthesis (ISS) of the silver nanoparticles.

The visual aspect of the hybrid thin films remained unaltered after the silver ($AgNO_3$) loading immersion step (transparent), although the silver cations (Ag^+) were already present in the thin films. However, the films showed a coloration change from transparent to golden-yellowish after the DMAB reduction immersion step. Such alteration of the visible absorption spectrum of the samples is directly related with the Localized Surface Plasmon Resonance (LSPR) phenomenon [39, 40] typical of gold and silver nanoparticles.

In Figure 2.2, it is shown the aspect of the thin films once fabricated with the initial hybrid matrix (TEOS, PAA and ethanol) and after the *in situ* synthesis (ISS) of the silver nanoparticles (AgNPs) via metal ion exchange and a further chemical reduction. This chemical reduction process was performed for a total number of 4 Loading/Reduction (L/R) cycles for a PAA concentration of 20 mM.

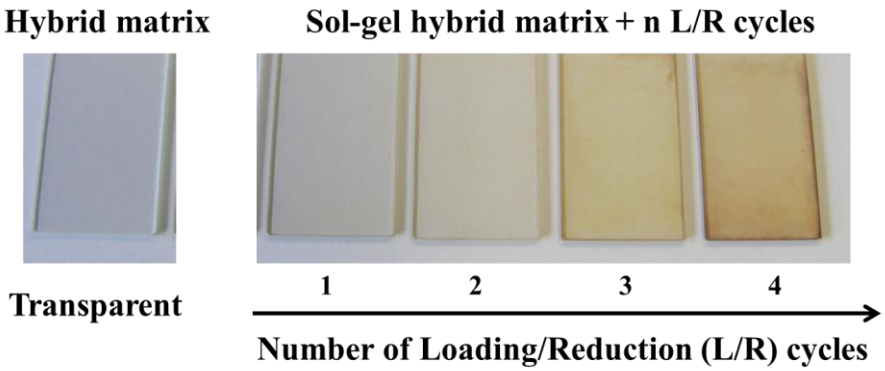

Figure 2.2. Aspect of the thin-films after the *in situ* synthesis (ISS) of the silver nanoparticles (AgNPs) into the sol-gel hybrid matrix (20 mM PAA) as a function of the number of L/R cycles (golden-yellowish color) in comparison with a film with only hybrid matrix (transparent).

In Figure 2.3, it is shown the UV-Vis spectra (20 mM PAA) of the thin films using this *in situ* synthesis (ISS) process as a function of the number of Loading/Reduction cycles. The existence of an absorption band at 410 nm with the resultant change coloration from transparent to yellow-orange is indicative that AgNPs have been successfully synthesized into the thin films.

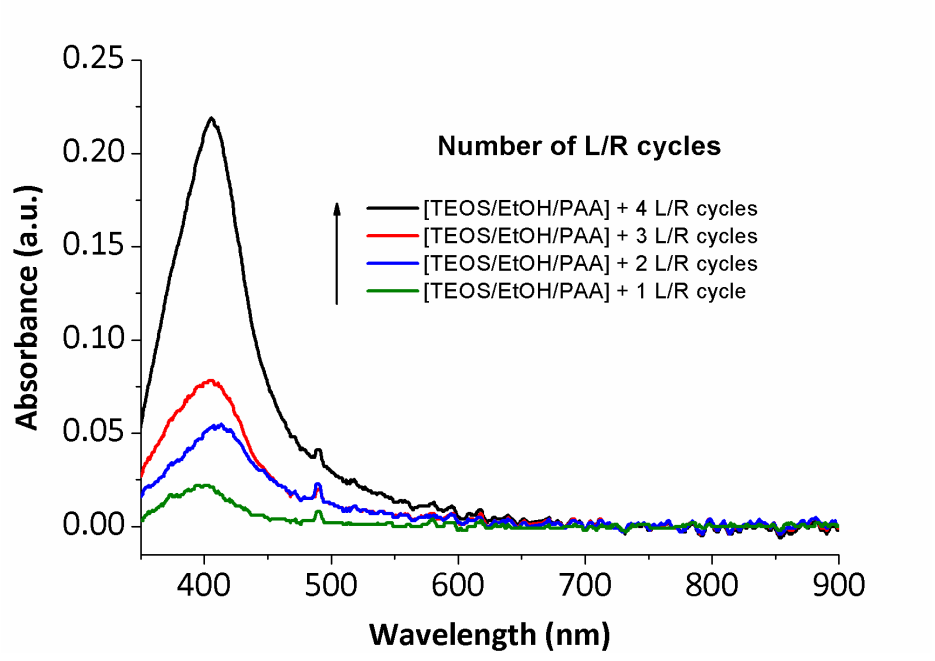

Figure 2.3. UV-Vis spectroscopy of the *in situ* synthesis (ISS) of the silver nanoparticles (AgNPs) into the hybrid sol-gel matrix for different number of Loading/Reduction cycles (1, 2, 3 and 4 L/R) and for a PAA concentration 20 mM.

As it was previously commented, such narrow absorption bands are due to the LSPR phenomenon of the silver nanoparticles synthesized inside the coating [56-58]. Furthermore, in order to get an additional evidence of the presence of silver within the hybrid coatings, an elemental analysis was obtained using the EDX technique (Figure 2.4). This EDX spectrum shows a peak at 3 keV that confirms the presence of silver within the coating. The rest of the lines of the EDX spectrum correspond to other elements which are present in the coating (mainly Si, O, and Na) and also present in the glass slide substrate. The EDX analysis together with the LSPR absorption band of the UV-VIS spectra make possible to confirm the reduction of silver ions (Ag^{+}) to silver nanoparticles (Ag^{0}) inside the organic/inorganic hybrid coating.

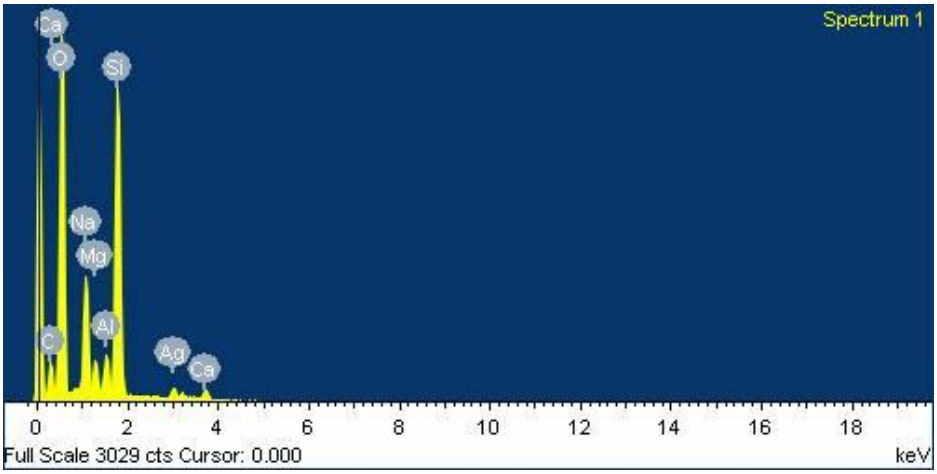

Figure 2.4. EDX analysis of the resultant hybrid coating after 4 L/R cycles with PAA molar concentration of 20 mM.

Another important consideration is the effect of the molar concentration of the PAA (1 mM or 20mM) in the initial hybrid matrix because it plays a key role in order to understand the further *in situ* synthesis (ISS) of the AgNPs into the thin films in comparison with a control coating based on only inorganic TEOS matrix without any PAA polyelectrolyte (no hybrid). In Figure 2.5, the evolution of the maxima absorption bands at LSPR wavelength position obtained by UV-Vis spectroscopy of three different coatings (control, hybrid PAA 1mM and hybrid PAA 20 mM) are shown. A growth in the intensity related to the LSPR bands can be observed when the number of L/R cycles is increased, although this effect is more notorious in the hybrid matrix with a higher PAA concentration (20 mM) in comparison with PAA 1 mM.

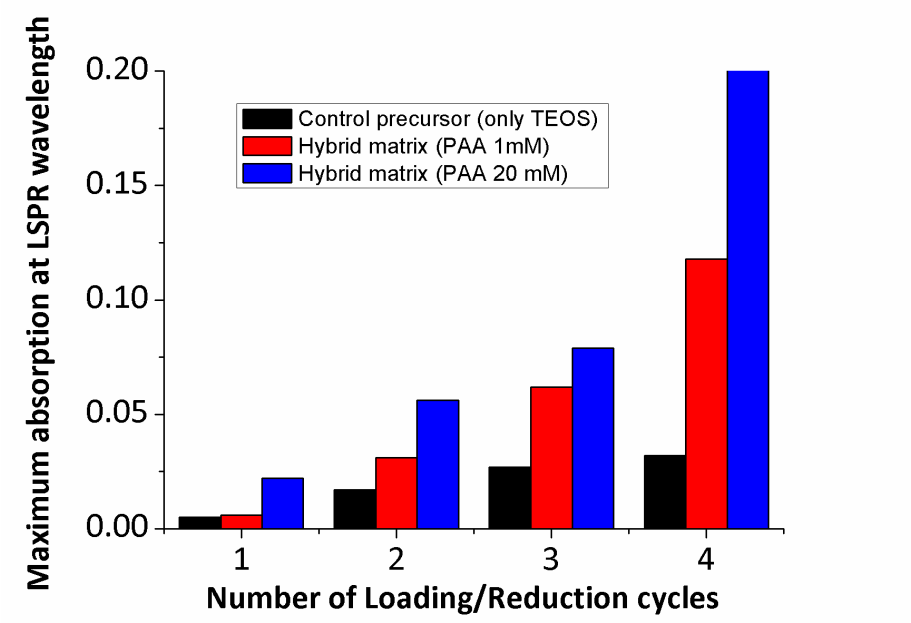

Figure 2.5. Evolution of LSPR absorption bands after the Loading/Reduction (L/R) cycles for a control (only TEOS) and variable PAA concentration (1 and 20 mM).

This result confirms the hypothesis that lower PAA concentration results in less nanoreactor host sites for the introduction of Ag^+ ions during the loading step, and the amount of synthesized AgNPs is significantly lower in the hybrid matrix. In addition, when this same Loading/Reduction (L/R) protocol was carried out in the control precursor (only TEOS) without any PAA polyelectrolyte, no significant LSPR absorption band was observed because there was not any nanoreactor host site available to incorporate the silver ions via ion exchange during the fabrication process. According to these results, a higher PAA concentration in the hybrid matrix makes possible to obtain a higher LSPR absorption band after the number of L/R cycles because there is an increase of nanoreactor host sites for synthesizing the AgNPs into the thin film. This result is corroborated by the increase of the color formation from transparent to golden-yellowish when both number of L/R cycles and PAA concentration are increased (see Figure 2.2).

Once it has been corroborated that a higher PAA concentration (20 mM) provides a higher number of nanoreactor host sites for the silver ions (Ag^+) during the loading immersion step by ion exchange which enables to obtain a higher amount of AgNPs during the reduction immersion step. Then, an important aspect is that there was not found any significant variation in the thickness evolution after the L/R cycles in comparison with the control coating (only TEOS and PAA), as it can be observed in Table 2.1.

Table 2.1. Average evolution thickness before and after Loading/Reduction (L/R) cycles.

Fabrication process	Thickness (nm)
[TEOS:EtOH:PAA/H_2O]	307.7 ± 6.1
[TEOS:EtOH:PAA/H_2O] + 4 L/R cycles	312.8 ± 7.2

A study of the influence of the temperature indicates that these hybrid thin films can be thermally treated at high temperature values due to the presence of the inorganic TEOS matrix. This high temperature is of great interest when it is necessary to improve the mechanical stability of the films [59] and a change from amorphous silver to crystalline silver is corroborated by X-ray diffraction (XRD) analysis (see Figure 2.12). The reflection peaks at 2θ values of 38.1º and 44.3º is indicative of the existence of crystal planes of the silver nanoparticles which corresponds to crystal phase of cubic silver.

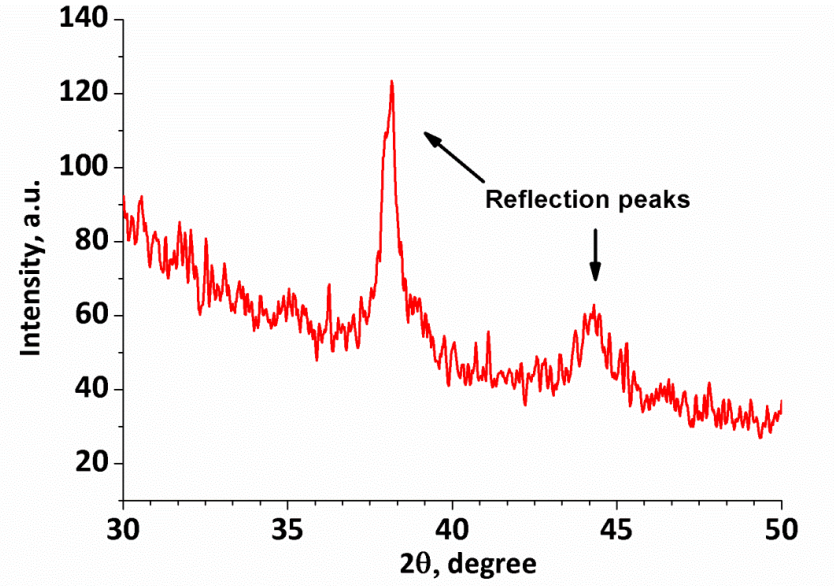

Figure 2.6. XRD of the hybrid matrix after thermal treatment of 450 ºC for 2 hours.

In Figure 2.7, it is possible to observe that the basic pH of the precursor solution gives macroporous aggregates (Fig. 2.7a) that can be assembled into thin films with the sol-gel dip coating technique [60, 61]. Then, once the *in situ* synthesis of the AgNPs has been performed, the porosity of the aggregates allows the ionic interchange with the external medium and at the same time,

no variation in the morphology and thickness of the hybrid films was observed (Fig. 2.7b). In addition, these films showed a sharp improvement of the mechanical strength in terms of manual scratching test after the thermal treatment. AFM analysis showed that there was no significant alteration in the morphology of the resultant films with a partial thickness reduction (Fig. 2.7c). This hybrid matrix shows an average roughness (Rq) of 29.8 nm (rms).

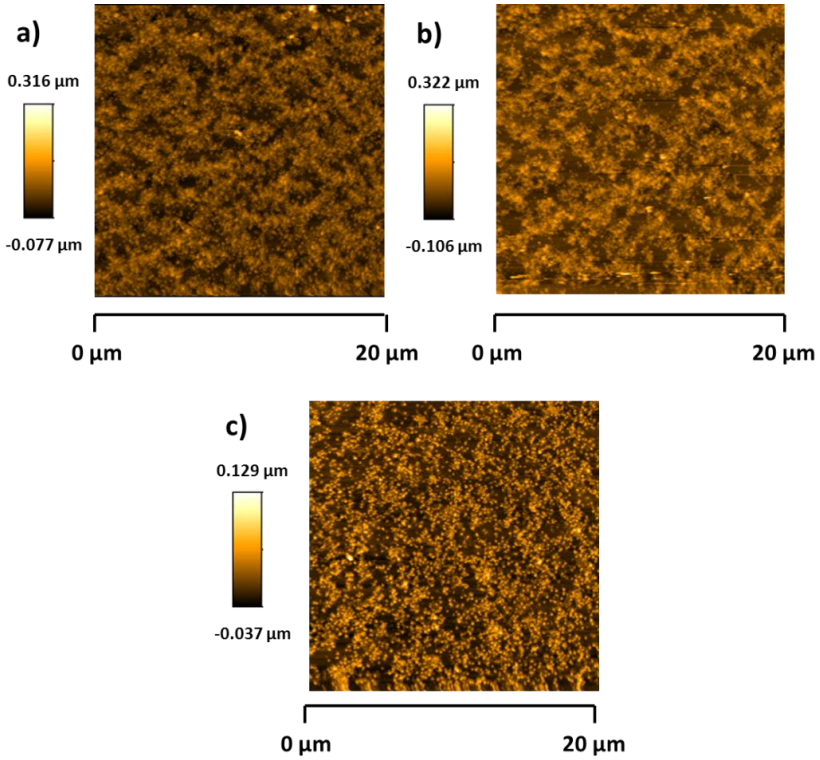

Figure 2.7. AFM images of the (a) hybrid coating (TEOS and PAA 20 mM); (b) hybrid coating after 4 L/R cycles and (c) hybrid coating after 4 L/R cycles and a thermal treatment of 450 ºC for 2 hours.

Finally, sol-gel process indicates that the amount of synthesized AgNPs is increased when PAA molar concentration is higher. However, problems of stability of the initial sol-gel host matrix are observed when PAA is increased and thin films with less transparency are obtained for higher PAA molar than 20 mM. Due to this, an alternative approach for the incorporation of a higher amount of AgNPs can be achieved using the LbL assembly as a host matrix. Polyelectrolytes exhibit a pH-dependent degree of dissociation that defines the amount of free carboxylic acid groups (nanoreactor host sites) which are responsible for binding Ag-ions by the metal-ion exchange mechanism.

2.3. In situ synthesis (ISS) of the silver nanoparticles into thin polymeric Layer-by-Layer (LbL) films

In order to obtain the *in situ* synthesis (ISS) of the silver nanoparticles (AgNPs) into the LbL films, the fabrication process has been performed in two steps. More details about the LbL assembly, experimental conditions and fabrication process can be found in Appendix 2.

Firstly, a polymeric coating has been fabricated using the LbL assembly by sequentially exposition the substrate to poly(allylamine hydrochloride) (PAH) as a polycation and poly(acrylic acid, sodium salt) (PAA) as a polyanion at a desired pH. This process has been repeated up to a total thickness of 40 bilayers. A bilayer is the combination of a cationic layer (PAH) and an anionic layer (PAA). Secondly, silver cations (Ag^{+}) have been immobilized into the previous polymeric matrix obtained by the LbL assembly via metal-ionic exchange when LbL films have been immersed into a silver nitrate solution ($AgNO_3$ 0.01 N). Afterwards, the silver loaded into the LbL polymeric coating has been reduced using dimethylamine borane complex solution (DMAB 0.01 N). This reducing agent (DMAB) makes possible the *in situ* synthesis (ISS) of the silver nanoparticles (Ag^{0}) into the LbL films [49, 51], as it was previously commented in Section 2.2. A schematic representation of this experimental process is shown in Figure 2.8.

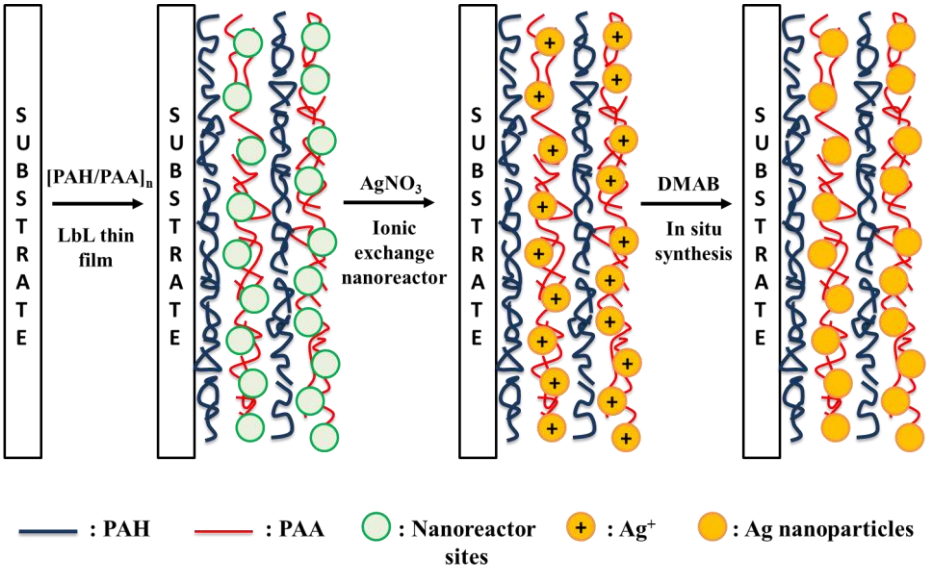

Figure 2.8. Schematic illustration of the ion exchange in the polymeric LbL matrix and a further *in situ* synthesis (ISS) of the silver nanoparticles into thin LbL films.

It has been found that it is possible to use the pH of the polyelectrolyte dipping solutions to control the number of free carboxylic acid groups present in the multilayer thin films constructed from weak polyacids such as PAA [62, 63]. This polyanion presents carboxylate and carboxylic acid groups at a suitable pH where the carboxylate groups are the responsible for the electrostatic attraction with the cationic groups of the polycation (PAH), forming ion pairs to build sequentially adsorbed multilayers in the LbL assembly [64-66]. However, the free carboxylic acid groups are responsible for binding Ag-ions by the metal-ion exchange mechanism with the proton (nanoreactor sites).

In Figure 2.9, two different pH values of the PAA, pH 7.0 and pH 9.0 respectively, are used to show how the silver nanoparticles are synthesized into the LbL films. A color change from transparent to yellow-orange has been pointed as an interesting result to corroborate the *in situ* synthesis (ISS) of the silver nanoparticles (AgNPs) during the loading ($AgNO_3$) and a further reduction (DMAB) process into the polymeric film. This Loading/Reduction (L/R) process has been repeated up to 4 times because it has been demonstrated that AgNPs have been synthesized in the polymeric LbL film.

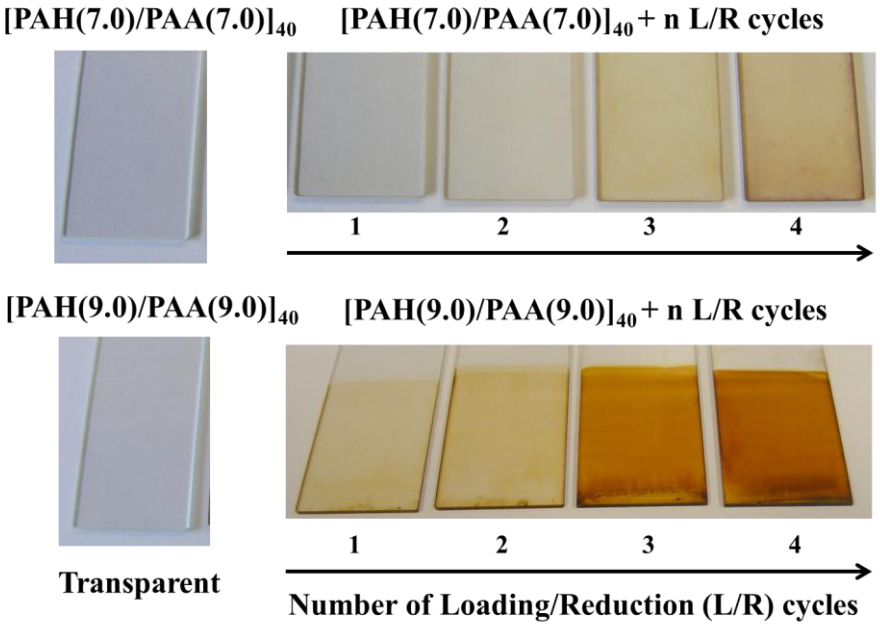

Figure 2.9. *In situ* synthesis (ISS) of the AgNPs into LbL films as a function of the number of L/R cycles and the pH value of the dipping polyelectrolyte solutions (PAH and PAA, respectively).

It is possible to appreciate the difference between a glass slide with only polymeric coating $[PAH/PAA]_{40}$ obtained by the LbL assembly at pH 7.0 or 9.0 (transparent), and the evolution of the yellow-orange coloration after the successive Loading/Reduction (L/R) cycles. When a higher number of L/R cycles has been performed, a better definition of the orange coloration in the LbL films can be observed, which is indicative that AgNPs have been synthesized into the polymeric LbL films. In addition, a higher number of nanoractor sites are available at pH 9.0, enabling a higher ion exchange and as a result, a higher number of the *in situ* synthesis (ISS) of silver nanoparticles is obtained into the LbL film. Due to this, the films show a higher intense orange coloration at pH 9.0 in comparison with the films at pH 7.0.

In Figure 2.10, UV-Vis spectra of the LbL films are shown after the *in situ* synthesis (ISS) of the silver nanoparticles (AgNPs) at pH 9.0. The presence of the LSPR absorption band at a specific wavelength position (420 nm) is indicative that AgNPs with a spherical shape have been synthesized into the LbL films. In addition, an increase in intensity of the LSPR absorption bands is observed when the number of L/R cycles is increased. This result is due to a higher amount of AgNPs are incorporated into the LbL films when the number of L/R cycles is increased during the fabrication process.

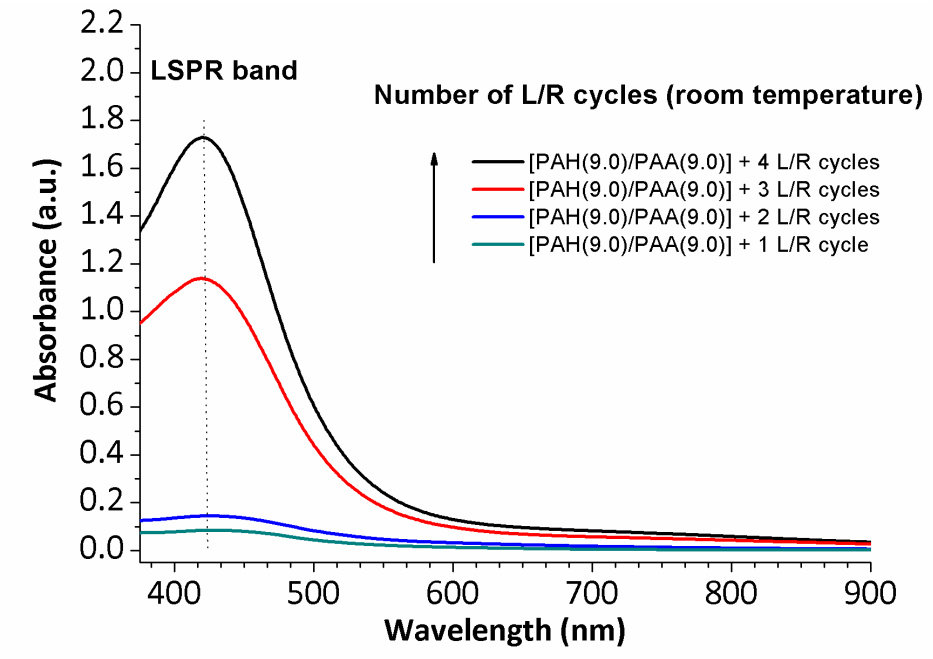

Figure 2.10. UV-Vis spectroscopy of the *in situ* synthesis (ISS) of the silver nanoparticles (AgNPs) into LbL films for different number Loading/Reduction cycles (1, 2, 3 and 4 L/R cycles).

The influence of the temperature in the LbL films has been also evaluated. The films have been thermally treated at 150 ºC to improve their mechanical stability and promote a chemical crosslink between the polymeric chains of both polyelectrolytes, PAH and PAA. An amide bond is formed between the carboxylic acid groups (COOH) of the PAA and the amine groups (NH_2) of the PAH. In addition, it is important to remark that higher values of temperature (i.e. melting point) produces a total evaporation of the polymeric chains and so, the only contribution of the silver nanoparticles (AgNPs) will be observed in the films.

In Figure 2.11, UV-Vis spectra of the LbL films are shown after thermal treatment of 150 ºC for 2 hours. The maxima of the LSPR absorption bands have been shifted in wavelength position (from 420 nm to 425 nm) and increased in intensity. This aspect related to LSPR evolution band can be better observed in Figure 2.12 where the intensity of the LSPR bands after thermal treatment is duplicated for the higher number of L/R cycles (n= 3, 4) in comparison with the films at room temperature.

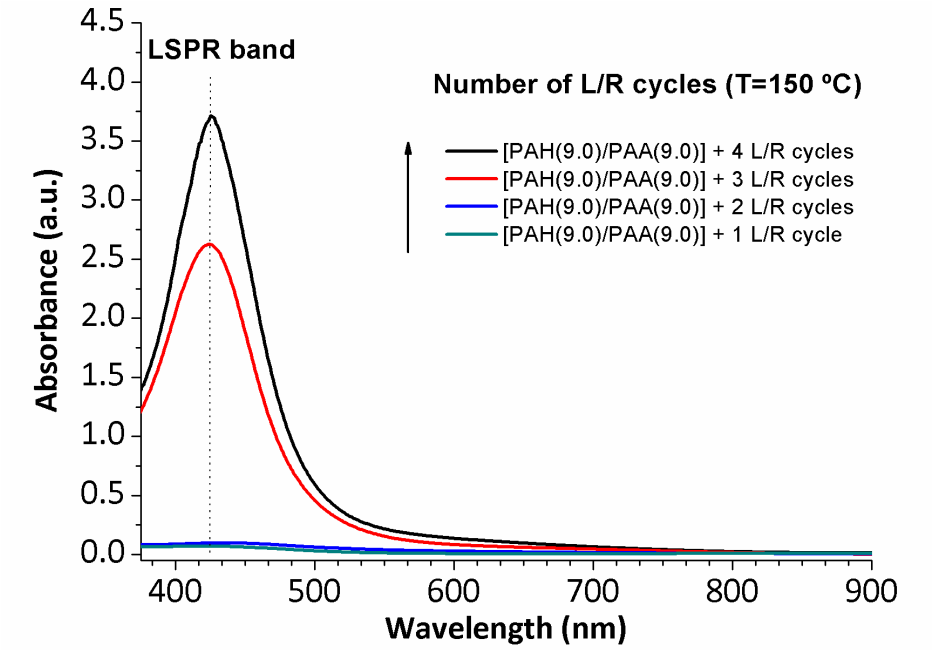

Figure 2.11. UV-Vis spectroscopy of the *in situ* synthesis (ISS) of the silver nanoparticles (AgNPs) into LbL films for different number Loading/Reduction cycles (1, 2, 3 and 4 L/R cycles) after thermal treatment of 150 ºC for 2 hours..

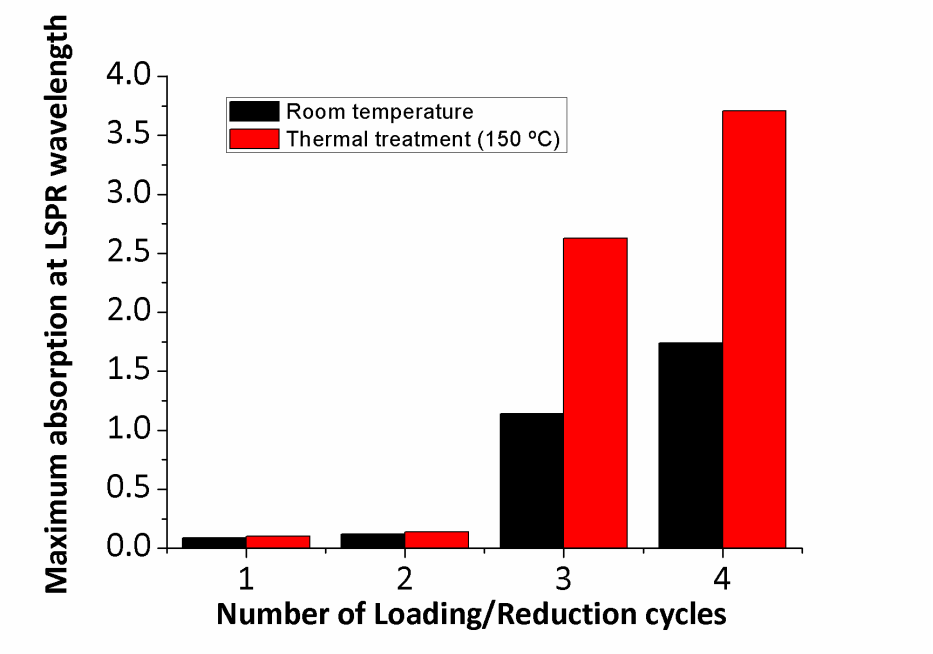

Figure 2.12. Comparative study of the intensity of the LSPR absorption bands as a function of the number of Loading/Reduction (L/R) cycles at room temperature and after thermal treatment of 150ºC for 2 hours .

In all the cases of study, an increase in intensity of the LSPR absorption bands has been observed in the UV-Vis spectroscopy after thermal treatment (150 ºC). A conclusion of this result can be due to a better proximity of the *in situ* synthesis of the AgNPs in the LbL films and so, a higher value in intensity of the LSPR absorption bands is observed.

In order to understand this thermal effect related to the drastic increase of the LSPR absorption bands, an AFM analysis was performed to study the thickness evolution (see Table 2.2) and the morphology of the resultant LbL films at room temperature and after thermal treatment (150 ºC). The thickness evolution after n cycles of L/R (n=1-4) is very similar that only polymeric LbL coating $[PAH(9.0)/PAA(9.0)]_{40}$, so that no change in the resultant thickness is observed after the *in situ* synthesis (ISS) of the AgNPs into the LbL films. In addition, the effect of the temperature results in a partial thickness reduction (around 20%) with no significant changes between initial control coating (only polymeric LbL film) and the coatings based on *in situ* synthesis of the silver nanoparticles (AgNPs) after the Loading/Reduction (L/R) process.

Table 2.2. Average evolution thickness as a function of the Loading/Reduction (L/R) cycles added.

Fabrication process	Thickness (nm) (room temperature)	Thickness (nm) (T 150 ºC)
$[PAH(9.0)/PAA(9.0)]_{40}$	287.7 ± 4.9	229.3 ± 5.2
$[PAH(9.0)/PAA(9.0)]_{40}$ + 1 L/R cycle	291.1 ± 4.2	234.1 ± 6.2
$[PAH(9.0)/PAA(9.0)]_{40}$ + 2 L/R cycles	289.4 ± 6.1	231.4 ± 4.5
$[PAH(9.0)/PAA(9.0)]_{40}$ + 3 L/R cycles	295.9 ± 7.9	233.9 ± 5.8
$[PAH(9.0)/PAA(9.0)]_{40}$ + 4 L/R cycles	293.8 ± 8.3	235.8 ± 6.9

According to this result of no variation of the thickness after L/R cycles, the morphology of the resultant films has been evaluated. In Figure 2.13, AFM analysis (1x1 µm) show a random distribution of the *in situ* synthesis (ISS) of the AgNPs with a spherical shape and variable size into the polymeric LbL films, as it can be observed in both height (a) and phase (b) images. These AFM images are of [PAH(9.0)/PAA(9.0)]+4 L/R cycles coating in tapping mode at room temperature and show an average in roughness of 1.39 nm (rms). The light spots observed in the height image correspond to the *in situ* synthesis (ISS) of the silver nanoparticles (AgNPs) into the LbL films which can be perfectly observed in the phase image.

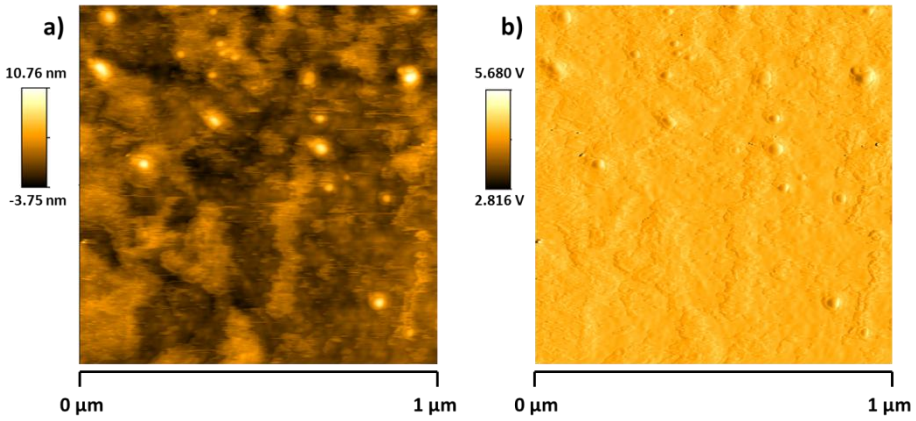

Figure 2.13. AFM images (1x1 µm) in tapping mode of height (a) and phase (b) for a coating [PAH(9.0)/PAA(9.0)] + 4 L/R cycles before thermal treatment (room temperature).

A totally different aspect of the *in situ* synthesis of the AgNPs in the topographic distribution can be observed after thermal treatment (150 ºC) for the [PAH(9.0)/PAA(9.0)] + 4 L/R cycles coating (see Figure 2.14). For this specific case, AFM images (1x1 µm) in tapping mode reveal a random distribution with an aggregation of the silver nanoparticles (AgNPs) in the polymeric LbL overlay. This aggregation of the AgNPs makes that the resultant films have increased in roughness with an average of 4.76 nm (rms). This thermal treatment induces an aggregation of the *in situ* synthesis of the AgNPs into the LbL films due to the partial thickness reduction of the films and so, an increase of the LSPR absorption bands (UV-Vis spectra) is obtained.

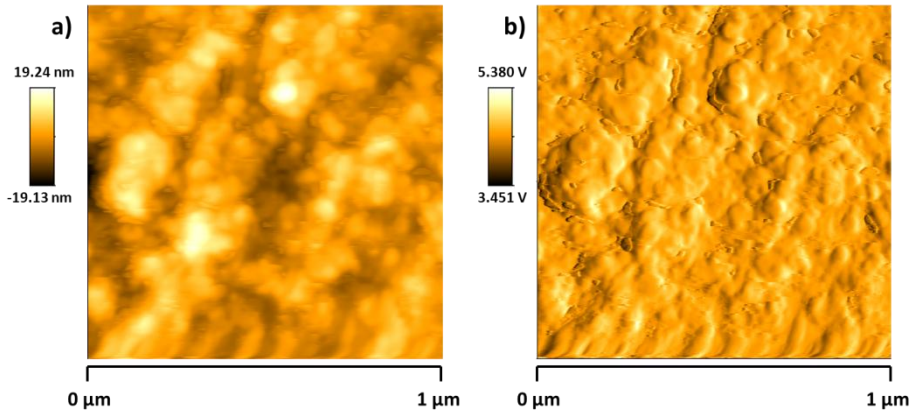

Figure 2.14. AFM images (1x1 µm) in tapping mode of height (a) and phase (b) for a coating [PAH(9.0)/PAA(9.0)] + 4 L/R cycles after thermal treatment of 150 ºC for 2 hours.

2.4. Comparison between sol-gel deposition process and Layer-by-Layer (LbL) assembly using in situ synthesis (ISS) of silver nanoparticles

In this section, it will emphasize the advantages and limitations of both techniques in the world of materials science for fabricating thin films. One of the main advantages of both techniques is the simplicity and versatility without the need of using expensive substances or equipment to perform the process. In addition, another benefit is that the coatings can be fabricated at room temperature based on aqueous solutions (wet chemistry) that yield metallic silver nanoparticles (LSPR).

According to the results observed in the UV-Vis spectra, the maxima values related to LSPR absorption bands in the sol-gel process are lower in intensity in comparison with the values obtained in the LbL assembly, using the same synthetic route for *in situ* synthesis (ISS) of AgNPs. The main reason of this result is that there is less PAA available groups in the hybrid sol-gel matrix, and as result, the amount of nanoreactor sites for a further metal ion exchange by silver ions in the loading step is lower when the substrates are immersed in the $AgNO_3$ solution.

An alternative to obtain higher PAA available groups in the sol-gel process could be to increase the number of dips in the initial hybrid precursor solution (only TEOS and PAA) before doing L/R protocol and so, the further *in situ* chemical reduction allows a higher ionic exchange with the resultant increase of the AgNPs. As a result, an increase of the resultant thickness is obtained and a change from nanometer to micrometer scale is observed. Due to this, applications where a precise control of the evolution thickness at nanometric scale is required as it can be in optical devices, the sol-gel dip-coating deposition technique is not an adequate process. However, applications where the thickness is not a crucial parameter, sol-gel method can be applied due to the easy way of implementing the deposition process. As an example, antibacterial surfaces proposed in Chapter 4 where only the presence of silver nanoparticles into the thin films will be the key to obtain a biocide effect and prevent the bacteria growth in a desired surface.

In addition, an important consideration in the sol-gel process is that a variable period of time is necessary to observe a change from sol to gel which depends on several parameters such as molecular alkoxyde precursor (TEOS), concentration and nature of the catalyst or water to silane ratio. This sol ageing time strongly affects in the final properties of the film obtained by dip-coating deposition technique. It has been corroborated that deposition processes performed at different period of time of a same sol-gel solution produces coatings with a different thickness.

To overcome the limitation of the thickness precision, LbL assembly can be a good alternative for obtaining thin films with a nanometric variation because the resultant thickness can be perfectly controlled with a high precision and accuracy as a function of the number of bilayers deposited onto the substrate. In addition, the composition and thickness of an individual bilayer can be controlled by adjusting the deposition parameters such as concentration, pH and immersion time in the aqueous weak polyelectrolyte solutions. Due to this precise control of the coating thickness at a nanoscale level, LbL method is chosen to fabricate optical fiber sensors for measuring Relative Humidity (RH) changes. A small change in the resultant thickness as a function of the number of bilayers added in the coating during the LbL fabrication process makes possible the apparition of new absorption resonant bands in the visible or infrared region, called Lossy Mode Resonance (LMRs) which are very sensitive to humidity changes with an adequate monitoring. More details about this variation of the LMR bands as well as LSPR bands related to the metallic silver nanoparticles (AgNPs) are extensively explained in Chapter 5, as a function of the number of bilayers added (thickness).

To sum up, a scheme of the results obtained of both LbL assembly and sol-gel process using the *in situ* synthesis (ISS) of silver nanoparticles is shown in Table 2.3.

Table 2.3. A scheme of the results obtained by *in situ* synthesis (ISS) process using the LbL assembly and sol-gel process.

In situ synthesis (ISS) of silver nanoparticles (AgNPs)	
Layer-by-Layer (LbL) assembly	Higher intensity of the LSPR bands Synthesis of spherical AgNPs and aggregates Nanometer thickness evolution (bilayers added) No high temperature values (evaporation polymeric chains)
Sol-gel process	Lower intensity of the LSPR bands Synthesis of inorganic macroaggregates Micrometer thickness evolution (dips added) High temperature values (450 ºC) Higher values in average roughness

2.5. Conclusions

In this chapter, a method for the *in situ* synthesis (ISS) of AgNPs into thin films is explained using two different deposition techniques, the sol-gel process and the Layer-by-Layer (LbL) assembly. In both cases of study, firstly, a thin film is fabricated using these two deposition processes and secondly, a further *in situ* synthesis of the silver nanoparticles into the thin films is performed.

This approach of the *in situ* synthesis (ISS) is based on the pH-dependent dissociation of weak polyacids such as PAA, as a function of the pH, where both ionized (carboxylate) and non-ionized (carboxylic) groups are obtained. The presence of the free carboxylic acid groups makes possible to bind metal ions via a simple aqueous ion exchange procedure, and a further chemical reduction step with a reducing agent, leads to obtain the silver nanoparticles within the thin film. As a result, a final golden-yellowish (sol-gel) or orange coloration (LbL) is observed which it is indicative that AgNPs have been successfully incorporated into the thin films. In addition, UV-Vis spectra show an intense absorption band at 410-420 nm which it is due to the LSPR of the spherical silver nanoparticles. However, a random distribution of the AgNPs nanoparticles with a partial aggregation as well as variable size and shape is observed in the AFM images (topographic distribution).

According to these results, a precise control over nanoparticles size and distribution into the thin films is not easy to achieve with the *in situ* synthesis (ISS) process and as a result, only yellow or orange coloration is observed. To overcome this situation, a new methodology, known as Layer-by-Layer Embedding (LbL-E) deposition technique, will be proposed in Chapter 3. As a result, a greater degree control over silver nanoparticles (shape and size distribution) in the resultant films is observed and variable multicolor films are obtained, maintaining the initial aggregation state of the nanoparticles.

Bibliography

[1] Cotí, K. K.; Belowich, M. E.; Liong, M.; Ambrogio, M. W.; Lau, Y. A.; Khatib, H. A.; Zink, J. I.; Khashab, N. M.; Stoddart, J. F. Mechanised Nanoparticles for Drug Delivery. Nanoscale 2009, 1, 16-39.
[2] Cozzoli, P. D.; Pellegrino, T.; Manna, L. Synthesis, Properties and Perspectives of Hybrid Nanocrystal Structures. Chem. Soc. Rev. 2006, 35, 1195-1208.
[3] Dufrêne, Y. F. TowardsNanomicrobiology using Atomic Force Microscopy. Nature Reviews Microbiology 2008, 6, 674-680.
[4] Ebert, P. Nano-Scale Properties of Defects in Compound Semiconductor Surfaces. Surface Science Reports 1999, 33, 121-303.
[5] Gimzewski, J. K.; Joachim, C. Nanoscale Science of Single Molecules using Local Probes. Science 1999, 283, 1683-1688.
[6] Gyurcsányi, R. E. Chemically-Modified Nanopores for Sensing. TrAC - Trends in Analytical Chemistry 2008, 27, 627-639.
[7] Hegmann, T.; Qi, H.; Marx, V. M. Nanoparticles in Liquid Crystals: Synthesis, Self-Assembly, Defect Formation and Potential Applications. Journal of Inorganic and Organometallic Polymers and Materials 2007, 17, 483-508.
[8] Lu, W.; Lieber, C. M. Semiconductor Nanowires. J. Phys. D 2006, 39, R387-R406.
[9] Mann, S. Self-Assembly and Transformation of Hybrid Nano-Objects and Nanostructures Under Equilibrium and Non-Equilibrium Conditions. Nature Materials 2009, 8, 781-792.
[10] Rajagopal, K.; Schneider, J. P. Self-Assembling Peptides and Proteins for Nanotechnological Applications. Curr.Opin.Struct. Biol. 2004, 14, 480-486.
[11] Slota, J. E.; He, X.; Huck, W. T. S. Controlling Nanoscale Morphology in Polymer Photovoltaic Devices. Nano Today 2010, 5, 231-242.
[12] Zanetti, M.; Lomakin, S.; Camino, G. Polymer Layered Silicate Nanocomposites. Macromolecular Materials and Engineering 2000, 279, 1-9.
[13] Hughes, G. A. Nanostructure-Mediated Drug Delivery. Nanomedicine: Nanotechnology, Biology, and Medicine 2005, 1, 22-30.
[14] Jain, K. K. Applications of Nanobiotechnology in Clinical Diagnostics. Clin. Chem. 2007, 53, 2002-2009.
[15] Jain, K. K. Nanotechnology in Clinical Laboratory Diagnostics. ClinicaChimicaActa 2005, 358, 37-54.
[16] Lapotko, D. Plasmonic Nanoparticle-Generated Photothermal Bubbles and their Biomedical Applications. Nanomedicine 2009, 4, 813-845.
[17] Liu, H.; Webster, T. J. Nanomedicine for Implants: A Review of Studies and Necessary Experimental Tools. Biomaterials 2007, 28, 354-369.
[18] Russ Algar, W.; Massey, M.; Krull, U. J.The Application of Quantum Dots, Gold Nanoparticles and Molecular Switches to Optical Nucleic-Acid Diagnostics.TrAC - Trends in Analytical Chemistry 2009, 28, 292-306.
[19] Arregui, F. J.; Matias, I. R.; Corres, J. M.; Del Villar, I.; Goicoechea, J.; Zamarrenoa, C. R.; Hernáez, M.; Claus, R. O. In In Optical fiber sensors based on layer-by-layer nanostructured films; Procedia Engineering; 2010; Vol. 5, pp 1087-1090.
[20] Arregui, F. J.; Matias, I. R.; Liu, Y.; Lenahan, K. M.; Claus, R. O. Optical Fiber Nanometer-Scale Fabry-Perot Interferometer Formed by the Ionic Self-Assembly Monolayer Process. Opt. Lett. 1999, 24, 596-598.
[21] Galbarra, D.; Arregui, F. J.; Matias, I. R.; Claus, R. O. Ammonia Optical Fiber Sensor Based on Self-Assembled Zirconia Thin Films. Smart Mater.Struct. 2005, 14, 739-744.
[22] Corres, J. M.; Sanz, A.; Arregui, F. J.; Matías, I. R.; Roca, J. Fiber Optic Glucose Sensor Based on Bionanofilms. Sensors and Actuators, B: Chemical 2008, 131, 633-639.
[23] Hrudey, P. C. P.; Taschuk, M.; Tsui, Y. Y.; Fedosejevs, R.; Sit, J. C.; Brett, M. J. Evaporated Nanostructured Y 2O 3:Eu Thin Films. Journal of Nanoscience and Nanotechnology 2005, 5, 229-234.

[24] Kamiya, S.; Takahashi, H.; Saka, M.; Abé, H. Evaluation and Improvement of the Adhesive Fracture Toughness of CVD Diamond on Silicon Substrate. J Electron Packag, Trans ASME 2002, 124, 271-276.
[25] Shin, D. O.; Lee, D. H.; Moon, H. -.; Jeong, S. -.; Kim, J. Y.; Mun, J. H.; Cho, H.; Park, S.; Kim, S. O. Sub-Nanometer Level Size Tuning of a Monodisperse Nanoparticle Array Via Block Copolymer Lithography. Advanced Functional Materials 2011, 21, 250-254.
[26] Song, J.; Jensen, D. S.; Hutchison, D. N.; Turner, B.; Wood, T.; Dadson, A.; Vail, M. A.; Linford, M. R.; Vanfleet, R. R.; Davis, R. C. Carbon-Nanotube-TemplatedMicrofabrication of Porous Silicon-Carbon Materials with Application to Chemical Separations. Advanced Functional Materials 2011, 21, 1132-1139.
[27] Schmidt, H. Chemistry of Material Preparation by the Sol-Gel Process. J. Non Cryst. Solids
[28] Livage, J.; Sanchez, C. Sol-Gel Chemistry. J. Non Cryst. Solids 1992, 145, 11-19.
1988, 100, 51-64.
[29] Wencel, D.; Barczak, M.; Borowski, P.; McDonagh, C. The Development and Characterisation of Novel Hybrid Sol-Gel-Derived Films for Optical pH Sensing. Journal of Materials Chemistry 2012, 22, 11720-11729.
[30] Estella, J.; Wencel, D.; Moore, J. P.; Sourdaine, M.; McDonagh, C. Fabrication and Performance Evaluation of Highly Sensitive Hybrid Sol-Gel-Derived Oxygen Sensor Films Based on a Fluorinated Precursor. Anal.Chim.Acta 2010, 666, 83-90.
[31] Berg, M. C.; Choi, J.; Hammond, P. T.; Rubner, M. F. Tailored Micropatterns through Weak Polyelectrolyte Stamping. Langmuir 2003, 19, 2231-2237.
[32] Yoo, D.; Shiratori, S. S.; Rubner, M. F. Controlling Bilayer Composition and Surface Wettability of Sequentially Adsorbed Multilayers of Weak Polyelectrolytes. Macromolecules 1998, 31, 4309-4318.
[33] Berg, M. C.; Zhai, L.; Cohen, R. E.; Rubner, M. F. Controlled Drug Release from Porous Polyelectrolyte Multilayers. Biomacromolecules 2006, 7, 357-364.
[34] Fendler, J. H. Self-Assembled Nanostructured Materials. Chemistry of Materials 1996, 8, 1616-1624.
[35] Fendler, J. H.; Meldrum, F. C. The Colloid Chemical Approach to Nanostructured Materials.Adv Mater 1995, 7, 607-632.
[36] Bico, J.; Thiele, U.; Quéré, D. Wetting of Textured Surfaces. Colloids Surf. Physicochem. Eng. Aspects 2002, 206, 41-46.
[37] Carbone, L.; Cozzoli, P. D. Colloidal HeterostructuredNanocrystals: Synthesis and Growth Mechanisms. Nano Today 2010, 5, 449-493.
[38] Liz-Marzán, L. M. Nanometals: Formation and Color. Materials Today 2004, 7, 26-31.
[39] Pastoriza-Santos, I.; Serra-Rodríguez, C.; Liz-Marzán, L. M. Self-Assembly of Silver Particle Monolayers on Glass from Ag+ Solutions in DMF. J. Colloid Interface Sci. 2000, 221, 236-241.
[40] Rivero, P. J.; Goicoechea, J.; Urrutia, A.; Arregui, F. J. Effect of both Protective and Reducing Agents in the Synthesis of Multicolor Silver Nanoparticles. Nanoscale Research Letters 2013, 8, 1-9.
[41] Kan, C. -.; Zhu, J. -.; Zhu, X. -. Silver Nanostructures with Well-Controlled Shapes: Synthesis, Characterization and Growth Mechanisms. J. Phys. D 2008, 41.
[42] Zhang, W. C.; Wu, X. L.; Kan, C. X.; Pan, F. M.; Chen, H. T.; Zhu, J.; Chu, P. K. Surface-Enhanced Raman Scattering from Silver Nanostructures with Different Morphologies. Applied Physics A: Materials Science and Processing 2010, 100, 83-88.
[43] Fernanda Cardinal, M.; Rodríguez-González, B.; Alvarez-Puebla, R. A.; Pérez-Juste, J.; Liz-Marzán, L. M. Modulation of Localized Surface Plasmons and SERS Response in Gold Dumbbells through Silver Coating. Journal of Physical Chemistry C 2010, 114, 10417-10423.
[44] Abalde-Cela, S.; Ho, S.; Rodríguez-González, B.; Correa-Duarte, M. A.; Álvarez-Puebla, R. A.; Liz-Marzán, L. M.; Kotov, N. A. Loading of Exponentially Grown LBL Films with Silver Nanoparticles and their Application to Generalized SERS Detection. AngewandteChemie - International Edition 2009, 48, 5326-5329.
[45] Koktysh, D. S.; Liang, X.; Yun, B. -.; Pastoriza-Santos, I.; Matts, R. L.; Giersig, M.; Serra-Rodríguez, C.; Liz-Marzán, L. M.; Kotov, N. A. Biomaterials by Design: Layer-by-Layer Assembled Ion-Selective and Biocompatible Films of TiO2 Nanoshells for Neurochemical Monitoring. Advanced Functional Materials 2002, 12, 255-265.

[46] Liz-Marzán, L. M.; Lado-Touriño, I. Reduction and Stabilization of Silver Nanoparticles in Ethanol by Nonionic Surfactants. Langmuir 1996, 12, 3585-3589.
[47] Pastoriza-Santos, I.; Liz-Marzán, L. M. ColloidalSilverNanoplates. State of the Art and Future Challenges. Journal of Materials Chemistry 2008, 18, 1724-1737.
[48] Schmidt, H. Nanoparticles by Chemical Synthesis, Processing to Materials and Innovative Applications. Applied Organometallic Chemistry 2001, 15, 331-343.
[49] Rivero, P. J.; Urrutia, A.; Goicoechea, J.; Zamarreño, C. R.; Arregui, F. J.; Matías, I. R. An Antibacterial Coating Based on a polymer/sol- Gel Hybrid Matrix Loaded with Silver Nanoparticles. Nanoscale Research Letters 2011, 6, X1-7.
[50] Wang, T. C.; Rubner, M. F.; Cohen, R. E. Polyelectrolyte Multilayer Nanoreactors for Preparing Silver Nanoparticle Composites: Controlling Metal Concentration and Nanoparticle Size. Langmuir 2002, 18, 3370-3375.
[51] Rivero, P. J.; Urrutia, A.; Goicoechea, J.; Matias, I. R.; Arregui, F. J. A Lossy Mode Resonance Optical Sensor using Silver Nanoparticles-Loaded Films for Monitoring Human Breathing. Sensors and Actuators, B: Chemical 2012, 187,40-44.
[52] Rivero, P. J.; Urrutia, A.; Goicoechea, J.; Arregui, F. J. Optical Fiber Humidity Sensors Based on Localized Surface Plasmon Resonance (LSPR) and Lossy-Mode Resonance (LMR) in Overlays Loaded with Silver Nanoparticles. Sensors and Actuators, B: Chemical 2012, 173, 244-249.
[53] Rivero, P. J.; Urrutia, A.; Goicoechea, J.; Arregui, F. J.; Matias, I. R. In In Humidity sensor based on silver nanoparticles embedded in a polymeric coating; Proceedings of the International Conference on Sensing Technology, ICST; 2011; , pp 376-379.
[54] Rivero, P. J.; Urrutia, A.; Goicoechea, J.; Arregui, F. J.; Matías, I. R. Humidity Sensor Based on Silver Nanoparticles Embedded in a Polymeric Coating. International Journal on Smart Sensing and Intelligent Systems 2012, 5, 71-83.
[55] Rivero, P. J.; Urrutia, A.; Goicoechea, J.; Rodríguez, Y.; Corres, J. M.; Arregui, F. J.; Matías, I. R. An Antibacterial Submicron Fiber Mat with in Situ Synthesized Silver Nanoparticles. J ApplPolymSci 2012, 126, 1228-1235.
[56] Cobley, C. M.; Skrabalak, S. E.; Campbell, D. J.; Xia, Y. Shape-Controlled Synthesis of Silver Nanoparticles for Plasmonic and Sensing Applications. Plasmonics 2009, 4, 171-179.
[57] Sepúlveda, B.; Angelomé, P. C.; Lechuga, L. M.; Liz-Marzán, L. M. LSPR-Based Nanobiosensors. Nano Today 2009, 4, 244-251.
[58] Rycenga, M.; Cobley, C. M.; Zeng, J.; Li, W.; Moran, C. H.; Zhang, Q.; Qin, D.; Xia, Y. Controlling the Synthesis and Assembly of Silver Nanostructures for Plasmonic Applications. Chem. Rev. 2011, 111, 3669-3712.
[59] Patel, A. C.; Li, S.; Wang, C.; Zhang, W.; Wei, Y. Electrospinning of Porous Silica Nanofibers Containing Silver Nanoparticles for Catalytic Applications. Chemistry of Materials 2007, 19, 1231-1238.
[60] Boonamnuayvitaya, V.; Tayamanon, C.; Sae-Ung, S.; Tanthapanichakoon, W. Synthesis and Characterization of Porous Media Produced by a Sol-Gel Method. Chemical Engineering Science 2006, 61, 1686-1691.
[61] Lvov, Y.; Ariga, K.; Onda, M.; Ichinose, I.; Kunitake, T. Alternate Assembly of Ordered Multilayers of SiO2 and Other Nanoparticles and Polyions. Langmuir 1997, 13, 6195-6202.
[62] Ershov, B. G.; Henglein, A. Time-Resolved Investigation of Early Processes in the Reduction of Ag + on Polyacrylate in Aqueous Solution. J PhysChem B 1998, 102, 10667-10671.
[63] Ershov, B. G.; Henglein, A. Reduction of Ag + on Polyacrylate Chains in Aqueous Solution. J PhysChem B 1998, 102, 10663-10666.
[64] Machado, G.; Beppu, M. M.; Feil, A. F.; Figueroa, C. A.; Correia, R. R. B.; Teixeira, S. R. Silver Nanoparticles obtained in PAH/PAA-Based Multilayers by Photochemical Reaction. Journal of Physical Chemistry C 2009, 113, 19005-19010.
[65] Veletanlic, E.; Cynthia Goh, M. Polyelectrolyte Multilayer Films as Templates for the in Situ Photochemical Synthesis of Silver Nanoparticles. Journal of Physical Chemistry C 2009, 113, 18020-18026.
[66] Logar, M.; Jancar, B.; Šturm, S.; Suvorov, D. Weak Polyion Multilayer-Assisted in Situ Synthesis as a Route Toward a Plasmonic Ag/TiO2 Photocatalyst. Langmuir 2010, 26, 12215-12224.

CHAPTER 3. Synthesis of multicolor silver nanoparticles and their incorporation into thin films using the Layer-by-Layer Embedding (LbL-E) deposition technique

In this chapter, the synthesis of AgNPs with different shape, size, aggregation state and coloration is studied. In addition, the evolution of their optical properties related to the wavelength position of the Localized Surface Plasmon Resonance (LSPR) is shown. Then, a further incorporation of the synthesized AgNPs into polyelectrolyte multilayer thin films using the Layer-by-Layer Embedding (LbL-E) deposition technique is presented. This is the first time that a study about the color formation based on AgNPs is investigated in LbL-E thin films preserving the original color of the AgNPs dispersions.

3.1. Introduction to the synthesis of metal nanoparticles

Metal nanoparticles are of great interest in a high number of disciplines because of their potential applications in diverse fields such as antibacterials [1-5], catalysis [6-10], chemical sensors [11-15], drug delivery [16-19], electronics [20], photochemistry [21, 22] or photonics [23-25]. Their special optical properties arise from Localized Surface Plasmon Resonance (LSPR) which occurs when the conduction electrons in metal nanostructures collectively oscillate, as a result of their interaction with an incident electromagnetic radiation [26-28]. One of the most relevant aspects of the synthesis of AgNPs is that their optical properties (resultant color) present a high dependence with their crystal morphology [29-31]. A monitoring of the evolution of the LSPR wavelength position by UV-Vis measurements and the corresponding color formation makes possible to obtain nanoparticles with a desirable shape and size [32-35].

A wide variety of synthesis methodologies to obtain metallic nanoparticles are focused on a control of several parameters such as the shape, size, surface functionalization or interparticle distance which affect their final properties. A fine control of these parameters is a challenging goal, and a large number of reports have been published [36-48]. Among them, the synthesis routes based on the chemical reduction in organic solvents or in which polymers can act simultaneously as a stabilizer and reducing agent to obtain metal nanoparticles have been investigated [49-52]. However, the use of organic media and the

synthesis of polydisperse nanoparticles limit their use for some specific applications where monodisperse nanoparticles are required [53, 54].

It is not intended here to describe all the existing methods for the preparation of metallic nanoparticles. In fact, this work will be restricted to one of the most widely used methods based on chemical reactions in solution (known as wet chemistry). Alternative procedures for the synthesis of gold (AuNPs) or silver nanoparticles (AgNPs) are based on the use of water soluble polymers with the aim of achieving size-controlled nanoparticles. Wang and co-workers have obtained AuNPs in aqueous solution in the 1–5 nm size range with the use of poly (methacrylic acid) (PMMA) [55, 56]. Keuker-Baumann and co-workers reported a study about the formation of AgNPs with a high control and a characteristic plasmon band at 410 nm is observed using dilute solutions of long-chain sodium polyacrylates (NaPA) by exposing the solution to UV-radiation [57] where the coil size of the polymeric chains acts as a collector of silver cations (Ag^+). Other researches have investigated the formation of AgNPs and intermediate clusters in polyacrylate aqueous solutions by chemical reduction of Ag^+ using a reducing agent, gamma radiation or ambient light [58-61]. The use of polyacrylate anions with uncoordinated carboxylate groups enables to bind metallic cations such as silver (Ag^+ salts) via a simple aqueous ion exchange procedure and a posterior chemical reduction step with a reducing agent, forming intermediate charged clusters [62-65].

In this work, the first part, section 3.2, is focused on the development of a chemical reduction method to synthesize both clusters and silver nanoparticles of different colors in aqueous polymeric solution at room temperature and in a short period of time with a well-defined shape. An experimental matrix (known as multicolor silver map) of 56 possible combinations as a function of variable molar ratios between both protective and reducing agents will be presented, enabling a wide range of colors (yellow, orange, red, violet, blue, green, brown), shapes and sizes [66]. Then, once metal nanoparticles have been synthesized, the second part of this work, section 3.3, is devoted to the incorporation of three types of these synthesized AgNPs (violet, green and orange coloration) into a polyelectrolyte multilayer thin film using the Layer-by-Layer assembly. Henceforward, this process of incorporating the previous synthesized silver nanoparticles with a specific coloration and well-controlled shape into multilayer thin films will be called Layer-by-Layer Embedding (LbL-E) deposition technique.

As was explained in Chapter 2, the Layer-by-Layer (LbL) is based on the alternating deposition of oppositely charged polyelectrolytes in water solution (polycations and polyanions) on substrates where the electrostatic interaction between these two components of different charge is the driving force for the multilayer assembly [67-71]. More details can be found in Appendix 2. In

addition, LbL assembly makes possible to incorporate the earlier mentioned nanoparticles into thin films due to the use of poly(acrylic acid, sodium salt) (PAA) as a protective agent which maintains unaltered the aggregation state of the AgNPs. However, previous LbL approaches are based on the *in situ* synthesis (ISS) of AgNPs into the polyelectrolyte multilayers via counterion exchange and a further chemical reduction, using weak or strong polyelectrolytes [72-80], without preserving the aggregation state of the nanoparticles. Although the film thickness of the polymeric matrix can be controlled by the number of bilayers deposited onto the substrate, a better control over particles size and distribution in the films is not easy to achieve with the *in situ* synthesis (ISS) and as a result, only yellow or orange coloration is observed. This aspect related to color formation based on the *in situ* synthesis (ISS) of AgNPs is also corroborated using other deposition techniques such as sol-gel or electrospining process [81-85].

In order to obtain a specific color in the resultant LbL films is necessary to have a greater control over distribution of the nanoparticles into the films, maintaining their aggregation state and preserving their agglomeration. All these aspects can be controlled with the Layer-by-Layer Embedding (LbL-E) deposition technique where AgNPs with a desired shape, size and color are successfully incorporated into multilayer thin films. To our knowledge, this is the first time that a study about the color formation in films based on AgNPs and preserving the original color of the precursor solutions containing the AgNPs is presented.

3.2. Synthesis of multicolor silver nanoparticles

In this section, an analysis about the generation of multicolor silver nanoparticles will be presented. Then, the effect of both protective and reducing agents in the synthesis process will be evaluated. To our knowledge, this is the first time that an experimental study based on the influence of both PAA and DMAB molar concentrations to obtain colored silver nanoparticles and clusters has been reported in the literature.

3.2.1. Preparation of the multicolor silver map

A chemical reduction method at room temperature was performed using silver nitrate ($AgNO_3$) as a loading agent, dimethylaminoborane (DMAB) as a reducing agent and poly(acrylic acid, sodium salt) (PAA) as a protective agent. In order to investigate the influence of both PAA and DMAB on the color formation, several concentrations of this water soluble polymer (from 1 mM to 250 mM PAA) and reducing agent (from 0.033 mM to 6.66 mM DMAB) were prepared [66]. This synthesis process was repeated several times under the same experimental conditions (room temperature and storage), and no significant difference in the optical absorption spectra of the AgNPs was observed.

The samples were prepared by adding freshly variable DMAB concentration (0.033, 0.066, 0.16, 0.33, 0.66, 1.66, 3.33 and 6.66 mM) to vigorous stirred solutions which contained different PAA concentration (1.0, 2.5, 5.0, 10.0, 25.0, 100.0 and 250.0 mM) and constant $AgNO_3$ concentration (3.33 mM). The final molar ratio between reducing and loading agent (DMAB:$AgNO_3$ ratio) was 1:100, 1:50, 1:20, 1:10, 1:5, 1:2, 1:1 and 2:1. The final molar ratio between protective agent and loading agent (PAA:$AgNO_3$ ratio) was 0.3:1, 0.75:1, 1.5:1, 3:1, 7.5:1, 30:1 and 75:1. Once the reaction was completed, the color was stable without any further modification.

In Figure 3.1, it is possible to appreciate the experimental matrix with a total number of 56 different combinations which were obtained when both PAA and DMAB molar concentrations have been varied. From these 56 combinations, a wide range of AgNPs can be obtained with different colors (yellow, orange, red, violet, blue, green, brown) and tunable shape and size (corroborated by TEM micrographs). The synthesized AgNPs dispersions showed no changes of their optical absorption bands even after a year of storage at room conditions.

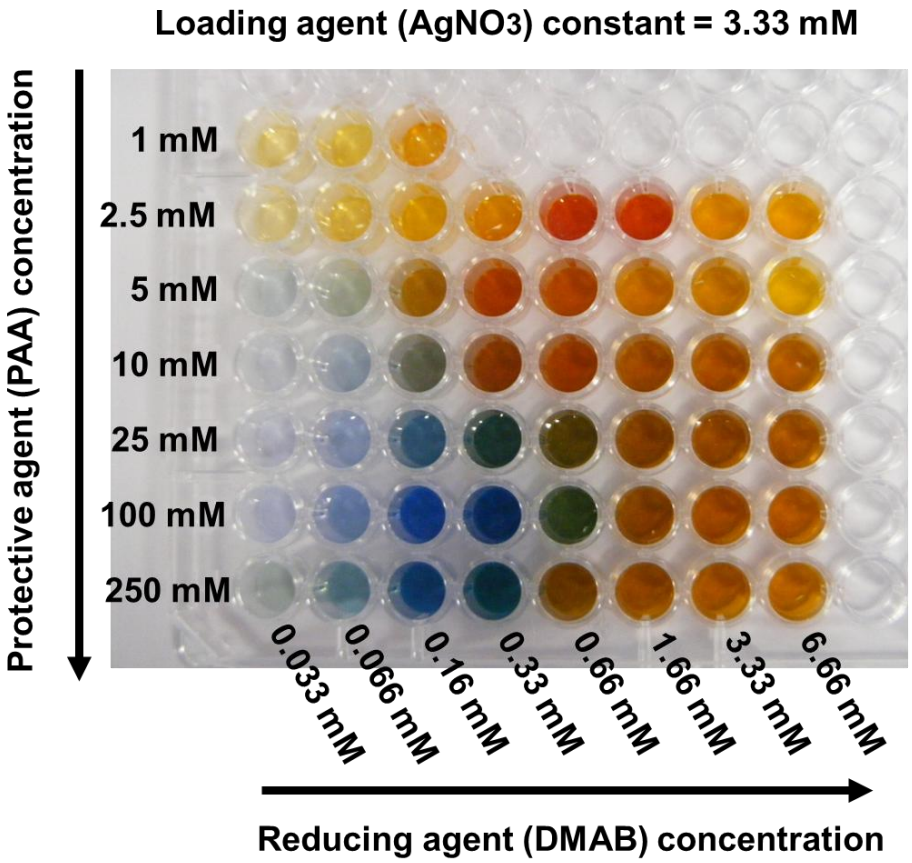

Figure 3.1. Photograph of the multicolor silver map obtained as a function of variable protective agent (PAA) and reducing agent (DMAB).

3.2.2. Characterization of the silver map

Transmission Electron Microscopy (TEM) was used to determine the morphology of both silver nanoparticles and clusters. TEM analysis was carried out with a Carl Zeiss Libra 120. Samples for TEM were prepared by dropping and evaporating the solutions onto a collodion-coated copper grid.

UV-Visible spectroscopy (UV-Vis) was used to characterize the optical properties of the multicolor silver map. The measurements were carried out with a Jasco V-630 spectrophotometer.

3.2.3. Effect of the protective agent in the synthesis process

One of the major findings of the present study was the significant influence of the PAA concentration on the final color of each sample. Due to its molecular structure with PA− in water solution, the binding of PA^- with metal cations (silver) was made possible, forming Ag^+PA^- complexes wherein a posterior reduction of the silver cations to silver nanoparticles takes place [60-65]. Moreover, PAA concentration plays a key role for the stabilization of silver nanoparticles and metal clusters along the polymeric chains, controlling their size and shape. In fact, the multicolor silver map of Figure 3.1 demonstrates that with a lower PAA concentration (1 mM or 2.5 mM), stable silver nanoparticles are generated showing only yellow, orange and red colors. These AgNPs showed no changes in the spectral position of their optical absorption bands even after a year. Our study demonstrates that by increasing PAA concentration from 5mM to 250 mM, a wider range of colors (violet, blue, green, brown, orange) is obtained with a high stability in time. In fact, a higher range of blue colors is obtained for higher PAA concentration (25, 100 or 250 mM), see Figure 3.1. This blue color has been reported in previous works using photochemical or chemical reduction [58, 59, 64], but no using DMAB as a reducing agent in the presence of various PAA concentrations.

Figure 3.2 shows the UV-Vis spectra for different PAA concentrations, from 2.5 mM to 250 mM when the DMAB concentration was kept constant (0.33 mM) corresponding to the fourth column of Figure 3.1. It has been observed experimentally that 1 mM PAA for this DMAB concentration or higher DMAB concentration produces a complete precipitation of silver and no color formation is obtained. The UV-Vis spectra reveal the evolution of two spectral regions (region 1 the 400-500 nm band and region 2 the 600-700 nm band) as a function of PAA concentration. Initially, according to the yellow and orange color obtained for the lower PAA concentrations of 2.5 and 5 mM, an intense absorption band is obtained at short wavelengths with the wavelength of maximum absorbance located at 435 and 445 nm respectively (region 1). As PAA concentration is increased (10 mM), the absorption band in region 1 is decreased in intensity and is shifted to longer wavelengths with a change in the resulting color (brown, 10 mM) and at the same time a new absorption band appears in region 2 (600-700 nm), indicating the synthesis of silver nanoparticles of different shapes than the previously obtained with lower PAA concentration. In addition, when PAA molar concentration is increased from 25 to 250 mM, generation of new colors is achieved (blue or green) with an increase in the intensity of their absorption bands in the region 2, whereas simultaneously a gradual decrease in the intensity in the region 1 is observed.

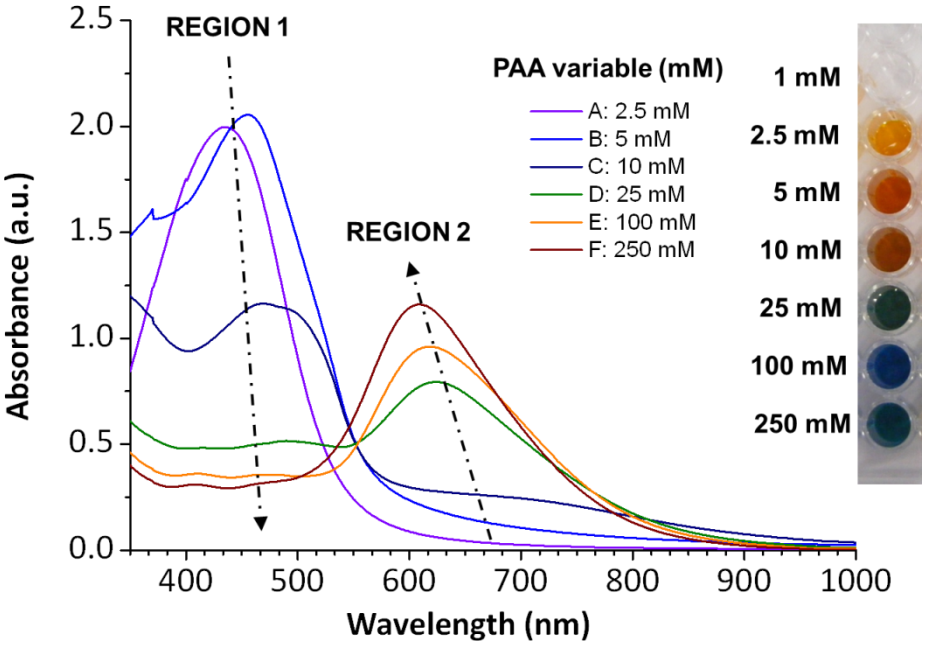

Figure 3.2. UV-Vis absorption spectra of silver solutions for different PAA concentrations (2.5, 5, 10, 25, 100 and 250 mM) at a constant DMAB concentration (0.33 mM). This plot corresponds to the fourth column of the multicolor silver map.

Figure 3.3 was also plotted in order to show a clearer picture of the evolution of the optical absorption bands (region 1 and 2) when molar PAA concentration was increased. As can be deduced from this Figure, PAA plays a key role in the formation of the resulting color because it is clearly observed well defined positions of the maximum absorption bands as a function of the PAA concentration added to the solution. These changes in color from orange (lower PAA concentration with an intense absorption band in region 1) to blue (higher PAA concentration with an absorption band in region 2) can be controlled during the synthesis process as a function of PAA and DMAB added in the initial solution.

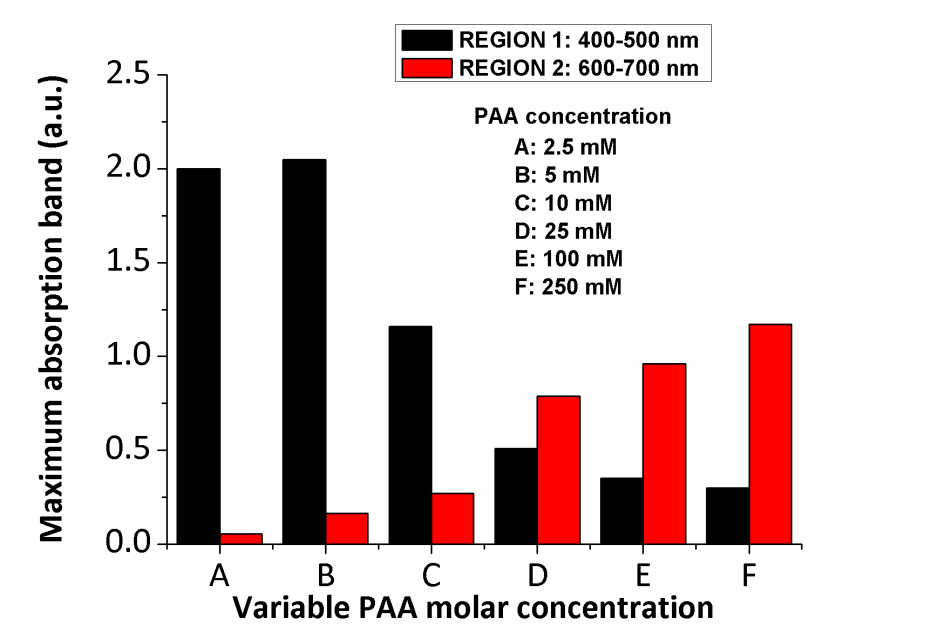

Figure 3.3. Evolution of the UV-Vis maxima absorption bands of the silver samples in region 1 and region 2 (400-500 nm and 600-700 nm respectively) prepared with different PAA concentration at a constant molar DMAB concentration (0.33 mM).

The reason for the gradual absence of the plasmonic resonance band in the region 1 (around 410 nm) for higher PAA concentrations is due to the gradual absence of silver nanoparticles with a spherical shape and the gradual appearance of silver nanoparticles with new shapes. This hypothesis is corroborated by the results obtained by TEM micrographs. As can be seen in Figure 3.4, variable PAA concentrations from 5 to 250 mM lead to the formation of new shapes (rods, cylinders, triangles, cubic, hexagons) with a considerable increase in the size with respect to the AgNPs obtained with lower PAA concentrations (1 or 2.5 mM) where only spherical shapes were observed.

The results observed in Figure 3.4 reveal that varying PAA concentration induces a change in the corresponding shape and the size of the particles from 100-300 nm (nanoparticles) with lower PAA concentrations (orange coloration) to 0.5-1 um (clusters) with higher PAA concentrations (brown, green or blue coloration).

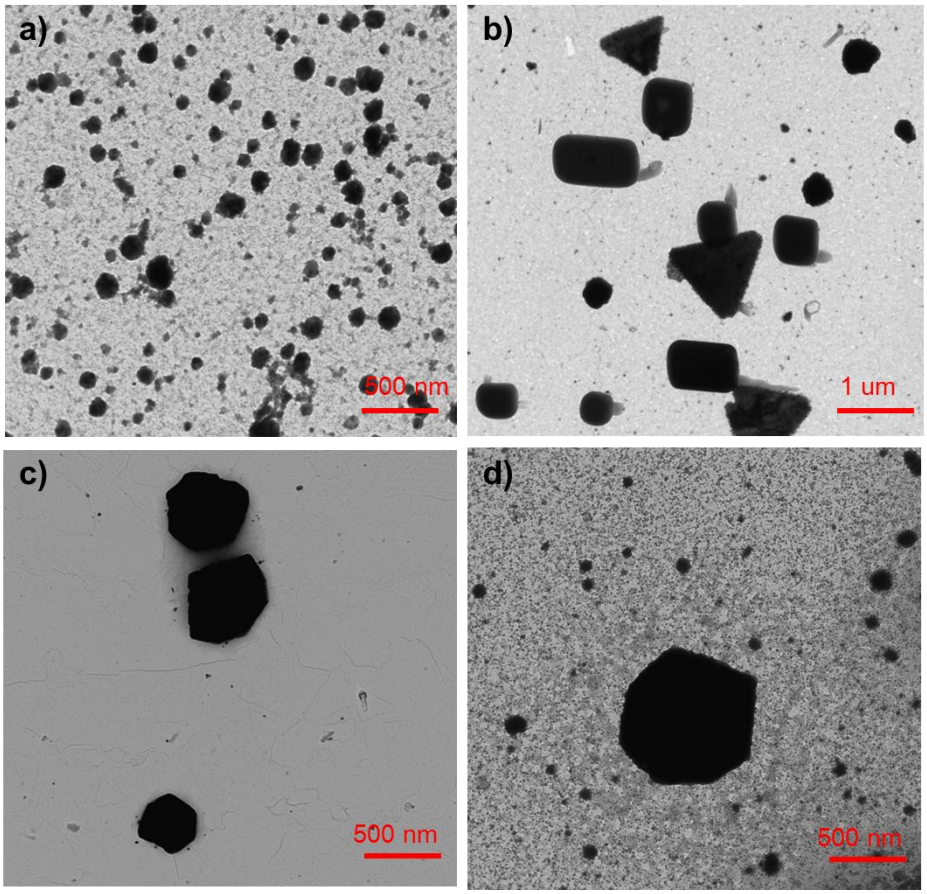

Figure 3.4. TEM micrographs that show the formation of AgNPs with different shapes for different PAA concentrations (a) spherical shape for 2.5 mM PAA; (b) several shapes (triangle, rod, cube, bar) for 10 mM PAA; (c and d) hexagonal shapes for 100 and 250 mM PAA, respectively. The DMAB concentration was 0.33 mM.

3.2.4. Effect of the reducing agent in the synthesis process

In the previous Section 3.2.3, the influence of the PAA concentration in the synthesis process to obtain the metallic silver nanoparticles or clusters was investigated. Here, the reduction of silver cations (Ag^{+}) at different reducing: loading agent molar ratios (DMAB: $AgNO_3$) is studied.

When the reducing agent (DMAB) is increased from 0.033 to 6.66 mM in the same mixture of $AgNO_3$ and PAA, the maximum absorption band is shifted to shorter wavelengths (region 1). Figure 3.5 shows the UV-Vis absorption bands when the DMAB concentration is increased for a 25 mM PAA solution (fifth line in Figure 3.1). An increase of the reducing agent

DMAB produces an absorption band shift to shorter wavelengths. An intense absorption band at 410 nm is observed when the highest DMAB proportion (6.66 mM) is added to the mixture and an orange coloration is obtained, indicating the synthesis of Ag NPs with spherical shape (corroborated by TEM micrographs).

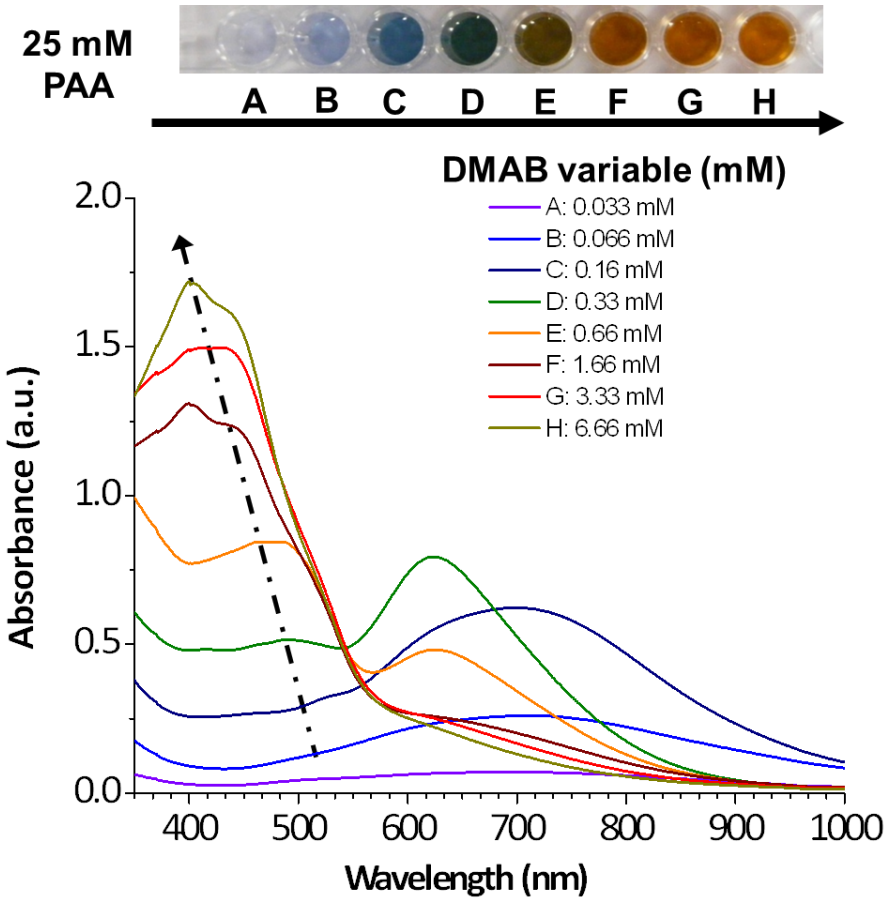

Figure 3.5. UV-Vis spectra of silver solutions prepared with different DMAB concentrations at a constant PAA concentration of 25 mM (fifth line of the silver multicolor map of Figure 3.1).

The spectra observed in Figure 3.5 reveal that the evolution of the absorption bands as a function of the DMAB added to the solution shows just the opposite behavior to the phenomenon observed when PAA was added (see Figure 3.2). The position of the maximum absorption bands shifts to shorter wavelengths when DMAB concentration was increased and the resulting colors are formed in a different order (from violet to orange) during the synthesis process.

According to the results observed in Figure 3.5, the evolution of both regions demonstrated that an absorption band at long wavelengths (region 2) is obtained in the first steps of color formation (violet or blue) with lower DMAB molar in the solution. However, when this DMAB molar is increased, the maximum absorption band shifts at shorter wavelengths (region 1) with the corresponding change of color (green or brown). Furthermore, when higher DMAB molar is added to the solution (only orange color), a new intense absorption band appears at 410 nm which is indicative of formation of silver nanoparticles with a spherical shape. These same spectral absorption variations in both regions have been observed with higher PAA concentrations (100 or 250 mM, respectively). In Figure 3.6 it is possible to appreciate the UV-Vis spectra corresponding to 250 mM PAA and variable DMAB molar concentration.

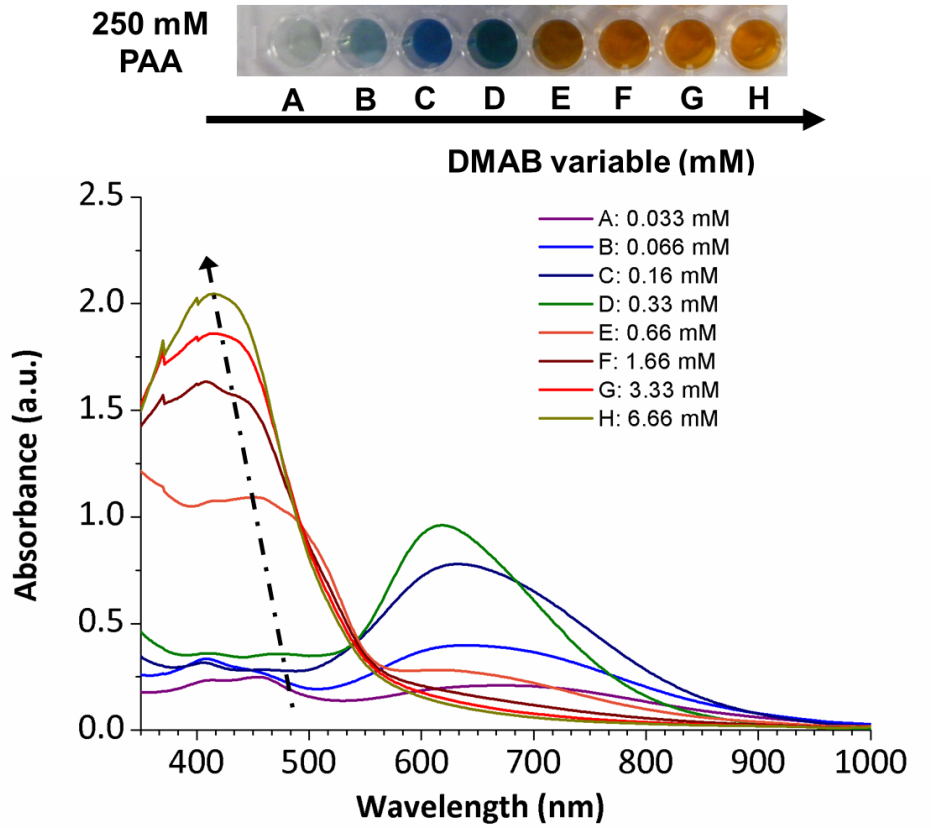

Figure 3.6. UV-Vis spectra of silver solutions prepared with different DMAB concentrations at a constant PAA concentration of 250 mM (seventh line of the silver multicolor map of Figure 3.1).

Similarly to what was made in the preceding Section 3.2.3, the Figure 3.7 is plotted in order to show a clearer picture of the evolution of the optical absorption bands in both regions (region 1 and 2) when the molar

concentration of DMAB is increased for a constant molar PAA concentration of 25 mM. In this Figure 3.7, it is easy to identify the increase in absorbance of region 2 from 0.033 to 0.33 mM DMAB. Conversely, from 0.33 to 6.66 mM DMAB, the absorbance in region 2 is decreased. However, the absorbance of region 1 always increases with the DMAB concentration. In view of these results, the influence of the DMAB concentration in the color of the synthesized AgNPs is also clear.

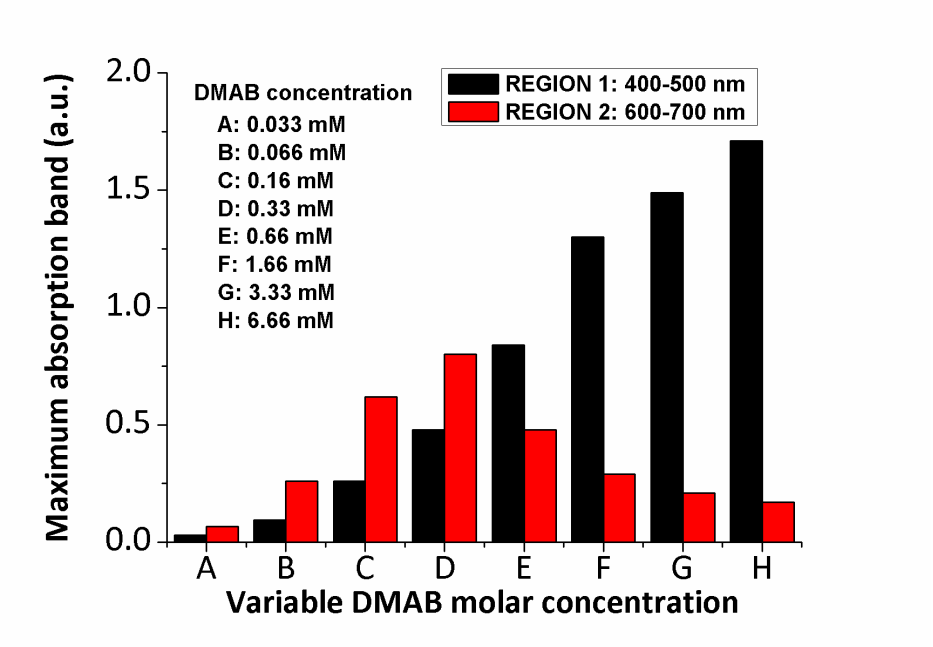

Figure 3.7. Evolution of the UV-Vis maxima absorption bands of the silver samples in region 1 and region 2 (400-500 nm and 600-700 nm respectively) prepared with different DMAB concentrations at a constant molar PAA concentration (25mM).

Figure 3.8 shows TEM micrographs of the synthesized silver nanoparticles and clusters with different DMAB molar ratios in the presence of 25 mM PAA, and in all cases, different shapes can be obtained. Initially, specific shape (triangle or hexagonal) were obtained when lower DMAB molar (0.066 or 0.16 mM respectively) was added (Figure 3.8a and 3.8b). However, these shapes and the resultant color dramatically changes (brown or orange color) when higher DMAB molar (0.66 and 3.33 mM) was added to the solution. The final position of their maximum absorption bands (UV-Vis spectroscopy) at 410 nm and the resultant orange color indicates the excitation of the Localized Surface Plasmon Resonance (LSPR) of spherical shapes (Figure 3.8d).

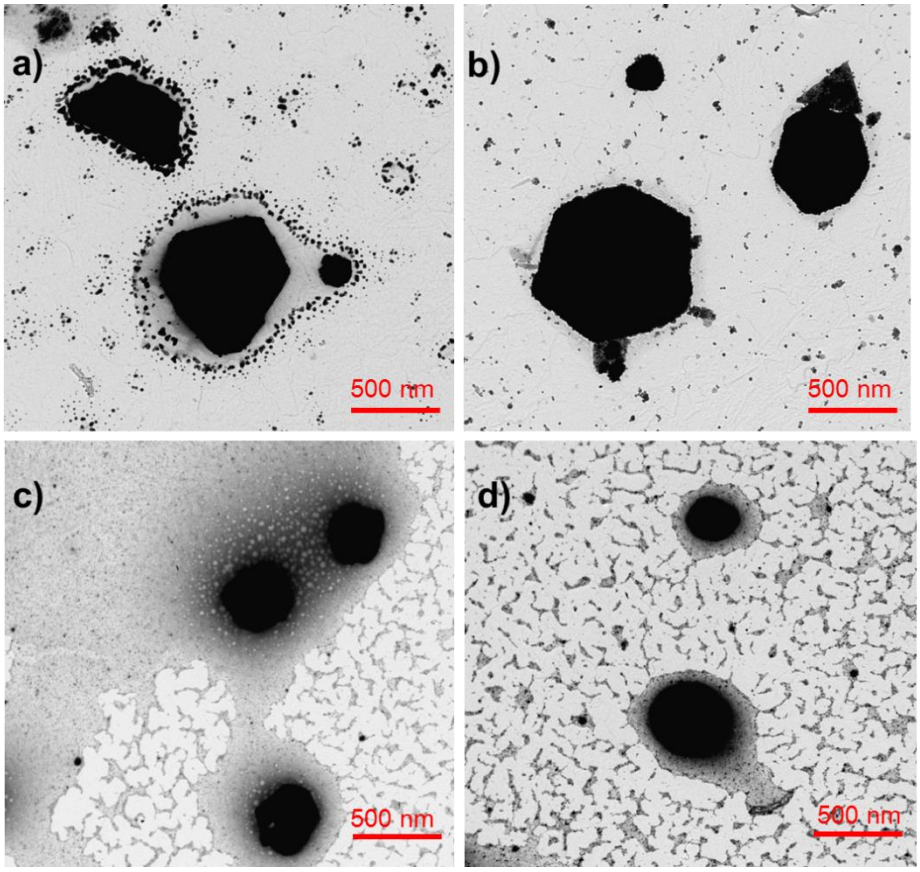

Figure 3.8. TEM micrographs show the formation of AgNPs with different shapes for different DMAB concentrations (a) triangle shape with 0.066 mM DMAB; (b) hexagonal shape with 0.16 mM DMAB; (c) quasispherical shape with 0.66 mM DMAB; (d) spherical shape with 3.33 mM DMAB. The PAA concentration was 25 mM.

An important aspect observed in this study is the same shape evolution (rod, triangle, hexagonal and spherical) for different PAA concentration when DMAB molar is gradually increased. Figure 3.9 shows similar evolution in the resulting shapes as a function of DMAB molar added in the presence of 10 mM PAA. Initially, rod or triangle shapes are observed for lower DMAB molar (0.033 and 0.066 mM), but a change in the shape to hexagonal or spherical are observed when DMAB molar is increased (0.66 or 6.66 mM respectively).

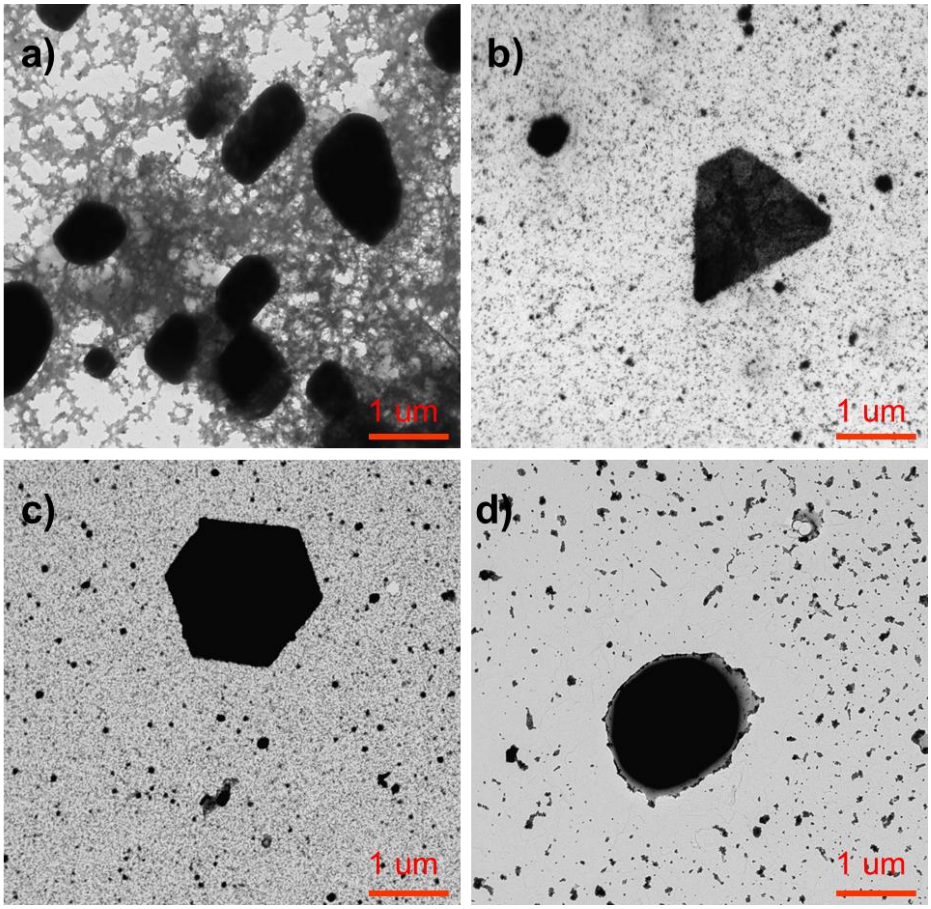

Figure 3.9. TEM micrographs show the formation of AgNPs with different shapes for different DMAB concentrations (a) rod shape with 0.033 mM DMAB; (b) triangle shape with 0.066 mM DMAB; (c) hexagonal shape with 0.66 mM DMAB; (d) spherical shape with 6.66 mM DMAB. The PAA concentration was 10mM.

To sum up, UV-Vis spectra are congruent with the nanoparticles shapes and sizes observed in the TEM micrographs. In these spectra, firstly an absorption band is obtained in the region 2 (600-700 nm) corresponding to rod, triangle or hexagonal shapes and secondly, this absorption band is displaced to shorter wavelength in the region 1 (400-500 nm), appearing an intense absorption band at 410 nm due to the synthesis of spherical nanoparticles.

3.2.5. Other considerations

A relevant aspect of this work is the synthesis of silver reddish nanoparticles in the presence of 2.5 mM PAA because this color is not obtained with lower or higher PAA concentrations. In figure 3.10 (left), it is possible to appreciate the evolution of the maximum absorption band (UV-Vis spectroscopy) when variable DMAB molar is added to the solution. It is worth noting that the intensity of the peak corresponding to red solution is broader than yellow or orange solution, indicating a considerable increase and aggregation in the number of synthesized silver nanoparticles. The maximum absorption band of this reddish solution is gradually shifted to lower wavelength (425 nm) in comparison with orange (435 nm) or yellow (445 nm) solution. These colors (yellow, orange or red), the position of their maximum absorption bands in the region 1 (400-500 nm) and the absence of absorption bands in region 2 (600-700 nm) indicate the complete synthesis of nanoparticles with a spherical shape which it is corroborated by TEM image (Figure 3.10, right).

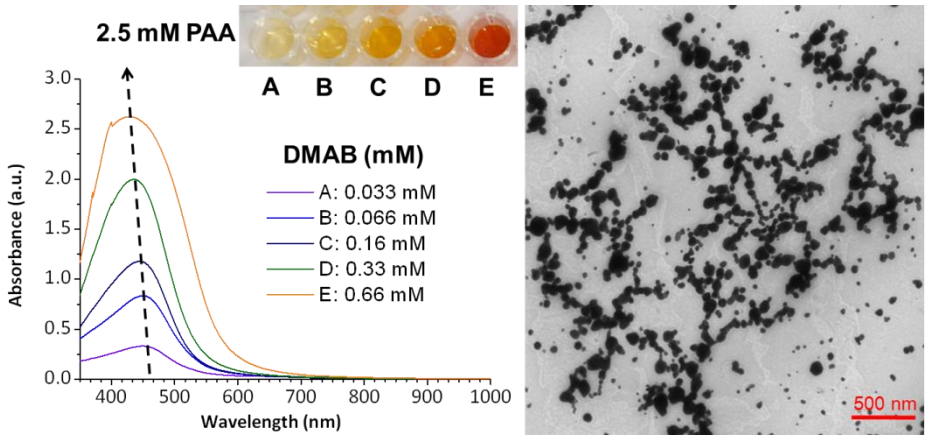

Figure 3.10. UV-Vis absorption spectra of silver solutions prepared with different DMAB concentrations at a constant PAA concentration of 2.5 mM (left); TEM micrograph of the reddish sample (0.66 mM DMAB) with aggregation of spherical nanoparticles (right).

3.2.6. Conclusions of the multicolor silver map

The fine control of two parameters in the AgNPs synthesis, PAA and DMAB molar concentration, makes possible the selection of the color of the AgNPs solutions, from violet to red, as well as the shape (spherical, rod, triangle, hexagonal, cube) and size (from nanometer to micrometer) of the nanoparticles. In Figure 3.11, a summary of the results obtained in the

multicolor silver map is presented as a function of the molar variation of PAA and DMAB. These synthesized AgNPs are unique in the sense that prior studies using different encapsulating agents to synthesize silver nanoparticles indicate that only an orange coloration is obtained without any color variation. In addition, the resultant AgNPs dispersions showed an excellent long-term stability since no changes in the position of their absorption bands have been observed after more than one year of storage at room conditions, corroborated by UV-Vis spectroscopy.

To our knowledge, this is the first time that an experimental matrix showing multicolor silver nanoparticles solutions with well-defined shape and size using both protective agent (PAA) and reducing agent (DMAB) has been reported in the bibliography.

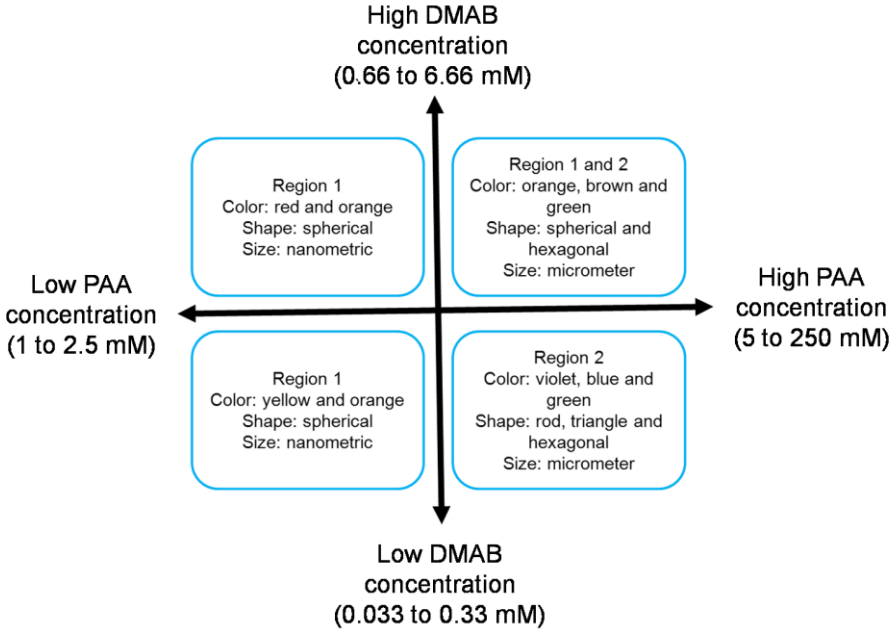

Figure 3.11. Evolution of the color formation, shape, size and region of the absorption bands as a function of PAA and DMAB molar concentration of the multicolor silver map.

3.3. Incorporation of silver nanoparticles into thin films using the Layer-by-Layer Embedding (LbL-E) deposition technique

In previous section 3.2, an analysis to obtain silver nanoparticles or clusters with a wide range of colors (violet, blue, green, brown, yellow, red, orange), sizes (from nanometer to micrometer) and shapes (cubic, rod, triangle, hexagonal, spherical) was presented by means of a fine control of protective (PAA) and reducing agent (DMAB) molar concentrations.

In this section, the incorporation of these previously synthesized silver nanoparticles with a specific coloration (violet, green and orange) into polyelectrolyte multilayer thin films using the Layer-by-Layer Embedding (LbL-E) deposition technique is presented. The aim of this section is to fabricate colored thin films which have the same coloration than initial AgNPs dispersions obtained in the previous section. The immobilization of AgNPs with different shape and size into thin films would open up a new interesting perspective to fabricate multicolor nanocomposites based on AgNPs.

3.3.1. Layer-by-Layer Embedding (LbL-E) deposition technique

This deposition technique is based on a first step of synthesis of AgNPs with a desired shape using PAA as a protective agent (PAA-AgNPs) and then, a second step, where the Layer-by-Layer Embedding (LbL-E) deposition technique of the previously synthesized AgNPs into a thin film is performed.

Silver nanoparticles have been synthesized at room temperature via chemical reduction process of an aqueous solution of silver precursor (silver nitrate, $AgNO_3$) with an aqueous solution of dimethylamine borane complex (DMAB) which acts as a reducing agent, as was previously explained in Section 3.2. In this synthesis process, the reduction of silver ions (Ag^+) to silver nanoparticles (Ag^0) is possible thanks to the use of a protective agent, poly(acrylic acid, sodium salt) (PAA) which can control the shape/size of the resultant nanoparticles and prevent their agglomeration or precipitation.

In this synthetic route for preparing the AgNPs, the protective agent used (PAA) is of vital importance in a further incorporation of the nanoparticles into a thin film using the Layer-by-Layer Embedding (LbL-E). This is due to the presence of free carboxylate groups at a suitable pH which are used to build the sequentially multilayer film in the LbL assembly. To perform this deposition technique, the electrostatic attraction between monolayers of opposite charge such as the cationic polyelectrolytes (PAH) and the anionic polyelectrolytes with the nanoparticles incorporated (PAA-AgNPs), makes

possible to obtain a thin multilayer film with a structure homogeneous, resistant and compact. The final coloration of the thin films can be tuned as a function of several parameters such as, the initial color of the AgNPs dispersions, the number of bilayers added or the pH of the dipping solutions. In Figure 3.12, a schematic representation of the LbL-E deposition technique is shown for an incorporation of AgNPs with spherical shape (orange color). However, the LbL-E process can be performed for AgNPs with a different shape, size and coloration, as it will be demonstrated in the following sections.

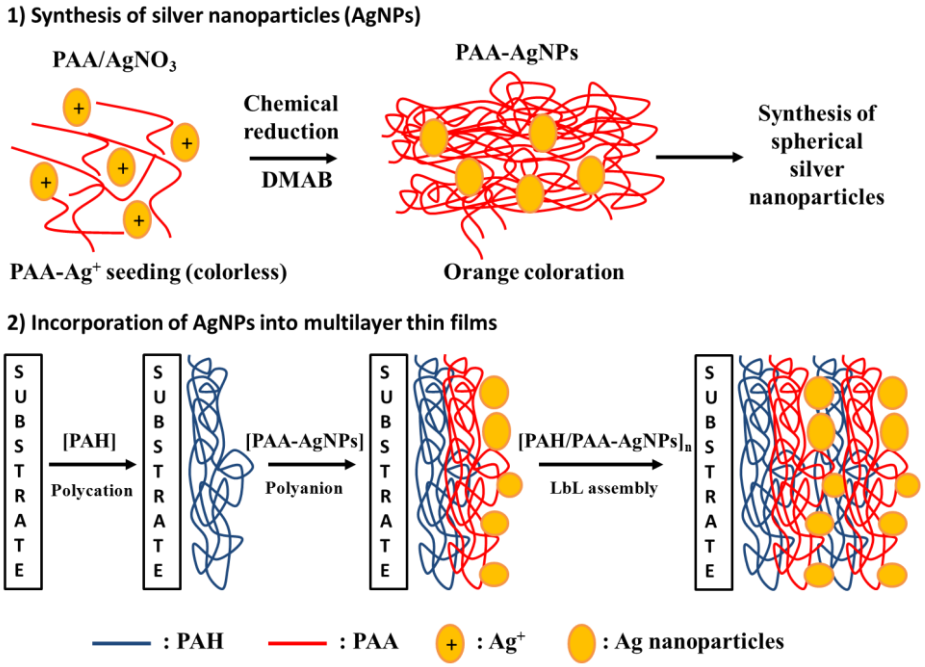

Figure 3.12. A schematic representation of the AgNPs synthesis (orange coloration; spherical shape) and a further progressive incorporation into thin films using the Layer-by-Layer Embedding (LbL-E) deposition technique.

3.3.2. Characterization

UV-Visible spectroscopy (UV-Vis) was used to characterize the optical properties of the multicolor silver nanoparticles and the resultant coatings obtained by LbL-E deposition technique. Measurements were carried out with a Jasco V-630 spectrophotometer.

Transmission electron microscopy (TEM) was used to determine the morphology (shape and size) of the silver nanoparticles obtained in aqueous solution. This TEM analysis was carried out with a Carl Zeiss Libra 120.

Samples for TEM were prepared by dropping and evaporating the solutions onto a collodion-coated copper grid.

Atomic force microscope (AFM) in tapping mode (Innova, Veeco Inc.) has been used in order to show the distribution of the AgNPs, thickness evolution of the films obtained by the LbL-E deposition technique.

3.3.3. Fabrication of orange colored films using the LbL-E

Initial experiments for the fabrication of colored thin films have been done at a specific concentration of PAA (10 mM, fourth line of the silver map of Figure 3.1) in order to compare the results with the *in situ* synthesis (ISS) of the AgNPs, obtained in chapter 2, where both weak polyelectrolytes (PAH and PAA) have been deposited at this concentration (10 mM). In addition, the same pH value (pH 9.0), number of bilayers and effect of the temperature have been investigated using the LbL-E deposition technique.

Silver nanoparticles are prepared by adding freshly reducing agent (dimethylamine borane, DMAB) to a stirred solution which contained 10 mM PAA concentration and constant $AgNO_3$ concentration (3.33 mM). The final molar ratio between reducing and loading agent (DMAB:$AgNO_3$ ratio) is 1:1. The final molar ratio between protective agent and loading agent (PAA:$AgNO_3$ ratio) is 3:1. Once the reaction was completed, the color was stable without any further modification. In Figure 3.13, the orange PAA-AgNPs synthesized and their further incorporation into thin films using the LbL-E deposition technique is shown. As was previously commented, the molar concentrations of both polyelectrolytes, PAH and PAA-AgNPs, are 10 mM and the pH value of the dipping solutions is 9.0.

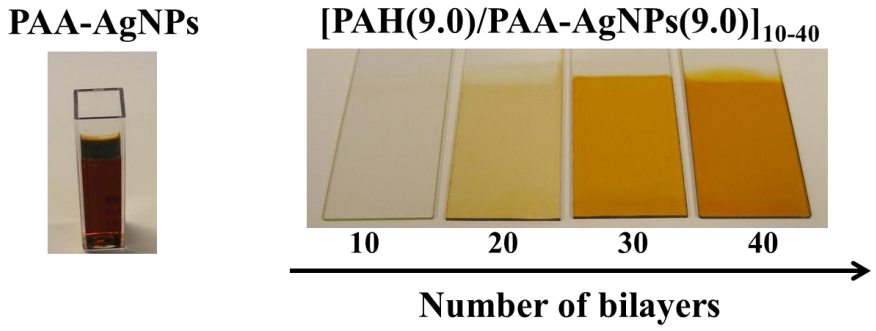

Figure 3.13. Synthesis of silver nanoparticles (AgNPs) with an orange coloration and a further incorporation into thin films using LbL-E as a function of the number of bilayers deposited.

It is worth noting that UV-Vis spectrum corresponding to the PAA-AgNPs shows an intense absorption band around 430 nm, as can be seen in Figure 3.14. One of the important properties of the metallic nanoparticles (i.e. silver) is the coherent oscillations of the metal electrons in resonance with light of a certain frequency called Localized Surface Plasmon Resonance (LSPR) [28-31]. The presence of this resonant absorption band at a desired wavelength depends on strongly of the particle size and shape [32-35], as was explained in Section 3.2. For this synthetic route of AgNPs, the orange coloration of the solution and the location of the band at this specific wavelength position (430 nm) indicate us that AgNPs with a spherical shape have been successfully synthesized.

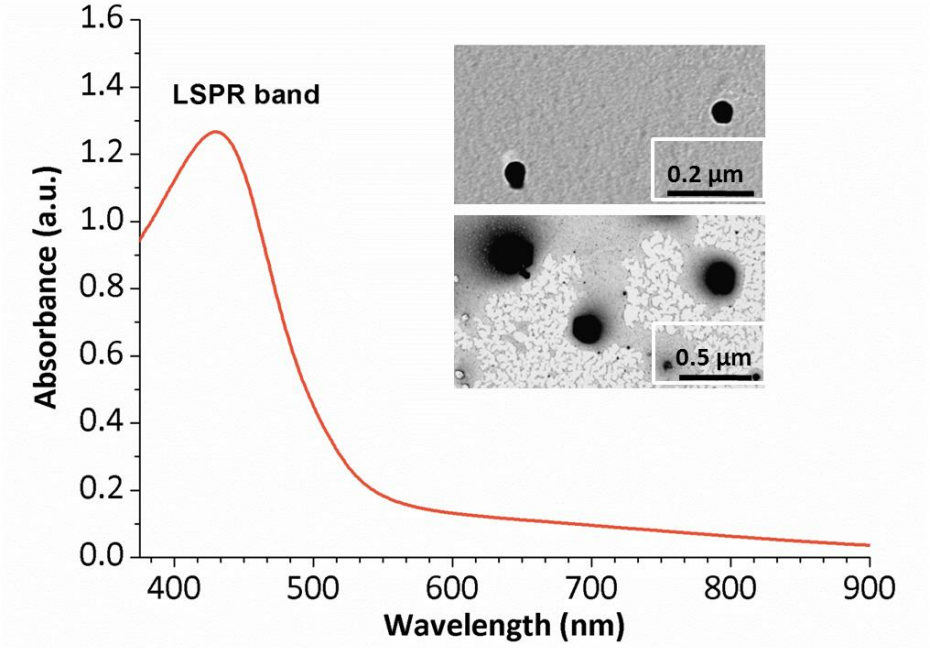

Figure 3.14. UV-Vis spectroscopy of silver nanoparticles (PAA-AgNPs) and the spherical shape with variable size obtained by TEM image (scale bar of 200 and 500 nm, respectively).

Once silver nanoparticles (AgNPs) with a spherical shape have been synthesized, a further incorporation of them into thin films using the LbL Embedding (LbL-E) deposition technique is performed. As was previously commented, the use of the PAA with its free carboxylate groups at a desired pH (pH 9.0) makes possible the binding with cationic polyelectrolytes such as PAH, being the electrostatic attraction between monolayers of opposite charge (cationic and anionic) the main force to obtain the thin films. In addition, in this specific synthetic process, it can be observed an increase of the orange coloration of the LbL-E films when the number of bilayers is increased from

10 to 40 bilayers (see Figure 3.13). These results of a better definition of the orange coloration when a higher number of bilayers are deposited indicate a higher incorporation of the spherical silver nanoparticles into the LbL-E films. In Figure 3.15, UV-Vis spectra of the LbL-E films as a function of the number of bilayers deposited are shown. A better definition in intensity of the LSPR band at 430 nm is observed when a higher number of bilayers are deposited.

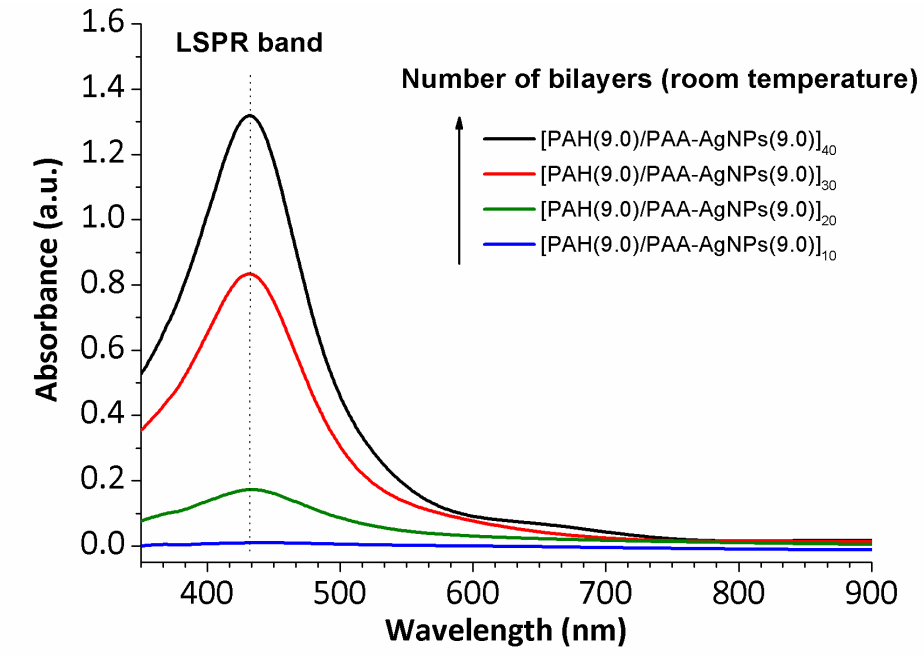

Figure 3.15. UV-Vis spectra of the orange multilayer films obtained by LbL-E deposition technique for different number of bilayers (10, 20, 30 and 40).

The influence of the temperature in these LbL-E films has been also evaluated. The coatings have been thermally treated at 150 ºC for two hours to improve the mechanical stability of the films and promote a chemical crosslink between the polymeric chains of both polyelectrolytes, PAH and PAA, as was explained in chapter 2. In addition, it is important to remark that higher values of temperature (i.e. melting point) produce a total evaporation of the polymeric chains (PAH and PAA) and so, the only contribution of the silver nanoparticles will be observed in the films.

In Figure 3.16, UV-Vis spectra of the LbL-E films after a thermal treatment of 150 ºC are shown as a function of the number of bilayers deposited (from 10 to 40 bilayers). In all the cases of study, an increase in intensity of the LSPR absorption bands has been observed in the UV-Vis spectra after this thermal treatment. This can be due to a better proximity of the synthesized

silver nanoparticles (AgNPs) into the LbL-E films after the thermal treatment and as a result, a higher value in intensity related to the LSPR band [83].

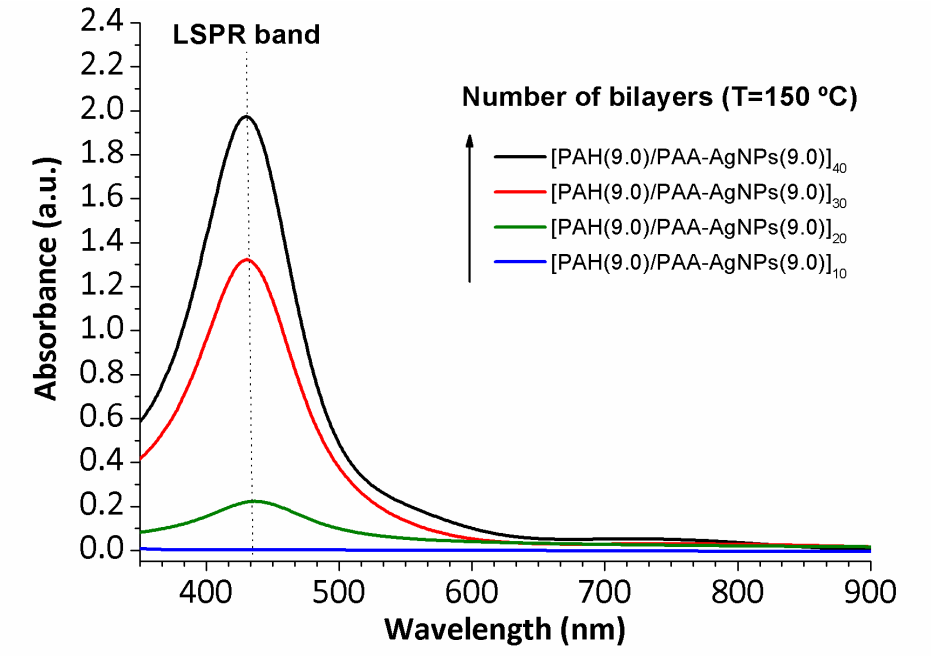

Figure 3.16. UV-Vis spectra of the orange multilayer films obtained by LbL-E deposition technique for different number of bilayers (10, 20, 30 and 40) after a thermal treatment (150 ºC).

In Figure 3.17, it is shown a comparison between the number of bilayers deposited (from 10 to 40 bilayers) and the maximum intensity at the LSPR wavelength position at room temperature and after thermal treatment (150 ºC). As was previously commented, a higher intensity of the LSPR absorption bands is observed when a higher thickness (number of bilayers) is deposited onto the substrate. This result is due to a higher number of AgNPs have been incorporated into the LbL-E films when the number of bilayers is increased during the fabrication process. In addition, the thermal treatment of the LbL-E films induces higher values in intensity at the LSPR wavelength position for all the cases of study (from 10 to 40 bilayers), as was also observed in the *in situ* synthesis of the AgNPs in Chapter 2 (section 2.3). The main reason of this increase in intensity of the LSPR absorption band can be due to the partial thickness reduction (see Table 3.1) after thermal treatment, and as a result the better proximity of the AgNPs.

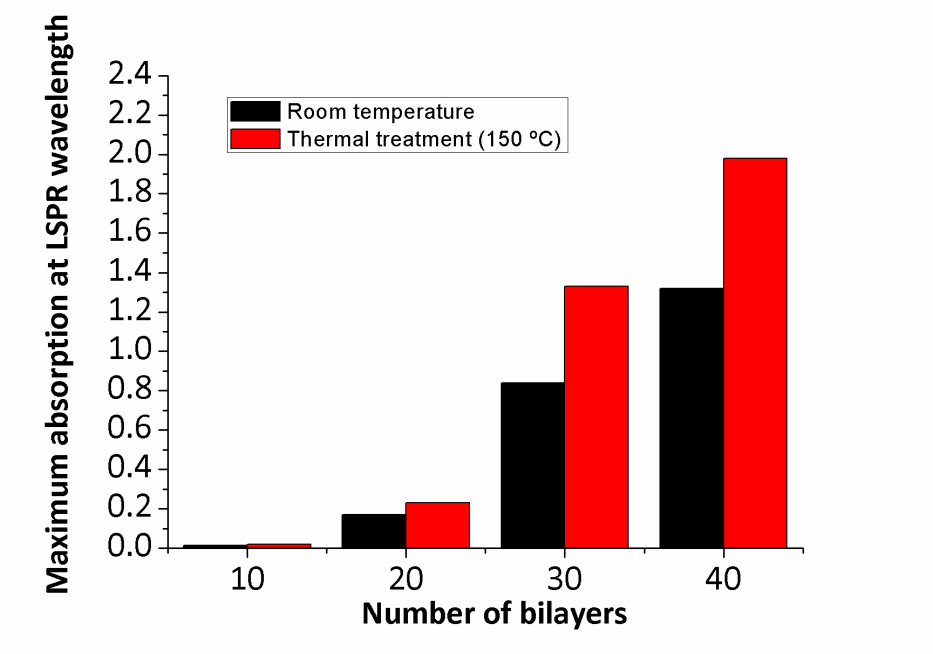

Figure 3.17. Evolution LSPR absorption bands at room temperature and after thermal treatment.

Table 3.1. Average evolution thickness as a function of the number of bilayers added.

Fabrication process	Thickness (nm) (room temperature)	Thickness (nm) (T 150 ºC)
$[PAH(9.0)/PAA\text{-}AgNPs(9.0)]_{10}$	62.7 ± 4.8	47.7 ± 5.1
$[PAH(9.0)/PAA\text{-}AgNPs(9.0)]_{20}$	164.7 ± 4.4	120.4 ± 6.5
$[PAH(9.0)/PAA\text{-}AgNPs(9.0)]_{30}$	507.3 ± 15. 7	433.9 ± 12.3
$[PAH(9.0)/PAA\text{-}AgNPs(9.0)]_{40}$	641.7 ± 12.3	497.3 ± 12.6

In this section, it has been demonstrated the possibility of obtaining orange colored LbL-E thin films due to the succesive incorporation of orange AgNPs during the fabrication process which was corroborated by UV-Vis spectra and the visual appearance of the films (glass slides). However, the possibility of obtaining multicolored films as a function of the initial colored AgNPs has not yet been studied. In the next section, the fabrication of multicolored thin films using the LbL-E deposition technique will be presented.

3.3.4. Fabrication of multicolored thin films using the LbL-E

In order to obtain multicolored thin films, the LbL-E corresponding to PAA-AgNPs for a concentration of 25 mM has been selected. The main reason of this decision is due to a wide range of colors with a better definition for PAA 25 mM (fifth line of silver map) in the same experimental conditions have been obtained in comparison with PAA 10 mM (fourth line), as can be seen in Figure 3.1. This section will be divided in several subsections such as, the preparation of the multicolor AgNPs, effect of the pH, fabrication of the multicolored LbL-E thin films and their thickness evolution.

3.3.4.1. Synthesis of silver nanoparticles of the multicolor map

Multicolor silver nanoparticles have been prepared by adding freshly variable DMAB concentration (0.033, 0.33 and 3.33 mM) to vigorously stirred solution which contained constant PAA (25 mM) and $AgNO_3$ concentrations (3.33 mM). This yields a molar ratio between the protective and loading agent ([PAA]/[$AgNO_3$] ratio of 7.5:1. The final molar ratios between the reducing and loading agents ([DMAB]/[$AgNO_3$] ratio) were 1:100, 1:10 and 1:1.

In Figure 3.18, it is possible to appreciate three different colors obtained (violet, green and orange) using PAA as an encapsulating agent (PAA-AgNPs) when DMAB concentration is increased (from 0,033 mM to 3.33 mM).

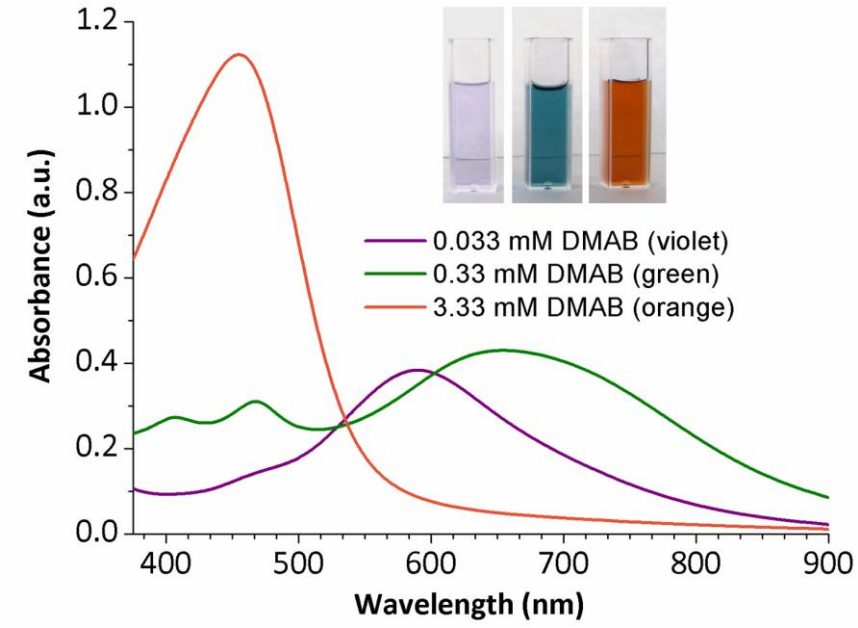

Figure 3.18. UV-Vis spectra of the multicolored silver nanoparticles (violet, green and orange) as a function of variable DMAB concentration (0.033, 0.33 and 3.33 mM).

Initially, the mixture of 25mM PAA with $AgNO_3$ is colorless (control), but after the addition of 0.033 mM of DMAB, the mixture turns quickly to violet with a plasmonic absorption peak with a maximum centered at 600 nm. When DMAB concentration is increased (0.33 mM), the sample changes from violet to green. The absorption band distribution in the UV-Vis spectrum was altered significantly. The initial absorption band was increased significantly, and it was also shifted toward longer-wavelengths (at 650 nm). Furthermore, a new absorption band was found at 480 nm related with the coexistence of different AgNPs aggregation states or shapes. Finally, when DMAB concentration is increased to 3.33 mM, the solution turned to orange color and only an intense absorption band around 440 nm was observed, indicating the complete synthesis of spherical silver nanoparticles. The evolution of these absorption bands in two well separated regions (region 1 for the 400- 500 nm and region 2 for the 600-700 nm) has been discussed in the previous section 3.2.

These changes in the UV-vis spectra (colors) are related to changes in the shape, size and aggregation state of the AgNPs. In order to corroborate this hypothesis, TEM micrographs (500 nm and 2 μm) of the different samples (PAA-AgNPs) were performed (see Figure 3.19).

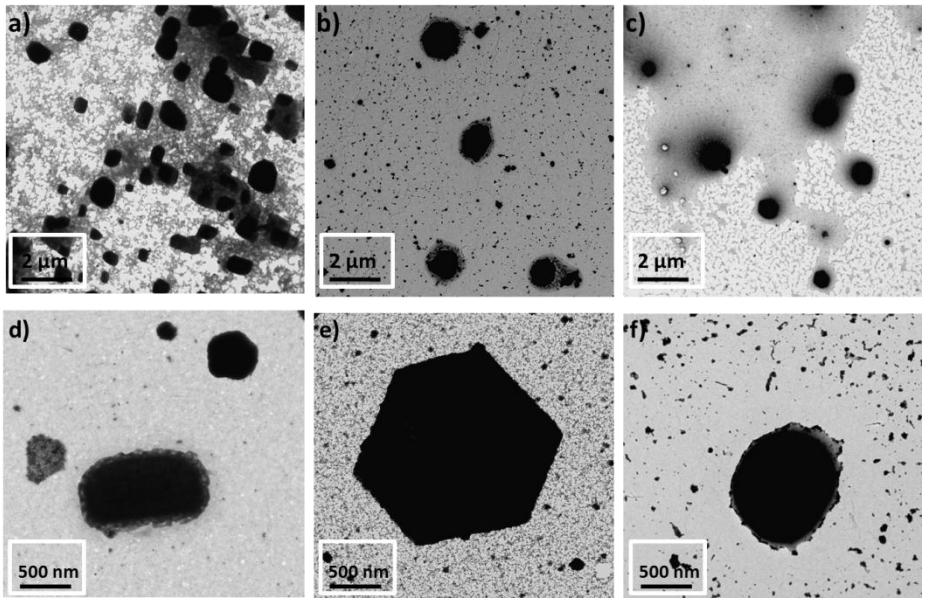

Figure 3.19. TEM micrographs of the multicolored silver nanoparticles at different scale (500 nm and 2 μm). (a,d) rod shape (violet coloration); (b,e) hexagonal shape (green coloration); (c,f) spherical shape (orange coloration).

According to the results observed in Figures 3.18 and 3.19, when molar DMAB concentration added in the reaction mixture is low, violet coloration ([DMAB]/[$AgNO_3$]=0.01) or green coloration ([DMAB]/[$AgNO_3$] = 0.1) is

obtained with a typical long-wavelength absorption band (600-700 nm). In addition, a new absorption band at 480 nm can be observed for green coloration, which it corresponds to complexes of small positively charged metal clusters and polymer ligands of the polyacrylate anions (PAA) [59-61]. However, other authors report that the presence of two distinct plasmon bands could be related to transverse and longitudinal electron oscillations when the synthesized metal nanoparticles show a slight variation from spherical geometry [29, 30]. And finally, when molar DMAB concentration is increased ([DMAB]/[$AgNO_3$] = 1), an orange coloration with an only intense absorption band at 440 nm is observed. In addition, it has been also found that AgNPs with a specific shape and size (see Figure 3.19) can be perfectly obtained. Nanorods of variable size are synthesized for violet coloration. Additionally, clusters with a hexagonal shape (from 0.5-1 µm) mixed with spherical particles of nanometric size are found for green coloration. And spherical nanoparticles with a variable size are observed for orange coloration.

These results corroborate that the excess of free Ag^+ cations immobilized into the polyelectrolyte chains of the PAA respect to the reducing agent, plays a key role in the synthesis process, yielding different nanoparticle size distributions and aggregation states. It is important to remark that changes in the plasmonic absorption bands (resultant color) basically depend on the relationship between the aggregation state of the nanoparticles (even in the cluster formation) and the final shape/size of the resultant nanoparticles. A control of all these parameters is the key to understand the color formation in the resultant films. In Table 3.2, a summary of the different AgNPs dispersions as well as molar concentration [DMAB]/[$AgNO_3$], their corresponding shapes and sizes are shown for a constant PAA concentration (25mM) is shown.

Table 3.2. Characteristics of the PAA-AgNPs dispersions reported in previous sections

Color	[DMAB] / [$AgNO_3$]	Shape vs size
Violet	0.01	Rod (variable nm or µm)
Green	0.1	Hexagonal (0.5-1 µm) Spherical (nm)
Orange	1	Spherical (variable nm or µm)

3.3.4.2. Effect of the pH in the colored PAA-AgNPs dispersions

An important consideration of this work is the pH value of the AgNPs solutions when the deposition process is performed. As can be seen in Figure 3.20, keeping PAA-AgNPs at pH 7.0 or higher pH values plays a key role in order to preserve the aggregation state of the nanoparticles during the synthesis process with a good control of the resultant color without any further precipitation. However, when the pH of the dipping solutions (PAA-AgNPs) is lowered below 7.0, a change of the coloration is observed in all the experiments. An increase in opacity and a further precipitation with a complete loss of color (transparent solutions) at low pH values (pH 4.0 or lower) of the PAA-AgNPs are obtained. Due to these changes concerning to the resultant coloration as a function of the pH for PAA-AgNPs, the reason of choosing pH 7.0 or higher values is the base to obtain the multicolored LbL-E films.

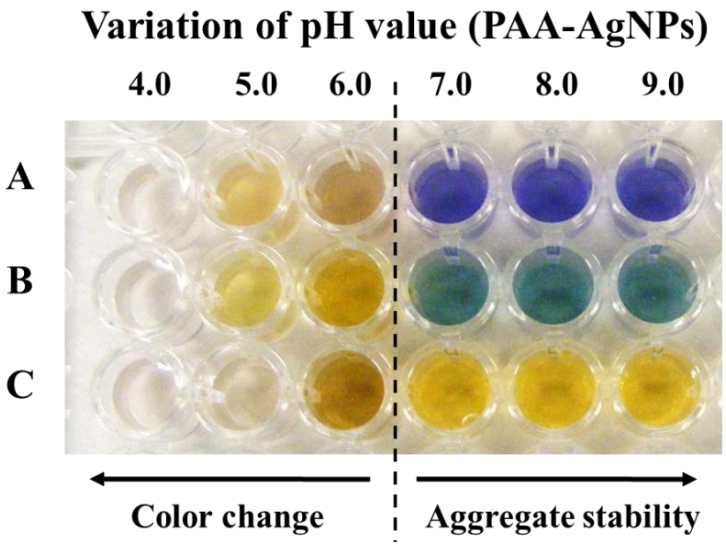

Figure 3.20. Variation of the multicolored silver nanoparticles (PAA-AgNPs) as a function of the pH value for violet (file A), green (file B) and orange coloration (file C).

Once multicolored silver nanoparticles (AgNPs) have been successfully synthesized and the pH value has been evaluated, the next step is the incorporation of them in a polyelectrolyte multilayer film using the LbL-E deposition technique. The main goal is to get coatings with the similar coloration that the initial colored PAA-AgNPs solutions (violet, green and orange).

3.3.4.3. Experimental conditions of the LbL-E deposition technique

Aqueous solutions of PAH and PAA-AgNPs with a concentration of 25 mM with respect to the repetitive unit were prepared using ultrapure deionized water (18.2 MΩ·cm). The pH was adjusted to 7.5 by the addition of a few drops of NaOH or HCl. The LbL-E deposition technique was performed by sequentially exposing the glass slide (substrate) to cationic polyelectrolyte poly(allylamine hydrochloride) (PAH) and anionic polyelectrolyte PAA loaded with the silver nanoparticles previously synthesized (PAA-Ag NPs) with an immersion time of 5 minutes. A rinsing step of 1 minute in deionized water was performed between the two polyelectrolytes baths and a drying step of 30 seconds was performed after each rinsing step. The combination of a cationic monolayer with an anionic monolayer is called bilayer.

3.3.4.4. Fabrication of the multicolored LbL-E films

The effect of the pH of the dipping solutions is the key to understand the color formation in the films. During the fabrication process, a pH of 7.5 for both PAH and PAA-AgNPs is chosen to fabricate the LbL-E thin films. In addition, the fundamental element to obtain the multilayer buildup is the presence of ionized groups of these weak polyelectrolytes, which they are responsible for the electrostatic assembly and the spatial control of the previously silver nanoparticles distribution (colored PAA-AgNPs) in the multilayer LbL-E films when the number of bilayers is increased.

In Figure 3.21, a detail of the evolution of the absorption bands (UV-Vis spectra) and their corresponding color formation during the LbL-E deposition technique for both PAH and PAA-AgNPs (orange coloration) is shown as a function of the number of bilayers added to the film. From these results, it can be said that a successful deposition of orange colored LbL-E films was obtained when the number of bilayers was increased. This result related to orange coloration of the LbL-E films was previously obtained for lower molar concentrations of both polyelectrolytes (10 mM PAH and PAA-AgNPs) as can be seen in Figure 3.13. A LSPR absorption peak centred at 430 nm grows as a function of the number of bilayers deposited onto glass slides via LbL-E deposition technique (10, 20, 30 and 40 bilayers, respectively). The increase of both intensity of the absorption band at 430 nm and the orange coloration of the LbL-E films during the fabrication process (higher number of bilayers), is the result of a successful incorporation of spherical AgNPs into the thin films.

The next step will be to incorporate violet silver nanoparticles in the LbL-E thin films. In Figure 3.22, the evolution of the absorption bands corresponding to PAH and PAA-AgNPs (violet) is studied for the same number of bilayers.

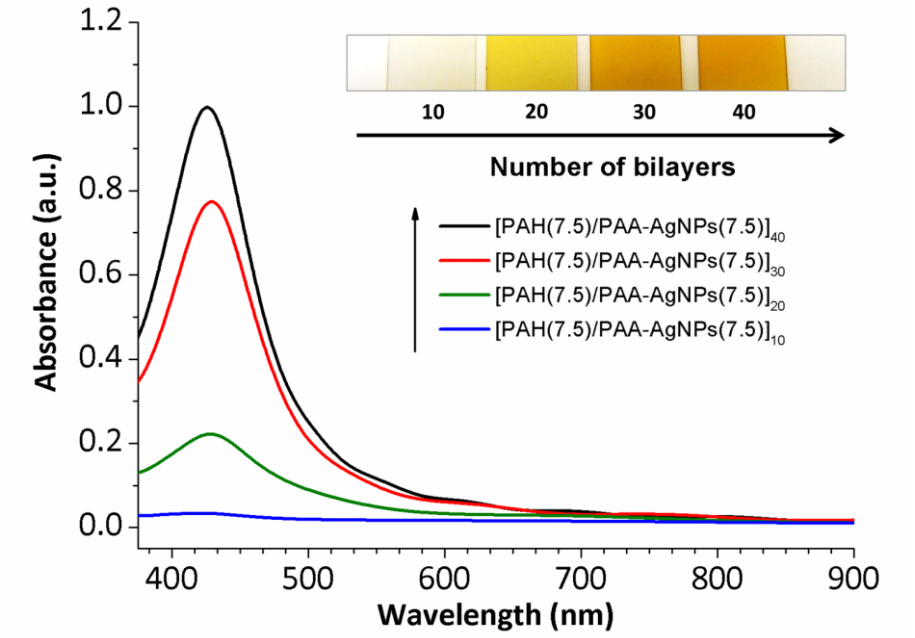

Figure 3.21. UV-Vis spectra of the orange multilayer films obtained by LbL-E deposition technique for different number of bilayers (10, 20, 30 and 40) and photographs of the coatings.

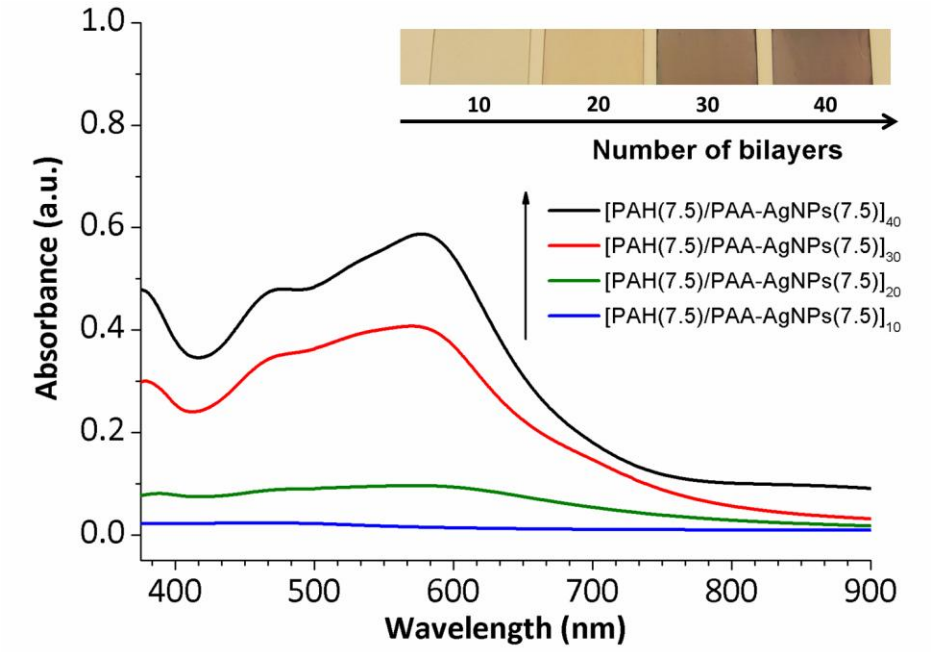

Figure 3.22. UV-Vis spectra of the violet multilayer films obtained by LbL-E deposition technique for different number of bilayers (10, 20, 30 and 40) and photographs of the coatings.

According to the results observed in Figure 3.22, an increase of the absorption peak from 10 bilayers to 40 bilayers at a specific wavelength position is observed. The location of this absorption band, which is higher in intensity when the thickness of the coating is increased, maintains the same position that initial synthesized violet silver nanoparticles (PAA-AgNPs) at 600 nm (see Figure 3.18). In view of these results, UV-Vis spectra reveal identical absorption peaks for both LbL-E deposition technique and the synthesized PAA-AgNPs (violet solution), which it means that silver nanoparticles with a specific shape (mostly rods) have been successfully incorporated into the multilayer films.

In Figure 3.23, the evolution of the absorption bands corresponding to the coating of PAH and PAA-AgNPs (green) during LbL-E is shown. The UV-Vis spectra of the resulting coatings at different number of bilayers confirm the existence of two absorption peaks during the multilayer assembly, one at 620 nm typical of green AgNPs which is lower in intensity and the other one, higher in intensity at 440 nm. For this case, it is possible to appreciate a difference in the UV-Vis spectra between the LbL-E films and the previously green colored PAA-AgNPs (see Figure 3.18).

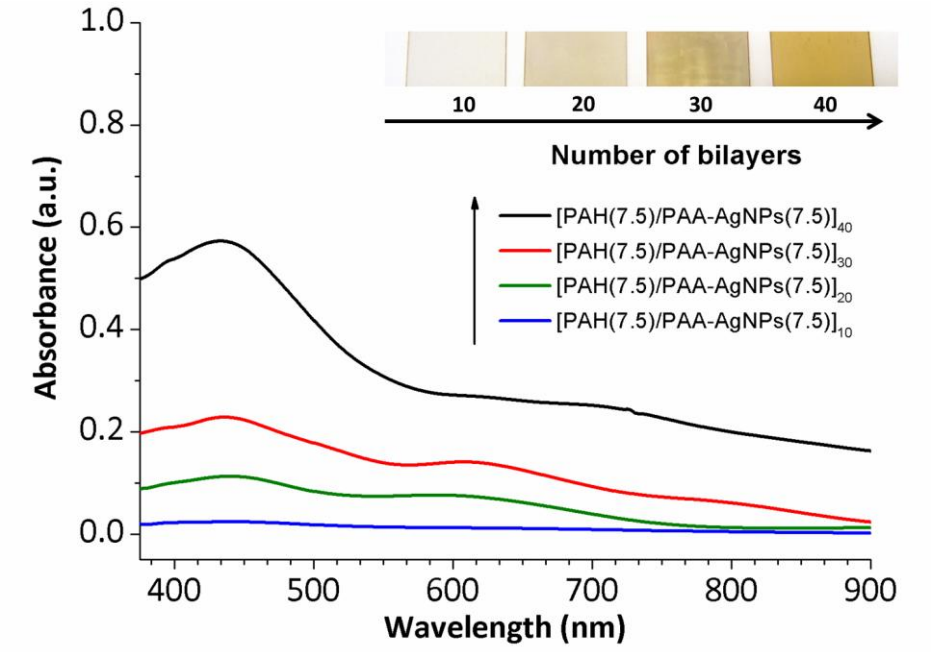

Figure 3.23. UV-Vis spectra of the green multilayer films obtained by LbL-E deposition technique for different number of bilayers (10, 20, 30 and 40) and photographs of the coatings.

The presence of a higher and broader absorption band at 440 nm can be due to an agglomeration and higher number of the AgNPs inside of the thin film

and the presence of AgNPs with different shape (not only hexagonal shape). This approach is corroborated by the final coloration of the resultant coatings where a light orange coloration instead of clearly green coloration is observed. A possible reason of this spectral change (color) in comparison with previously green PAA-AgNPs could be associated to the reduction of the metal clusters with a partial positive charge by the amine groups [85-88] of the PAH during the LbL assembly.

However, this hypothesis has not been confirmed for the violet coloration (Figure 3.22) when the number of bilayers onto glass slides was continuously increased, so we can conclude that a reduction by the amine groups of PAH and a further *in situ* generation of the spherical AgNPs is not observed. According to the results, the presence of the absorption band at 440 nm is associated to the incorporation of AgNPs with less size (mostly spherical nanoparticles) during the fabrication process (observed by TEM images), whereas the absorption band at 620 nm is lower in intensity because of a more difficult incorporation of higher size particles (metal clusters with hexagonal shape) in the multilayer LbL-E films for a total number of 40 bilayers. As conclusion, a selective absorption process is observed and as result, the partial orange coloration of the resultant films is due to a higher presence of spherical AgNPs in comparison with hexagonal clusters.

3.3.4.5. Thickness evolution of the colored LbL-E thin films

In previous sections, a study of the position of the absorption bands with their corresponding intensities and the aspect in coloration of the LbL-E films has been analyzed to understand the incorporation of the multicolor AgNPs. However, to create a template of well-defined coloration, the thickness of the resulting films to incorporate the AgNPs also plays a key role, which can be controlled by two parameters, pH value of the polyelectrolyte solutions (PAH and PAA-AgNPs) and the number of bilayers added onto glass slides [89-92].

When the pH of the dipping solutions is 7.5, both PAH and PAA-AgNPs are adsorbed as fully charged polyelectrolytes and very thin films are obtained. For a total of 40 bilayers, the final average thickness is varied from 185.2 nm (PAH/PAA-AgNPs violet coating), 223.3 nm (PAH/PAA-AgNPs orange coating) to 293.4 nm (PAH/PAA-AgNPs green coating). In table 3.3, a summary of the thickness evolution related to these multicolored LbL-E thin films is presented for a specific number of bilayers added.

Table 3.3. Average evolution thickness of the multicolored LbL-E films (violet, green and orange) for a pH deposition of 7.5 as a function of the number of bilayers added.

Number of bilayers	Violet	Orange	Green
$[PAH(7.5)/PAA\text{-}AgNPs(7.5)]_{10}$	34.6 ± 2.6 nm	38.3 ± 2.5 nm	44.1 ± 2.8 nm
$[PAH(7.5)/PAA\text{-}AgNPs(7.5)]_{20}$	87.1 ± 5.2 nm	100.7 ± 3.6 nm	94.3 ± 6.8 nm
$[PAH(7.5)/PAA\text{-}AgNPs(7.5)]_{30}$	138.4 ± 3.6 nm	154.7 ± 7.5 nm	167.2 ± 6.5 nm
$[PAH(7.5)/PAA\text{-}AgNPs(7.5)]_{40}$	185.2 ± 4.1 nm	223.3 ± 4.3 nm	293.4 ± 7.5 nm

The evolution of the thickness for different number of bilayers (10, 20, 30 and 40, respectively) with their corresponding error bars in this pH regime (7.5) is shown for each LbL-E film in Figure 3.24.

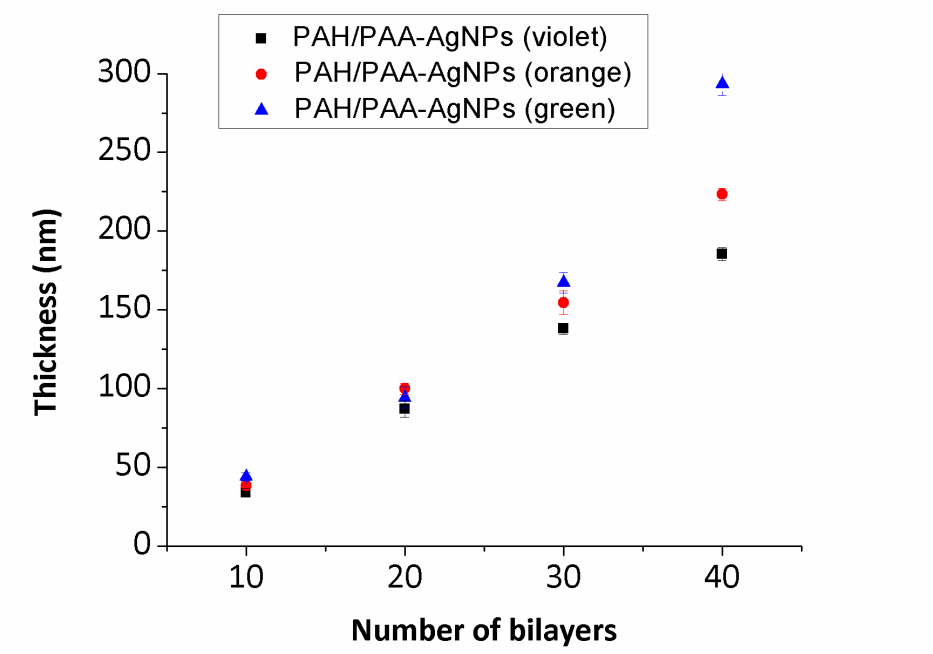

Figure 3.24. Evolution thickness of the PAH/PAA-AgNPs multilayer assemblies (violet, green, orange) for different number of bilayers (10, 20, 30 and 40) with their error bars.

As was previously commented, the effect of the pH of the dipping solutions plays a key role in order to understand the thickness contribution in the LbL-E films. In Table 3.1, when the pH of the dipping solutions is 9.0, the PAA polymeric chains are adsorbing in their fully ionized state whereas PAH polymeric chains at this pH start to lose protons and become less ionized. This combination of layer totally ionized (PAA) with a layer partially ionized (PAH) results in thicker coatings. However, when the pH of the dipping solutions is 7.5, both polyelectrolytes PAH and PAA are adsorbing as fully charged species and as a result, thinner coatings are obtained (see Table 3.3). This aspect related to thickness contribution of the polymeric chains of both PAH and PAA, has been corroborated in literature [90, 91]. More specifically, the [PAH/PAA] at pH 7.5 contributes with a thickness of 0.5 nm/bilayer, whereas [PAH/PAA] at pH 9.0 contributes with a resultant thickness of 10.7 nm/bilayer [90]. As conclusion, the pH-dependent bilayer behavior is demonstrated for two pH values, 7.5 and 9.0, making possible to obtain thin films with variable thickness as a function of the degree of ionization of the polymeric chains PAH and PAA controlled by the pH, and the number of bilayers incorporated during the LbL-E deposition technique [93].

According to these results observed in Tables 3.1 and 3.3, the resultant thickness of the LbL-E films depends strongly on degree of ionization of the weak polyelectrolytes (pH of both PAH and PAA) and the number of bilayers. In addition, the color of the LbL-E films depends on the shape and size of the AgNPs incorporated. Obviously, in all the cases of study, the final coloration (intensity of the LSPR bands) will increase when a higher number of AgNPs are incorporated during the LbL-E process (thicker coatings).

3.3.4.6. Morphological aspect of the multicolored LbL-E thin films

In order to show the final aspect and morphologies of the LbL-E thin films, AFM images of $[PAH(7.5)/PAA\text{-}AgNPs(7.5)]_{40}$ have been performed. In all the cases of study, the polymeric chains of the weak polyelectrolytes are predominant in the outer surface, whereas the visible AgNPs show a random distribution in the outer surface of these LbL-E films. In Figure 3.25, the light spots in height images (a, c, f) are the AgNPs observed in the outer surface which have been incorporated during the fabrication process. These AFM images correspond to a $[PAH(7.5)/PAA\text{-}AgNPs(7.5)]_{40}$ coating (violet, orange and green color) and the resultant films show a high uniformity with a smooth roughness. In order to show the presence of these AgNPs in the LbL-E thin films, a thermal curing of 450 ºC was applied to the LbL-E films with the idea of a complete evaporation of the polymeric chains (PAH and PAA) and so, the contribution of the AgNPs can be appreciated in the LbL-E films.

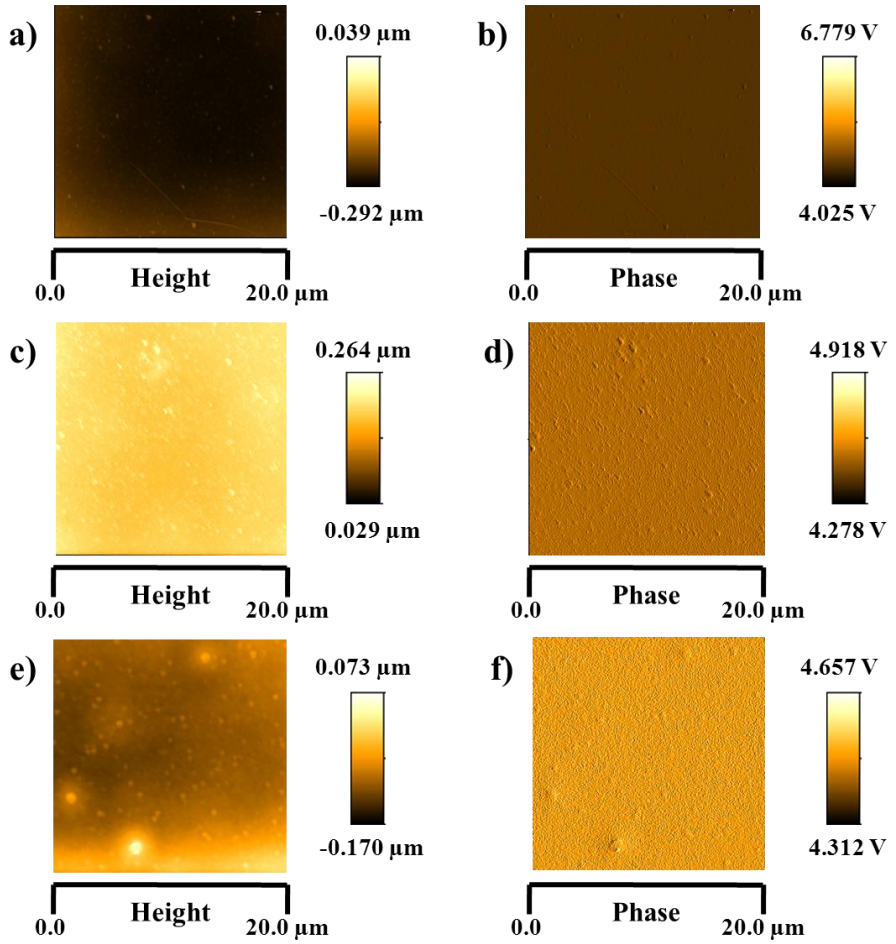

Figure 3.25. AFM images in tapping and phase mode of a coating of $[PAH(7.5)/PAA\text{-}AgNPs(7.5)]_{40}$ (a,b) violet coloration; (c,d) orange coloration and (e,f) green coloration.

In Figure 3.26, AFM images corresponding to 10, 20, 30 and 40 bilayers of [PAH(7.5)/PAA-AgNPs(7.5)] (violet color) after a thermal curing of 450 ºC are shown. According to the AFM images, when the thickness coating is lower (10 bilayers), it is possible to appreciate how well-separated AgNPs are incorporated into the LbL-E films. However, when the thickness is gradually increased, a higher number of AgNPs are being incorporated into LbL-E films. In addition, after this thermal treatment, the total evaporation of the polymeric chains induces an agglomeration of the AgNPs without preserving their distribution along the LbL-E, as can be observed in Fig. 3.26 b, c, d).

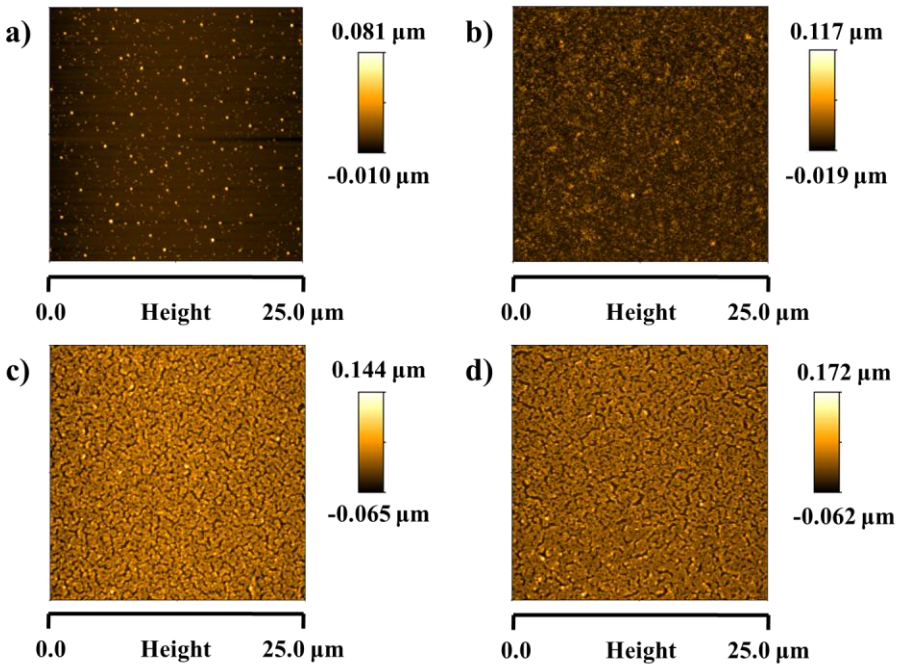

Figure 3.26. AFM images (tapping mode, 25x25 µm) of [PAH(7.5)/PAA-AgNPs(7.5)] (violet color) (a) 10 bilayers; (b) 20 bilayers; (c) 30 bilayers and (d) 40 bilayers, after thermal curing of 450 ºC.

In order to show an incorporation of AgNPs with a specific shape during the LbL-E deposition technique, AFM images in tapping mode with a smaller scan were performed. In Figure 3.27, AgNPs with nanorod shape (violet coloration) can be perfectly observed after the thermal curing of 450 ºC (a). The nanorods showed an approximated size of 200 nm (b).

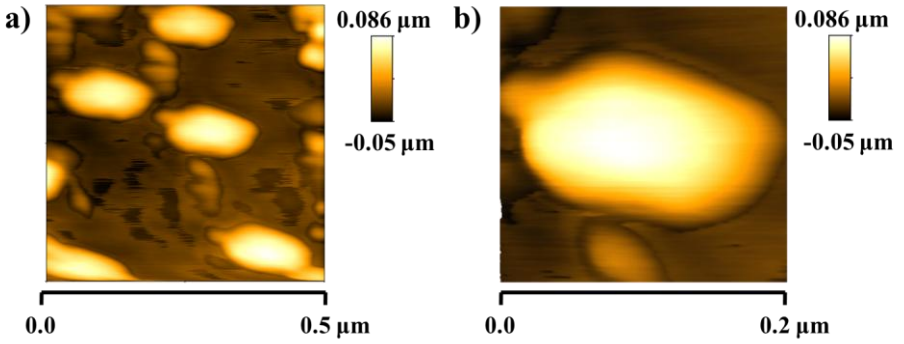

Figure 3.27. AFM image (tapping) of [PAH(7.5)/PAA-AgNPs(7.5)] (violet coloration) (a) scan 0.5x0.5 µm, nanorods distribution; (b) scan 0.2x0.2 µm, nanorod size, after thermal curing of 450 ºC.

In Figure 3.28, AFM images related to a coating based on PAA-AgNPs dispersions with a green coloration, AFM images reveal that the coating is composed of nanoparticles with a higher size (b) mixed with spherical nanoparticles (b), as was commented in previous sections (corroborated by TEM images and UV-Vis spectra). The LbL-E related to a coating of 40 bilayers showed a light orange coloration instead of green coloration due to a selective absorption process of the nanoparticles of lower size (spherical) and as result, partial orange coloration is observed. The AFM image corroborates this aspect where both spherical and particles of higher size (clusters) are being embedded during the LbL-E deposition technique.

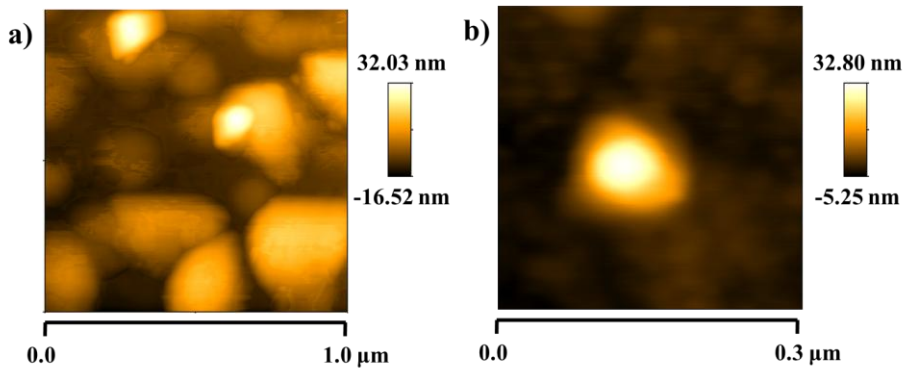

Figure 3.28. AFM image (tapping) of [PAH(7.5)/PAA-AgNPs(7.5)] (green coloration) (a) scan 1.0x1.0 µm, clusters mixed with spherical nanopartilcles; (b) scan 0.3x0.3 µm, spherical shape, after thermal curing of 450 ºC.

3.3.4.7. Final aspect of the multicolored LbL-E thin films

As a conclusion of the previous sections, in order to entrap AgNPs with a higher size (mostly hexagonal clusters of 0.5-1 µm) into the LbL-E thin films, a higher number of bilayers during the fabrication process (80 bilayers), and consequently, a higher thickness of the resultant films, promote a better definition of the color, mostly in the green coloration. For this specific case, a better entrapment of both initial clusters (hexagons with higher size) with nanometric spherical AgNPs in the multilayer assembly is observed due to a clearer green coloration instead of light orange (observed in Section 3.3.4.4).

In Figure 3.29, [PAH(7.5)/PAA-AgNPs(7.5)$_{80}$ coatings have been fabricated in order to show clearly the final coloration of the films onto glass slides as a function of the initial synthesized multicolor silver nanoparticles (PAA-AgNPs). In all the cases, LbL-E films with an orange (a), green (b) and violet (c) coloration are shown. In Figure 3.29d, the visual appearance of all the LbL-E thin films (orange, green and violet) indicate us the possibility of obtaining the multicolored thin films with a better definition of the resultant color when

a high number of the AgNPs with a specific shape and size are incorporated during the fabrication process.

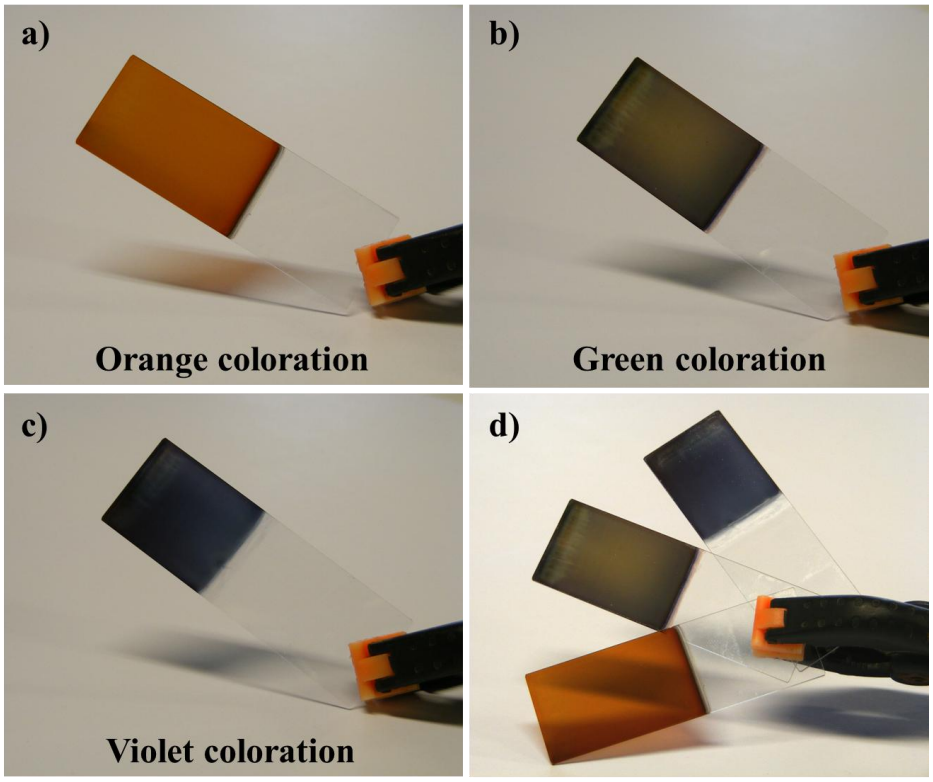

Figure 3.29. Final aspect of the multicolored LbL-E thin films $[PAH(7.5)/PAA\text{-}AgNPs(7.5)]_{80}$ (a) orange coloration; (b) green coloration; (c) violet coloration and (d) all together multicolored LbL-E thin films (orange, green and violet coloration).

Finally, UV-Vis spectra of the LbL-E thin films prepared with this thickness (80 bilayers) is shown in Figure 3.30. The spectra reveal that the position of the absorption bands is the same than previous spectra (Figure 3.21, 3.22 and 3.23) but with a considerable increase in intensity of the absorption peaks due to a higher number of the metallic silver nanoparticles that have been incorporated into the multilayer film. Therefore, when the thickness is increased, it is possible to corroborate the presence of the same aggregates species or AgNPs than the original colloidal solutions (PAA-AgNPs). In other words, when the thickness is increased, the final coloration of the resultant LbL-E films (orange, green and violet) is similar than the color of the original colloidal PAA-AgNPs solutions. These results of coloration as a function of number bilayers indicate that a higher thickness leads to a better incorporation

of higher size aggregates (clusters) in the resultant LbL-E films, as it has been confirmed for the green coloration.

This is the first time that a study about colored AgNPs synthesis and their further incorporation into multicolored LbL-E thin films (orange, green and violet) has been investigated.

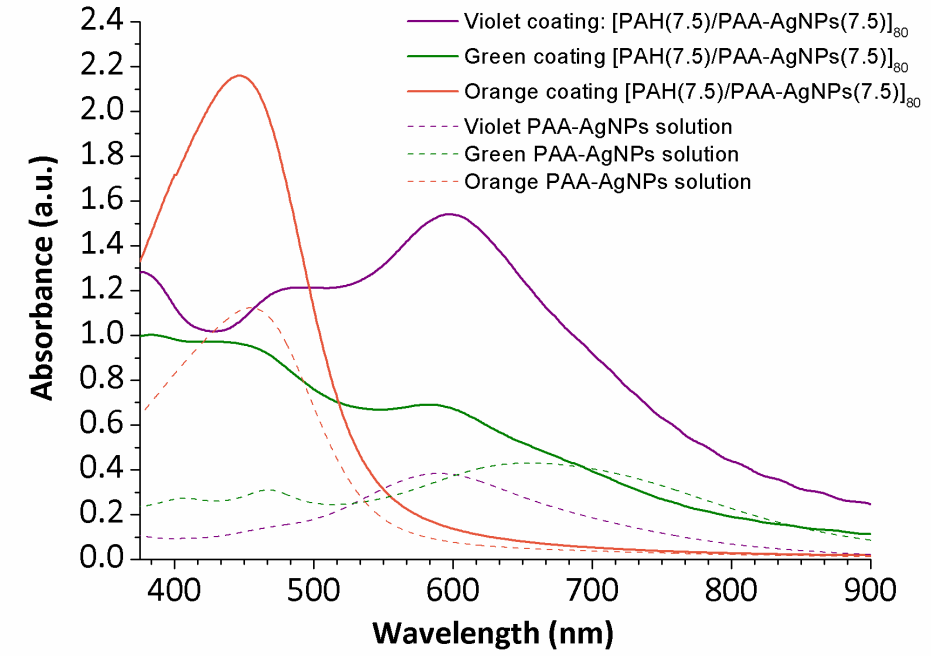

Figure 3.26. UV-Vis spectra of the multicolored LbL-E thin films of [PAH(7.5)/PAA-AgNPs(7.5]$_{80}$ (orange, green and violet coloration) in comparison with initial colored PAA-AgNPs solutions.

3.4. Conclusions

In this chapter, two complementary studies are presented. The first work deals with the synthesis of multicolor silver nanoparticles or clusters as a function of variable protective (PAA) and reducing (DMAB) molar concentration with a constant molar concentration of silver cations ($AgNO_3$), using a water-based chemical reduction method. The second study is about the incorporation of these multicolored AgNPs or aggregates into LbL-E films with the goal of keeping the same coloration that initial AgNPs dispersions.

It has been demonstrated that a fine control of both PAA and DMAB molar concentration makes possible to obtain a wide range of colors with a specific shape, size and aggregation state. Initially, only yellow, orange or red coloration is obtained with lower PAA concentration (1.0 or 2.5 mM PAA), whereas violet, blue, green, brown or orange coloration are obtained with higher PAA concentration (from 5 to 250 mM). In addition, a study of the evolution of their maximum absorption bands in two well-separated spectral regions (region 1, the 400-500 nm and region 2, the 600-700 nm bands) has been evaluated.

Two experimental series were performed, firstly when PAA concentration varies (from 1 to 250 mM) for a constant DMAB concentration (0.33 mM) and, secondly when DMAB concentration varies (from 0.033 to 6.66 mM) for a constant PAA concentration (25 mM). The results indicate that for higher PAA or lower DMAB molar concentrations an absorption band at longer wavelengths (region 2) appears, which implies violet, blue or green solutions of AgNPs with rod, triangle and hexagonal shape respectively. On the other hand, for lower PAA or higher DMAB concentrations, an intense absorption band at shorter wavelengths (region 1) appears, which implies orange-red solutions of AgNPs of spherical shape.

In Table 3.4, a summary of the different AgNPs dispersions with their corresponding color formation, shapes, sizes and absorption bands in a specific region is presented. A specific molar concentration of reducing agent (DMAB) respect to the Ag^+ cations (($DMAB/AgNO_3$) and the weak polyelectrolyte nature of the protective agent ($PAA/AgNO_3$) makes possible to achieve nanoparticles or clusters with different shapes, sizes and aggregation states.

Table 3.4. Summary of the multicolor silver map (regions, shape, size) as a function of variable molar concentration of protective (PAA) and reducing (DMAB) agents.

	Low PAA (1 to 2.5 mM)	**High PAA (5 to 250 mM)**
Low DMAB (0.033 to 0.33 mM)	Region 1 Color: yellow and orange Shape: spherical Size: nanometer	Region 2 Color: violet, blue and green Shape: rod, triangle, hexagonal Size: micrometer
High DMAB (0.066 to 6.66 mM)	Region 1 Color: red and orange Shape: spherical Size: nanometer	Region 1 and 2 Color: orange, brown and green Shape: spherical and hexagonal Size: micrometer

With respect to the incorporation of three different colored AgNPs dispersions (violet, green and orange) into LbL-E thin films, several steps were taken. In order to obtain the proper coloration of the LbL-E films, a study about the influence of the number of PAH/PAA-AgNPs bilayers (10, 20, 30, 40 and 80, respectively), the position of the absorption bands (UV-vis spectra) and the pH value of the weak polyelectrolytes (pH 7.5 or 9.0) solutions was performed. It was experimentally observed that a pH value of 7.0 or higher pH values of the PAA-AgNPs dispersions is the key to preserve the aggregation state of the AgNPs without any further precipitation or loss of coloration.

The incorporation of these AgNPs with a specific shape was corroborated for LbL-E violet coating where nanorods have been succesfully embedded within the LbL-E films. These nanorods were present in the initial PAA-AgNPs dispersion which it is indicative that after the fabrication process is preserved the original color, shape and size of the nanoparticles.

In addition, when the size of the nanoparticles is higher, even cluster formation (green PAA-AgNPs dispersion), a better definition of the coloration in the LbL-E films is observed when a higher number of bilayers are added because of a better entrapment of both clusters and nanometric spherical nanoparticles. In this case a selective absorption process of the nanoparticles of lower size (spherical) is observed when less number of bilayers are added, and as a result light orange coloration instead of green coloration is observed because of the mostly presence of spherical nanoparticles. However, a drastic color change is observed when the number of bilayers is increased up to 80 bilayers, where a green coloration is obtained as a result of incorporation of hexagonal clusters into the LbL-E films. To our knowledge, this is the first time that colored PAA-AgNPs of different size and shape are synthesized and incorporated later into LbL-E, preserving the original color of the dispersions.

Bibliography

[1] Abdullayev, E.; Sakakibara, K.; Okamoto, K.; Wei, W.; Ariga, K.; Lvov, Y. Natural Tubule Clay Template Synthesis of Silver Nanorods for Antibacterial Composite Coating. ACS Applied Materials and Interfaces 2011, 3, 4040-4046.

[2] Malcher, M.; Volodkin, D.; Heurtault, B.; André, P.; Schaaf, P.; Möhwald, H.; Voegel, J. -.; Sokolowski, A.; Ball, V.; Boulmedais, F.; Frisch, B. Embedded Silver Ions-Containing Liposomes in Polyelectrolyte Multilayers: Cargos Films for Antibacterial Agents. Langmuir 2008, 24, 10209-10215.

[3] Baker, C.; Pradhan, A.; Pakstis, L.; Pochan, D. J.; Shah, S. I. Synthesis and Antibacterial Properties of Silver Nanoparticles. Journal of Nanoscience and Nanotechnology 2005, 5, 244-249.

[4] Morones, J. R.; Elechiguerra, J. L.; Camacho, A.; Holt, K.; Kouri, J. B.; Ramírez, J. T.; Yacaman, M. J. The Bactericidal Effect of Silver Nanoparticles. Nanotechnology 2005, 16, 2346-2353.

[5] Sharma, V. K.; Yngard, R. A.; Lin, Y. Silver Nanoparticles: Green Synthesis and their Antimicrobial Activities. Adv. Colloid Interface Sci. 2009, 145, 83-96.

[6] Kidambi, S.; Bruening, M. L. Multilayered Polyelectrolyte Films Containing Palladium Nanoparticles: Synthesis, Characterization, and Application in Selective Hydrogenation. Chemistry of Materials 2005, 17, 301-307.

[7] Kidambi, S.; Dai, J.; Li, J.; Bruening, M. L. Selective Hydrogenation by Pd Nanoparticles Embedded in Polyelectrolyte Multilayers. J. Am. Chem. Soc. 2004, 126, 2658-2659.

[8] Daniel, M. -.; Astruc, D. Gold Nanoparticles: Assembly, Supramolecular Chemistry, Quantum-Size-Related Properties, and Applications Toward Biology, Catalysis, and Nanotechnology. Chem. Rev. 2004, 104, 293-346.

[9] Haruta, M.; Daté, M. Advances in the Catalysis of Au Nanoparticles. Applied Catalysis A: General 2001, 222, 427-437.

[10] Narayanan, R.; El-Sayed, M. A. Catalysis with Transition Metal Nanoparticles in Colloidal Solution: Nanoparticle Shape Dependence and Stability. J Phys Chem B 2005, 109, 12663-12676.

[11] Xi, Q.; Chen, X.; Evans, D. G.; Yang, W. Gold Nanoparticle-Embedded Porous Graphene Thin Films Fabricated Via Layer-by-Layer Self-Assembly and Subsequent Thermal Annealing for Electrochemical Sensing. Langmuir 2012, 28, 9885-9892.

[12] Devadoss, A.; Spehar-Délèze, A. -.; Tanner, D. A.; Bertoncello, P.; Marthi, R.; Keyes, T. E.; Forster, R. J. Enhanced Electrochemiluminescence and Charge Transport through Films of Metallopolymer-Gold Nanoparticle Composites. Langmuir 2010, 26, 2130-2135.

[13] Haes, A. J.; Zou, S.; Schatz, G. C.; Van Duyne, R. P. A Nanoscale Optical Biosensor: The Long Range Distance Dependence of the Localized Surface Plasmon Resonance of Noble Metal Nanoparticles. J Phys Chem B 2004, 108, 109-116.

[14] Liu, J.; Lu, Y. A Colorimetric Lead Biosensor using DNAzyme-Directed Assembly of Gold Nanoparticles. J. Am. Chem. Soc. 2003, 125, 6642-6643.

[15] Willets, K. A.; Van Duyne, R. P. Localized Surface Plasmon Resonance Spectroscopy and Sensing. Annual Review of Physical Chemistry 2007, 58, 267-297.

[16] Dreaden, E. C.; Alkilany, A. M.; Huang, X.; Murphy, C. J.; El-Sayed, M. A. The Golden Age: Gold Nanoparticles for Biomedicine. Chem. Soc. Rev. 2012, 41, 2740-2779.

[17] Cheng, Y.; Meyers, J. D.; Agnes, R. S.; Doane, T. L.; Kenney, M. E.; Broome, A. -.; Burda, C.; Basilion, J. P. Addressing Brain Tumors with Targeted Gold Nanoparticles: A New Gold Standard for Hydrophobic Drug Delivery? Small 2011, 7, 2301-2306.

[18] Doane, T. L.; Burda, C. The Unique Role of Nanoparticles in Nanomedicine: Imaging, Drug Delivery and Therapy. Chem. Soc. Rev. 2012, 41, 2885-2911.

[19] Lu, F.; Doane, T. L.; Zhu, J. -.; Burda, C. Gold Nanoparticles for Diagnostic Sensing and Therapy. Inorg. Chim. Acta 2012, 393, 142-153.

[20] Shang, L.; Wang, Y.; Huang, L.; Dong, S. Preparation of DNA-Silver Nanohybrids in Multilayer Nanoreactors by *in Situ* Electrochemical Reduction, Characterization, and Application. Langmuir 2007, 23, 7738-7744.

[21] Bracko, I.; Jancar, B.; Logar, M.; Caglic, D.; Suvorov, D. Silver Nanoparticles on Titanate Nanobelts Via the Self-Assembly of Weak Polyelectrolytes: Synthesis and Photocatalytic Properties. Nanotechnology 2011, 22.

[22] Logar, M.; Jancar, B.; Šturm, S.; Suvorov, D. Weak Polyion Multilayer-Assisted in Situ Synthesis as a Route Toward a Plasmonic Ag/TiO2 Photocatalyst. Langmuir 2010, 26, 12215-12224.
[23] Nolte, A. J.; Rubner, M. F.; Cohen, R. E. Creating Effective Refractive Index Gradients within Polyelectrolyte Multilayer Films: Molecularly Assembled Rugate Filters. Langmuir 2004, 20, 3304-3310.
[24] Zhai, L.; Nolte, A. J.; Cohen, R. E.; Rubner, M. F. PH-Gated Porosity Transitions of Polyelectrolyte Multilayers in Confined Geometries and their Application as Tunable Bragg Reflectors. Macromolecules 2004, 37, 6113-6123.
[25] Wang, T. C.; Cohen, R. E.; Rubner, M. F. Metallodielectric Photonic Structures Based on Polyelectrolyte Multilayers. Adv Mater 2002, 14, 1534-1537.
[26]Mayer, K. M.; Hafner, J. H. Localized Surface Plasmon Resonance Sensors. Chem. Rev. 2011, 111, 3828-3857.
[27] Zhao, J.; Zhang, X.; Yonzon, C. R.; Haes, A. J.; Van Duyne, R. P. Localized Surface Plasmon Resonance Biosensors. Nanomedicine (London, England) 2006, 1, 219-228.
[28] Otte, M. A.; Sepúlveda, B.; Ni, W.; Juste, J. P.; Liz-Marzán, L. M.; Lechuga, L. M. Identification of the Optimal Spectral Region for Plasmonic and Nanoplasmonic Sensing. ACS Nano 2010, 4, 349-357.
[29] Liz-Marzán, L. M. Nanometals: Formation and Color. Materials Today 2004, 7, 26-31.
[30] Cobley, C. M.; Skrabalak, S. E.; Campbell, D. J.; Xia, Y. Shape-Controlled Synthesis of Silver Nanoparticles for Plasmonic and Sensing Applications. Plasmonics 2009, 4, 171-179.
[31] Henry, A. -.; Bingham, J. M.; Ringe, E.; Marks, L. D.; Schatz, G. C.; Van Duyne, R. P. Correlated Structure and Optical Property Studies of Plasmonic Nanoparticles. Journal of Physical Chemistry C 2011, 115, 9291-9305.
[32] Angelomé, P. C.; Mezerji, H. H.; Goris, B.; Pastoriza-Santos, I.; Pérez-Juste, J.; Bals, S.; Liz-Marzán, L. M. Seedless Synthesis of Single Crystalline Au Nanoparticles with Unusual Shapes and Tunable LSPR in the Near-IR. Chemistry of Materials 2012, 24, 1393-1399.
[33] Sepúlveda, B.; Angelomé, P. C.; Lechuga, L. M.; Liz-Marzán, L. M. LSPR-Based Nanobiosensors. Nano Today 2009, 4, 244-251.
[34] Anker, J. N.; Hall, W. P.; Lyandres, O.; Shah, N. C.; Zhao, J.; Van Duyne, R. P. Biosensing with Plasmonic Nanosensors. Nature Materials 2008, 7, 442-453.
[35] Haes, A. J.; Zou, S.; Schatz, G. C.; Van Duyne, R. P. A Nanoscale Optical Biosensor: The Long Range Distance Dependence of the Localized Surface Plasmon Resonance of Noble Metal Nanoparticles. J Phys Chem B 2004, 108, 109-116.
[36] Vigderman, L.; Khanal, B. P.; Zubarev, E. R. Functional Gold Nanorods: Synthesis, Self-Assembly, and Sensing Applications. Adv Mater 2012, 24, 4811-4841.
[37] Jeon, S. -.; Xu, P.; Zhang, B.; MacK, N. H.; Tsai, H.; Chiang, L. Y.; Wang, H. -. Polymer-Assisted Preparation of Metal Nanoparticles with Controlled Size and Morphology.Journal of Materials Chemistry 2011, 21, 2550-2554.
[38] Zhang, J.; Sun, Y.; Zhang, H.; Xu, B.; Zhang, H.; Song, D. Preparation and Application of Triangular Silver nanoplates/chitosan Composite in Surface Plasmon Resonance Biosensing. Anal.Chim. Acta 2013, 769, 114-120.
[39] Aliev, F. G.; Correa-Duarte, M. A.; Mamedov, A.; Ostrander, J. W.; Giersig, M.; Liz-Marzán, L. M.; Kotov, N. A. Layer-by-Layer Assembly of Core-Shell Magnetite Nanoparticles: Effect of Silica Coating on Interparticle Interactions and Magnetic Properties. Adv Mater 1999, 11, 1006-1010.
[40] Wang, Y.; Biradar, A. V.; Duncan, C. T.; Asefa, T. Silica Nanosphere-Supported Shaped Pd Nanoparticles Encapsulated with Nanoporous Silica Shell: Efficient and Recyclable Nanocatalysts. Journal of Materials Chemistry 2010, 20, 7834-7841.
[41] Wang, Y.; Biradar, A. V.; Wang, G.; Sharma, K. K.; Duncan, C. T.; Rangan, S.; Asefa, T. Controlled Synthesis of Water-Dispersible Faceted Crystalline Copper Nanoparticles and their Catalytic Properties. Chemistry - A European Journal 2010, 16, 10735-10743.
[42] Barbosa, S.; Agrawal, A.; Rodríguez-Lorenzo, L.; Pastoriza-Santos, I.; Alvarez-Puebla, R. A.; Kornowski, A.; Weller, H.; Liz-Marzán, L. M. Tuning Size and Sensing Properties in Colloidal Gold Nanostars. Langmuir 2010, 26, 14943-14950.

[43] Liz-Marzán, L. M. Tailoring Surface Plasmons through the Morphology and Assembly of Metal Nanoparticles. Langmuir 2006, 22, 32-41.
[44] Pazos-Pérez, N.; Baranov, D.; Irsen, S.; Hilgendorff, M.; Liz-Marzán, L. M.; Giersig, M. Synthesis of Flexible, Ultrathin Gold Nanowires in Organic Media. Langmuir 2008, 24, 9855-9860.
[45] Pastoriza-Santos, I.; Liz-Marzán, L. M. Colloidal Silver Nanoplates. State of the Art and Future Challenges. Journal of Materials Chemistry 2008, 18, 1724-1737.
[46] Pastoriza-Santos, I.; Liz-Marzán, L. M. Synthesis of Silver Nanoprisms in DMF. Nano Letters 2002, 2, 903-905.
[47] Pastoriza-Santos, I.; Liz-Marzán, L. M. Formation of PVP-Protected Metal Nanoparticles in DMF. Langmuir 2002, 18, 2888-2894.
[48] Sánchez-Iglesias, A.; Pastoriza-Santos, I.; Pérez-Juste, J.; Rodríguez-González, B.; García De Abajo, F. J.; Liz-Marzán, L. M. Synthesis and Optical Properties of Gold Nanodecahedra with Size Control. Adv Mater 2006, 18, 2529-2534.
[49] Hoppe, C. E.; Lazzari, M.; Pardiñas-Blanco, I.; López-Quintela, M. A. One-Step Synthesis of Gold and Silver Hydrosols using Poly(N-Vinyl-2- Pyrrolidone) as a Reducing Agent. Langmuir 2006, 22, 7027-7034.
[50] Sakai, T.; Alexandridis, P. Spontaneous Formation of Gold Nanoparticles in Poly(Ethylene Oxide)-Poly(Propylene Oxide) Solutions: Solvent Quality and Polymer Structure Effects. Langmuir 2005, 21, 8019-8025.
[51] Sakai, T.; Alexandridis, P. Mechanism of Gold Metal Ion Reduction, Nanoparticle Growth and Size Control in Aqueous Amphiphilic Block Copolymer Solutions at Ambient Conditions. J Phys Chem B 2005, 109, 7766-7777.
[52] Sardar, R.; Park, J. -.; Shumaker-Parry, J. S. Polymer-Induced Synthesis of Stable Gold and Silver Nanoparticles and Subsequent Ligand Exchange in Water. Langmuir 2007, 23, 11883-11889.
[53] Pellegrino, T.; Kudera, S.; Liedl, T.; Javier, A. M.; Manna, L.; Parak, W. J. On the Development of Colloidal Nanoparticles Towards Multifunctional Structures and their Possible use for Biological Applications. Small 2005, 1, 48-63.
[54] Boyer, D.; Tamarat, P.; Maali, A.; Lounis, B.; Orrit, M. Photothermal Imaging of Nanometer-Sized Metal Particles among Scatterers. Science 2002, 297, 1160-1163.
[55] Hussain, I.; Graham, S.; Wang, Z.; Tan, B.; Sherrington, D. C.; Rannard, S. P.; Cooper, A. I.; Brust, M. Size-Controlled Synthesis of Near-Monodisperse Gold Nanoparticles in the 1-4 Nm Range using Polymeric Stabilizers. J. Am. Chem. Soc. 2005, 127, 16398-16399.
[56] Wang, Z.; Tan, B.; Hussain, I.; Schaeffer, N.; Wyatt, M. F.; Brust, M.; Cooper, A. I. Design of Polymeric Stabilizers for Size-Controlled Synthesis of Monodisperse Gold Nanoparticles in Water. Langmuir 2007, 23, 885-895.
[57] Huber, K.; Witte, T.; Hollmann, J.; Keuker-Baumann, S. Controlled Formation of Ag Nanoparticles by Means of Long-Chain Sodium Polyacrylates in Dilute Solution. J. Am. Chem. Soc. 2007, 129, 1089-1094.
[58] Kiryukhin, M. V.; Sergeev, B. M.; Prusov, A. N.; Sergeev, V. G. Formation of Nonspherical Silver Nanoparticles by the Photochemical Reduction of Silver Cations in the Presence of a Partially Decarboxylated Poly(Acrylic Acid). Polymer Science - Series B 2000, 42, 324-328.
[59] Kiryukhin, M. V.; Sergeev, B. M.; Prusov, A. N.; Sergeyev, V. G. Photochemical Reduction of Silver Cations in a Polyelectrolyte Matrix. Polymer Science - Series B 2000, 42, 158-162.
[60] Ershov, B. G.; Henglein, A. Time-Resolved Investigation of Early Processes in the Reduction of Ag + on Polyacrylate in Aqueous Solution. J Phys Chem B 1998, 102, 10667-10671.
[61] Ershov, B. G.; Henglein, A. Reduction of Ag + on Polyacrylate Chains in Aqueous Solution. J Phys Chem B 1998, 102, 10663-10666.
[62] Sergeev, B. M.; Lopatina, L. I.; Prusov, A. N.; Sergeev, G. B. Borohydride Reduction of AgNO3 in Polyacrylate Aqueous Solutions: Two-Stage Synthesis of "Blue Silver". Colloid Journal 2005, 67, 213-216.
[63] Janata, E.; Henglein, A.; Ershov, B. G. First Clusters of Ag+ Ion Reduction in Aqueous Solution. J. Phys. Chem. 1994, 98, 10888-10890.

[64] Sergeev, B. M.; Lopatina, L. I.; Prusov, A. N.; Sergeev, G. B. Formation of Silver Clusters by Borohydride Reduction of AgNO3 in Polyacrylate Aqueous Solutions. Colloid Journal 2005, 67, 72-78.
[65] Sergeev, B. M.; Lopatina, L. I.; Sergeev, G. B.The Influence of Ag+ Ions on Transformations of Silver Clusters in Polyacrylate Aqueous Solutions. Colloid Journal 2006, 68, 761-766.
[66] Rivero, P. J.; Goicoechea, J.; Urrutia, A.; Arregui, F. J. Effect of both Protective and Reducing Agents in the Synthesis of Multicolor Silver Nanoparticles. Nanoscale Research Letters 2013, 8, 1-9.
[67] Decher, G. Fuzzy Nanoassemblies: Toward Layered Polymeric Multicomposites. Science 1997, 277, 1232-1237.
[68] Decher, G.; Eckle, M.; Schmitt, J.; Struth, B. Layer-by-Layer Assembled Multicomposite Films. Current Opinion in Colloid and Interface Science 1998, 3, 32-39.
[69] Yoo, D.; Shiratori, S. S.; Rubner, M. F. Controlling Bilayer Composition and Surface Wettability of Sequentially Adsorbed Multilayers of Weak Polyelectrolytes. Macromolecules 1998, 31, 4309-4318.
[70] Yoo, D.; Shiratori, S. S.; Rubner, M. F. Controlling Bilayer Composition and Surface Wettability of Sequentially Adsorbed Multilayers of Weak Polyelectrolytes. Macromolecules 1998, 31, 4309-4318.
[71] Berg, M. C.; Choi, J.; Hammond, P. T.; Rubner, M. F. Tailored Micropatterns through Weak Polyelectrolyte Stamping. Langmuir 2003, 19, 2231-2237.
[72] Lee, D.; Cohen, R. E.; Rubner, M. F. Antibacterial Properties of Ag Nanoparticle Loaded Multilayers and Formation of Magnetically Directed Antibacterial Microparticles. Langmuir 2005, 21, 9651-9659.
[73] Wang, T. C.; Rubner, M. F.; Cohen, R. E. Polyelectrolyte Multilayer Nanoreactors for Preparing Silver Nanoparticle Composites: Controlling Metal Concentration and Nanoparticle Size. Langmuir 2002, 18, 3370-3375.
[74] Logar, M.; Jancar, B.; Suvorov, D.; Kostanjšek, R. In Situ Synthesis of Ag Nanoparticles in Polyelectrolyte Multilayers.Nanotechnology 2007, 18.
[75] Gao, S.; Yuan, D.; Lü, J.; Cao, R. In Situ Synthesis of Ag Nanoparticles in Aminocalix[4]Arene Multilayers. J. Colloid Interface Sci. 2010, 341, 320-325.
[76] Rivero, P. J.; Urrutia, A.; Goicoechea, J.; Matias, I. R.; Arregui, F. J. A Lossy Mode Resonance Optical Sensor using Silver Nanoparticles-Loaded Films for Monitoring Human Breathing. Sensors and Actuators, B: Chemical 2012, 187, 40-44.
[77] Veletanlic, E.; Cynthia Goh, M. Polyelectrolyte Multilayer Films as Templates for the in Situ Photochemical Synthesis of Silver Nanoparticles. Journal of Physical Chemistry C 2009, 113, 18020-18026.
[78] Zan, X.; Su, Z. Incorporation of Nanoparticles into Polyelectrolyte Multilayers Via Counterion Exchange and in Situ Reduction. Langmuir 2009, 25, 12355-12360.
[79] Zan, X.; Su, Z. Polyelectrolyte Multilayer Films Containing Silver as Antibacterial Coatings. Thin Solid Films 2010, 518, 5478-5482.
[80] Zan, X.; Su, Z. Counterions in Polyelectrolyte Multilayers: A Vehicle for Introducing Functionalities. Thin Solid Films 2009, 518, 116-119.
[81] Rivero, P. J.; Urrutia, A.; Goicoechea, J.; Rodríguez, Y.; Corres, J. M.; Arregui, F. J.; Matías, I. R. An Antibacterial Submicron Fiber Mat with in Situ Synthesized Silver Nanoparticles. J Appl Polym Sci 2012, 126, 1228-1235.
[82] Mahanta, N.; Valiyaveettil, S. In Situ Preparation of Silver Nanoparticles on Biocompatible Methacrylated Poly(Vinyl Alcohol) and Cellulose Based Polymeric Nanofibers. RSC Advances 2012, 2, 11389-11396.
[83] Rivero, P. J.; Urrutia, A.; Goicoechea, J.; Zamarreño, C. R.; Arregui, F. J.; Matías, I. R. An Antibacterial Coating Based on a polymer/sol- Gel Hybrid Matrix Loaded with Silver Nanoparticles. Nanoscale Research Letters 2011, 6, X1-7.
[84] Zayat, M.; Einot, D.; Reisfeld, R. In-Situ Formation of AgCl Nanocrystallites in Films Prepared by the Sol-Gel and Silver Nanoparticles in Silica Glass Films. J. Sol Gel Sci. Technol. 1997, 10, 67-74.

[85] Urrutia, A.; Rivero, P. J.; Ruete, L.; Goicoechea, J.; Matías, I. R.; Arregui, F. J. Single-Stage in Situ Synthesis of Silver Nanoparticles in Antibacterial Self-Assembled Overlays. Colloid Polym. Sci. 2012, 290, 785-792.

[86] Newman, J. D. S.; Blanchard, G. J. Formation and Encapsulation of Gold Nanoparticles using a Polymeric Amine Reducing Agent. *Journal of Nanoparticle Research* **2007***, 9*, 861-868.

[87] Wu, K. H.; Chang, Y. C.; Tsai, W. Y.; Huang, M. Y.; Yang, C. C. Effect of Amine Groups on the Synthesis and Antibacterial Performance of Ag Nanoparticles Dispersed in Aminosilanes-Modified Silicate. *Polym. Degrad. Stab.* **2010***, 95*, 2328-2333.

[88] Frattini, A.; Pellegri, N.; Nicastro, D.; De Sanctis, O. Effect of Amine Groups in the Synthesis of Ag Nanoparticles using Aminosilanes. Mater. Chem. Phys. 2005, 94, 148-152.

[89] Shiratori, S.; Yamada, M.; Ito, T.; Wang, T. C.; Rubner, M. F. In In Nanoscale control of layer thickness for EL devices by mass-controlled layer-by-layer sequential adsorption process; Materials Research Society Symposium - Proceedings; 2000; Vol. 598, pp BB1.9.1-BB1.9.6.

[90] Shiratori, S. S.; Rubner, M. F. PH-Dependent Thickness Behavior of Sequentially Adsorbed Layers of Weak Polyelectrolytes. Macromolecules 2000, 33, 4213-4219.

[91] Choi, J.; Rubner, M. F. Influence of the Degree of Ionization on Weak Polyelectrolyte Multilayer Assembly. Macromolecules 2005, 38, 116-124.

[92] Itano, K.; Choi, J.; Rubner, M. F. Mechanism of the pH-Induced Discontinuous swelling/deswelling Transitions of Poly(Allylamine Hydrochloride)-Containing Polyelectrolyte Multilayer Films. Macromolecules 2005, 38, 3450-3460.

[93] Rivero, P. J.; Goicoechea, J.; Urrutia, A.; Matias, I. R.;Arregui, F. J. Multicolor layer-by-layer films using weak polyelectrolyte assisted synthesis of silver nanoparticles. Nanoscale Research Letters 2013, 8, 1-10.

CHAPTER 4. Implementation of nanostructured coatings based on silver nanoparticles as antibacterial surfaces

In this chapter, the fabrication of low-cost and highly efficient antibacterial surfaces is presented. These coatings based on the immobilization of silver nanoparticles (AgNPs) have been fabricated using the in situ synthesis (ISS) process and the Layer-by-Layer Embedding (LbL-E) deposition technique. All the coatings were tested with gram-positive bacterial cultures (Lactobacillus plantarum). The implementation of these coatings opens the door in the design of novel materials as antibacterial surfaces.

4.1. Introduction

In previous chapters, silver nanoparticles (AgNPs) have been incorporated into thin films using two alternative methods, the *in situ* synthesis (ISS) process and the Layer-by-Layer Embedding (LbL-E) deposition technique. In this chapter, a specific property related to the AgNPs will be studied, their antimicrobial activity. This property of the AgNPs makes possible the fabrication of antibacterial films, being of great interest in optical fiber sensors when are placed in high humidity environments in order to prevent the growth of microorganisms onto the sensor coating.

Microbes and bacteria are the most abundant of all living organisms and a large number of them are pathogens and disease-causing organisms. Because of this, there is a high concern in preventing the emergence of germs in products which are directly or indirectly used by humans. Consequently, to avoid the apparition of these microorganisms in instrumentals, devices, labs or operating rooms, there is an enormous interest among researchers about developing highly efficient and low-cost antibacterial surface treatments and coatings [1-4].

It is well known that silver is considered a very good antibacterial agent and silver ions show a notorious broad spectrum biocide effect. In fact, there are several known biological mechanisms that explain why silver shows an extraordinary toxicity for bacteria [5-10]. Moreover, silver is particularly attractive because it combines a high bacterial killing efficiency with a low toxicity for humans [11-18]. Its disinfectant properties for hygienic and medicinal purposes are known since ancient times, and for example it has been extensively used to prevent wound infection since World War I [19].

Most of the approaches for achieving antibacterial surfaces are based on doping some elements with silver particles which act as silver ions source, for example, in textiles [20, 21], surgical instruments [22], and other surfaces [23]. The biocide efficiency of such coatings depends on the ability of the trapped silver to release ions. Consequently, silver particles with a high specific area show more efficient ion release mechanisms and therefore the antibacterial effect is enhanced. Some authors have reported how silver nanoparticles, nanorods, or nanotubes are especially efficient antibacterial agents because of their large surface to volume ratio [24-30]. In the most usual approach, such silver nanoparticles have been immobilized on inorganic porous hosts such as zeolites, calcium phosphate, and carbon fiber [31-33]. Moreover, silver-supported silica materials, such as silica glass [34], silica thin films [35], and silica nanoparticles [36], are also good candidates for antibacterial materials due to their fine chemical durability and high antibacterial activity. Other authors have proposed other efficient approaches based on alternative biocide mechanisms that not involve AgNPs such as the contact with quaternary amine compounds [37-39], phosphonium salts [40] or titanium oxide particles [41]. There is a wide variety of coating techniques that have been used for fabricating antibacterial coatings, such as PVD [42], spin-coating [43], or electrospinning [44-47]. However, specific experimental conditions and expensive equipment are required to obtain the films [48-50] onto a desired substrate.

Recently, the use of nanotechnology has made possible the fabrication of new nanostructured coatings with an extremely high specific surface area. In addition, the use of eco-friendly green chemistry or water based methods to make nanomaterials could be a good alternative for fabricating thin films because of their low cost and the possibility of being upscalable. Among the different thin film fabrication techniques, the sol-gel process [51-59] and the Layer-by-Layer (LbL) assembly [60-69] will be used due to their simplicity, flexibility, versatility and the possibility of obtaining organic-inorganic hybrid materials, such metal nanoparticles (silver) and polymeric chains.

In this work, we report the immobilization of silver nanoparticles (AgNPs) into thin films, using the two methods which were previously presented, *in situ* synthesis (ISS) process in Chapter 2 [4, 47], and the Layer-by-Layer Embedding (LbL-E) deposition technique in Chapter 3 [70]. In all the cases of study, the surfaces were tested against a specific type of bacteria which are gram positive (*Lactobacillus plantarum*), showing a very good antibacterial behavior against this type of bacteria. The high biocide efficiency of such AgNPs loaded thin films could be of great interest in applications where bacteria could grow onto the films damaging the device or becoming a risk for health. One of these applications could be high Relative Humidity sensors,

since it is well known that bacteria are prone to grow onto organic films in good conditions of temperature and hydratation.

4.2. Experimental section

4.2.1. Materials

A non-pathogen gram-positive bacteria was chosen to carry out the antibacterial tests. The gram-positive membrane characteristic was chosen to elucidate more precisely the behavior of other gram-positive pathogen bacteria and bacilli such as *Staphylococcus aureus*, *Streptococcus pneumonia*, *Clostridium tetani*, or even *Bacillus anthracis*. More precisely *Lactobacillus plantarum* were obtained from CECT (The Spanish Type Culture Collection University from Valencia). These bacteria are gram-positive, rod, aerotolerant and belong to risk group I.

Tryptic Soy Broth (TSB) and Tryptic Soy Agar were provided from the company Sigma Aldrich.

4.2.2. Fabrication of the thin films

The thin films were fabricated using the two methods presented in previous chapters 2 and 3, respectively. Firstly, the *in situ* synthesis (ISS) process of silver nanoparticles from a source of silver ions. And secondly, the Layer-by-Layer Embedding (LbL-E) deposition technique of silver nanoparticles with an orange coloration is performed.

It is important to remark that thin films with the higher number of L/R cycles in the *in situ* synthesis process (4 cycles of L/R) as well as thin films with the higher number of bilayers ($[PAH(9.0)/PAA\text{-}AgNPs(9.0]_{40}$) in the LbL-E deposition technique have been tested as antibacterial surfaces.

4.2.3. Bacteriologic test method

The antibacterial activity of the nanostructured coatings based on AgNPs against the *Lactobacillus plantarum* bacteria was assessed by a viable cell-counting method [4, 46, 68, 71]. *L. plantarum* was inoculated in a Tryptic Soy Broth aqueous medium and incubated at 37ºC for 24 hours. The obtained bacterial suspension had approximately $4.8 \cdot 10^8$ Colony Formation Units per milliliter (CFU/mL).

The bacterial suspension was shaken and diluted 10^6 times. "Tryptic Soy Agar" was autoclaved at 121ºC for 30 minutes and cooled in sterile Petri-dishes to form a 3 mm thick slab. Then, 0.1 mL bacterial suspension dilution was spread uniformly on the surface of the nutrient agar slab. The substrates coated with AgNPs (ISS and LbL-E) were then placed onto the agar slab. Bare glass slides were also placed as reference control (previously disinfected by dipping in isopropyl alcohol and treated by contact flame) by the same way. Then, Petri-dishes were introduced into an incubator for 24 hours at 37ºC and the colonies were counted. To measure the effect of an antimicrobial film, the percentage of cell reduction between the control sample and the test sample is calculated according to the Equation 4.1.

$$Cell\ reduction(\%) = \left(1 - \frac{Test\ Sample(CFU/ml)}{Control(CFU/ml)}\right) \times 100 \qquad \text{Eq. 4.1}$$

A coating is considered biocide if the cell reduction is higher than 99% [72].

4.3. Antibacterial results of the nanostructured thin films

4.3.1. *In situ* synthesis (ISS) of the silver nanoparticles

In Figure 4.1, the UV-Vis spectrum as well as the final aspect of the thin film based on the *in situ* synthesis (ISS) of silver nanoparticles into the hybrid matrix is presented. As it was previously commented in Chapter 2, the existence of an absorption peak at 410 nm which is related to the LSPR of the AgNPs with a spherical shape and the resultant change of coloration from transparent to golden-yellowish after the 4 L/R cycles is indicative that AgNPs have been successfully synthesized into the sol-gel hybrid matrix and deposited onto the glass slide substrate, being coherent with experimental results obtained in Chapter 2.

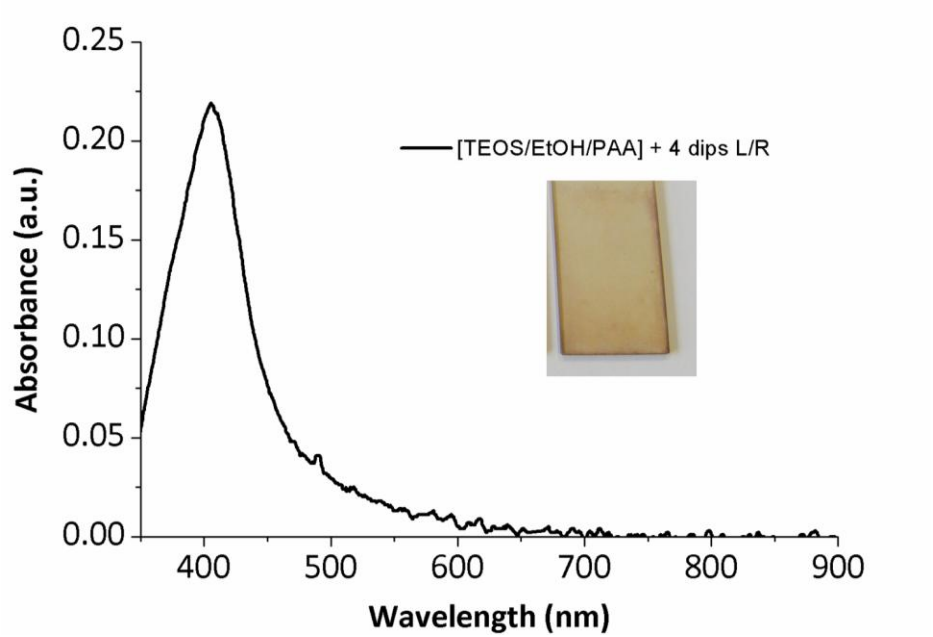

Figure 4.1. UV-Vis spectroscopy of the *in situ* synthesis (ISS) of the silver nanoparticles (AgNPs) into hybrid sol-gel matrix for 4 dips Loading/Reduction (L/R) and the aspect of the thin film. The LSPR maximum was observed around 410nm.

The antibacterial activity against *Lactobacillus plantarum* of the coating can be observed in Figure 4.2 where it is shown the antibacterial results of two samples placed on agar slabs after 24 hours. Figure 4.2a shows a reference substrate (bare glass slide) and it is clearly seen that a higher number of *Lactobacillus plantarum* colonies (white spots) grow up randomly throughout the whole agar slab. However, Figure 4.2b has a coated area based on the *in situ* synthesis of silver nanoparticles where there is no growth of colonies, whereas a growth of colonies can be clearly observed in the uncoated area as it happens in the reference substrate. In addition, Figure 4.2b shows an inhibition zone around the coated area where bacterial growth was not observed, indicating the high killing efficiency of the coating. All the experiments were performed by triplicated and the treated surfaces reached more than 99.9% of killing efficiency.

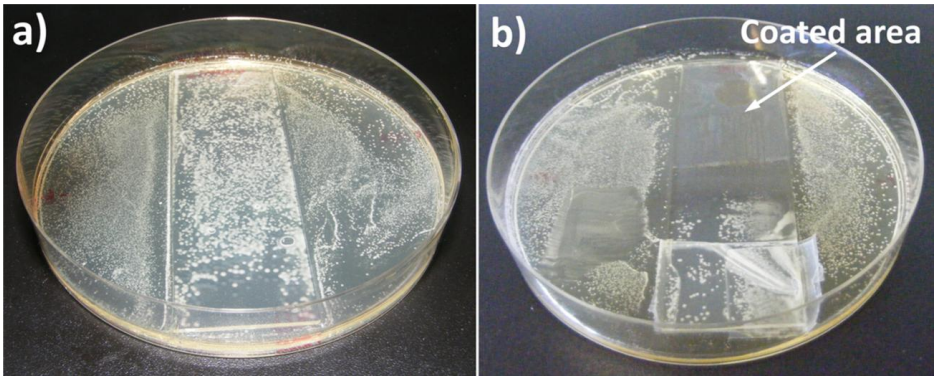

Figure 4.2. Bacteria growth on culture plates after 24 hours: (a) reference substrate (bare glass slide); (b) coated substrate based on silver nanoparticles into a hybrid sol-gel matrix. The coated area is clearly visible, as far as it inhibits the bacteria growth (no white spots of bacteria colonies).

This same procedure was performed for the *in situ* synthesis (ISS) using as a host matrix of the AgNPs a coating obtained by the Layer-by-Layer (LbL) assembly instead of sol-gel process. In this case, a more intense LSPR band than in the case of the sol-gel process was observed. This implies that a higher amount of AgNPs have been incorporated into the LbL polymeric thin film during the fabrication process.

Finally, the results indicate that the coatings exhibited an excellent behavior against *Lactobacillus plantarum*, showing a killing effieciency higher than 99.9%. As conclusion of both results of the ISS obtained by sol-gel process and LbL assembly, the coatings showed a high kill efficiency to be considered biocide surfaces.

4.3.2. Layer-by-Layer Embedding (LbL-E) deposition technique

In Figure 4.3, the UV-Vis spectrum as well as the final aspect of the thin film based on the LbL-E of the silver nanoparticles with an orange coloration is presented. The location of the LSPR peak at 430 nm indicates that AgNPs have been successfully incorporated into the LbL thin film, which is perfectly coherent with the results obtained in Chapter 3.

In Figure 4.4, the antibacterial behavior against *Lactobacillus plantarum* is shown. In order to corroborate that the killing efficiency is due to the only presence of AgNPs into the thin films, two different kind of coatings have been tested. The first one corresponds to a reference substrate based on LbL polymeric thin film of $[PAH(9.0)/PAA(9.0)]_{40}$ and the second one corresponds to the LbL-E coating of $[PAH(9.0)/PAA\text{-}AgNPs(9.0)]_{40}$. It can be observed that in the reference substrate (Figure 4.4a), bacteria growth was observed in the whole agar slab and the coated area also showed a random distribution of

the bacteria (white spots). However, the LbL-E coating based on AgNPs (Figure 4.4b) showed no bacteria growth in the coated area (yellowish-orange color), whereas the uncoated area (transparent) clearly showed a growth of bacteria colonies in the glass slide. The killing efficiency of the coating is higher than 99.9% which is considered as a biocide surface.

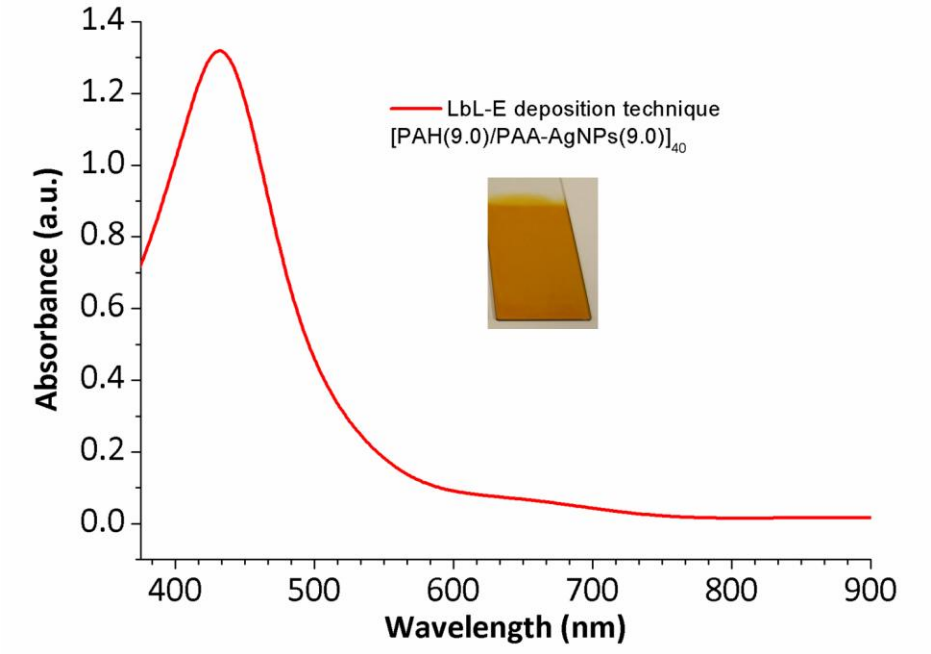

Figure 4.3. UV-Vis spectroscopy of the LbL-E of the silver nanoparticles (orange coloration) and the aspect of the LbL-E thin film after the deposition process. The LSPR maximum is observed at 430nm, which is coherent with the LSPR band of the previously synthesized AgNPs.

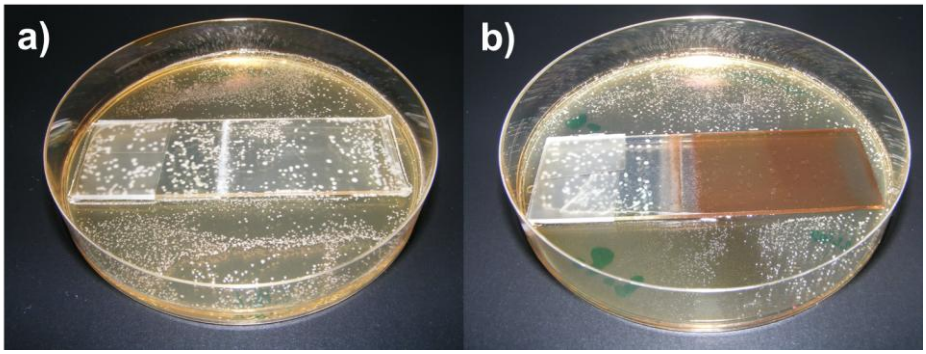

Figure 4.4. Bacteria growth on culture plates after 24 hours: (a) reference substrate (only polymeric LbL coating); (b) coated substrate based on silver nanoparticles (LbL-E of orange nanoparticles). The orange coated area is clearly visible, as far as it inhibits the bacteria growth (no white spots).

These results corroborate that both methods based on the incorporation of silver nanoparticles into thin films, *in situ* synthesis (ISS) process and LbL-E deposition technique respectively, showed great results as biocide surfaces. In addition, this antibacterial behavior is even observed when a lower intensity related to LSPR band is obtained as it happens for the ISS process using as host matrix a sol-gel coating (see Figure 4.1 and 4.2).

4.4. Conclusions

In this chapter, the design and development of novel antibacterial surfaces is presented using two different methods such as, *in situ* synthesis (ISS) of silver nanoparticles and the Layer-by-Layer Embedding (LbL-E) deposition technique of orange nanoparticles. These methods have been extensively discussed in previous chapters and it has been demonstrated how silver nanoparticles have been successfully incorporated into the thin-films. The great advantages of these methods are their low-cost fabrication, easy implementation, simplicity and versatility.

All the coatings have been tested against *Lactobacillus plantarum* (gram positive bacteria) and the results reveal high killing efficiency (higher than 99% in all cases) against the bacteria in comparison with reference substrates where a random distribution and growth of bacteria colonies were observed. In addition, it is important to remark that the coated areas with both processes showed an inhibition zone around them, indicating the high biocide effect of the coatings by the presence of the silver nanoparticles.

To sum up, both approaches for obtaining biocide surfaces can be used for different applications in a wide range of fields like in buildings, pharmaceutical tools or other instrumental devices, and humidity sensor coatings operating near tropical environmental conditions, as it will be shown in the following chapter.

Bibliography

[1] Mcdonnell, G.; Russell, A. D. Antiseptics and Disinfectants: Activity, Action, and Resistance. Clin. Microbiol. Rev. 1999, 12, 147-179.
[2] Russell, A. D. Biocide use and Antibiotic Resistance: The Relevance of Laboratory Findings to Clinical and Environmental Situations. Lancet Infectious Diseases 2003, 3, 794-803.
[3] Russell, A. D. Mechanisms of Antimicrobial Action of Antiseptics and Disinfectants: An Increasingly Important Area of Investigation. J. Antimicrob. Chemother. 2002, 49, 597-599.
[4] Rivero, P. J.; Urrutia, A.; Goicoechea, J.; Zamarreño, C. R.; Arregui, F. J.; Matías, I. R. An Antibacterial Coating Based on a polymer/sol- Gel Hybrid Matrix Loaded with Silver Nanoparticles. Nanoscale Research Letters 2011, 6, X1-7.
[5] Klasen, H. J. A Historical Review of the use of Silver in the Treatment of Burns. II. Renewed Interest for Silver. Burns 2000, 26, 131-138.
[6] Klasen, H. J. Historical Review of the use of Silver in the Treatment of Burns. I. Early Uses. Burns 2000, 26, 117-130.
[7] Lansdown, A. B. Silver. I: Its Antibacterial Properties and Mechanism of Action. J. Wound Care 2002, 11, 125-130.
[8] Li, W. -.; Xie, X. -.; Shi, Q. -.; Duan, S. -.; Ouyang, Y. -.; Chen, Y. -. Antibacterial Effect of Silver Nanoparticles on Staphylococcus Aureus. Biometals 2011, 24, 135-141.
[9] Li, W. -.; Xie, X. -.; Shi, Q. -.; Zeng, H. -.; Ou-Yang, Y. -.; Chen, Y. -. Antibacterial Activity and Mechanism of Silver Nanoparticles on Escherichia Coli. Appl. Microbiol. Biotechnol. 2010, 85, 1115-1122.
[10] Bragg, P. D.; Rainnie, D. J. The Effect of Silver Ions on the Respiratory Chain of Escherichia Coli. Can. J. Microbiol. 1974, 20, 883-889.
[11] Ilic, V.; Šaponjic, Z.; Vodnik, V.; Molina, R.; Dimitrijevic, S.; Jovancic, P.; Nedeljkovic, J.; Radetic, M. Antifungal Efficiency of Corona Pretreated Polyester and Polyamide Fabrics Loaded with Ag Nanoparticles. J. Mater. Sci. 2009, 44, 3983-3990.
[12] Jain, J.; Arora, S.; Rajwade, J. M.; Omray, P.; Khandelwal, S.; Paknikar, K. M. Silver Nanoparticles in Therapeutics: Development of an Antimicrobial Gel Formulation for Topical use. Molecular Pharmaceutics 2009, 6, 1388-1401.
[13] Miranda, M.; Fernández, A.; Díaz, M.; Esteban-Tejeda, L.; López-Esteban, S.; Malpartida, F.; Torrecillas, R.; Moya, J. S. Silver-Hydroxyapatite Nanocomposites as Bactericidal and Fungicidal Materials. International Journal of Materials Research 2010, 101, 122-127.
[14] Monteiro, D. R.; Gorup, L. F.; Takamiya, A. S.; Ruvollo-Filho, A. C.; Camargo, E. R. d.; Barbosa, D. B. The Growing Importance of Materials that Prevent Microbial Adhesion: Antimicrobial Effect of Medical Devices Containing Silver. Int. J. Antimicrob. Agents 2009, 34, 103-110.
[15] Panácek, A.; Kolár, M.; Vecerová, R.; Prucek, R.; Soukupová, J.; Kryštof, V.; Hamal, P.; Zboril, R.; Kvítek, L. Antifungal Activity of Silver Nanoparticles Against Candida Spp. Biomaterials 2009, 30, 6333-6340.
[16] Travan, A.; Marsich, E.; Donati, I.; Benincasa, M.; Giazzon, M.; Felisari, L.; Paoletti, S. Silver-Polysaccharide Nanocomposite Antimicrobial Coatings for Methacrylic Thermosets. Acta Biomaterialia 2011, 7, 337-346.
[17] Travan, A.; Pelillo, C.; Donati, I.; Marsich, E.; Benincasa, M.; Scarpa, T.; Semeraro, S.; Turco, G.; Gennaro, R.; Paoletti, S. Non-Cytotoxic Silver Nanoparticle-Polysaccharide Nanocomposites with Antimicrobial Activity. Biomacromolecules 2009, 10, 1429-1435.
[18] Greulich, C.; Kittler, S.; Epple, M.; Muhr, G.; Köller, M. Studies on the Biocompatibility and the Interaction of Silver Nanoparticles with Human Mesenchymal Stem Cells (hMSCs). Langenbeck's Archives of Surgery 2009, 394, 495-502.
[19] Chen, X.; Schluesener, H. J. Nanosilver: A Nanoproduct in Medical Application. Toxicol. Lett. 2008, 176, 1-12.
[20] Yuranova, T.; Rincon, A. G.; Bozzi, A.; Parra, S.; Pulgarin, C.; Albers, P.; Kiwi, J. Antibacterial Textiles Prepared by RF-Plasma and Vacuum-UV Mediated Deposition of Silver. J. Photochem. Photobiol. A. 2003, 161, 27-34

[21] Lee, H. Y.; Park, H. K.; Lee, Y. M.; Kim, K.; Park, S. B. A Practical Procedure for Producing Silver Nanocoated Fabric and its Antibacterial Evaluation for Biomedical Applications. Chemical Communications 2007, 2959-2961.
[22] Gao, Y.; Cranston, R. Recent Advances in Antimicrobial Treatments of Textiles. Text. Res. J. 2008, 78, 60-72.
[23] Blaker, J. J.; Nazhat, S. N.; Boccaccini, A. R. Development and Characterisation of Silver-Doped Bioactive Glass-Coated Sutures for Tissue Engineering and Wound Healing Applications. Biomaterials 2004, 25, 1319-1329.
[24] Ahmad, N.; Sharma, S.; Rai, R. Rapid Green Synthesis of Silver and Gold Nanoparticles using Peels of Punica Granatum. Advanced Materials Letters 2012, 3, 376-380.
[25] Singhal, G.; Bhavesh, R.; Kasariya, K.; Sharma, A. R.; Singh, R. P. Biosynthesis of Silver Nanoparticles using Ocimum Sanctum (Tulsi) Leaf Extract and Screening its Antimicrobial Activity. Journal of Nanoparticle Research 2011, 13, 2981-2988.
[26] Sharma, V. K.; Yngard, R. A.; Lin, Y. Silver Nanoparticles: Green Synthesis and their Antimicrobial Activities. Adv. Colloid Interface Sci. 2009, 145, 83-96.
[27] Dallas, P.; Sharma, V. K.; Zboril, R. Silver Polymeric Nanocomposites as Advanced Antimicrobial Agents: Classification, Synthetic Paths, Applications, and Perspectives. Adv. Colloid Interface Sci. 2011, 166, 119-135.
[28] Sharma, J.; Imae, T. Recent Advances in Fabrication of Anisotropic Metallic Nanostructures. Journal of Nanoscience and Nanotechnology 2009, 9, 19-40.
[29] Wang, J. -.; Wen, L. -.; Wang, Z. -.; Chen, J. -. Immobilization of Silver on Hollow Silica Nanospheres and Nanotubes and their Antibacterial Effects. Mater. Chem. Phys. 2006, 96, 90-97.
[30] Wang, J. -.; Wen, L. -.; Wang, Z. -.; Wang, M.; Shao, L.; Chen, J. -. Facile Synthesis of Hollow Silica Nanotubes and their Application as Supports for Immobilization of Silver Nanoparticles. Scr. Mater. 2004, 51, 1035-1039.
[31] Kawashita, M.; Toda, S.; Kim, H. -.; Kokubo, T.; Masuda, N. Preparation of Antibacterial Silver-Doped Silica Glass Microspheres. Journal of Biomedical Materials Research - Part A 2003, 66, 266-274.
[32] Rivera-Garza, M.; Olguín, M. T.; García-Sosa, I.; Alcántara, D.; Rodríguez-Fuentes, G. Silver Supported on Natural Mexican Zeolite as an Antibacterial Material. Microporous and Mesoporous Materials 2000, 39, 431-444.
[33] Park, S. -.; Jang, Y. -. Preparation and Characterization of Activated Carbon Fibers Supported with Silver Metal for Antibacterial Behavior. J. Colloid Interface Sci. 2003, 261, 238-243.
[34] Masuda, N.; Kawashita, M.; Kokubo, T. Antibacterial Activity of Silver-Doped Silica Glass Microspheres Prepared by a Sol-Gel Method. Journal of Biomedical Materials Research - Part B Applied Biomaterials 2007, 83, 114-120.
[35] Soto, G.; Tiznado, H.; Contreras, O.; Pérez-Tijerina, E.; Cruz-Reyes, J.; Del Valle, M.; Portillo, A. Preparation of a Ag/SiO2 Nanocomposite using a Fluidized Bed Microwave Plasma Reactor, and its Hydrodesulphurization and Escherichia Coli Bactericidal Activities. Powder Technol 2011, 213, 55-62.
[36] Bravo, J.; Zhai, L.; Wu, Z.; Cohen, R. E.; Rubner, M. F. Transparent Superhydrophobic Films Based on Silica Nanoparticles. Langmuir 2007, 23, 7293-7298.
[37] Grapski, J. A.; Cooper, S. L. Synthesis and Characterization of Non-Leaching Biocidal Polyurethanes. Biomaterials 2001, 22, 2239-2246.
[38] Lin, J.; Tiller, J. C.; Lee, S. B.; Lewis, K.; Klibanov, A. M. Insights into Bactericidal Action of Surface-Attached Poly(Vinyl-N-Hexylpyridinium) Chains. Biotechnol. Lett. 2002, 24, 801-805.
[39] Tiller, J. C.; Lee, S. B.; Lewis, K.; Klibanov, A. M. Polymer Surfaces Derivatized with Poly(Vinyl-N-Hexylpyridinium) Kill Airborne and Waterborne Bacteria. Biotechnol. Bioeng. 2002, 79, 465-471.
[40] Popa, A.; Davidescu, C. M.; Trif, R.; Ilia, G.; Iliescu, S.; Dehelean, G. Study of Quaternary 'Onium' Salts Grafted on Polymers: Antibacterial Activity of Quaternary Phosphonium Salts Grafted on 'Gel-Type' Styrene-Divinylbenzene Copolymers. React Funct Polym 2003, 55, 151-158.
[41] Sunada, K.; Watanabe, T.; Hashimoto, K. Studies on Photokilling of Bacteria on TiO2 Thin Film. J. Photochem. Photobiol. A. 2003, 156, 227-233.

[42] Daniel, A.; Le Pen, C.; Archambeau, C.; Reniers, F. Use of a PECVD-PVD Process for the Deposition of Copper Containing Organosilicon Thin Films on Steel. Appl. Surf. Sci. 2009, 256, S82-S85.
[43] Li, J.; Zivanovic, S.; Davidson, P. M.; Kit, K. Production and Characterization of Thick, Thin and Ultra-Thin chitosan/PEO Films. Carbohydr. Polym. 2011, 83, 375-382.
[44] Yang, Q. B.; Li, D. M.; Hong, Y. L.; Li, Z. Y.; Wang, C.; Qiu, S. L.; Wei, Y. Preparation and Characterization of a PAN Nanofibre Containing Ag Nanoparticles Via Electrospinning. Synth. Met. 2003, 137, 973-974.
[45] Hong, K. H.; Park, J. L.; Hwan Sul, I. N.; Youk, J. H.; Kang, T. J. Preparation of Antimicrobial Poly(Vinyl Alcohol) Nanofibers Containing Silver Nanoparticles. J. Polym. Sci. Part B 2006, 44, 2468-2474.
[46] Jin, W. -.; Lee, H. K.; Jeong, R. H.; Park, W. H.; Youk, J. H. Preparation of Polymer Nanofibers Containing Silver Nanoparticles by using Poly(N-Vinylpyrrolidone). Macromolecular Rapid Communications 2005, 26, 1903-1907.
[47] Rivero, P. J.; Urrutia, A.; Goicoechea, J.; Rodríguez, Y.; Corres, J. M.; Arregui, F. J.; Matías, I. R. An Antibacterial Submicron Fiber Mat with in Situ Synthesized Silver Nanoparticles. J Appl Polym Sci 2012, 126, 1228-1235.
[48]Hrudey, P. C. P.; Taschuk, M.; Tsui, Y. Y.; Fedosejevs, R.; Sit, J. C.; Brett, M. J. Evaporated Nanostructured Y 2O 3:Eu Thin Films. Journal of Nanoscience and Nanotechnology 2005, 5, 229-234.
[49] Kamiya, S.; Takahashi, H.; Saka, M.; Abé, H. Evaluation and Improvement of the Adhesive Fracture Toughness of CVD Diamond on Silicon Substrate. J Electron Packag, Trans ASME 2002, 124, 271-276.
[450] Shin, D. O.; Lee, D. H.; Moon, H. -.; Jeong, S. -.; Kim, J. Y.; Mun, J. H.; Cho, H.; Park, S.; Kim, S. O. Sub-Nanometer Level Size Tuning of a Monodisperse Nanoparticle Array Via Block Copolymer Lithography. Advanced Functional Materials 2011, 21, 250-254.
[51] Hench, L. L.; West, J. K. The Sol-Gel Process. Chem. Rev. 1990, 90, 33-72.
[52] Brinker, C. J.; Scherer, G. W. Sol → Gel → Glass: I. Gelation and Gel Structure. J. Non Cryst. Solids 1985, 70, 301-322.
[53] Brinker, C. J.; Scherer, G. W.; Roth, E. P. Sol → Gel → Glass: II. Physical and Structural Evolution during Constant Heating Rate Experiments. J. Non Cryst. Solids 1985, 72, 345-368.
[54] Scherer, G. W.; Brinker, C. J.; Roth, E. P. Sol → Gel → Glass: III. Viscous Sintering. Journal of Non-Crystalline Solids 1985, 72, 369-389.
[55] Lin, J.; Brown, C. W. Sol-Gel Glass as a Matrix for Chemical and Biochemical Sensing. TrAC - Trends in Analytical Chemistry 1997, 16, 200-211.
[56] Schmidt, H. Chemistry of Material Preparation by the Sol-Gel Process. J. Non Cryst. Solids
[57] Wencel, D.; Barczak, M.; Borowski, P.; McDonagh, C. The Development and Characterisation of Novel Hybrid Sol-Gel-Derived Films for Optical pH Sensing. Journal of Materials Chemistry 2012, 22, 11720-11729.
[58] Livage, J.; Sanchez, C.; Henry, M.; Doeuff, S. The Chemistry of the Sol-Gel Process. Solid State Ionics 1989, 32-33, 633-638.
[59] Livage, J.; Sanchez, C. Optical Properties of Sol-Gel Films. Molecular Crystals and Liquid Crystals Science and Technology Section B: Nonlinear Optics 1999, 21, 125-141.
[60] Decher, G. Fuzzy Nanoassemblies: Toward Layered Polymeric Multicomposites. Science 1997, 277, 1232-1237.
[61] Choi, J.; Rubner, M. F. Influence of the Degree of Ionization on Weak Polyelectrolyte Multilayer Assembly. Macromolecules 2005, 38, 116-124.
[62] Hammond, P. T. Form and Function in Multilayer Assembly: New Applications at the Nanoscale. Adv Mater 2004, 16, 1271-1293.
[63] Choi, J.; Rubner, M. F. Influence of the Degree of Ionization on Weak Polyelectrolyte Multilayer Assembly. Macromolecules 2005, 38, 116-124.
[64] Shiratori, S.; Yamada, M.; Ito, T.; Wang, T. C.; Rubner, M. F. In In Nanoscale control of layer thickness for EL devices by mass-controlled layer-by-layer sequential adsorption process; Materials Research Society Symposium - Proceedings; 2000; Vol. 598, pp BB1.9.1-BB1.9.6.
[65] Shiratori, S. S.; Rubner, M. F. PH-Dependent Thickness Behavior of Sequentially Adsorbed Layers of Weak Polyelectrolytes. Macromolecules 2000, 33, 4213-4219.

[66] Berg, M. C.; Choi, J.; Hammond, P. T.; Rubner, M. F. Tailored Micropatterns through Weak Polyelectrolyte Stamping. Langmuir 2003, 19, 2231-2237.
[67] Yoo, D.; Shiratori, S. S.; Rubner, M. F. Controlling Bilayer Composition and Surface Wettability of Sequentially Adsorbed Multilayers of Weak Polyelectrolytes. Macromolecules 1998, 31, 4309-4318.
[68] Fendler, J. H. Self-Assembled Nanostructured Materials. Chemistry of Materials 1996, 8, 1616-1624.
[69] Urrutia, A.; Rivero, P. J.; Ruete, L.; Goicoechea, J.; Matías, I. R.; Arregui, F. J. Single-Stage in Situ Synthesis of Silver Nanoparticles in Antibacterial Self-Assembled Overlays. Colloid Polym. Sci. 2012, 290, 785-792.
[70] Rivero, P. J.; Goicoechea, J.; Urrutia, A.; Matias, I. R.; Arregui, F. J. Multicolor Layer-by-Layer Films using Weak Polyelectrolyte Assisted Synthesis of Silver Nanoparticles. Nanoscale Research Letters 2013, 8, 1-10.
[71] Urrutia, A.; Rivero, P. J.; Ruete, L.; Goicoechea, J.; Fernández-Valdivieso, C.; Arregui, F. J.; Matías, I. R. An Antibacterial Surface Coating Composed of PAH/SiO2 Nanostructurated Films by Layer by Layer. Physica Status Solidi (C) Current Topics in Solid State Physics 2010, 7, 2774-2777.
[72] JIS Z 2801: Japanese Industrial Standard, Japanese Standard Association. 2000.

CHAPTER 5. Optical fiber humidity sensors based on Localized Surface Plasmon Resonance (LSPR) and Lossy Mode Resonance (LMR)

In previous chapters, different methodologies for synthesizing silver nanoparticles and their incorporation into thin films have been reported. Additionally, their antibacterial behavior has been demonstrated. In this chapter, optical fiber sensors based on silver nanoparticles are shown and their potential applications as humidity sensors. A study about the different types of electromagnetic resonances generated onto an optical fiber core as a function of the characteristics of the silver nanoparticles and thickness coating will be studied here. Finally, it is presented for the first time the fabrication of an optical fiber humidity sensor based on the simultaneous observation of Localized Surface Plasmon Resonance (LSPR) and Lossy Mode Resonance (LMR).

5.1. Introduction to electromagnetic resonances

In the last years, surface plasmon resonance (SPR) is one of the most widely studied optical resonant phenomena for sensing. Since the first demonstration of SPR for the study of processes at the surfaces of metals and sensing gases in the early 1980s [1,2], a large number of structures based on this optical phenomenon have been described in terms of both development of the technology and its applications for detection of chemical and biological species [3]. The SPR phenomenon consists in a resonant coupling between an incident electromagnetic wave and the surface of a metallic-thin film, where some of the energy of the light is transferred to the surface free electrons of the metal, causing an electronic wave at the metal-dielectric interface. This energy transfer only occurs under certain resonant conditions between the wavalenth and the angle of incidence of the light and the thickness and refractive index of the dielectric medium. This results in the apparition of a sharp absorption peak in the transmitted light. A change in the refractive index of the dielectric medium will produce a wavelength shift of this resonant peak [4,5]. This phenomenon has been applied in the design and fabrication of sensors for different applications because SPR coupling condition is extremely sensitive to variation in the properties of the surrounding medium and metal layer [6-11].

First studies about SPR generation used a prism to excite surface wave (known as Kretschmann configuration) [6]. However, this prism-based SPR sensing setup presents several shortcomings, such as a big size, presence of fragile mechanic parts or the impossibility for remote sensing applications. To overcome these limitations, the use of optical fiber instead of a prism is developed by Jorgenson and Yee [12] where it is possible to combine the typical advantages of optical fiber (small size, low weight or immunity to electromagnetic interference) with the possibility excellent sensitivity of this sensing SPR-device [13-15]. Due to this, numerous optical fiber sensors based on SPR phenomenon have been reported [16-28]. However, this kind of devices presents some limitations. On one hand, SPR phenomenon can be only produced by TM polarized light and it is necessary a specialoptical fiber which maintains the polarization to obtain a sharp absorption peak in the transmitted light. On the other hand, all the SPR-devices are limited to the use of specific metals that can fulfill the SPR condition. The most used materials are noble metals, especially gold or silver, because their SPR resonances show sharp and intense attenuation bands in the visible region of the spectrum.

It is important to remark what happens with the SPR phenomenon when the metallic medium is confined into a nanoparticle. In this case, the charge-density oscillation does not affect only to the nanoparticle surface, but the whole nanoparticle electronic distribution is altered. Therefore the Localized Surface Plasmon Resonance (LSPR) is in fact a particularization of the classic SPR phenomenon for the case of metallic nanoparticles suspended into a particular dielectric medium like a fluid or a coating [29-41]. LSPR has also been used for the creation of optical sensors [42, 43], nevertheless they show additional issues such as the short range of sensitivity of the change of refractive index around the nanoparticle (4-5 nm), and the small wavelength shifts observed in operation.

Very recently, an alternative resonant phenomenon has been reported, named Lossy Mode Resonance (LMR). This LMR presents very different characteristics which can overcome the some of the previously described limitations of the SPR-sensor devices [44-46]. One of these advantages is that LMR can be generated by using a broader range of supporting materials, not only electrically conductive materials as in the SPR and LSPRoptical sensors. Another important advantage is that the LMR-devices allow the generation of resonances with standard optical fiber because these LMR are generated by both, TE and TM, light polarizations. Furthermore, dramatically higher wavelength shifts have been observed using LMR technology. Due to these advantages, a considerable increase of publications based on LMR-devices has been reported in recent works during the last four years [47-52].

Both phenomena will be presented and analyzed in this chapter. The differences between LMR and LSPR will be theoretically and experimentally

explained. Those phenomena will be studied for the particular case of an optical waveguide coated with a thin-film loaded with silver nanoparticles (AgNPs). Finally, practical applications as humidity sensing devices based on these electromagnetic resonances will be presented, emphasizing their great importance in the field of optical fiber sensors. This is the first time that both LSPR and LMR phenomena are reported in the bibliograghy in a same device which could yield self-referenced optical sensors, as it is discussed in the following sections.

5.2. Lossy Mode Resonances (LMR) and Localized Surface Plasmon Resonance (LSPR) for sensing applications

When an ultrathin coating is deposited onto an optical waveguide (see Figure 5.1), the propagation of the light is affected at a specific wavelength range. If the refractive index of the resulting coating has an imaginary part different to zero, it introduces losses that can produce electromagnetic resonances. According to this, three different cases of electromagnetic resonances can be distinguished as a function of the materials involved in the system (optical waveguide, coating and external medium):

a) The first case occurs when the real part of the thin-film permittivity is negative and higher in magnitude than both its own imaginary part and the permittivity of the material surrounding the thin film (i.e. the optical waveguide and the surrounding medium in contact with the thin film). In this case, coupling occurs between light propagating through the waveguide and a surface plasmon, which is called Surface Plasmon Polariton (SPP). This phenomenon produces a resonance called Surface Plasmon Resonance (SPR).

b) The second case occurs when the real part of the thin-film permittivity is positive and higher in magnitude than both its own imaginary part and the permittivity of the material surrounding the thin film. Some authors consider these modes as long-range guided modes [31], whereas others call them lossy modes [32, 33]. In this work, they will be called lossy modes to make a difference between them and the rest of guided modes. These lossy modes will produce the second type of resonances: the Lossy Mode Resonance (LMR).

c) The third case occurs when the real part of the thin-film permittivity is close to zero, while the magnitude of its imaginary part is large [31]. This case, known as long-range surface exciton polariton (LRSEP), falls beyond the scope of this study and will no longer be studied.

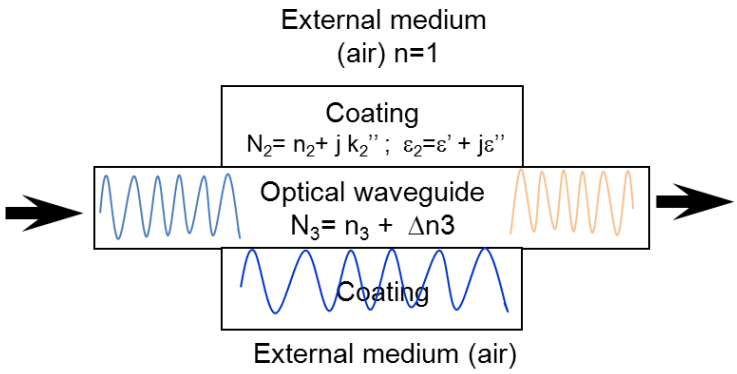

Figure 5.1. Schematic representation of the optical system used to obtain electromagnetic resonances.

The permittivity of a material can be expressed in terms of its complex refractive index (N=n+jk) according to Eq. 5.1.

$$\varepsilon = \varepsilon' + j\varepsilon'' = N^2 = (n + jk)^2 = n^2 - k^2 + j2nk \qquad (5.1)$$

In Table 5.1, a summary of these conditions in terms of its permittivity is presented.

Table 5.1. Summary of the conditions needed to obtain the three different types of electromagnetic resonances with the system represented in Figure 5.1 in terms of its permittivity.

Resonance	Permittivity
Surface Plasmon Resonance **SPR**	$\varepsilon_2' < 0$ $\varepsilon_2' > \varepsilon_2''$ $\varepsilon_2' > \varepsilon_3'$
Lossy Mode Resonance **LMR**	$\varepsilon_2' > 0$ $\varepsilon_2' > \varepsilon_2''$ $\varepsilon_2' > \varepsilon_3'$
Long-Range Surface Exciton Polariton **LRSEP**	$\varepsilon_2' \approx 0$ ε_2'' ↑↑

As was previously commented, this thesis is based on the synthesis of AgNPs and a further incorporation into a polymeric or hybrid matrix obtained by Layer-by-Layer assembly or sol-gel process. The physical phenomenon of SPR changes when the metallic material is distributed into nanoparticles instead of a thin-film onto the optical waveguide. For this specific case, the phenomenon is called Localized Surface Plasmon Resonance (LSPR). According to the scope of this work which is devoted to the synthesis of metallic silver nanoparticles (AgNPs), consequently the focus is placed in the fabrication and design of LSPR-sensors instead of SPR-devices.

Another important consideration is that LSPR sensors have been deeply studied during the last two decades and the number of publications related to this optical phenomenon is higher than LMR. Moreover, although initial publications related to LMR are based on theoretical studies about the light propagation through semiconductor-cladded waveguides [44, 45], there is an increase of publications based on experimental studies as sensing devices (basically optical fiber refractometers), using semiconductor materials [53-62]. The characteristics of these materials are adequate for generation of lossy modes. In these cases, the attenuation maxima of the light propagating through the waveguide are obtained for specific thickness [63, 64]. This effect is produced as a consequence of a coupling between a waveguide mode and a particular lossy mode of the semiconductor thin film.

In this chapter, both LSPR and LMR phenomena will be separately analyzed in sensing devices, thanks to the synthesis and incorporation of silver nanoparticles (AgNPs) in a polymeric coating fabricated onto the optical fiber core, using the two different synthetic methodologies, *in situ* synthesis (ISS) and Layer-by-Layer Embedding (LbL-E) of the AgNPs. Finally, an optical fiber humidity sensor based on the simultaneous observation LSPR and LMR will be experimentally demonstrated for the first time, emphasizing the advantages of using this device in terms of a dual-reference as well as their response to fast changes of Relative Humidity (RH) such as human breathing.

5.3. Optical fiber configuration and propagation of light through a thin-film coated optical fiber core

To characterize the electromagnetic resonances (LSPR or LMR), an optical fiber transmission setup was used. The cladding of a segment of 2 cm of the optical fiber was removed. This uncladded segment is where the sensitive coatings will be created and will be called "sensitive region". The setup consists of a halogen lamp as white light source and a spectrometer connected at the opposite end of the fiber in order to collect the light after passing through the sensitive region in which a thin-film was deposited, see Figure 5.2 (top). The light passes through the sensitive region which is located between the light source and the spectrometer. This region is where the optical fiber core is coated with AgNPs loaded polymeric thin film. Such film will generate different kind of resonances depending on its fabrication parameters. A detail of the cross and longitudinal section of this sensitive region is shown in Figure 5.2 (down).

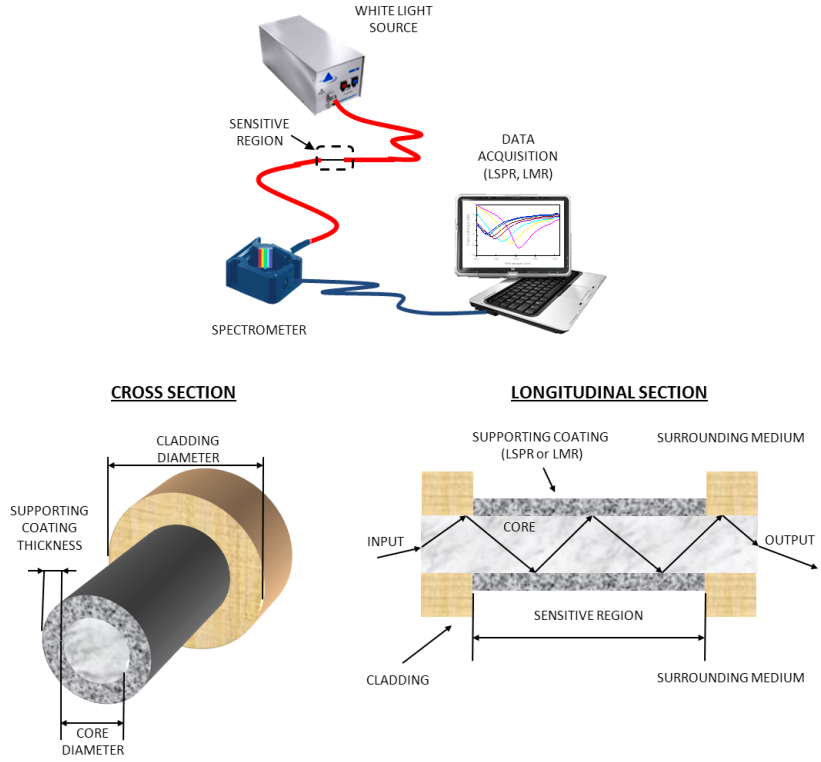

Figure 5.2. Optical fiber configuration used to characterize the electromagnetic resonances (top); detail of the cross and longitudinal section of the sensitive region coated with a supporting coating (LSPR or LMR) (down). The cladding of the optical fiber was chemically removed.

5.4. Optical fiber humidity sensors based on LSPR

The LSPR resonant condition is strongly affected by the composition, size, shape, aggregation state or the surrounding environment of the metallic nanoparticles. Moreover, the location of the LSPR in the visible region of the electromagnetic spectrum as a function of these plasmonic properties, mostly related to the synthesis of silver or gold nanoparticles, make possible the design of LSPR-based devices.

In this section, we propose the synthesis of silver nanoparticles (AgNPs), and their incorporation into thin films using the Layer-by-Layer Embedding (LbL-E) deposition technique. The central wavelength of the resonant peak (LSPR) depends on multiple factors such as nanoparticle size, shape and interparticle interaction. Moreover, these nanoparticles (AgNPs) have been widely used in antibacterial surfaces because silver ions show a notorious broad spectrum biocide effect. More specifically, silver is particularly attractive because it combines a high toxicity for bacteria with a low toxicity for humans [65-76].

In fact, this dual behavior of the AgNPs, generation of the LSPR in the visible region and a very good antibacterial agent, makes AgNPs an adequate candidate in sensing devices where the growth of microorganisms can affect the final behavior of the sensor. This is the case of a high humidity ambient because the bacteria are very likely to grow at these conditions, and enabling an incorrect monitoring of the system. Due to this, AgNPs can avoid the growth of the bacteria and, at the same time, it is possible to monitor the changes of Relative Humidity (RH) as a function of the plasmon resonance position.

5.4.1. Fabrication of the thin-films onto the sensitive region

A 2 cm segment of uncladded optical fiber core (sensitive region) is coated using the LbL-E deposition technique, as it was commented in Chapter 3. It is initially used the LbL-E because it allows the monitorization and control of the coating thickness with a high accuracy during the fabrication process.

To perform this process, layers of opposite-charged materials are alternated. Electrostatic attraction between cationic and anionic layers makes the resultant multilayer structure homogeneous and compact [77, 78]. Here, PAH is used as polycation and PAA-AgNPs (orange coloration) [79] is used as polyanion. The final yellowish-orange coloration of the thin films indicates that AgNPs with a spherical shape has been successfully incorporated into the films, as it was previously commented in Chapter 3 (section 3.3) [80].

It is important to remark that the polymeric structure (PAH/PAA) shows a shighly hydrophilic behavior that makes it sensitive to changes in the relative humidity. The PAH/PAA structure changes its effective refractive index when it absorbs/desorbs water from the environment. Furthermore the thickness and roughness of the (PAH/PAA) LbL coatings can be accurately adjusted [81-83] (see also Appendix 2) and let us tailor its overall properties as desired. This makes LbL films ideal to characterize and understand the evolution of the optical measurements collected from the following optical sensors.

5.4.2. Device characterization

The experimental setup used to perform the analysis is shown in Figure 5.3. This setup consists of a white halogen lamp connected to one end of the optical fiber and a CCD-based UV-VIS spectrometer (OceanOptics HR4000) connected to the other end of the fiber. This combination of optical source and detector allows us to show transmitted spectra in the wavelength range from 350 to 1000 nm. This study will focus on this specific interval because the LSPR position corresponding to the synthesized AgNPs is obtained in this specific region of wavelength, specifically at 430-440 nm (yellowish-orange color). The optical fiber (FT silica/TEQS, Thorlabs Inc.) has 200/225 μm of core/cladding diameter and it is made of fused silica.

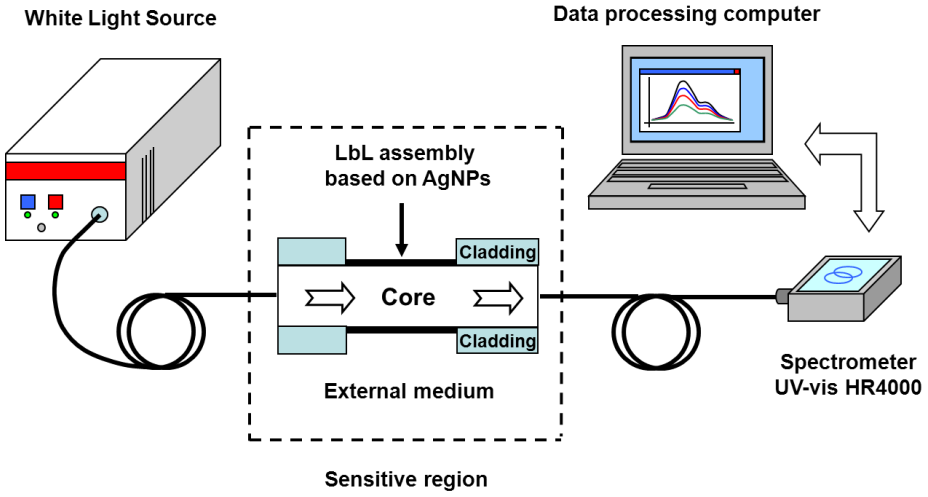

Figure 5.3. Experimental setup used to obtain and characterize the LSPR in the visible region.

Light passes through the sensitive region, which it is located between the light source and the detector. Transmitted light is affected by the new boundary conditions created by the LbL-E coating based on AgNPs. Then, an environmental chamber (Angelantoni Inc.) was used to control both the Relativity Humidity (RH) and the temperature of the sensor surrounding medium. The optical fiber sensor was exposed to humidity changes in the climatic chamber from 20%RH to 70%RH and the temperature was kept constant at 25ºC during the whole RH cycle.

5.4.3. Generation of LSPR band during the LbL-E deposition

When the LbL-E is sequentially created onto the sensitive region, an alteration of the visible absorption spectrum is observed at the detector. This aspect is directly related to the Localized Surface Plasmon Resonance (LSPR) phenomenon of the silver nanoparticles (AgNPs). In fact, the UV-Vis spectra were used to monitor the multilayer buildup LbL assembly in order to confirm the existence of this absorption peak of the LSPR at this specific wavelength region around 430nm.

In Figure 5.4, UV-Vis spectra are shown when the LbL-E was built up at different thickness coatings as a function of the number of bilayers added in the final coating (from 1 to 15 bilayers). The spectra show a direct relation between the number of bilayers added and the increasing absorbance of the LSPR absorption bands, at 440 nm. In other words, the results confirm that the optical absorbance of the coating increases directly with the number of bilayers. This confirms the hypothesis that the amount of AgNPs within the coating increases directly with the number of bilayers. Moreover, the wavelength position of the LSPR at 440 nm and the initial yellowish-orange coloration of the nanoparticles are indicative of a complete incorporation of spherical AgNPs in the final coating.

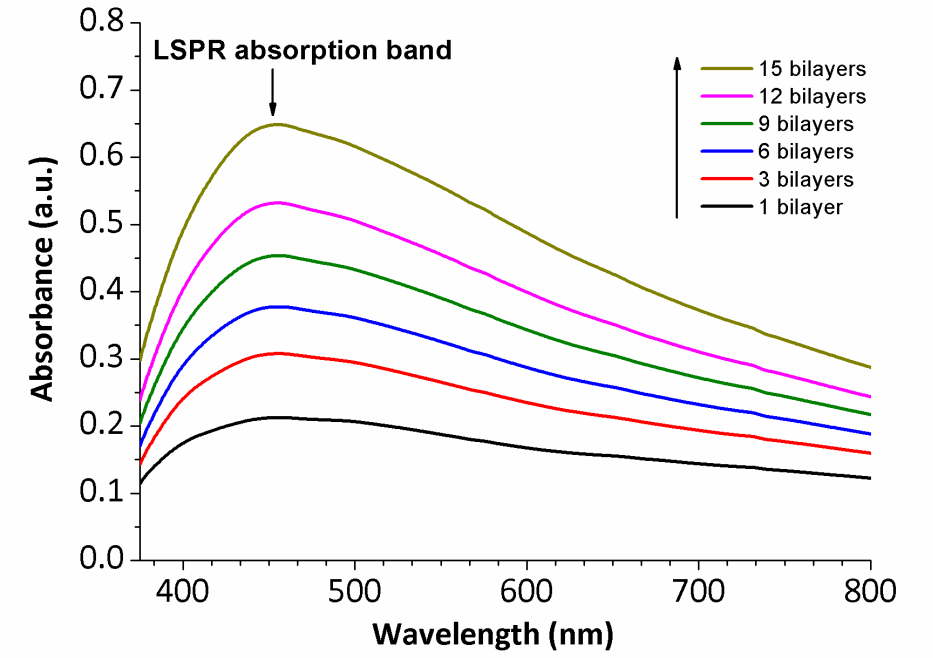

Figure 5.4. UV-Vis spectra when the LbL-E of the silver nanoparticles (AgNPs) is performed. The main absorption band is the LSPR corresponding to the AgNPs incorporated into the thin film. The curves plotted are for 1, 3, 6, 9, 12 and 15 bilayers.

5.4.4. Response of the LSPR to variation of RH changes

As it has been demonstrated in previous works, coatings based on weak polyelectrolytes (PAH/PAA) can modify their thickness and refractive index with Relative Humidity (RH) changes due to the swelling/deswelling phenomenon [84-88]. In Figure 5.5, the optical fiber sensor was experimentally tested to RH changes from 20% to 70% RH at constant temperature.

The results displayed in Figure 5.5 indicate that only a change in intensity of the LSPR attenuation band was observed as RH is varied. The intensity of the LSPR peak showed a linear response to RH changes as it can be seen in Figure 5.5 (inset). Nevertheless, no significant wavelength dependence with these RH changes was observed in the position of the LSPR band (440 nm). This change in wavelength was almost negligible respect to the change in intensity [42].

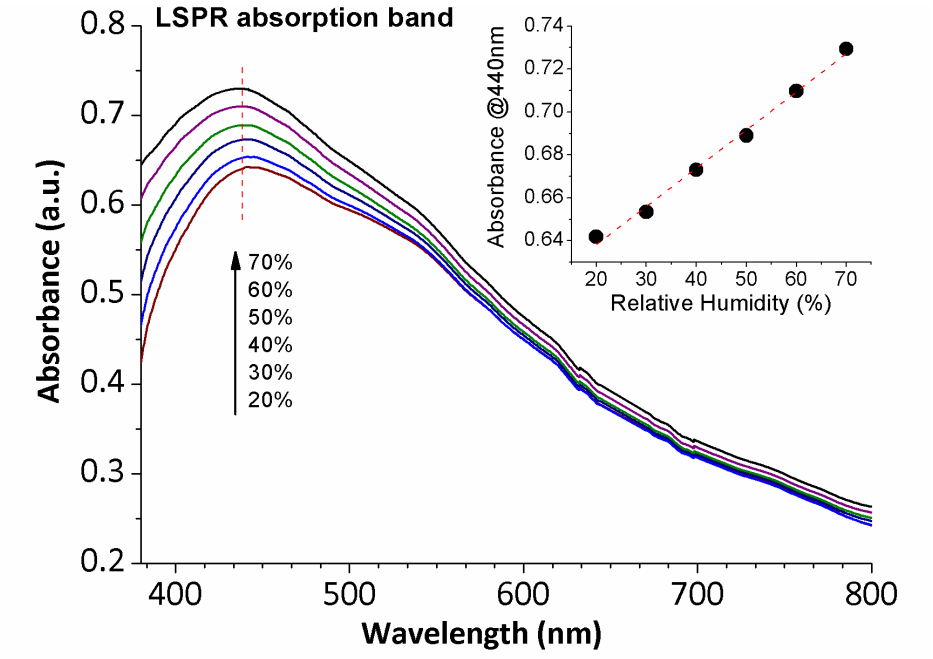

Figure 5.5. Spectral response of the device to RH changes from 20% to 70% RH at a constant temperature of 25ºC.

5.5. Optical fiber humidity sensor based on LMR

In previous section, an optical fiber humidity sensor based on LSPR was presented. In this section, a novel optical fiber humidity sensor based on a new optical phenomenon, known as Lossy-mode resonance (LMR) will be shown.

This new type of resonances (LMR) can be supported by thin-film coated optical waveguides. These optical resonances occur when the real part of the thin film permittivity is positive and higher in magnitude than both its own imaginary part and the real part of the material surrounding the thin film [44-46]. LMR-based devices have been explored for the fabrication of optical fiber pH sensors [51, 52], humidity sensors [57] or refractometers [58-62].

These devices based on LMR bands can be made of diverse materials such as polymers or ceramics. Furthermore, LMR-based devices make possible the generation of multiple resonant absorption bands and it is possible to obtain sensing signals as a function of the thickness and refractive index of optical fiber overlay.

5.5.1. Fabrication of the thin-films onto the sensitive region

In this section, the chemical route used for the incorporation of the metallic nanoparticles into thin films is the *in situ* synthesis (ISS) process, as it was explained in Chapter 2 (section 2.3). This process based on the *in situ* synthesis of AgNPs makes possible to obtain a resonant band (LMR) in the infrared region (900-1600 nm). The utilization of these metallic AgNPs for optical sensors produces an increasing of the refractive index of the thin film and permits the generation of a LMR band in this spectral range of study (infrared, NIR).

5.5.1.1. Fabrication of the polymeric coating

A polymeric matrix has been synthesized using the Layer-by-Layer technique (LbL) by sequentially exposing the optical fiber core to the cationic polyelectrolyte poly(allylamine hydrochloride) (PAH) and to the anionic polyelectrolyte poly(acrylic acid, sodium salt) (PAA).

This process was repeated until reaching a [PAH/PAA] polymeric structure of 40 bilayers (see appendix 2).

5.5.1.2. In situ synthesis of silver nanoparticles into the polymeric coating

Once the polymeric overlay was deposited onto the optical fiber core (sensitive region), the *in situ* synthesis (ISS) process was performed in order to incorporate the AgNPs into the polymeric matrix. Then, the loading/reduction

(L/R) process has been repeated up to 6 times in order to locate the LMR band in the infrared region.

A color change from transparent to orange has been pointed as an interesting result to corroborate the synthesis of the silver nanoparticles (AgNPs) during the Loading/Reduction process into the polymeric coating obtained by the LbL assembly [89]. In Figure 5.6, it is possible to appreciate the difference between a glass slide with only [PAH/PAA] polymeric coating obtained by the LbL assembly (totally transparent) and, a glass slide after the six loading/reduction (L/R) cycles (golden-yellowish), which it is indicative that AgNPs have been correctly synthesized and incorporated into the polymeric overlay onto the sensitive region.

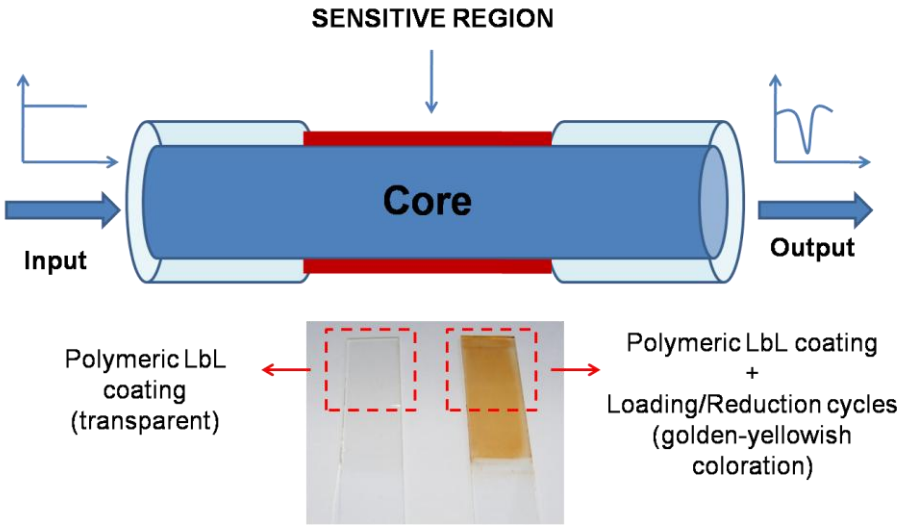

Figure 5.6. Schematic representation of the device based on the *in situ* synthesis (ISS) of AgNPs into the polymeric LbL matrix. The orange coloration indicates that AgNPs have been synthesized onto the optical fiber core.

This colored appearance is the result of the presence of a LSPR absorption band of the metallic AgNPs synthesized inside the polymeric coating, and makes possible the apparition of a strong absorption band in the visible region (410-450 nm) This light coupling results in an orange coloration of the coating as far as the LSPR absorption of spherical AgNPs is typically located around 410-450 nm, as it was previously demonstrated in Chapter 2.

5.5.2. Device characterization

The main aim of this section is to monitor the evolution of the LMR absorption band in the near infrared region (NIR). The experimental setup is very similar to the shown in Section 5.4.2.

In this case, the experimental setup consisted of a white halogen lamp (Ando Inc.) used as the excitation source which was connected to one end of the fiber and a CCD-based NIR spectrometer (NIR512 from Oceanoptics Inc.) which was connected to the other end of the fiber in order to obtain spectral information in the range between 900 and 1600 nm (infrared region). In order to observe the wavelength shift of the LMR absorption peak, the sensitive fragment is subjected to RH changes. The same environmental chamber (Angelantoni Inc.) of the previous section was used to control both RH and temperature surrounding the sensor.

5.5.3. Generation and shift of LMR band during the deposition

The *in situ* synthesis of the AgNPs as a function of the number of Loading/Reduction (L/R) cycles makes possible the generation of a new absorption band (LMR) in the infrared region (NIR). As it has been previously demonstrated in Chapter 2, the thickness of the LbL film was kept unaltered as the L/R cycles were carried out, and the only change is the amount of silver that has been loaded into the LbL film. The amount and size of the metal nanoparticles synthesized in the LbL polymeric coating modifies the overall refractive index of the film. Due to this, the wavelength of the LMR band maximum is shifted to longer wavelengths as a higher number of L/R cycles were performed, as it can be observed in Figure 5.7. An evolution of the LMR band with 4, 5 and 6 L/R cycles is observed in the infrared region (see Figure 5.8). A wavelength displacement of 150 nm from the 3rd cycle to the 6th cycle is observed during the *in situ* synthesis (ISS) of the AgNPs.

It is important to remark that this synthetic route makes possible the monitoring of the optical response of the optical fiber during the whole synthesis process. This allows us to stop the AgNPs growth during the Loading/Reduction cycles when the LMR position band is located at the desired wavelength in the infrared region, 1150 nm in this case.

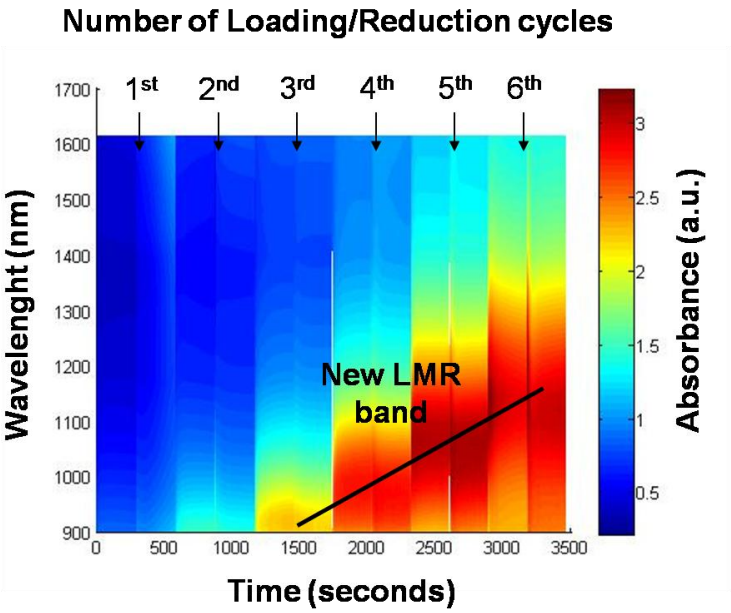

Figure 5.7. Spectral response at infrared region (NIR) as a function of the number of Loading/Reduction (L/R) cycles onto the optical fiber core.

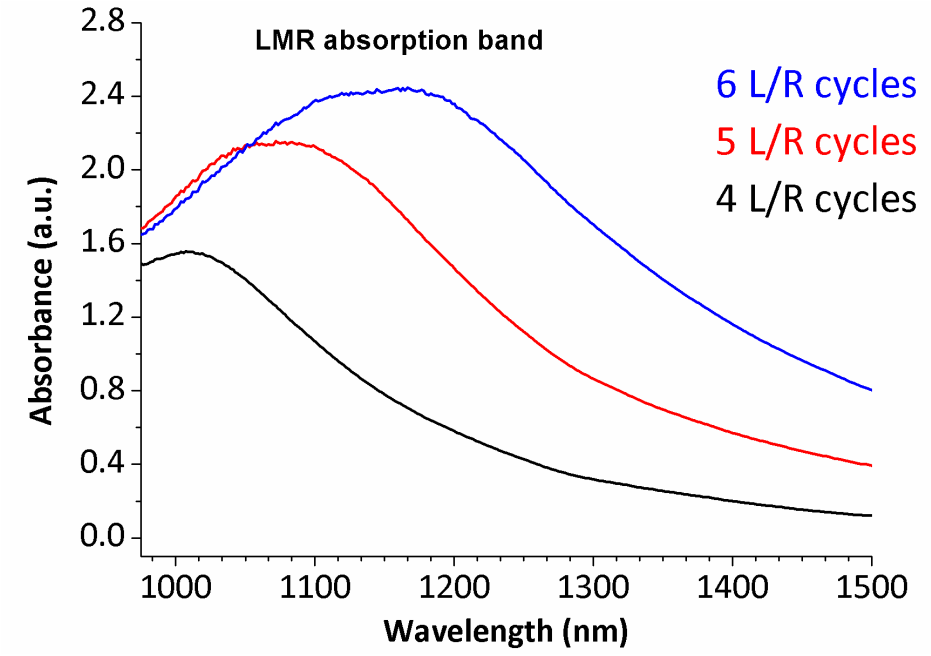

Figure 5.8. Evolution of the UV-Vis spectra of the LMR absorption band in the infrared region as a function of 4, 5 and 6 Loading/Reduction (L/R) cycles.

5.5.4. Response of the LMR to variation of RH changes

Once the sensor was fabricated in order to position the working point of the sensor (LMR position band) in the sensitivity region (NIR) at 1150 nm, the device was tested to variations of RH. In Figure 5.9, the dynamic response of the device (LMR band, black line) to different RH values between 20% and 80% for several cycles is shown. The results indicate that the dynamic range of the device in the studied range (NIR) is 27.3 nm which corresponds to a sensitivity of 0.455 nm per %RH. However, this device shows a high value of hysteresis (17.3%) because of the important difference between the rise and fall cycle when the maxima wavelength of LMR band is tested to RH changes.

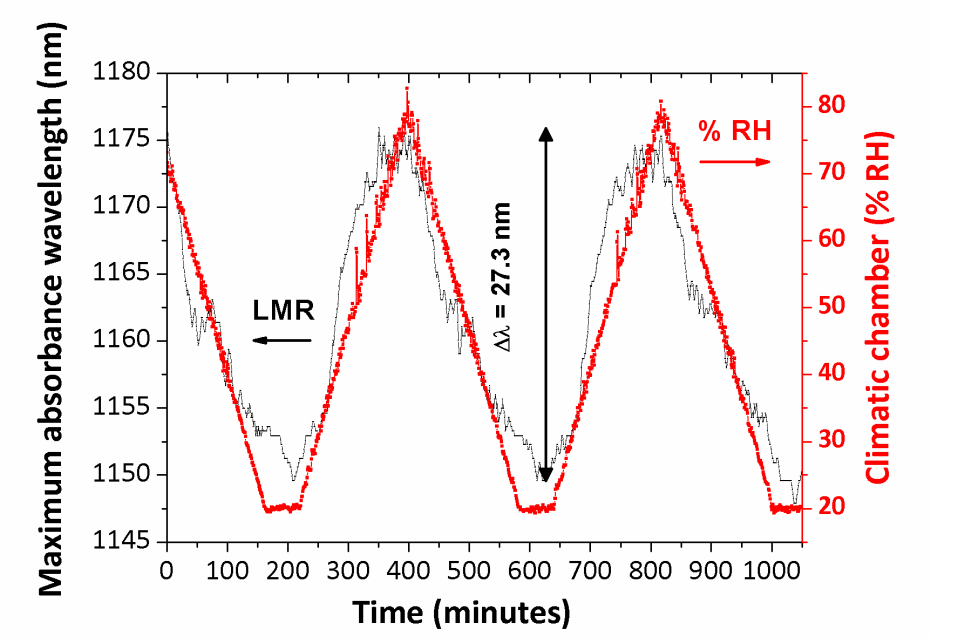

Figure 5.9. Dynamic response of the device (LMR maximum sensitivity) to RH changes from 20 to 80% at a constant temperature of 25ºC.

Finally, this device has been experimentally tested for human breathing changes at LMR wavelength position (1150 nm) to evaluate the response time. The results of the experiment to these quick changes of RH measurements are shown in Figure 5.10. The observed response time of the sensor was 692 and 839 ms for the rise and fall, respectively. The response of this device is very fast, periodic and repetitive, as it can be observed in the inset of the Figure.

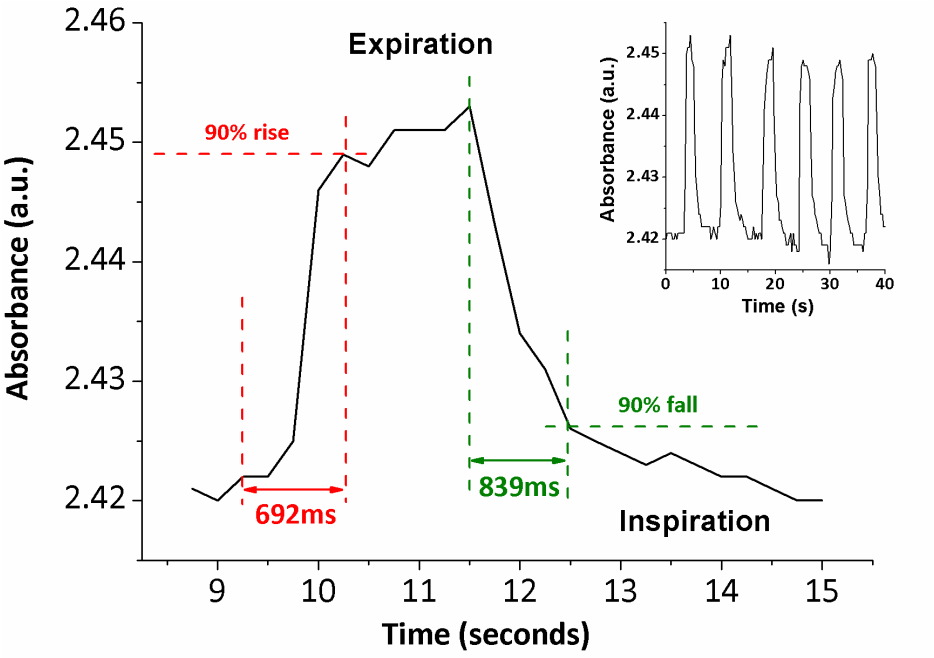

Figure 5.10. Response of the sensor to several consecutive human breathing cycles.

5.6. Optical fiber humidity sensors based on the simultaneous measurement of both LSPR and LMR

After observing separately the behavior of both LSPR and LMR phenomena when the sensitive region is supporting by a thin-film based loaded with AgNPs, new supporting coatings were selected to continue with this study. Particularly, thicker LbL-E thin films based on the same synthetic process shown in section 5.4 were developed. This leads us to the present work, the fabrication and design of coatings for a novel optical fiber sensor based on the simultaneous measurement of both LSPR and LMR for monitoring humidity changes.

The LbL-E deposition technique permits to control and monitor the transmission spectra while the coating is being deposited as a function of the number of bilayers added to the coating (directly related with its thickness). This is an important advantage for research purposes because it enables to observe the generation of the different electromagnetic resonances, such as Lossy mode resonances (LMR) as the coating thickness is increased.

As it was previously commented, one of the main advantages of the use of AgNPs in a polymeric matrix is the alteration in intensity of the LSPR when a change of the refractive index of the polymeric overlay is produced due to the swelling/deswelling phenomenon. However, a thicker coating based on the deposition of these AgNPs, allows an improvement of the sensitivity to RH changes of the device because of the presence of the LMRs. These LMR bands present a peak wavelength shift that depends on the thickness and refractive index of the overlay and that can be monitored. Due to this, it is possible to register humidity changes as a function of the wavelength displacement of the LMR, and not only with an intensity shift of the LSPR as it was observed in section 5.4. Moreover, the fabrication process (LbL-E) can be stopped at the desired moment when LMR band appears in the transmission spectra [45, 52].

As it will be explained in the following section, the presence of this dual-peak, LSPR and LMR respectively, permits to obtain more accurate measurements of the device. Thus, in this section, the transmission spectra of devices fabricated with LbL-E films of different thickness will be analyzed, trying to explain the generation and shift of the LSPR and LMR, testing its response to changes in the RH and comparing these results with the previously LSPR-device.

5.6.1. Fabrication of the thin-films onto the sensitive region

Optical fiber sensors with two different thicknesses (25 and 40 bilayers) were fabricated using the LbL-E deposition technique. For all the cases it is assumed that the sensitive region consists of both AgNPs (LSPR) and a polymeric matrix (PAH/PAA) which it is sensitive to the RH changes. Moreover, the presence of AgNPs allows an improvement of the visibility of the LMR bands with a smaller thickness in comparison with a sensor with a polymeric overlay without silver nanoparticles. An important advantage of the use of LMR as a sensing signal is the possibility of selecting the wavelength of operation and tuning the sensitivity by just tuning the thickness of the coating.

Here, it will be shown the successive evolution of the apparition of the different absorption bands when the thickness coating is increased up to a number total of 40 bilayers. For this case, firstly LSPR band will appear at a typical wavelength of 430-450 nm, which it is typical of spherical AgNPs without a significant wavelength-dependence (section 5.4), and secondly, the apparition of the LMR bands will be observed to sweep all the spectral range as the thickness coating is increased [42, 43].

5.6.1.1. Generation of the LSPR and a single LMR

The UV-Vis spectra was used to monitor the transmitted light during the LbL-E deposition technique, in order to study the apparition of the different resonant absorption peaks caused by the coating based on AgNPs.

In Figure 5.11, when the coating thickness has less than 20 bilayers it is possible to appreciate only a LSPR absorption band. This first absorption band (LSPR) was found centered around 450 nm, and it is attributed to the optical properties of the AgNPs. In addition, when the thickness of the LbL coating is increased up to 30 bilayers, a new absorption band attributed to the LMR phenomenon is observed (LMR 1). This resonant condition for LMR 1 strongly depends on the thickness and refractive index of the optical fiber overlay.

In fact, this LMR 1 attenuation band presents a shift of 300 nm of the maximum with a thickness increase of only 5 bilayers. The central wavelength of such LMR 1 is shifted from 650 nm to 950 nm in the spectral range as the number total of bilayers is increased from 25 to 30 bilayers, as it can be observed in Figure 5.11.

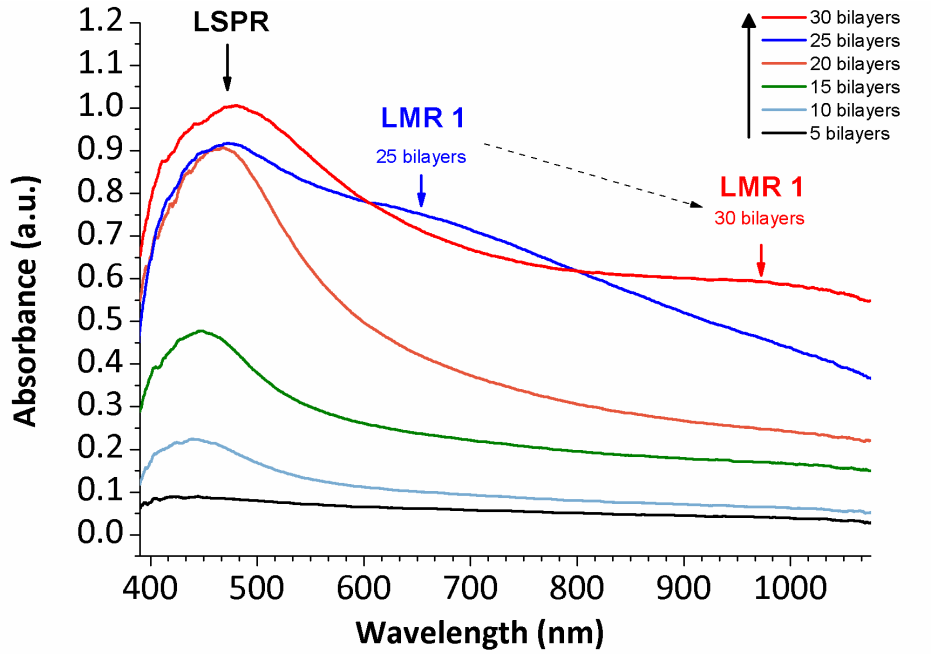

Figure 5.11. UV-Vis spectroscopy of the sensor as a function of the number of bilayers added using the LbL-E deposition technique. The curves plotted are for 5, 10, 15, 20, 25 and 30 bilayers.

5.6.1.2. Generation of multiple LMRs

A detail of the last 5 bilayers of the fabrication process (from 36 to 40 bilayers) is observed in Figure 5.12, where the apparition of both LMR 2 and LMR 3 absorption bands and their displacement as more bilayers are added can be easily appreciated. These resonances (LMR 2 and LMR 3) remained visible within the studied spectral range at the end of the fabrication process, while LMR 1 exceeded this range (more than 1100 nm) for a number of bilayers higher than 30. Moreover, it is possible to observe an overall displacement of the central wavelength of both LMR 2 and LMR 3 of 110 nm and 30 nm respectively, when the thickness coating is increased from 36 to 40 bilayers.

As it can be observed in Figures 5.11 and 5.12, it is possible to detect multiple absorption peaks (LMRs) in a polymeric coating fabricated with these AgNPs by means of the LbL-E deposition technique, even LSPR and LMR simultaneously. This fabrication technique allows the on-line optical monitorization during the fabrication process, and therefore it is possible to stop the LbL-E deposition when the optimal optical response is obtained.

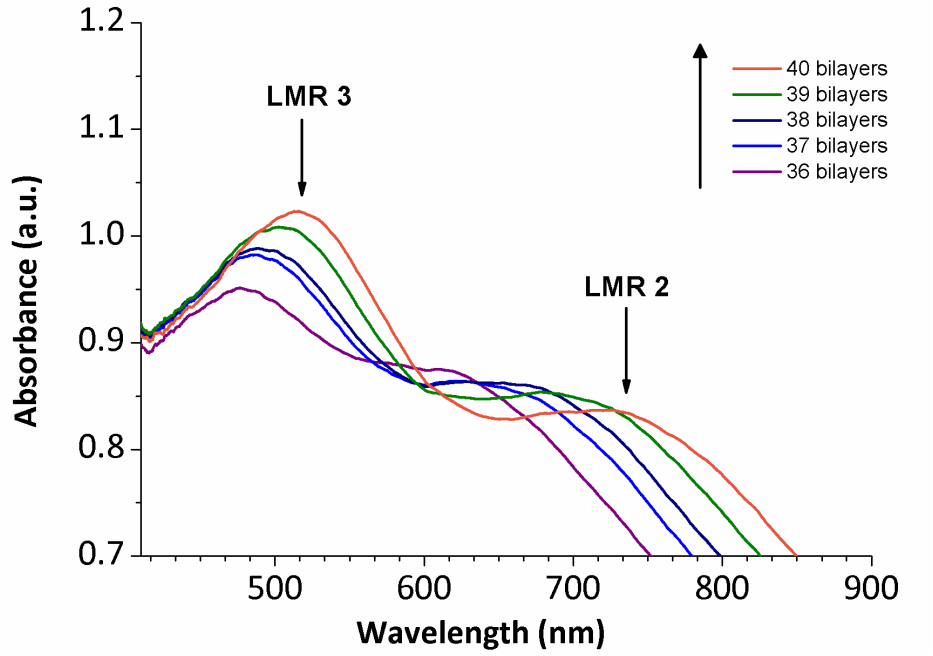

Figure 5.12. UV-Vis spectroscopy of the sensor as a function of the number of bilayers added using the LbL-E deposition technique. The curves plotted are for 36, 37, 38, 39 and 40 bilayers.

In Figure 5.13, it is displayed the evolution of the spectral response as the number of bilayers is increased up to 40 bilayers. This figure can help us to analyze the apparition of the different resonant bands (LSPR and LMRs) as the thickness of the LbL-E overlay is increased from 1 bilayer to 40 bilayers.

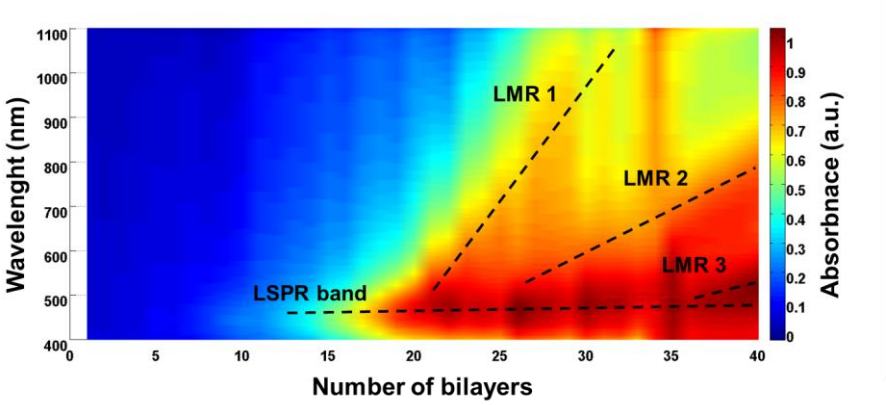

Figure 5.13. Spectral response observed as a function of the number of bilayers added.

These transmission spectra confirm that no LMR bands are observed when the coating thickness is very thin (from 1 to 20 bilayers), so the optical

response of the device is dominated by the LSPR absorption band of AgNPs centered at 450 nm. Nevertheless, when the coating thickness is increased (from 25 to 40 bilayers), several LMR absorption bands are observed in the spectral range studied. Finally, it is possible to appreciate their maxima wavelength dependence of these LMR with the thickness of the LbL coating as a higher number of bilayers are added to the final coating.

5.6.2. Response of both LSPR and LMR to variation of RH changes

In this section, two devices with different number of bilayers (25 and 40 bilayers) were fabricated in order to show the spectral response of the different absorption bands (LSPR and LMRs) to variation of RH changes.

5.6.2.1. Spectral response of 25 bilayers device

On the one hand, a sensor with 25 bilayers has been fabricated in order to show clearly both LSPR and LMR 1 bands. LSPR position band is found around a wavelength of 440 nm, while LMR 1 position band is located around 610 nm. The dynamic response of both LSPR and LMR 1 are shown in Figure 5.14 when the device is tested for RH changes between 20% and 70% for several cycles. It can be observed that LSPR shift (green line) showed no significant wavelength dependence, while LMR 1 shift (black line) showed a high wavelength displacement when RH varies between 20% and 70% RH.

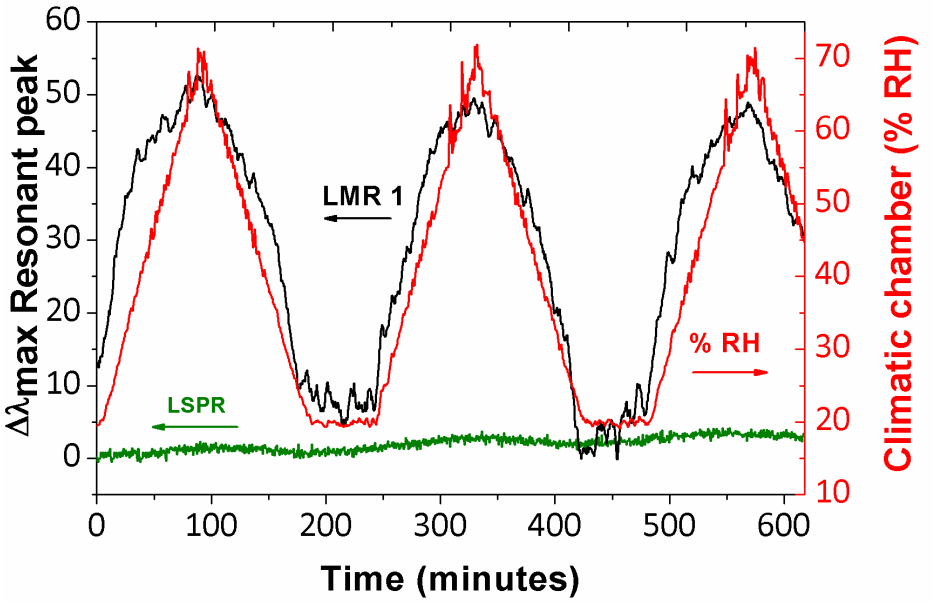

Figure 5.14. Dynamic response observed of the device (25 bilayers). The wavelength shift of both LSPR and LMR 1 are monitored simultaneously to RH cycles from 20 to 70 %RH at 25ºC.

The sensor shows a dynamical range of only 3 nm for LSPR, and a dynamical range of 50.8 nm for LMR 1. The results reveal that LSPR only shows a sensitivity of 0.06 nm per %RH corresponding to this slight variation in wavelength. This behavior of the LSPR has been previously observed in Figure 5.5 (15 bilayers) where only a linear response in intensity of the LSPR band was obtained without any significant change in the wavelength position. The results for LMR 1 band are more relevant because of this high wavelength shift to the same RH changes which corresponds to a sensitivity of 1.016 nm per %RH. This sensitivity to RH changes corresponding to LMR 1 is seventeen times higher than LSPR band, which indicates the great difference in wavelength displacement between both LSPR and LMR as a function of RH changes and enables the fabrication of OFHS suitable to be used in practical RH monitoring applications due the high dynamic range of LMR 1 band. In addition, it is important to note the great importance of this device (25 bilayers) because it is possible to observe two differentiated resonances at different wavelength-position (LSPR and LMR 1) which it enables to perform dual reference measurements, with its associated improvement in accuracy. In Figure 5.15, it is presented the transfer function of the variation of the maxima wavelength of both LSPR and LMR 1 to different RH values from 20% RH to 70% RH. The LSPR shows the same behavior to the rise and fall cycle with the same slope. However, LMR 1 shows a hysteresis of 6.3%.

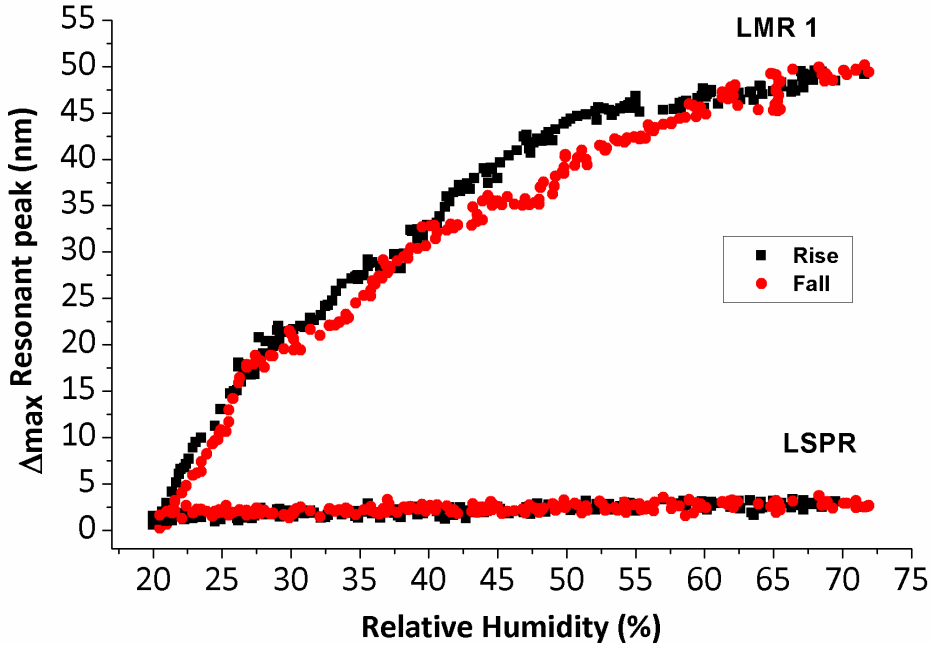

Figure 5.15. Transfer function of 25 bilayers device for humidification and desiccation (20% RH-70% RH-20% RH).

5.6.2.2. Spectral response of 40 bilayers device

On the other hand, another device of 40 bilayers has been fabricated in order to show the behavior to RH changes of both LMR 2 and LMR 3 bands. As it was previously commented, this sensor of 40 bilayers is based on the same approach than previous device of 25 bilayers because it is possible to appreciate both LSPR and LMR bands in the same spectral range (see Figure 5.13). The LSPR remains at a fixed wavelength position reference while LMR bands present a wavelength displacement in order to monitor RH changes of the surrounding medium. As it was previously commented, a higher number of LMR bands, LMR 2 and LMR 3 bands, are observed for this LbL-E thickness coating (40 bilayers), but LMR 1 band is not observed in this spectral range of study.

The dynamic response of LMR 2 is shown in Figure 5.16 when the device is tested for RH changes between 25 and 70 %RH for several cycles using the same experimental setup of previous sections. For this case, it can be observed that LMR 2 (black line) showed a very large resonance wavelength shift of 42.4 nm for a RH range between 25 and 70 % RH. This result confirms that LMR 2 presents a sensitivity of 0.943 nm per %RH, very similar to the result obtained by LMR 1 in 25 bilayers-device (1.016 nm per %RH).

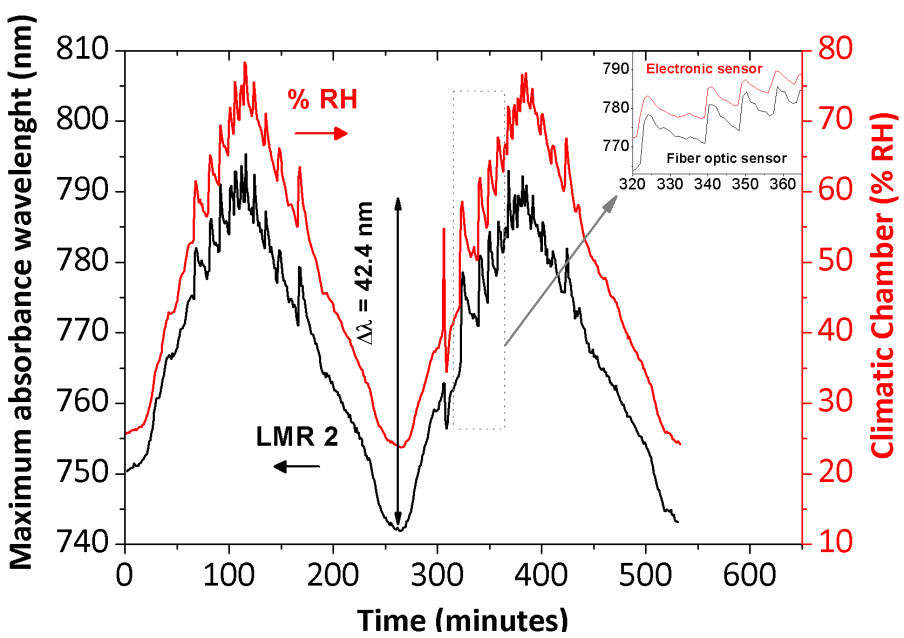

Figure 5.16. Dynamic response observed of 40 bilayers device (LMR 2) to RH changes from 25 to 70% RH at 25ºC.

An important aspect to remark is that the resonance wavelength variation fits well with the electronic RH sensor response, sensor which is located in the climatic chamber. The optical fiber sensor response is due to fast RH changes produced by the climatic chamber as result as normal operation (see Figure 5.16 inset). For this case, it is possible to appreciate that the fiber optic sensor (LMR 2) shows the same fluctuations than the electronic sensor.

Similarly, the dynamic response of LMR 3 (black line) to RH changes from 25% to 70% is shown in Figure 5.17. The wavelength displacement in the studied range is 5.7 nm, which it corresponds to a sensitivity of 0.126 nm per %RH. These results indicate that LMR 2 (0.943 nm per %RH) improves the sensitivity of LMR 3 (0.126 nm per %RH) in more than seven times. Furthermore, it can be observed the high repeatability of the sensor where the difference between the values at the end and the beginning of the cycle are very similar to the two different LMRs (LMR 1 and LMR 2).

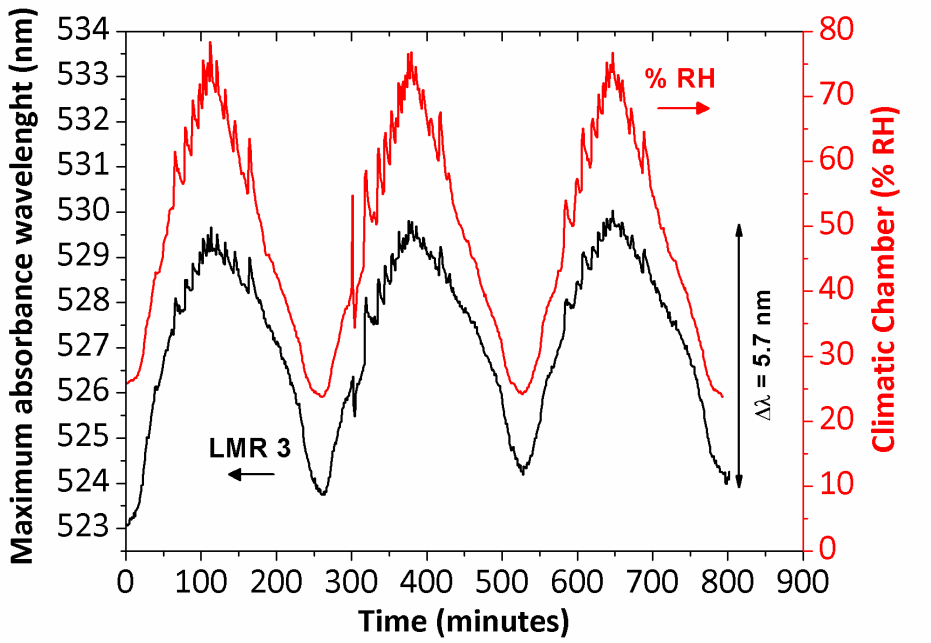

Figure 5.17. Dynamic response observed of 40 bilayers device (LMR 3) to RH changes from 25 to 70% RH at 25ºC.

In Figure 5.18, it is presented the transfer function of the variation of the maxima wavelength of both LMR 2 and LMR 3 to different RH values from 25% to 70% RH. The LMR 3 shows the same behavior to the rise and fall cycle with a high linearity and with almost the same slope, while LMR 2 shows a low hysteresis of 2.7%. This value of hysteresis corresponding to

LMR 2 is lower than previous device (LMR 1, 25 bilayers) with a higher value of hysteresis (6.3%).

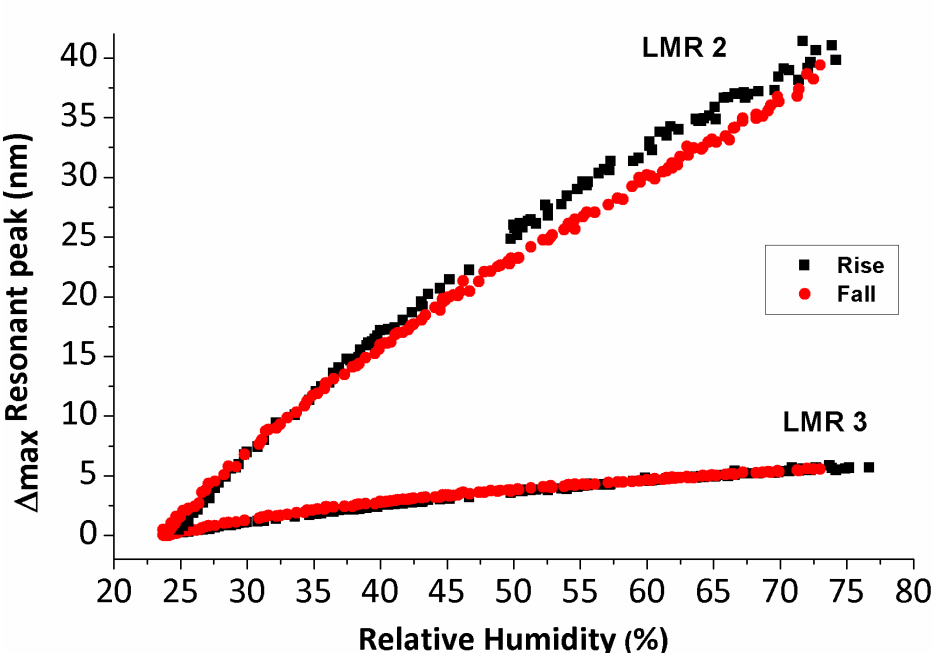

Figure 5.18. Transfer function of 40 bilayers device for humidification and desiccation (25% RH-70% RH-25% RH).

An interestingaspect of this kind of devices is that LMR allows the generation of multiple resonances as the thickness coating is increased. This property makes LMR appropriate for fabricating multi-peak sensors with a better sensitivity and multiple-wavelength optical filters. In addition, these devices take the additional advantage of a dual-peak reference (LSPR-LMR) with a high immunity to optical power fluctuations. This large wavelength displacement is not observed in the LSPR-based devices which showed only LSPR lineal intensity dependence with RH variations and negligible variation in wavelength of the LSPR band.

After monitoring this high wavelength displacement corresponding to the LMR 2 absorption band, the response time of the sensor was evaluated by exposing the device to quick RH changes. The results of this experiment are shown in Figure 5.19. The observed response time of the sensor was 476 and 447 ms for the rise and fall, respectively. The response of this device is very fast, periodic and repetitive (see inset), which this system could be a good alternative to monitor breathing or respiration in medical applications.

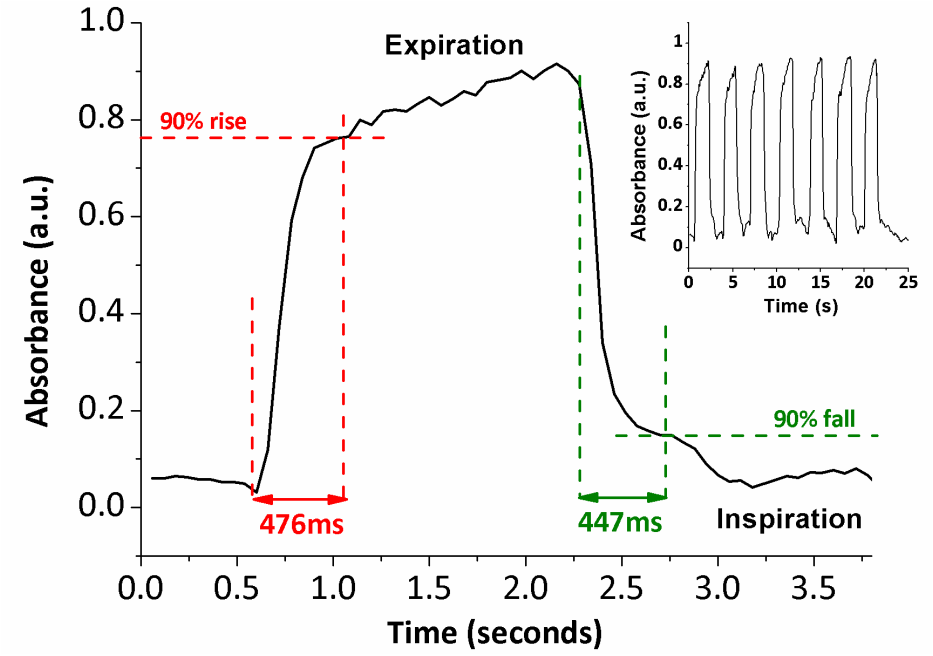

Figure 5.19. Response time of 40 bilayers device (LMR 2) to several consecutive human breathing cycles (rise and fall).

The hybrid inorganic-organic polymeric structure obtained by LbL-E deposition technique for these sensors (PAH/PAA-AgNPs) is sensitive to RH changes. This effect has been named in previous works as swelling/deswelling phenomenon of the PAH/PAA structure [88]. As a consequence of this variation, the effective refractive index of the structure changes, producing a shift of the different LMR bands. Moreover, the incorporation of AgNPs in this polymeric structure improves the sensitivity to RH changes, and also allows the visibility of the LMR bands with a smaller thickness in comparison with only polymeric overlay (PAH/PAA) which it implies an important reduction in the fabrication time. Other remarkable advantage is that AgNPs makes possible the use of LSPR reference at a fixed wavelength position around 450 nm whereas multiple LMR bands appear around visible spectra as a function of the thickness coating.

In Table 5.2, the most important characteristics of the different optical fiber humidity sensors presented in this section and obtained by LbL-E deposition technique are shown as a function of the number total of bilayers deposited onto the optical fiber core (sensitive region).

Table 5.2. Sensitivities of the optical fiber humidity sensors based on LSPR and LMR using the LbL-E deposition technique (25 and 40 bilayers) of the orange colored silver nanoparticles (AgNPs).

Thickness	Resonances (VIS)	Sensitivity
25 bilayers [PAH/PAA-AgNPs]	LSPR	0.06 nm/%RH
	LMR 1	1.016 nm/%RH (6.3% hysteresis)
40 bilayers [PAH/PAA-AgNPs]	LSPR	No measurement
	LMR 2	0.943 nm/%RH (2.7% hysteresis)
	LMR 3	0.126 nm/%RH

To summarize, a thicker coating (40 bilayers) makes possible the generation of a higher number of resonant peaks in the visible spectral range using the same fabrication process based on a successive loaded of AgNPs (LbL-E). In this case, a coating of 15 bilayers presents an only resonant peak (LSPR) (section 5.4), a coating of 25 bilayers presents two resonant peaks (LSPR and LMR1) and a coating of 40 bilayers presents three resonant bands (LSPR, LMR 2 and LMR 3). In addition, the presence of both LSPR and LMR absorption bands in a same device is of great interest because of the utilization of the LSPR band as a wavelength fixed reference, while LMR monitoring can be used to estimate the RH of the environment with a high sensitivity of the LMR band to these RH changes. It is important to remark that a better sensitivity of the device of 25 bilayers is observed with 1.016 nm/%RH whereas the device of 40 bilayers also presents a high sensitivity of 0.943 nm/%RH. However, the device with a higher thickness (40 bilayers) presents the additional advantage of a multiple reference of the LMR bands (LMR 2 and LMR 3) and a better appearance of the transfer function because LMR 3 shows a high linearity with almost the same slope, while LMR 2 only shows a low hysteresis of 2.7% in comparison with the hysteresis of the 25 bilayers device which it is of 6.3%.

5.7. Conclusions

In this chapter, a study about the generation of electromagnetic resonances when an optical waveguide is coated by a thin-film has been performed and the conditions to obtain the different types of resonances have been described. In particular, the presence of two phenomena, Localized Surface Plasmon Resonance (LSPR) and Lossy Mode Resonance (LMR) in a same device based on AgNPs, using an optical fiber configuration has been presented for the first time in the literature.

In all the cases of study, AgNPs loaded polymeric coating make possible to obtain these resonances in the spectral range of study. These AgNPs allows us to fabricate thin films with modified refractive index and can be used to estimate the Relative Humidity (RH) of the environment. In addition, AgNPs contribute to enhance lifetime of the devices in high RH environments due to the biocide behavior of AgNPs, as it was previously commented in Chapter 4, preventing the adverse bacterial apparition which could damage the sensitive coating.

In order to distinguish the difference between both LSPR and LMR, their properties have been experimentally demonstrated using two chemical different synthetic routes based on AgNPs onto the optical fiber core. These methods have been extensively described in Chapter 2 (ISS process) and in Chapter 3 (LbL-E deposition technique).

Once all the coatings have been fabricated, several aspects related to both LSPR and LMR should be remarked. The first difference is that LSPR condition presents only a single peak in the visible region. The position of this LSPR band at 410-450 nm is characteristic of AgNPs with a spherical shape and the orange coloration of the resulting films corroborates this hypothesis. However, LMR allows the generation of multiple resonances as the thickness coating is increased during the fabrication process. In addition, these LMR bands can be generated in different regions of the spectrum, visible as well as infrared region (NIR), as a function of the synthesis process selected onto the optical waveguide.

Other remarkable feature is that LMR bands present a high peak wavelength shift, whereas LSPR band presents a very slight wavelength displacement when the sensitive coating is tested to RH changes. This property makes LMR appropriate for fabricating multi-peak sensors with a better sensitivity and multiple- wavelength optical filters. In Table 5.3, a summary of the differences between both synthetic techniques as well as the sensitivities to RH changes of each device is shown.

Table 5.3. Characteristics of the optical fiber humidity sensors reported in the different sections.

Chemical synthesis	Number of bilayers	Region	Resonances
In Situ Synthesis (ISS)	40 bilayers [PAH/PAA] + 6 dips L/R	Infrared (NIR)	Single: LMR LMR: 0.455 nm/%RH
LbL-E [PAH/PAA-AgNPs]	15 bilayers	Visible (VIS)	Single (LSPR) LSPR: Slight wavelenght shift; Linear intensitiy variation
	25 bilayers	Visible (VIS)	Multiple (LSPR, LMR1) LSPR: low sensitivity (0.016nm/%RH) LMR 1: better sensitivity (1.016nm/%RH)
	40 bilayers	Visible (VIS)	Multiple (LSPR, LMR2, LMR3) LMR 2: high sensitivity (0.943 nm/%RH) LMR 3: 0.126 nm/%RH

It was observed in all the cases of study that the wavelength of the LMR is sensitive to the RH changes, independently of the method used to obtain the metallic nanoparticles (AgNPs) into the polymeric matrix. However, the sensitivity corresponding to the LbL-E deposition technique (25 or 40 bilayers device) is higher than the *in situ* synthesis (ISS), which it indicates that LMR peak obtained by LbL-E deposition shifts to higher wavelength in a faster way when the RH is increased. In addition, the sensitivity of the LMR shift corresponding to the LbL-E is higher when the thickness of the coating is lower. A coating thickness of 25 bilayers device presents a sensitivity of 1.016 nm/%RH (LMR 1) in comparison with a coating of 40 bilayers device with a sensitivity of 0.943 nm/%RH (LMR 2).

In addition, one of the most exigent applications for RH sensors is human breathing monitoring, as far as the expiration/inspiration cycles increase and decrease the RH air. A better response time corresponding to the LbL-E method with 476 ms and 447 ms for the rise/fall is observed in comparison with the ISS method with 692 ms and 839 ms for the rise/fall, respectively. In both cases, a fast and repetitive response in intensity of the LMR band is demonstrated in different spectral ranges (visible or infrared) as a function of

the chemical route of synthesis. These devices could be a good alternative to monitor human breathing in medical applications.

To summarize, the high sensitivity to the Relative Humidity (RH) of the LMR band opens the door to a wide range of applications in the optical fiber sensors field. Taking into account the success of optical fiber sensors based on LSPR, and due to the fact that some of their limitations are overcome by LMR sensors, this new phenomenon could be applied and combined with LSPR in a wide range of applications in the next years due to the associated advantages of both phenomena in a same optical device.

Bibliography

[1] Liedberg, B.; Nylander, C.; Lunström, I. Surface Plasmon Resonance for Gas Detection and Biosensing. Sensors and Actuators 1983, 4, 299-304.
[2] Nylander, C.; Liedberg, B.; Lind, T. Gas Detection by Means of Surface Plasmon Resonance. Sensors and Actuators 1982, 3, 79-88.
[3] Liedberg, B.; Nylander, C.; Lundstrom, I. Biosensing with Surface Plasmon Resonance - how it all Started. Biosensors and Bioelectronics 1995, 10, i-ix.
[4] Gupta, B. D.; Verma, R. K. Surface Plasmon Resonance-Based Fiber Optic Sensors: Principle, Probe Designs, and some Applications. Journal of Sensors 2009, 2009.
[5] Srivastava, S. K.; Verma, R.; Gupta, B. D. Surface Plasmon Resonance Based Fiber Optic Sensor for the Detection of Low Water Content in Ethanol. Sensors and Actuators, B: Chemical 2011, 153, 194-198.
[6] Homola, J.; Yee, S. S.; Gauglitz, G. Surface Plasmon Resonance Sensors: Review. Sensors and Actuators, B: Chemical 1999, 54, 3-15.
[7] Homola, J. Present and Future of Surface Plasmon Resonance Biosensors. Analytical and Bioanalytical Chemistry 2003, 377, 528-539.
[8] Homola, J. Surface Plasmon Resonance Sensors for Detection of Chemical and Biological Species. Chem. Rev. 2008, 108, 462-493.
[9] Stenberg, E.; Persson, B.; Roos, H.; Urbaniczky, C. Quantitative Determination of Surface Concentration of Protein with Surface Plasmon Resonance using Radiolabeled Proteins. J. Colloid Interface Sci. 1991, 143, 513-526.
[10] van Gent, J.; Lambeck, P. V.; Bakker, R. J.; Popma, T. H. J. A.; Sudhölter, E. J. R.; Reinhoudt, D. N. Design and Realization of a Surface Plasmon Resonance-Based Chemo-Optical Sensor. Sensors and Actuators: A.Physical 1991, 26, 449-452.
[11] Dougherty, G. Compact Optoelectronic Instrument with a Disposable Sensor Based on Surface Plasmon Resonance. Measurement Science and Technology 1993, 4, 697-699.
[12] Jorgenson, R. C.; Yee, S. S. A Fiber-Optic Chemical Sensor Based on Surface Plasmon Resonance. Sensors and Actuators: B.Chemical 1993, 12, 213-220.
[13] Cusano, A.; López-Higuera, J. M.; Matias, I. R.; Culshaw, B. Editorial Optical Fiber Sensor Technology and Applications. IEEE Sensors Journal 2008, 8, 1052-1054.
[14] Lee, B. Review of the Present Status of Optical Fiber Sensors. Optical Fiber Technology 2003, 9, 57-79.
[15] Wolfbeis, O. S. Fiber-Optic Chemical Sensors and Biosensors. Anal. Chem. 2004, 76, 3269-3284.
[16] Abdelghani, A.; Chovelon, J. M.; Jaffrezic-Renault, N.; Ronot-Trioli, C.; Veillas, C.; Gagnaire, H. Surface Plasmon Resonance Fibre-Optic Sensor for Gas Detection. Sensors and Actuators, B: Chemical 1997, 39, 407-410.
[17] Abdelghani, A.; Chovelon, J. M.; Jaffrezic-Renault, N.; Veilla, C.; Gagnaire, H. Chemical Vapour Sensing by Surface Plasmon Resonance Optical Fibre Sensor Coated with Fluoropolymer. Anal. Chim. Acta 1997, 337, 225-232.
[18] Cheng, S. -.; Chau, L. -. Colloidal Gold-Modified Optical Fiber for Chemical and Biochemical Sensing. Anal. Chem. 2003, 75, 16-21.
[19] He, Y. -.; Lo, Y. -.; Huang, J. -. Optical-Fiber Surface-Plasmon-Resonance Sensor Employing Long-Period Fiber Gratings in Multiplexing. J Opt Soc Am B 2006, 23, 801-811.
[20] Homola, J.; Ctyroký, J.; Skalský, M.; Hradilová, J.; Kolárová, P. A Surface Plasmon Resonance Based Integrated Optical Sensor. Sensors and Actuators, B: Chemical 1997, 39, 286-290.
[21] Homola, J.; Slavik, R. Fibre-Optic Sensor Based on Surface Plasmon Resonance. Electron. Lett. 1996, 32, 480-482.
[22] Mitsushio, M.; Miyashita, K.; Higo, M. Sensor Properties and Surface Characterization of the Metal-Deposited SPR Optical Fiber Sensors with Au, Ag, Cu, and Al. Sens Actuators A Phys 2006, 125, 296-303.

[23] Piliarik, M.; Homola, J.; Maníková, Z.; Ctyroký, J. Surface Plasmon Resonance Sensor Based on a Single-Mode Polarization-Maintaining Optical Fiber. Sensors and Actuators, B: Chemical 2003, 90, 236-242.
[24] Pollet, J.; Delport, F.; Janssen, K. P. F.; Jans, K.; Maes, G.; Pfeiffer, H.; Wevers, M.; Lammertyn, J. Fiber Optic SPR Biosensing of DNA Hybridization and DNA-Protein Interactions. Biosensors and Bioelectronics 2009, 25, 864-869.
[25] Slavík, R.; Homola, J.; Ctyroký, J. Single-Mode Optical Fiber Surface Plasmon Resonance Sensor. Sensors and Actuators, B: Chemical 1999, 54, 74-79.
[26] Slavík, R.; Homola, J.; Ctyroký, J. Miniaturization of Fiber Optic Surface Plasmon Resonance Sensor. Sensors and Actuators, B: Chemical 1998, 51, 311-315.
[27] Tang, J. -.; Cheng, S. -.; Hsu, W. -.; Chiang, T. -.; Chau, L. -. Fiber-Optic Biochemical Sensing with a Colloidal Gold-Modified Long Period Fiber Grating. Sensors and Actuators, B: Chemical 2006, 119, 105-109.
[28] Trouillet, A.; Ronot-Trioli, C.; Veillas, C.; Gagnaire, H. Chemical Sensing by Surface Plasmon Resonance in a Multimode Optical Fibre. Pure and Applied Optics (Print edition) (United Kingdom) 1996, 5, 227-237.
[29] Cao, J.; Sun, T.; Grattan, K. T. V. In In Development of gold nanorod-based localized surface plasmon resonance optical fiber biosensor; Proceedings of SPIE - The International Society for Optical Engineering; 2012; Vol. 8421.
[30] Cao, J.; Tu, M. H.; Sun, T.; Grattan, K. T. V. Wavelength-Based Localized Surface Plasmon Resonance Optical Fiber Biosensor. Sensors and Actuators, B: Chemical 2013, 181, 611-619.
[31] Chau, L. -.; Lin, Y. -.; Cheng, S. -.; Lin, T. -. Fiber-Optic Chemical and Biochemical Probes Based on Localized Surface Plasmon Resonance. Sensors and Actuators, B: Chemical 2006, 113, 100-105.
[32] Dhawan, A.; Muth, J. F. Plasmon Resonances of Gold Nanoparticles Incorporated Inside an Optical Fibre Matrix. Nanotechnology 2006, 17, 2504-2511.
[33] Hsieh, B. -.; Chang, Y. -.; Ng, M. -.; Liu, W. -.; Lin, C. -.; Wu, H. -.; Chou, C. Localized Surface Plasmon Coupled Fluorescence Fiber-Optic Biosensor with Gold Nanoparticles. Anal. Chem. 2007, 79, 3487-3493.
[34] Huang, C. -.; Jen, C. -.; Chao, T. -.; Wu, W. -.; Li, W. -.; Chau, L. -. A Novel Design of Grooved Fibers for Fiber-Optic Localized Plasmon Resonance Biosensors. Sensors 2009, 9, 6456-6470.
[35] Li, X.; Jiang, L.; Zhan, Q.; Qian, J.; He, S. Localized Surface Plasmon Resonance (LSPR) of Polyelectrolyte-Functionalized Gold-Nanoparticles for Bio-Sensing. Colloids Surf. Physicochem. Eng. Aspects 2009, 332, 172-179.
[36] Mitsui, K.; Handa, Y.; Kajikawa, K. Optical Fiber Affinity Biosensor Based on Localized Surface Plasmon Resonance. Appl. Phys. Lett. 2004, 85, 4231-4233.
[37] Shao, Y.; Xu, S.; Zheng, X.; Wang, Y.; Xu, W. Optical Fiber LSPR Biosensor Prepared by Gold Nanoparticle Assembly on Polyelectrolyte Multilayer. Sensors 2010, 10, 3585-3596.
[38] Srivastava, S. K.; Arora, V.; Sapra, S.; Gupta, B. D. Localized Surface Plasmon Resonance-Based Fiber Optic U-Shaped Biosensor for the Detection of Blood Glucose. Plasmonics 2012, 7, 261-268.
[39] Yeom, S. -.; Yuan, H.; Choi, W. -.; Eum, N. -.; Kang, S. -. Development of Localized Surface Plasmon Resonance Based Biosensor using Au Deposited Nano-Porous Aluminum Anodic Oxide Chip. Sensor Letters 2011, 9, 92-96.
[40] Zhang, Q.; Xue, C.; Yuan, Y.; Lee, J.; Sun, D.; Xiong, J. Fiber Surface Modification Technology for Fiber-Optic Localized Surface Plasmon Resonance Biosensors. Sensors 2012, 12, 2729-2741.
[41] Zhou, C. Localized Surface Plasmonic Resonance Study of Silver Nanocubes for Photonic Crystal Fiber Sensor. Optics and Lasers in Engineering 2012, 50, 1592-1595.
[42] Rivero, P. J.; Urrutia, A.; Goicoechea, J.; Arregui, F. J.; Matías, I. R. Humidity Sensor Based on Silver Nanoparticles Embedded in a Polymeric Coating. International Journal on Smart Sensing and Intelligent Systems 2012, 5, 71-83.
[43] Rivero, P. J.; Urrutia, A.; Goicoechea, J.; Arregui, F. J. Optical Fiber Humidity Sensors Based on Localized Surface Plasmon Resonance (LSPR) and Lossy-Mode Resonance (LMR) in overlays Loaded with Silver Nanoparticles. Sensors and Actuators, B: Chemical 2012, 173, 244-249.

[44] Del Villar, I.; Hernaez, M.; Zamarreno, C. R.; Sánchez, P.; Fernández-Valdivielso, C.; Arregui, F. J.; Matias, I. R. Design Rules for Lossy Mode Resonance Based Sensors. Appl. Opt. 2012, 51, 4298-4307.
[45] Del Villar, I.; Zamarreño, C. R.; Sanchez, P.; Hernaez, M.; Valdivielso, C. F.; Arregui, F. J.; Matias, I. R. Generation of Lossy Mode Resonances by Deposition of High-Refractive-Index Coatings on Uncladded Multimode Optical Fibers. Journal of Optics 2010, 12.
[46] Sanchez, P.; Zamarreno, C. R.; Hernaez, M.; Del Villar, I.; Matias, I. R.; Arregui, F. J. Considerations for Lossy-Mode Resonance-Based Optical Fiber Sensor. IEEE Sensors Journal 2013, 13, 1167-1171.
[47] Elosua, C.; Arregui, F. J.; Zamarreño, C. R.; Bariain, C.; Luquin, A.; Laguna, M.; Matias, I. R. Volatile Organic Compounds Optical Fiber Sensor Based on Lossy Mode Resonances. Sensors and Actuators, B: Chemical 2012, 173, 523-529.
[48] Elosúa, C.; Vidondo, I.; Arregui, F. J.; Bariain, C.; Luquin, A.; Laguna, M.; Matías, I. R. Lossy Mode Resonance Optical Fiber Sensor to Detect Organic Vapors. Sensors and Actuators, B: Chemical 2012.
[49] Razquin, L.; Zamarreno, C. R.; Munoz, F. J.; Matias, I. R.; Arregui, F. J. Thrombin detection by means of an aptamer based sensitive coating fabricated onto LMR-based optical fiber refractometer; Proceedings of IEEE Sensors; 2012; .
[50] Socorro, A. B.; Corres, J. M.; Del Villar, I.; Arregui, F. J.; Matias, I. R. Fiber-Optic Biosensor Based on Lossy Mode Resonances. Sensors and Actuators, B: Chemical 2012, 174, 263-269.
[51] Socorro, A. B.; Del Villar, I.; Corres, J. M.; Arregui, F. J.; Matias, I. R. Lossy Mode Resonance-based pH sensor using a tapered single mode optical fiber coated with a polymeric nanostructure; Proceedings of IEEE Sensors; 2011; , pp 238-241.
[52] Zamarreño, C. R.; Hernáez, M.; Del Villar, I.; Matías, I. R.; Arregui, F. J. Optical Fiber pH Sensor Based on Lossy-Mode Resonances by Means of Thin Polymeric Coatings. Sensors and Actuators, B: Chemical 2011, 155, 290-297.
[53] Del Villar, I.; Zamarreño, C. R.; Hernaez, M.; Arregui, F. J.; Matias, I. R. Lossy Mode Resonance Generation with Indium-Tin-Oxide-Coated Optical Fibers for Sensing Applications. J. Lightwave Technol. 2010, 28, 111-117.
[54] Hernáez, M.; Villar, I. D.; Zamarreño, C. R.; Arregui, F. J.; Matias, I. R. Optical Fiber Refractometers Based on Lossy Mode Resonances Supported by TiO2 Coatings. Appl. Opt. 2010, 49, 3980-3985.
[55] Hernaez, M.; Zamarreño, C. R.; Del Villar, I.; Matias, I. R.; Arregui, F. J. Lossy mode resonances supported by TiO2-coated optical fibers; Procedia Engineering; 2010; Vol. 5, pp 1099-1102.
[56] Zamarreño, C. R.; Hernaez, M.; Del Villar, I.; Matias, I. R.; Arregui, F. J. Sensing properties of ITO coated optical fibers to diverse VOCs; Procedia Engineering; 2010; Vol. 5, pp 653-656.
[57] Zamarreño, C. R.; Hernaez, M.; Sanchez, P.; Del Villar, I.; Matias, I. R.; Arregui, F. J. Optical fiber humidity sensor based on lossy mode resonances supported by TiO2/PSS coatings; Procedia Engineering; 2011; Vol. 25, pp 1385-1388.
[58] Zamarreño, C. R.; Lopez, S.; Hernaez, M.; Del Villar, I.; Matias, I. R.; Arregui, F. J. Resonance-Based Refractometric Response of Cladding-Removed Optical Fibers with Sputtered Indium Tin Oxide Coatings. Sensors and Actuators, B: Chemical 2012, 175, 106-110.
[59] Zamarreño, C. R.; Lopez, S.; Hernaez, M.; Del Villar, I.; Matias, I. R.; Arregui, F. J Resonance-based optical fiber refractometers; Proceedings of IEEE Sensors; 2011; , pp 1469-1471.
[60] Zamarreño, C. R.; Sanchez, P.; Hernaez, M.; Del Villar, I.; Fernandez-Valdivielso, C.; Matias, I. R.; Arregui, F. J. Sensing Properties of Indium Oxide Coated Optical Fiber Devices Based on Lossy Mode Resonances. IEEE Sensors Journal 2012, 12, 151-155.
[61] Zamarreño, C. R.; Sanchez, P.; Hernaez, M.; Del Villar, I.; Fernandez-Valdivielso, C.; Matias, I. R.; Arregui, F. J. LMR-based optical fiber refractometers based on transparent conducting and semiconducting oxide coatings: A comparative study; Proceedings of SPIE - The International Society for Optical Engineering; 2010; Vol. 7839.
[62] Zamarreño, C. R.; Del Villar, I.; Sanchez, P.; Hernaez, M.; Fernandez, C.; Matias, I. R.; Arregui, F. J. Lossy-mode resonance based refractometers by means of indium oxide coatings fabricated onto optical fibers; Proceedings of SPIE - The International Society for Optical Engineering; 2010; Vol. 7653.

[63] Batchman, T. E.; McWright, G. M. Mode Coupling between Dielectric and Semiconductor Planar Waveguides. IEEE J. Quant. Electron. 1982, QE-18, 782-788.
[64] Marciniak, M.; Grzegorzewski, J.; Szustakowski, M. Analysis of Lossy Mode Cut-Off Conditions in Planar Waveguides with Semiconductor Guiding Layer. IEE proceedings.Part J, Optoelectronics 1993, 140, 247-252.
[65] Rivero, P. J.; Urrutia, A.; Goicoechea, J.; Rodríguez, Y.; Corres, J. M.; Arregui, F. J.; Matías, I. R. An Antibacterial Submicron Fiber Mat with in Situ Synthesized Silver Nanoparticles. J Appl Polym Sci 2012, 126, 1228-1235.
[66] Rivero, P. J.; Urrutia, A.; Goicoechea, J.; Zamarreño, C. R.; Arregui, F. J.; Matías, I. R. An Antibacterial Coating Based on a polymer/sol- Gel Hybrid Matrix Loaded with Silver Nanoparticles. Nanoscale Research Letters 2011, 6, X1-7.
[67] Urrutia, A.; Rivero, P. J.; Ruete, L.; Goicoechea, J.; Matías, I. R.; Arregui, F. J. Single-Stage in Situ Synthesis of Silver Nanoparticles in Antibacterial Self-Assembled Overlays. Colloid Polym. Sci. 2012, 290, 785-792.
[68] Fabrega, J.; Fawcett, S. R.; Renshaw, J. C.; Lead, J. R. Silver Nanoparticle Impact on Bacterial Growth: Effect of pH, Concentration, and Organic Matter. Environmental Science and Technology 2009, 43, 7285-7290.
[69] Furno, F.; Morley, K. S.; Wong, B.; Sharp, B. L.; Arnold, P. L.; Howdle, S. M.; Bayston, R.; Brown, P. D.; Winship, P. D.; Reid, H. J. Silver Nanoparticles and Polymeric Medical Devices: A New Approach to Prevention of Infection? J. Antimicrob. Chemother. 2004, 54, 1019-1024.
[70] Lee, H. J.; Yeo, S. Y.; Jeong, S. H. Antibacterial Effect of Nanosized Silver Colloidal Solution on Textile Fabrics. J. Mater. Sci. 2003, 38, 2199-2204.
[71] Li, Q.; Mahendra, S.; Lyon, D. Y.; Brunet, L.; Liga, M. V.; Li, D.; Alvarez, P. J. J. Antimicrobial Nanomaterials for Water Disinfection and Microbial Control: Potential Applications and Implications. Water Res. 2008, 42, 4591-4602.
[72] Lok, C. -.; Ho, C. -.; Chen, R.; He, Q. -.; Yu, W. -.; Sun, H.; Tam, P. K. -.; Chiu, J. -.; Che, C. -. Silver Nanoparticles: Partial Oxidation and Antibacterial Activities. Journal of Biological Inorganic Chemistry 2007, 12, 527-534.
[73] Morones, J. R.; Elechiguerra, J. L.; Camacho, A.; Holt, K.; Kouri, J. B.; Ramírez, J. T.; Yacaman, M. J. The Bactericidal Effect of Silver Nanoparticles. Nanotechnology 2005, 16, 2346-2353.
[74] Panácek, A.; Kvítek, L.; Prucek, R.; Kolár, M.; Vecerová, R.; Pizúrová, N.; Sharma, V. K.; Nevecná, T.; Zboril, R. Silver Colloid Nanoparticles: Synthesis, Characterization, and their Antibacterial Activity. J Phys Chem B 2006, 110, 16248-16253.
[75] Sharma, V. K.; Yngard, R. A.; Lin, Y. Silver Nanoparticles: Green Synthesis and their Antimicrobial Activities. Adv. Colloid Interface Sci. 2009, 145, 83-96.
[76] Sondi, I.; Salopek-Sondi, B. Silver Nanoparticles as Antimicrobial Agent: A Case Study on E. Coli as a Model for Gram-Negative Bacteria. J. Colloid Interface Sci. 2004, 275, 177-182.
[77] Decher, G. Fuzzy Nanoassemblies: Toward Layered Polymeric Multicomposites. Science 1997, 277, 1232-1237.
[78] Decher, G.; Hong, J. D.; Schmitt, J. Buildup of Ultrathin Multilayer Films by a Self-Assembly Process: III. Consecutively Alternating Adsorption of Anionic and Cationic Polyelectrolytes on Charged Surfaces. Thin Solid Films 1992, 210-211, 831-835.
[79] Rivero, P. J.; Goicoechea, J.; Urrutia, A.; Arregui, F. J. Effect of both Protective and Reducing Agents in the Synthesis of Multicolor Silver Nanoparticles. Nanoscale Research Letters 2013, 8, 1-9.
[80] Rivero, P. J.; Goicoechea, J.; Urrutia, A.; Matias, I. R.;Arregui, F. J. Multicolor layer-by-layer films using weak polyelectrolyte assisted synthesis of silver nanoparticles. Nanoscale Research Letters 2013, 8, 1-10.
[81] Arregui, F. J.; Matías, I. R.; Cooper, K. L.; Claus, R. O. Simultaneous Measurement of Humidity and Temperature by Combining a Reflective Intensity-Based Optical Fiber Sensor and a Fiber Bragg Grating. IEEE Sensors Journal 2002, 2, 482-487.
[82] Arregui, F. J.; Liu, Y.; Matias, I. R.; Claus, R. O. Optical Fiber Humidity Sensor using a Nano Fabry-Perot Cavity Formed by the Ionic Self-Assembly Method. Sensors and Actuators, B: Chemical 1999, 59, 54-59.

[83] Choi, J.; Rubner, M. F. Influence of the Degree of Ionization on Weak Polyelectrolyte Multilayer Assembly. Macromolecules 2005, 38, 116-124.
[84] Shiratori, S.; Yamada, M.; Ito, T.; Wang, T. C.; Rubner, M. F. Nanoscale control of layer thickness for EL devices by mass-controlled layer-by-layer sequential adsorption process; Materials Research Society Symposium - Proceedings; 2000; Vol. 598, pp BB1.9.1-BB1.9.6.
[85] Shiratori, S. S.; Rubner, M. F. PH-Dependent Thickness Behavior of Sequentially Adsorbed Layers of Weak Polyelectrolytes. Macromolecules 2000, 33, 4213-4219.
[86] Yoo, D.; Shiratori, S. S.; Rubner, M. F. Controlling Bilayer Composition and Surface Wettability of Sequentially Adsorbed Multilayers of Weak Polyelectrolytes. Macromolecules 1998, 31, 4309-4318.
[87] Itano, K.; Choi, J.; Rubner, M. F. Mechanism of the pH-Induced Discontinuous swelling/deswelling Transitions of Poly(Allylamine Hydrochloride)-Containing Polyelectrolyte Multilayer Films. Macromolecules 2005, 38, 3450-3460.
[88] Goicoechea, J.; Zamarreño, C. R.; Matías, I. R.; Arregui, F. J. Optical Fiber pH Sensors Based on Layer-by-Layer Electrostatic Self-Assembled Neutral Red. Sensors and Actuators, B: Chemical 2008, 132, 305-311.
[89] Rivero, P. J.; Urrutia, A.; Goicoechea, J.; Matias, I. R.; Arregui, F. J. A Lossy Mode Resonance Optical Sensor using Silver Nanoparticles-Loaded Films for Monitoring Human Breathing. Sensors and Actuators, B: Chemical 2012, 187, 40-44.

CHAPTER 6. Conclusions and open research lines

6.1. Conclusions

Along this work, an original study about the synthesis of metallic silver nanoparticles into thin films has been presented. Two different methodologies, the *in situ* synthesis (ISS) process and the Layer-by-Layer Embedding (LbL-E) deposition technique, have been used for incorporating AgNPs into thin films, and applications of the resultant coatings as antibacterial surfaces or optical fiber devices have been evaluated. In particular, it is worth noting that the optical fiber sensors shown here have a common feature: all of them have been fabricated by depositing a nanostructured coating loaded with AgNPs onto the optical fiber core and the presence of two optical resonance phenomena, LSPR and LMR, in the same device results of great interest for the scientific community.

Two different deposition techniques have been used in order to incorporate the AgNPs into the thin films. Special attention has been paid to the Layer-by-Layer (LbL) assembly because it offers some important advantages such as nanometric thickness control of the coating, high versatility and, moreover, it does not require the utilization of expensive or complex instrumentation. Nevertheless, the sol-gel dip-coating technique has been also studied when the thickness control at nanometric scale was not so critical, showing good results as antibacterial sufaces.

In Chapter 2, a method for the *in situ* synthesis (ISS) of silver nanoparticles into thin films is presented. Firstly, an initial coating is fabricated by the sol-gel process or the LbL assembly and secondly, the *in situ* synthesis of the AgNPs into these previous deposited coatings is performed. In both cases (sol-gel or LbL), the key of a further incorporation of the *in situ* synthesis of AgNPs into the films is due to the presence of PAA. This weak polyelectrolyte presents carboxylate and carboxylic acid groups at a suitable pH where the free carboxylic acid groups are responsible for binding Ag-ions by the metal-ion exchange mechanism with the proton (nanoreactor sites). It has been demonstrated that when a higher number of nanoreactor sites are available in the coating, a higher number of AgNPs has been obtained. This aspect has been corroborated for the LbL assembly at pH 9.0 in comparison with films obtained at pH 7.0. The orange coloration, the location of the LSPR band at 410-420 nm and a post-thermal treatment of the thin films have been also

evaluated. This ISS process makes possible the synthesis of spherical AgNPs with a random distribution and partial aggregation into the films.

In Chapter 3, a multicolor silver nanoparticles map has been generated from water based solutions. The color is adjusted by controlling the molar ratio concentration between the protective and reducing agent. The synthesis of AgNPs with variable shapes (spherical, rod, hexagonal, triangle, cube), sizes (nanometric, micrometric or clusters), aggregation states and colors (orange, violet, green, blue, brown, red, yellow) as well as the evolution of the LSPR absorption bands in two regions (region 1 in 400-500 nm and region 2 in 600-700 nm) are presented. Then, in a second part of this chapter the further incorporation of these AgNPs with a specific coloration (violet, orange and green) into solid state thin films is also studied. The Layer-by-Layer Embedding (LbL-E) deposition technique is selected as a good candidate for the incorporation of the AgNPs into the films. A study about the pH of the dipping polyelectrolytes solutions as well as the number of bilayers is performed. The key to obtain multicolored films is a good control over the properties of the nanoparticles (shape and size) and their distribution into the thin films. The fabrication of multicolored thin films is not trivial and in the most of the approaches (i.e. *in situ* synthesis in Chapter 2), only yellowish-orange coloration was obtained. Attending to these results, this is the first time that a study about the color formation based on AgNPs is investigated in LbL films preserving the original color of the dipping solutions.

In Chapter 4, antibacterial surfaces have been obtained using the *in situ* synthesis (ISS) of AgNPs and the Layer-by-Layer Embedding (LbL-E) deposition technique. The coatings have been tested against bacterial cultures (*Lactobacillus plantarum*), preventing the bacteria growth in the coated area. This study is very interesting for applications such as sensors in tropical-like environmental conditions (high RH, high temperature) where bacteria are prone to grow over organic films. This biocide behavior of the AgNPs will contribute to extend the lifetime of the coatings in such harsh environments.

In Chapter 5, the simultaneous use of both Localized Surface Plasmon Resonance (LSPR) and Lossy Mode Resonance (LMR) in a same device has been described for the first time in the bibliography. In addition, remarkable differences in their sensitivities to the Relative Humidity (RH) changes have been observed. LSPR only showed an intense peak in the visible region (410-450 nm), lineal variation in intensity and a slight wavelength displacement. However, LMR can be generated in different regions of the spectrum, visible as well as infrared, as a function of the thickness of the films (LbL-E) or the amount of AgNPs incorporated (ISS). In addition, an important aspect related to LMRs is their high wavelength displacement with a good sensitivity when the LbL-E films of variable thickness (25 or 40 bilayers device) were tested to RH changes. For example, using the LbL-E of orange AgNPs, the sensitivities

of LMRs varied from 1.016 nm/%RH (LMR 1), 0.943 nm/%RH (LMR 2) or 0.126 nm/%RH (LMR 3). These values are higher compared to the slight LSPR variation of 0.016 nm/%RH. Finally, taking into account the limitations of the LSPR which can be overcome by LMR devices, the possibility of combining both phenomena in a same device opens the door to the design of a new group of self-referenced optical fiber sensors.

6.2. Open research lines

Once the conclusions of this study have been indicated, it is necessary to summarize the research lines that this thesis has opened and can be considered for future works.

Although this thesis is based on the synthesis of multicolored AgNPs from a source of silver ions ($AgNO_3$), using two parameters such as protective (PAA) and reducing agents (DMAB), it would be very interesting to apply this same study for synthesizing other type of nanoparticles. In particular, the synthesis of gold nanoparticles (AuNPs) could be a good alternative from a source of gold ions ($HAuCl_4$), and it should be studied if is possible to obtain different colors, using the same molar ratios of protective and reducing agents, as it appears in the multicolor silver map. Furthermore, it seems of interest to compare the results observed such as the optical properties (colors) of both LSPR bands (AgNPs and AuNPs), shapes, sizes or aggregation states. In addition, an interesting study would be to see if mixing both sources of silver and gold ions in the initial mixture, it is possible to appreciate both LSPR bands in the spectral range (UV-Vis spectroscopy), after the addition of the reducing agent (DMAB), because the LSPR band of AuNPs appears in a different wavelength position of the LSPR of AgNPs. If all this was possible, a novel comparative study between individual LSPR bands (AgNPs or AuNPs) and together LSPR bands can be performed as function of the final molar proportions of protective and reducing agents.

LSPR and LMR-devices for measuring Relative Humidity changes have been presented in Chapter 5. However, it would be interesting if these devices based on AgNPs can be used as optical fiber pH sensors or as refractometers, maintaining the high sensitivity for LMR (wavelength displacement), whereas LSPR shows a liner intensity variation with a negligible displacement in wavelength. If this occurs, novel applications of these devices based on both phenomena will be widely studied as an important aspect in the sensor fields.

In addition, LbL-E of AgNPs with an orange coloration was studied in Chapter 5. It has been demonstrated that LSPR of these AgNPs (spherical) are located in region 1 (410-450 nm) which it is corroborated in the LbL-E thin

films. An interesting approach would be to incorporate AgNPs whose LSPR bands are located in region 2 (600-700 nm) what is observed with bluish or purple coloration. In this case, once the LbL-E deposition technique of the AgNPs (blue or violet) is being performed onto the optical fiber core (sensitive region), a LSPR band related to AgNPs should appear at a fixed wavelength position in the region 2 since the beginning of the deposition. However, after the addition of several bilayers, a new LMR band should appear at lower wavelength (region 1) which it will be shifted to higher wavelength position when the number of bilayers is being increased. The ideal situation would be to stop the deposition process when both phenomena (LSPR and LMR) are perfectly observed at a specific number of bilayers and separated in wavelength position and then, monitoring their sensitivities to RH changes or other type of physical or chemical parameters.

Finally, according to the conclusions and future perspectives, the possibility of obtaining both LSPR and LMR phenomena using metal nanoparticles (Ag or AuNPs) loaded polymeric thin films in a same device, could open the door of the sensors market. The development and fabrication of low-cost portable kits based on LSPR and LMR for measuring RH, refractive index or pH values could be of great interest for the expansion of these devices.

APPENDIX 1. The sol-gel process

Ap1.1. Introduction

The sol-gel process is a technique for synthesizing porous, glass-like materials and ceramics. This process has been extensively investigated by scientific community because the sol-gel reactions can produce a high variety of inorganic networks which are prepared from metal alkoxyde solutions [1-6]. All these reactions follow the same evolution from a sol, a colloidal suspension of solid particles in a liquid, to produce a gel, a substance that contains a continuous solid skeleton enclosing a continuous liquid phase.

It has found that the sol-gel derived materials have important applications in fields as diverse as optics, chemistry, electronics, nanotechnology, medicine, biology or materials [7-19]. In addition, sol-gel derived materials show several benefits such as transparence in the UV or visible range and a high resistance to thermal or photochemical degradation. Another important benefit is that sol-gel reactions do not employ extreme reaction conditions because the reactions take place at room temperature and require only moderate temperature to cure the gel. All these factors along with simplicity and versatility of the process make the sol-gel process a suitable method to obtain thin films with special properties.

Ap1.2. Sol-gel chemical reactions

The sol-gel process consists of a chemical synthesis technique for preparing inorganic or hybrid inorganic-organic materials with a high purity through specific chemical reactions (hydrolysis and condensation) of metal alkoxydes at low or room temperature. The most widely used alkoxydes are silicon alkoxydes, such as tetramethoxysilane (TMOS) or tetraethoxysilane (TEOS).

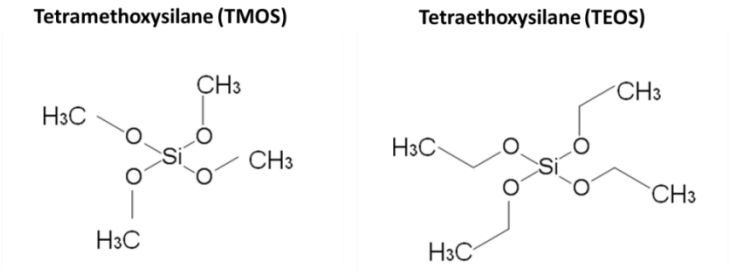

Figure Ap1.1. Chemical structure of both silicon alkoxydes, TMOS and TEOS, respectively.

The fundamental reaction principles are described using a silicon alkoxyde ($Si\text{-}(OR)_4$) as a model system. The sol-gel process is a simple three step reaction (hydrolysis, condensation and polycondensation) as it is shown in the following schematic reactions. It is important to remark that alkoxysilanes are used as an example but all of the metal alkoxydes (aluminates, titanates or zirconates) react similarly [20-23].

1. The hydrolysis is initiated by the addition of water to the silane solution under acidic, neutral or basic conditions. As a result of the hydrolysis of the silicon alkoxyde precursor, hydroxylated product (silanol groups) and the corresponding alcohol are generated.

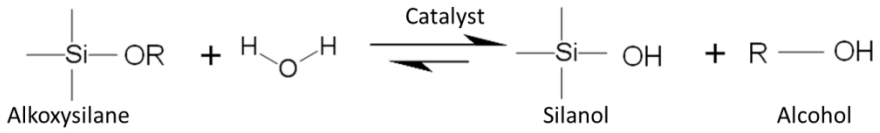

2. The condensation can be produced between an unhydroxylated alkoxide group and a hydroxyl group (alcohol condensation) or between two hydroxyl groups (water condensation), which eliminates the solvent, and making possible the formation of a colloidal mixture known as sol.

   (a) alcohol condensation:

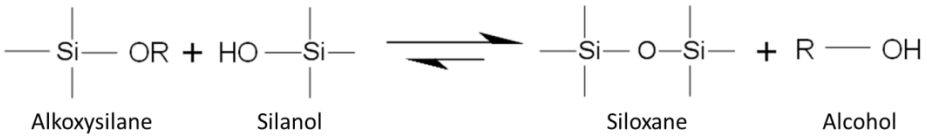

   (b) water condensation

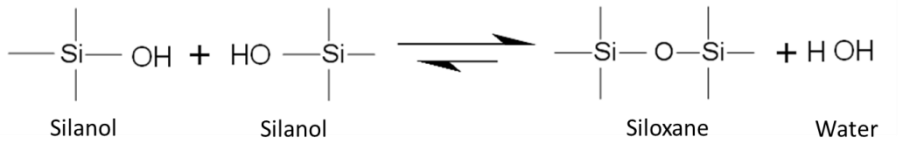

3. Polycondensation between sols or additional networking, resulting in a porous and three-dimensional (3D) crosslinked network. In this situation, the viscosity of the solution is gradually increased, and as result, the sol becomes interconnected to form a rigid and porous network known as gel. In Figure Ap1.2, all the steps of the sol-gel process are shown.

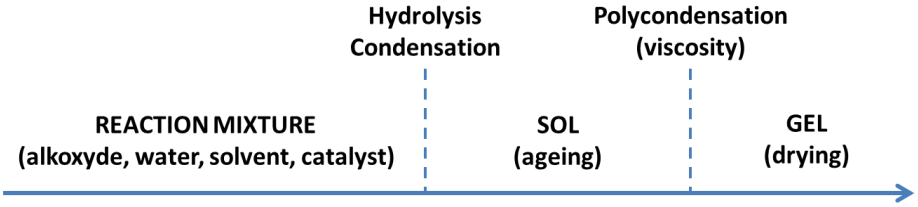

Figure Ap1.2. Steps of the sol-gel process.

The final properties of the resultant gel depend strongly on the sol-gel processing parameters, such as molecular precursor, concentration and nature of the catalyst, water to silane ratio, sol ageing time and temperature [24-30]. An important consideration is that the reaction mechanisms vary with a different kinetic if the process is catalyzed by acids (HCl, HNO_3, H_2SO_4) or by bases (NaOH, amines). Acid-catalyzed reactions promote the formation of linear polymers, whereas base-catalyzed reactions promote the formation of highly crosslinked polymers. In Figure Ap1.3, the difference in the chemical structure of the final polymers as a function of the experimental conditions is shown.

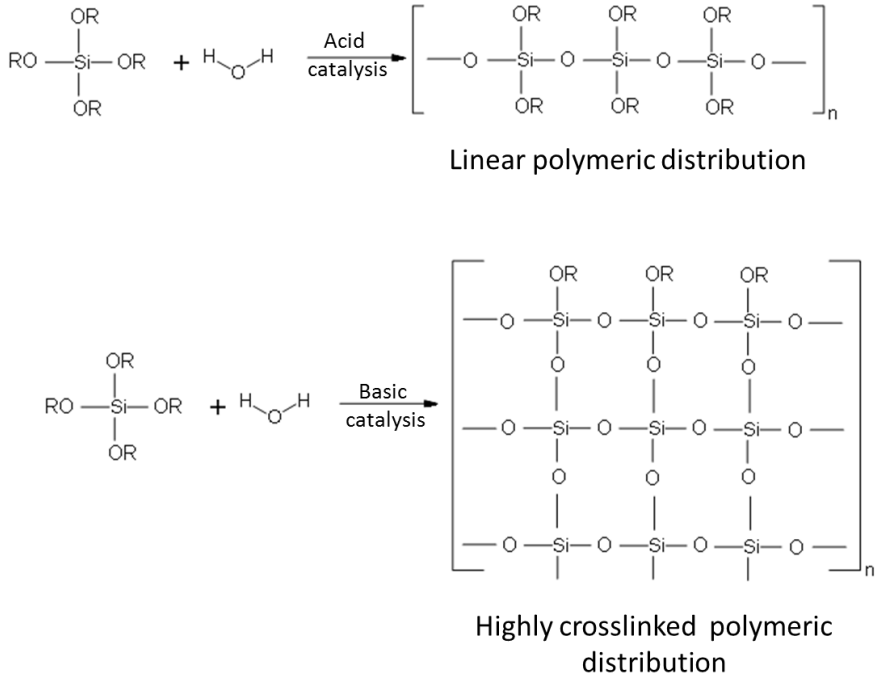

Figure Ap1.3. Polymeric distribution of the resultant gel as a function of acid or basic catalysis.

Ap1.3. Deposition procedure

Deposition techniques based on sol-gel chemistry are attracting a great interest due to their versatility and simplicity. In this work, a simple dip-coating technique has been applied to deposit hybrid sol-gel coatings based on polymeric chains and silver nanoparticles onto glass slides with the aim of obtaining antibacterial surfaces.

The general dip-coating deposition technique uses a solution which contains the precursor metal alkoxyde, water, co-solvent and catalyst. The changes observed in the solution during the process and the type of catalysts used (acid or basic) have a great influence in the final structure of the gel and, hence, in the resultant coating properties.

Once the sol-gel precursor is prepared and aged for a specific period of time, the substrate (glass slide), previously cleaned and treated, is immersed into it. After a determined period, it is pulled out from the gel. The extracting speed is an important parameter because the thickness of each layer highly

depends on it. Then, the substrate is dried during a fixed time. This step can include some additional processing, such as a heat treatment at specific conditions of temperature and pressure. These steps can be repeated until the coating has acquired the desired characteristics. Occasionally, a final processing is necessary to stabilize the film and tune its properties. In Figure Ap.1.4, a schematic representation of all these steps involved in a dip-coating deposition is shown.

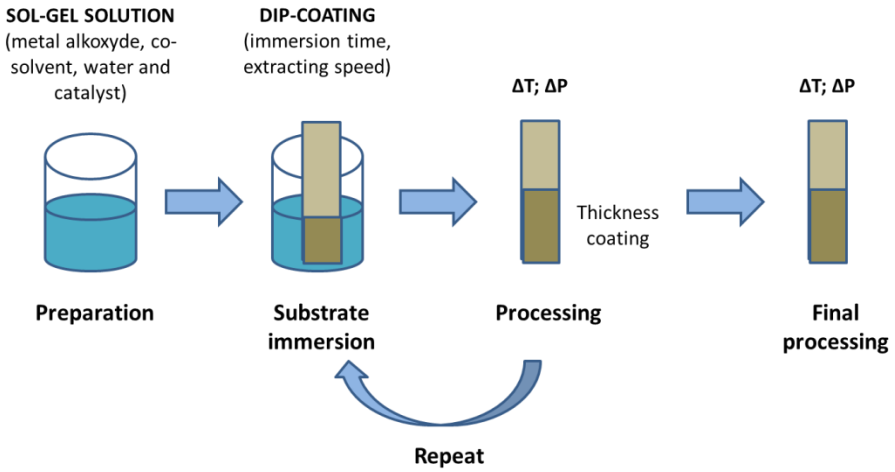

Figure Ap1.4. Schematic representation of the dip-coating deposition technique.

Bibliography

[1] Hench, L. L.; West, J. K. The Sol-Gel Process. Chem. Rev. 1990, 90, 33-72.
[2] Brinker, C. J.; Scherer, G. W. Sol → Gel → Glass: I. Gelation and Gel Structure. J. Non Cryst. Solids 1985, 70, 301-322.
[3] Brinker, C. J.; Scherer, G. W.; Roth, E. P. Sol → Gel → Glass: II. Physical and Structural Evolution during Constant Heating Rate Experiments. J. Non Cryst. Solids 1985, 72, 345-368.
[4] Scherer, G. W.; Brinker, C. J.; Roth, E. P. Sol → Gel → Glass: III. Viscous Sintering. Journal of Non-Crystalline Solids 1985, 72, 369-389.
[5] Lin, J.; Brown, C. W. Sol-Gel Glass as a Matrix for Chemical and Biochemical Sensing. TrAC - Trends in Analytical Chemistry 1997, 16, 200-211.
[6] Livage, J.; Sanchez, C.; Henry, M.; Doeuff, S. The Chemistry of the Sol-Gel Process. Solid State Ionics 1989, 32-33, 633-638.
[7] Livage, J.; Sanchez, C. Optical Properties of Sol-Gel Films. Molecular Crystals and Liquid Crystals Science and Technology Section B: Nonlinear Optics 1999, 21, 125-141.
[8] Sommerdijk, N. A. J. M.; Wright, J. D. Matrix Effects on Selective Chemical Sensing by Sol-Gel Entrapped Complexing Agent. J. Sol Gel Sci. Technol. 1999, 13, 565-568.
[9] Wallington, S. -.; Labayen, T.; Poppe, A.; Sommerdijk, N. A. J. M.; Wright, J. D. Sol-Gel Entrapped Materials for Optical Sensing of Solvents and Metal Ions. Sensors and Actuators, B: Chemical 1997, 38, 48-52.
[10] Schmidt, H.; Seiferling, B. In In CHEMISTRY AND APPLICATIONS OF INORGANIC-ORGANIC POLYMERS (ORGANICALLY MODIFIED SILICATES). Materials Research Society Symposia Proceedings; 1986; Vol. 73, pp 739-750.
[11] Rottman, C.; Ottolenghi, M.; Zusman, R.; Lev, O.; Smith, M.; Gong, G.; Kagan, M. L.; Avnir, D. Doped Sol-Gel Glasses as pH Sensors. Mater Lett 1992, 13, 293-298.
[12] Rottman, C.; Turniansky, A.; Avnir, D. Sol-Gel Physical and Covalent Entrapment of Three Methyl Red Indicators: A Comparative Study. J. Sol Gel Sci. Technol. 1999, 13, 17-25.
[13] Rottman, C.; Avnir, D. In In Effects of water/silane r-ratio and of humidity on properties of sol-gel entrapped indicators; Proceedings of SPIE - The International Society for Optical Engineering; 2003; Vol. 3943, pp 154-162.
[14] Zusman, R.; Rottman, C.; Ottolenghi, M.; Avnir, D. Doped Sol-Gel Glasses as Chemical Sensors. J. Non Cryst. Solids 1990, 122, 107-109.
[15] Kasemann, R.; Schmidt, H. K.; Wintrich, E. In In New type of a sol-gel-derived inorganic-organic nanocomposite; Materials Research Society Symposium - Proceedings; 1994; Vol. 346, pp 915-921.
[16] Krug, H.; Merl, N.; Schmidt, H. Fine Patterning of Thin Sol-Gel Films. J. Non Cryst. Solids 1992, 147-148, 447-450.
[17] Schmidt, H.; Wolter, H. Organically Modified Ceramics and their Applications. J. Non Cryst. Solids 1990, 121, 428-435.
[18] Wencel, D.; MacCraith, B. D.; McDonagh, C. High Performance Optical Ratiometric Sol-Gel-Based pH Sensor. Sensors and Actuators, B: Chemical 2009, 139, 208-213.
[19] Wencel, D.; Moore, J. P.; Stevenson, N.; McDonagh, C. Ratiometric Fluorescence-Based Dissolved Carbon Dioxide Sensor for use in Environmental Monitoring Applications. Analytical and Bioanalytical Chemistry 2010, 398, 1899-1907.
[20] Schmidt, H.; Scholze, H.; Kaiser, A. Principles of Hydrolysis and Condensation Reaction of Alkoxysilanes. J. Non Cryst. Solids 1984, 63, 1-11.
[21] Brinker, C. J. Hydrolysis and Condensation of Silicates: Effects on Structure. J. Non Cryst. Solids 1988, 100, 31-50.
[22] Brinker, C. J. In In Structural studies of sol-gel silicate glasses; Transactions of the American Crystallographic Association; 1991; Vol. 27, pp 163-190.
[23] Sanchez, C.; Livage, J.; Henry, M.; Babonneau, F. Chemical Modification of Alkoxide Precursors. J. Non Cryst. Solids 1988, 100, 65-76.

[24] Sommerdijk, N. A. J. M.; Van Eck, E. R. H.; Wright, J. D. Highly Defined Pore Size Distribution in Sol-Gel Silicate Glasses Induced by Incorporation of an Oligomeric Siloxane. Chemical Communications 1997, 159-160.
[25] Ying, J. Y.; Benziger, J. B. Structure and Energetics of Silica in the Sol-Gel to Ceramic Transitions. Colloids Surf. Physicochem. Eng. Aspects 1993, 74, 23-31.
[26] Ying, J. Y.; Benziger, J. B. Structure Tailoring of Alkoxide Silica. J. Non Cryst. Solids 1992, 147-148, 222-231.
[27] Ying, J. Y.; Benziger, J. B.; Navrotsky, A. Structural Evolution of Alkoxide Silica Gels to Glass: Effect of Catalyst pH. J Am Ceram Soc 1993, 76, 2571-2582.
[28] Rottman, C.; Grader, G.; Avnir, D. Polarities of Sol-Gel-Derived Ormosils and of their Interfaces with Solvents. Chemistry of Materials 2001, 13, 3631-3634.
[29] Schmidt, H. Organic Modification of Glass Structure New Glasses Or New Polymers? J. Non Cryst. Solids 1989, 112, 419-423.
[30] Schmidt, H. New Type of Non-Crystalline Solids between Inorganic and Organic Materials. J. Non Cryst. Solids 1985, 73, 681-691.

APPENDIX 2. The Layer-by-Layer (LbL) assembly

Ap2.1. Introduction

The Layer-by-Layer (LbL) assembly, also known as Electrostatic Self-Assembly Multilayer (ESAM), consists of the alternate immersion of the substrate into aqueous solutions with opposite electric charge, being the electrostatic attraction the main force to adsorb onto a surface. It was reported for the first time by Iler [1] in 1966. However, nobody followed this line of research after his death. In the first nineties, G. Decher and coworkers rediscovered the technique [2]. Since then, the number of publications related to LbL assembly has increased exponentially [3-5], being one of the most used methods in the nanoscale level.

This technique offers a high number of advantages in comparison with other techniques. One of them is its simplicity because it is not necessary any special or expensive equipment. In addition, LbL method can be applied onto surfaces with any shape (cylindrical, conical or plane) and the resultant thickness of the film can be perfectly controlled with a high precision by just selecting the number of deposited layers [6, 7]. Other great benefit of this technique is that it allows the deposition of a different kind of substances, such as polymers, fluorescent indicators, nanoparticles, quantum dots or colorimetric indicators [8-13].

This high versatility combined with the simplicity makes the LbL technique as a suitable method for fabricating optical fiber sensors based on thin films. As a consequence, the number of papers related to optical devices based on nanostructured coatings have been recently increased and different type of sensors such as humidity, pH, temperature, harmful gas,glucose or hydrogen peroxide sensors have been reported [14-18] using this technique deposition. In addition, as it was previously commented, this method can be also applied onto other surfaces (wood, glass) and novel nanocoatings have been fabricated with special properties as diverse as antibacterial, self-cleaning, fireproof, superhydrophilic, superhydrophobic or anti-scratching [19-25].

Ap2.2. Deposition procedure

The basis of the LbL method is the electrostatic attraction between the aqueous polyelectrolyte solutions of opposite charge. The charge of these polyelectrolyte solutions can be perfectly tuned with the pH and the ionic strength of the dipping solutions. This process involves different steps. First of all, the substrate is cleaned and treated to create a charged surface. After that, the substrate is alternately dipped in solutions with a cationic and anionic charge to create a multilayer thin film. In Figure Ap2.1, a schematic representation of this process with all the steps involved is presented. If the initial charge of the substrate is positive, the first monolayer will be a polyanion, and if it is negative, the first deposited monolayer will be a polycation. This way, a multilayer structure is formed by electrostatic attraction between each bilayer and the bilayer previously deposited. After each immersion, the substrate is dipped into ultrapure water to remove the excess of material deposited onto the surface. The molecular species of the anionic and the cationic components and the long-range physical order of the layers determine the resulting coating properties.

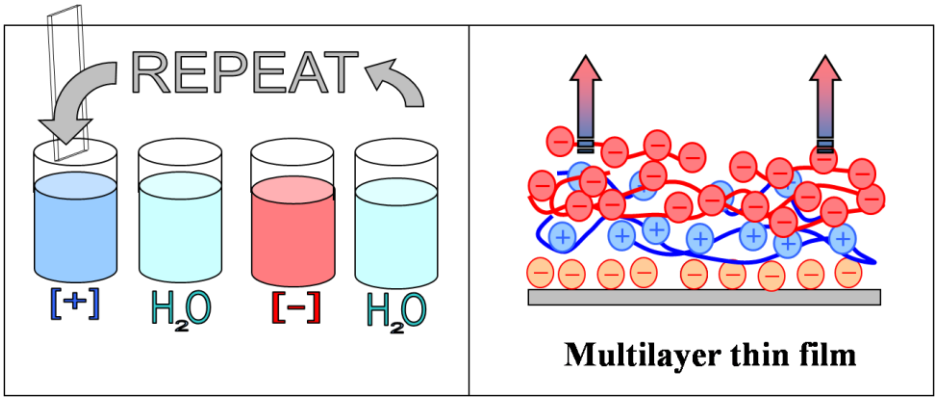

Figure Ap2.1. Schematic representation of the different steps involved in the deposition of a nanocoating by using the Layer by Layer method.

It is important to note that the polyanions and polycations overlap each other at the molecular level, and this produces a homogeneous optical material [3-5, 26, 27]. The pair of one anionic monolayer and one cationic monolayer will be called bilayer henceforward. The composition and thickness of an individual bilayer can be controlled by adjusting the deposition parameters (concentration of solutions, pH, temperature, immersion times, ionic strength, etc.).In addition, these coatings can be formed onto many different substrates (metals, plastics, ceramics or semiconductors) with different shapes.

In this thesis, two weak polyelectrolytes will be used for the LbL assembly, poly(allylamine hydrochloride) (PAH) as a polycation and Poly(acrylic acid, sodium salt) (PAA) as a polyanion, and will be the base of the electrostatic attraction onto the desired surface (optical fiber or glass slides). In Figure Ap2.2, the chemical structures of both weak polyelectrolytes are shown. The main advantage of these polyelectrolytes is that their linear charge densities can be varied over a wide range by simple adjustments of the pH of the dipping solutions. With this approach, it is possible to control the charge density of both an adsorbing polelectrolyte and the surface charge of a previously adsorbed polyelectrolyte in order to obtain the bilayer building block. The final thickness and the surface properties can be tuned in a very precise manner as a function of the number of bilayers deposited onto the surface of the substrate.

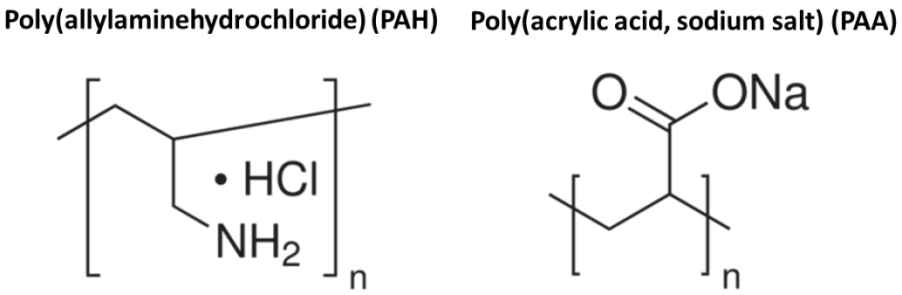

Figure Ap2.2. Chemical structure of both cationic and anionic polyelectrolytes (PAH and PAA).

Finally, the use of the PAA at a desired pH during the fabrication process is of great interest because this weak polyelectrolyte can be used as a protective agent of the silver nanoparticles which makes possible the control of their resultant shape and size, preventing their agglomeration or precipitation, as it was previously commented in Chapter 2 and 3. Due to these specific properties related to the PAA [5, 7, 28-33], the use of the LbL assembly as a tool to obtain thin films based on inorganic nanoparticles will be investigated in this thesis, using two different methods, known as in situ synthesis (ISS) and the Layer-by-Layer Embedding (LbL-E) deposition technique.

Bibliography

[1] Iler, R. K. Multilayers of Colloidal Particles. J. Colloid Interface Sci. 1966, 21, 569-594.
[2] Decher, G. Fuzzy Nanoassemblies: Toward Layered Polymeric Multicomposites. Science 1997, 277, 1232-1237.
[3] Choi, J.; Rubner, M. F. Influence of the Degree of Ionization on Weak Polyelectrolyte Multilayer Assembly. Macromolecules 2005, 38, 116-124.
[4] Hammond, P. T. Form and Function in Multilayer Assembly: New Applications at the Nanoscale. Adv Mater 2004, 16, 1271-1293.
[5] Choi, J.; Rubner, M. F. Influence of the Degree of Ionization on Weak Polyelectrolyte Multilayer Assembly. Macromolecules 2005, 38, 116-124.
[6] Shiratori, S.; Yamada, M.; Ito, T.; Wang, T. C.; Rubner, M. F. In In Nanoscale control of layer thickness for EL devices by mass-controlled layer-by-layer sequential adsorption process; Materials Research Society Symposium - Proceedings; 2000; Vol. 598, pp BB1.9.1-BB1.9.6.
[7] Shiratori, S. S.; Rubner, M. F. PH-Dependent Thickness Behavior of Sequentially Adsorbed Layers of Weak Polyelectrolytes. Macromolecules 2000, 33, 4213-4219.
[8] Ariga, K.; Lvov, Y.; Kunitake, T. Assembling Alternate Dye-Polyion Molecular Films by Electrostatic Layer-by-Layer Adsorption. J. Am. Chem. Soc. 1997, 119, 2224-2231.
[9] Lvov, Y.; Ariga, K.; Ichinose, I.; Kunitake, T. Layer-by-Layer Architectures of Concanavalin A by Means of Electrostatic and Biospecific Interactions. Journal of the Chemical Society, Chemical Communications 1995, 2313-2314.
[10] Liu, Y.; Wang, A.; Claus, R. Molecular Self-Assembly of TiO2/polymer Nanocomposite Films. J Phys Chem B 1997, 101, 1385-1388.
[11] Lenahan, K. M.; Wang, Y. -.; Liu, Y.; Claus, R. O.; Heflin, J. R.; Marciu, D.; Figura, C. Novel Polymer Dyes for Nonlinear Optical Applications using Ionic Self-Assembled Monolayer Technology. Adv Mater 1998, 10, 853-855.
[12] Lenahan, K. M.; Liu, Y.; Wang, Y.; Claus, R. O. Electrostatic Self-Assembly Processes for Noncentrosymmetric Thin Films and Devices. Proc SPIE Int Soc Opt Eng 1999, 3675, 104-112.
[13] Bertrand, P.; Jonas, A.; Laschewsky, A.; Legras, R. Ultrathin Polymer Coatings by Complexation of Polyelectrolytes at Interfaces: Suitable Materials, Structure and Properties. Macromolecular Rapid Communications 2000, 21, 319-348.
[14] Arregui, F. J.; Matías, I. R.; Claus, R. O. Optical Fiber Gas Sensors Based on Hydrophobic Alumina Thin Films Formed by the Electrostatic Self-Assembly Monolayer Process. IEEE Sensors Journal 2003, 3, 56-61.
[15] Rivero, P. J.; Urrutia, A.; Goicoechea, J.; Arregui, F. J. Optical Fiber Humidity Sensors Based on Localized Surface Plasmon Resonance (LSPR) and Lossy-Mode Resonance (LMR) in Overlays Loaded with Silver Nanoparticles. Sensors and Actuators, B: Chemical 2012, 173, 244-249.
[16] Rivero, P. J.; Urrutia, A.; Goicoechea, J.; Arregui, F. J.; Matias, I. R. In In Humidity sensor based on silver nanoparticles embedded in a polymeric coating; Proceedings of the International Conference on Sensing Technology, ICST; 2011; , pp 376-379.
[17] Rivero, P. J.; Urrutia, A.; Goicoechea, J.; Arregui, F. J.; Matías, I. R. Humidity Sensor Based on Silver Nanoparticles Embedded in a Polymeric Coating. International Journal on Smart Sensing and Intelligent Systems 2012, 5, 71-83.
[18] Rivero, P. J.; Urrutia, A.; Goicoechea, J.; Matias, I. R.; Arregui, F. J. A Lossy Mode Resonance Optical Sensor using Silver Nanoparticles-Loaded Films for Monitoring Human Breathing. Sensors and Actuators, B: Chemical 2012.
[19] Bravo, J.; Zhai, L.; Wu, Z.; Cohen, R. E.; Rubner, M. F. Transparent Superhydrophobic Films Based on Silica Nanoparticles. Langmuir 2007, 23, 7293-7298.
[20] Cassagneau, T.; Mallouk, T. E.; Fendler, J. H. Layer-by-Layer Assembly of Thin Film Zener Diodes from Conducting Polymers and CdSe Nanoparticles. J. Am. Chem. Soc. 1998, 120, 7848-7859.
[21] Cebeci, F. Ç.; Wu, Z.; Zhai, L.; Cohen, R. E.; Rubner, M. F. Nanoporosity-Driven Superhydrophilicity: A Means to Create Multifunctional Antifogging Coatings. Langmuir 2006, 22, 2856-2862.

[22] Itano, K.; Choi, J.; Rubner, M. F. Mechanism of the pH-Induced Discontinuous swelling/deswelling Transitions of Poly(Allylamine Hydrochloride)-Containing Polyelectrolyte Multilayer Films. Macromolecules 2005, 38, 3450-3460.
[23] Mwaura, J. K.; Pinto, M. R.; Witker, D.; Ananthakrishnan, N.; Schanze, K. S.; Reynolds, J. R. Photovoltaic Cells Based on Sequentially Adsorbed Multilayers of Conjugated Poly(p-Phenylene Ethynylene)s and a Water-Soluble Fullerene Derivative. Langmuir 2005, 21, 10119-10126.
[24] Urrutia, A.; Rivero, P. J.; Ruete, L.; Goicoechea, J.; Fernández-Valdivieso, C.; Arregui, F. J.; Matías, I. R. An Antibacterial Surface Coating Composed of PAH/SiO2 Nanostructurated Films by Layer by Layer. Physica Status Solidi (C) Current Topics in Solid State Physics 2010, 7, 2774-2777.
[25] Urrutia, A.; Rivero, P. J.; Ruete, L.; Goicoechea, J.; Matías, I. R.; Arregui, F. J. Single-Stage in Situ Synthesis of Silver Nanoparticles in Antibacterial Self-Assembled Overlays. Colloid Polym. Sci. 2012, 290, 785-792.
[26] Berg, M. C.; Choi, J.; Hammond, P. T.; Rubner, M. F. Tailored Micropatterns through Weak Polyelectrolyte Stamping. Langmuir 2003, 19, 2231-2237.
[27] Yoo, D.; Shiratori, S. S.; Rubner, M. F. Controlling Bilayer Composition and Surface Wettability of Sequentially Adsorbed Multilayers of Weak Polyelectrolytes. Macromolecules 1998, 31, 4309-4318.
[28] Ershov, B. G.; Henglein, A. Time-Resolved Investigation of Early Processes in the Reduction of Ag + on Polyacrylate in Aqueous Solution. J Phys Chem B 1998, 102, 10667-10671.
[29] Ershov, B. G.; Henglein, A. Reduction of Ag + on Polyacrylate Chains in Aqueous Solution. J Phys Chem B 1998, 102, 10663-10666.
[30] Machado, G.; Beppu, M. M.; Feil, A. F.; Figueroa, C. A.; Correia, R. R. B.; Teixeira, S. R. Silver Nanoparticles obtained in PAH/PAA-Based Multilayers by Photochemical Reaction. Journal of Physical Chemistry C 2009, 113, 19005-19010.
[31] Veletanlic, E.; Cynthia Goh, M. Polyelectrolyte Multilayer Films as Templates for the in Situ Photochemical Synthesis of Silver Nanoparticles. Journal of Physical Chemistry C 2009, 113, 18020-18026.
[32] Logar, M.; Jancar, B.; Šturm, S.; Suvorov, D. Weak Polyion Multilayer-Assisted in Situ Synthesis as a Route Toward a Plasmonic Ag/TiO2 Photocatalyst. Langmuir 2010, 26, 12215-12224.
[33] Wang, T. C.; Rubner, M. F.; Cohen, R. E. Polyelectrolyte Multilayer Nanoreactors for Preparing Silver Nanoparticle Composites: Controlling Metal Concentration and Nanoparticle Size. Langmuir 2002, 18, 3370-3375.

APPENDIX 3. Publications

Ap3.1. Articles published in JCR indexed journals

[1] P. J. Rivero, A. Urrutia, J. Goicoechea, C. R. Zamarreño, F. J. Arregui and I. R. Matias, "An antibacterial coating based on a polymer/sol- gel hybrid matrix loaded with silver nanoparticles," *Nanoscale Research,* vol. 6, pp. 1-7, 2011.

[2] A. Urrutia, P. J. Rivero, L. Ruete, J. Goicoechea, I. R. Matias and F. J. Arregui, "Single-stage in situ synthesis of silver nanoparticles in antibacterial self-assembled overlays," *Colloid and Polymer Science,* vol. 290, pp. 785-792, 2012.

[3] P. J. Rivero, A. Urrutia, J. Goicoechea and F. J. Arregui, "Optical Fiber Humidity Sensors Based on Localized Surface Plasmon Resonance (LSPR) and Lossy-Mode Resonance (LMR) in Overlays Loaded with Silver Nanoparticles," *Sensors and Actuators, B: Chemical,* vol. 173, pp. 244-249, 2012.

[4] P. J. Rivero, A. Urrutia, J. Goicoechea, Y. Rodriguez, J.M. Corres, F. J. Arregui and I. R. Matias, "An Antibacterial Submicron Fiber Mat with in Situ Synthesized Silver Nanoparticles," *Journal of Applied Polymer Science,*" vol. 126, pp. 1228-1235, 2012.

[5] P. J. Rivero, A. Urrutia, J. Goicoechea, I. R. Matias and F. J. Arregui, "A Lossy Mode Resonance Optical Sensor using Silver Nanoparticles-Loaded Films for Monitoring Human Breathing," *Sensors and Actuators, B: Chemical,* vol. 187, pp. 40-44, 2013.

[6] P. J. Rivero, J. Goicoechea, A. Urrutia, and F. J. Arregui, "Effect of both protective and reducing agents in the synthesis of multicolor silver nanoparticles," *Nanoscale Research,* vol. 8, pp. 1-9, 2013.

[7] A. Urrutia, J. Goicoechea, P. J. Rivero, I. R. Matias and F. J. Arregui, "Electrospun nanofiber mats for evanescent optical fiber sensors," *Sensors and Actuators, B: Chemical,* vol. 176, pp. 569-576, 2013.

[8] P. J. Rivero, J. Goicoechea, A. Urrutia, I. R. Matias and F. J. Arregui, "Multicolor Layer-by-Layer films using weak polyelectrolyte assisted synthesis of silver nanoparticles," *Nanoscale Research,* vol. 8, pp. 1-10, 2013.

Ap3.2. Additional articles published in other scientific journals

[1] A. Urrutia, P. J. Rivero, L. Ruete, J. Goicoechea, C. Fernandez-Valdivielso, F. J. Arregui and I. R. Matias, "An antibacterial surface coating composed of PAH/SiO_2 nanostructurated films by layer by layer," *Physica Status Solidi (C) Current Topics in Solid State Physics,* vol. 7, pp. 2774-2777, 2010.

[2] P. J. Rivero, A. Urrutia, J. Goicoechea, F. J. Arregui and I. R. Matias, "Humidity Sensor Based on Silver Nanoparticles Embedded in a Polymeric Coating," *International Journal on Smart Sensing and Intelligent Systems,* vol. 5, pp. 71-83, 2012.

Ap3.3. International conferences

[1] A. Urrutia, P. J. Rivero, L. Ruete, J. Goicoechea, I. R. Matias and F. J. Arregui, "An antibacterial surface coating composed of PAH/SiO_2 nanostructurated films by layer by layer", *TNT 2009*, Barcelona (Spain), 2009.

[2] A. Urrutia, P. J. Rivero, J. Goicoechea, F. J. Arregui and I. R. Matias "Humidity sensor based on a long-period fiber grating coated with a hydrophobic thin film,", *Proceedings of SPIE - the International Society for Optical Engineering, EWOFS 2010*, Porto (Portugal), 2010.

[3] P. J. Rivero, A. Urrutia, , P. Aldaz, J. Goicoechea, I. R. Matias and F. J. Arregui "An antibacterial coating based on a polymer/sol- gel hybrid matrix loaded with silver nanoparticles", *TNT 2010*, Braga (Portugal), 2010.

[4] C. R. Zamarreño, M. Hernaez, I. Del Villar, P. J. Rivero, I. R. Matias and F. J. Arregui, "Lossy mode resonance based optical fiber pH sensors," *TNT 2010*, Braga (Portugal), 2010.

[5] P. J. Rivero, A. Urrutia, J. Goicoechea, F. J. Arregui and I. R. Matias, "Humidity Sensor Based on Silver Nanoparticles Embedded in a Polymeric Coating," *Proceedings of The 5th International Conference on Sensing Technology, ICST 2011,* Palmerston North (New Zealand), 2011.

[6] A. Urrutia, P. J. Rivero, J. Goicoechea, F. J. Arregui and I. R. Matias, "Optical sensor based on polymer electrospun nanofibers for sensing humidity," *Proceedings of The 5th International Conference on Sensing Technology, ICST 2011,* Palmerston North (New Zealand), 2011.

[7] P. J. Rivero, A. Urrutia, J. Goicoechea, F. J. Arregui and I. R. Matias, " An optical resonance sensor using silver nanoparticles-loaded films for monitoring human breathing," *Proceedings of The 14th International Meeting on Chemical Sensing, IMCS 2012,* Nuremberg (Germany), 2012.

[8] A. Urrutia, P. J. Rivero, J. Goicoechea, Y. Rodriguez, F. J. Arregui and I. R. Matias, "Silver Nanoparticles Loaded Electrospun Nanofibers for Humidity Optical Fiber Sensing," *Proceedings of The 14th International Meeting on Chemical Sensing, IMCS 2012,* Nuremberg (Germany), 2012.

[9] J. M. Corres, F. J. Arregui, J. Goicoechea, Y. Rodriguez and P. J. Rivero, "Optical Fiber pH Sensor using Electrospun Nanowebs of poly(acrylic acid) PAA," *2nd International Conference on Electrospinning, Electrospin 2012,* Jeju (Korea), 2012.

[10] A. Urrutia, P. J. Rivero, J. Goicoechea, Y. Rodriguez-Garcia, F. J. Arregui and I. R. Matias, "Optical fiber ammonia sensors based on fluorescent electrospun nanofibers," *2nd International Conference on Electrospinning, Electrospin 2012,* Jeju (Korea), 2012.

[11] F. J. Arregui, I. R. Matias, C. Bariain, J. M. Corres, C. Fernandez-Valdivielso, I. Del Villar, J. Goicoechea, C. R. Zamarreño, M. Hernaez, C. Elosua, P. J. Rivero, A. Urrutia, A. B. Socorro, P. Sanchez-Zabal, I. Vidondo, L. Razquin, J. Ascorbe, "Optical fiber sensors based on Lossy Mode Resonances," *6èmes Journées Franco-espagnoles*, IBERNAM-CMC2 2012, Marseille (France), 2012.

[12] A. Urrutia, D. Wencel, S. O´Driscoll, B. O´Reilly, T. Abel, M. Somers, P. J. Rivero, F. J. Arregui and C. McDonagh, "A novel camera phone-based platform for sol-gel-derived fluorescence-based pH sensing," *XIII International Sol-Gel Conference , Sol-Gel 2013,* Madrid (Spain), 2013.

[13] F. J. Arregui, P. J. Rivero, M. Hernaez, J. Goicoechea and I. R. Matias, "Lossy-Mode resonances and Localized surface plasmons generated by layer-by-layer assemblies for sensing," *Layer-by-Layer (LbL) assemblies: Science and Technology Conference*, New Jersey (EEUU), 2014.

[14] P. J. Rivero, M. Hernaez, J. Goicoechea, I. R. Matias and F. J. Arregui, "Optical fiber refractometers based on localized surface plasmon resonance (LSPR) and lossy mode resonance (LMR)" *Proceedings of The 23rd International Conference on Optical Fibre Sensor, OFS23*, Santander (Spain), 2014.

Ap3.4. Submitted articles

[1] P. J. Rivero, J. Goicoechea, I. R. Matias and F. J. Arregui, "A comparative study of two different approaches for the incorporation of silver nanoparticles into Layer-by-Layer films" *Nanoscale Research (under revision).*

Ap3.5. Other publications

[1] C. R. Zamarreño, M. Hernaez, J. Goicoechea, P. J. Rivero, I. R. Matias and F. J. Arregui, "Optical sensors for corrosion monitoring," in the book entitled "*Intelligent Coatings for Corrosion Monitoring*", Elservier Publications, USA (Butterworth-Heinemann); 1st edition (2014), ISBN 9780124114678.